Department of Pure and Applied Chemistry

University of Strathclyde

Glasgow

THE GEOCHEMISTRY OF A LATE PRECAMBRIAN WEATHERING PROFILE NORTHWEST SCOTLAND

by

Fidel A. Cardenas S., B.Sc., M.E.

A thesis submitted in part fulfilment of the requirements for the degree of Doctor of Philosophy.

January, 1986

To ALLAN,
who has given a new dimension
to his parents' life!

A C K N O W L E D G E M E N T S

The main body of the investigation was carried out at the Department of Pure and Applied Chemistry, in collaboration with the Department of Applied Geology, of the University of Strathclyde. I wish to thank Professor J.M. Ottaway and Professor M.J. Russell, from the departments of Chemistry and Geology, respectively, for providing the facilities for this project.

I particularly thank Dr B.G. Cooksey, my supervisor, from the Department of Chemistry for his much appreciated guidance and contributions to the development of this project. I also thank Dr I. Allison, from the Department of Geology, for his valuable cooperation in the Mineralogical Analysis and the critical reading of the manuscript.

My thanks also go to Mrs Barbara Ottaway for her ever kind collaboration as well as to the technicians of the Geochemistry laboratory.

Major and Trace Element Analysis of the samples was performed at the Department of Geology of the University of Glasgow, and Microprobe Analysis for Pyrophyllite at the Grant Institute of Geology of the University of Edinburgh. I therefore express my thanks to Dr C. Farrow, for providing the facilities for the analysis, and to Dr R. Hall, from the Grant Institue, who performed the Microprobe Analysis.

The author remains greatly indebted to the British Council for its financial support through a "Technical Cooperation" scholarship to undertake this research.

Thanks are also due to the Universidad Pedagogica Nacional de Bogota, Colombia, for their financial support in the early stages of this project and for allowing me the time to develop it.

To my wife, Rosa Isabel, my love and thanks for her ever positive and stimulating attitude towards this work.

Thanks also to my colleagues and particularly to Mr Stephen Cook for his collaboration at the beginning of my studies at the University of Strathclyde.

Fidel A. Cardenas

A B S T R A C T

In an attempt to understand the environment of the Precambrian weathering at Rispond, and compare it with weathering processes taking place at the present time, samples weathered to different degrees have been taken at various distances immediately below the Cambrian Unconformity. These samples have been subjected to chemical analysis by X-ray fluorescence spectometry and wet analysis, and to mineralogical analysis by X-ray diffraction and polarised light microscopy.

Interpretation of these results indicate that the samples represent a weathering profile (although not necessarily an unchanged one as these rocks have been subjected to a maximum temperature of 250°C during burial subsequent to the deposition of the Cambrian strata). This is inferred from the minerals present in the soil, the nature of the chemical changes observed, the similarities of the data on the Kronberg weathering diagram to those of present-day weathering, and the position of the profile immediately below the unconformity.

Further interpretation of the results in terms of the thermodynamic properties of the minerals present in the profile, the chemical reactions believed to have taken place, the geological evidence and a survey of the chemical composition of present-day surface waters leads to the conclusion that the rocks below the Cambrian Unconformity at Rispond represent a fossil soil profile. These rocks contain pyrophyllite, considered to have been formed by low-grade metamorphism rather than by weathering. Three possible modes

of origin have been considered, and that involving the weathering of potassium feldspar to kaolinite alone in an acid environment rejected. The two mechanisms involving the weathering of the feldspar to illite in an arid alkaline environment with restricted drainage are considered to be more likely. The illite produced in these mechanisms was further weathered to produce, in the one case, kaolinite, and in the other one, potassium beidellite as a mixed layer mineral with illite. These two mechanisms can be mixed in any proportion, the exact amount of potasium beidellite present depending upon the relative thermodynamic stabilities of kaolinite and beidellite. As the latter is unknown, further accuracy cannot be achieved at present.

The presence of abundant potassium feldspar in the Fucoid Beds, and the existence of trace fossil planolites in such rocks as well as the temperature to which they have been heated (about 250°C) suggested the possible existence of an ammonium feldspar in the area. Therefore, a method to measure the amount of ammonia content in these rocks has been designed. The results of twenty-two samples from the Cambro-Ordovician succession of N.W. Scotland analysed by this method show that the ammonia content is very low. If all the ammonia is present as an ammonium feldspar (buddingtonite), it represents about 0.3% of the mineral in the shales and even less in other rock types.

I N D E X

CHAPTER I

INTRODUCTION

Page No.

CHAPTER II

EXPERIMENTAL

CHAPTER III

PRESENT-DAY WEATHERING PROCESSES BEARING ON THE WEATHERING OF LEWISIAN GNEISS

CHAPTER IV

RESULTS AND DISCUSSION

CHAPTER V

DETERMINATION OF AMMONIA IN ROCKS

CHAPTER I

I N T R O D U C T I O N

1.0. General

The world's two largest known sedimentary deposits of chemically precipitated feldspar appear in Scotland, where 10^{10} tonnes of orthoclase and 10^{7} tonnes of barium feldspar of early Cambrian and latest Precambrian age respectively are formed (1). It is believed that weathering of Lewisian gneiss gave rise to fluids rich in potassium, aluminium and silicon, which flowed into the sea and were precipitated on the continental shelf as potassium feldspar in the lower Cambrian Fucoid Beds of Northwestern Scotland and into deeper basins, where the aluminium and silicon reacted with barium to form the barium feldspar.

The search for possible explanations of both the derivation of these potassium rich fluids and their precipitation as potassium feldspar in the Fucoid Beds originated this investigation. The project began with the search of an ammonium feldspar in the Cambrian Argyllites and included the development of a method for the determination of ammonia in rocks. This was originally an M.Sc. project, which was later extended to a Ph.D. by studying the Geochemistry of the rocks immediately below the Cambrian Unconformity thought to be the source of the Cambrian rocks. Thus the Ph.D. project aimed to compare weathering processes in the Precambrian with present-day weathering processes. The first four chapters of this thesis deal with the weathering processes, while the last chapter (Chapter V) refers to the search of an ammonium feldspar and the determination of ammonia in rocks.

1.1. The Aim of the Investigation

Rocks on the surface of the earth are continuously undergoing modifications due to physical and chemical action of agents such as carbon dioxide, water, air, oxygen and micro-organisms. The result of this complex process called weathering is a variety of soils. Of particular importance is the reaction that takes place between water and the mineral constituents of the rocks. This is because carbon dioxide, which is produced mainly by degradation of organic matter, photosynthesis and bacterial action, dissolves in water. Thus the water becomes acid and attacks rocks more easily than pure water would do.

In the Precambrian era, around 800 Ma (2.3), terrestrial plants had not yet evolved. In the absence of plants, the amount of carbon dioxide present in the soil atmosphere was less than it is today. It is the objective of this study to compare Precambrian weathering with that taking place at the present time in order to infer as much as possible about the chemical reactions taking place and the nature of the waters reacting with the Lewisian rocks. To do this, samples of Lewisian gneiss weathered to different degrees were taken at different distances beneath the Cambrian unconformity, and subjected to chemical and mineral analysis. These results were then interpreted with the aid of thermodynamics.

1.1.1. The Relevance of the Project

It is well known that potassium is essential for the metabolism of animals and plants and that the deficiency of this metal in soils makes them poor and inefficient for agricultural purposes. The Fucoid Beds, member of the

agricultural purposes. The Fucoid Beds, member of the Cambro-Ordovician succession in Northwestern Scotland represents a source of potassium. However, it is difficult to utilize this potassium because it is held in very slowly soluble aluminosilicates such as potassium feldspar and micas. The solubility of potassium feldspar and mica is very low, saturated solutions of microcline and muscovite contain 3 and 0.14 ppm of K respectively [see solubility products in Ref. (4)].

The Fucoid Beds do however have a potential value as a bulk fertilizer (5, 6, 7). The rock can be crushed and ground to a fine powder. This powder, when spread over terrains of poor potassium content becomes on weathering an abundant source of the metal because, under these circumstances, the solubility of the minerals is increased.

The investigation provides information about the chemistry and the geochemistry of the Precambrian/Cambrian boundary in Scotland as well as the understanding of the chemical weathering of Lewisian rocks. It is important to note that the research has revealed the presence of pyrophyllite along the unconformity, thus locating this mineral for any interested party.

This introductory chapter outlines some of the background information (i.e. Geology in Section 1.2. and weathering in Section 1.3.) and provides an elementary introduction to the relevant parts of chemical thermodynamics (Section 1.4.). The techniques of X-ray analysis are also discussed as these form the basis of the practical techniques employed in the analysis of the rocks examined (Section 1.5).

1.2. Geology

It is believed that approximately 4600 Ma the earth condensed from a cloud of dust and gas. Since then it has been changing and evolving, undergoing a variety of geological processes.

A great deal of effort and investigation has been devoted to reconstructing the history of the earth. The further back in time, the less certain are the inferences about geological history and the evolution of the earth. Since it is not the purpose of this work to discuss the history of the earth or the geology of the British Isles in depth, only a brief description of the relevant rock groups is given in this section.

Rocks of very different ages from the Archaean 25 Ma to the present are preserved in Britain. The stratigraphic units, which are referred to in this study, are the Lewisian Complex, the Torridonian and the Cambrian [see Anderton et al (8) and Craig (6) for reviews].

1.2.1. The Lewisian Complex

The Lewisian Complex includes the oldest rocks of the United Kingdom (3, 8, 9, 10) and consists of highly metamorphosed gneiss and schists with lesser amount of metasedimentary rocks (e.g. marbles), with ages between 2600 and 1400 Ma (8), according to radiometric data.

Most of these rocks are of igneous origin and include intrusions of basic igneous rocks of various ages. One suite of basic dykes, the Scourie dykes, is used as a time marker

to separate the older, Scourian gneiss from the younger, Laxfordian gneiss. The Scourian complex has metamorphic radiometric ages from about 2900 Ma to about 2200 Ma. The Laxfordian complex has metamorphic ages from about 2200 Ma to about 1500 Ma (10). Each of these geological formations represents a long succession of events, some of which are summarised in Table 1.

The history of the Laxfordian, after the intrusion of the Scourie dykes, has been summarised by Anderton et al. (8) in four phases:

a. deposition of sediments,
b. deformation and metamorphism,
c. intrusion of igneous rocks, and
d. uplifting and cooling.

As most of the rocks metamorphosed by the Laxfordian event had been in existance since the early Scourian metamorphism, the effect of the Laxfordian metamorphism was mainly to rework and deform existing gneiss rather than to form gneiss from the new igneous and sedimentary rocks. However, some post-Scourian sediments such as the Loch Marie group and the Gairloch metasediments were also affected.

The Laxfordian reworking was followed by intrusions of small granite sheets and extensive pegmatite veins. The granitic injection complex of Harris was probably the last major episode in the development of the Lewisian complex.

1.2.2. The Torridonian

The Torridonian is a sequence of sandstones and

conglomerates that unconformably rest on a rugged surface of the older Lewisian rocks in the northwest of Scotland (3). Its thickness reaches several thousand metres (11).

The Torridonian was deposited between the end of the Laxfordian about 1400 Ma and the beginning of the Cambrian period at 570 Ma. It consists of at least three different groups: the Stoer Group, the Torridon Group and the Sleat Group (12).

Torridonian rocks are found forming many of the prominent mountains along the western seaboard of the mainland, e.g., Suilven, Canisp, Liathach and An Teallach (Fig. 1).

The Stoer Group consists of breccio-conglomerates, derived from local gneiss and fluvially deposited exotic facies containing well rounded pebbles of gneiss and quartz, and also quartzites that are unknown in the basement.

The Torridon Group is mainly composed of unmetamorphosed red beds and some subordinated grey shales. The red beds occur lower in the succession and are interpreted as fanglomerates, transported only a few kilometres or less from their source. The overlying grey shales are interpreted as marine deposits.

The Sleat Group is made mainly of slightly metamorphosed sandstones and shales, underlying the Torridon Group. These sandstones differ from the Torridon Group in being poorly sorted.

Table 1: Major Scourian and Laxfordian events.- [After Anderton et al. (8)]

Million Years	Complex	Major Events	Local Events
1300			
1400	L		
1500	A	Uplift and Cooling	
1600	X		
1700	F	Intrusions	Intrusions of Granitic
1800	O	Laxfordian	Injection Complexes
1900	R	Metamorphism	South Harris, Rona.
	D		
2000	I		Deposition of Loch
	A		Marie Group and Gair-
2100	N		loch Sediments.
2200	_____	Intrusion of Scorie	
2300		Dykes	
2400	S		Inverian Metamorphism
2500	C		
2600	O		
2700	U	Badcallian	
2800	R	Metamorphism	Deposition of Sediments
2900	I		and Formation of Lay-
	A		ered Intrusions
3000	N	Formation of Con-	
		tinental Crust?	

Fig. 1: Map of Northwest Scotland showing the Cambrian, Lewisian and Torridonian rocks.

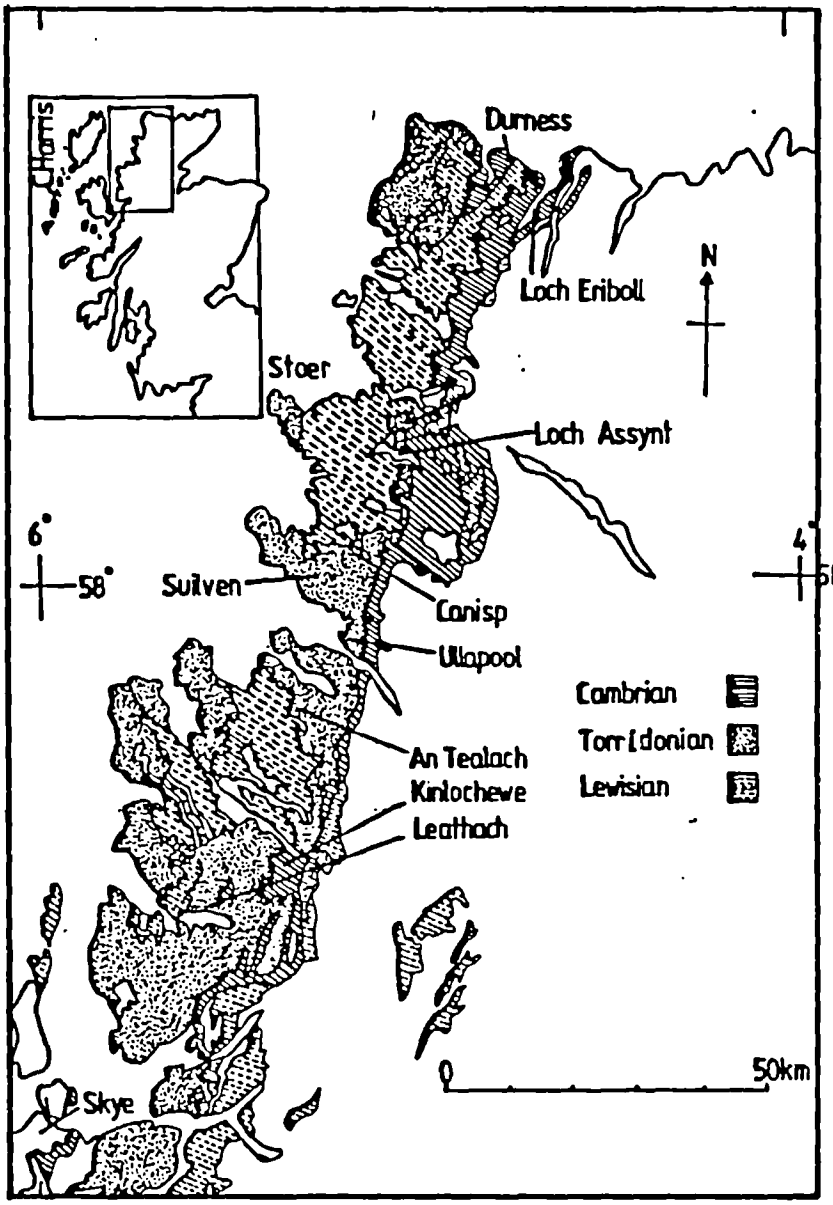

1.2.3. The Cambrian

Rocks of the Cambrian period are exposed over a strike length of about 200 km in a narrow, 2-3 km, strip that extends from the north coast to Skye (see Fig. 1). Made up chiefly of sandstones, siltstones, and carbonates, these beds were deposited in a sea, which gradually transgressed northwestwards over older Torridonian and Lewisian rocks, on which they rest with a remarkably planar unconformity.

The succession is divided into a lower, clastic, and an upper, carbonate, sequence (6). The succession is well seen in places like Durness and Loch Eriboll in the North (Fig. 1) and in the Assynt area, the neighbourhood of Ullapool and Kinlochewe in the South.

The lower sequence comprises: the basal quartzite, a cross-bedded arkose and sandstone, and the overlying Pipe Rock, a sandstone which gets its name from an abundance of vertical worm burrows called pipes that are present. The pipes are ascribed to the trace fossils Skolithos and Monocraterion. The sequence has been interpreted as being deposited in a tidal environment (6).

The overlying Fucoid Beds, usually less than 20 m thick, are dolomitic siltstones, that are named after the frequency of the horizontal worm tube trace fossil Planolites, which was originally mistaken for seaweed markings. Their brown ferruginous-coloured weathering makes the formation a marker horizon. It is considered that the Fucoid Beds were deposited in a shallow lagoonal environment.

One characteristic of the Fucoid Beds is their high

potassium content. Averages between 8% and 12% have been reported (13) and can be seen in Table 20 of this work, chemical analyses of samples 2, 3, and 5.

The potassium occurs as adularia, a low-temperature potassium feldspar, the dominant mineral in the siltstones. Its origin has been ascribed to three sources: a volcanic source (13), derivation from illite during dolomitization of the overlying limestones (14), and derivation by deep weathering of the Lewisian (15). The Salterella Grit, which directly overlies the Fucoid Beds, consists of sandstones with interleavings of shales. It takes its name from the presence of a small conical primitive mollusc, Salterella, which has been found in these rocks (16).

The upper sequence of the Durness Formation is predominantly made up of limestones and dolostones. A possible sequence of diagenesis has been suggested for these carbonates (17): partial recrystallization, dolomitization, silicification, calcitization and dolomitization.

1.3. Weathering Processes

Rocks exposed on the surface of the earth and those that are close to it are subjected to continuous alteration by physical, chemical and biotic processes. The physical and chemical alteration of these rocks is known as weathering (18). Igneous and metamorphic rocks as well as deeply buried and lithified sedimentary rocks were formed under high temperatures and pressures. On or near the surface of the earth, under lower temperatures and pressures, they are altered by weathering to new materials, which are more in equilibrium with the new conditions.

Disintegration of the original rock into material of smaller size but with virtually no change in chemical or mineralogical composition is known as physical or mechanical weathering. In contrast to physical weathering, chemical alteration may induce thorough decomposition of most or all of the primary minerals of the rock, resulting in the formation of new minerals, particularly clay minerals. Weathering due to living organisms is largely prevalent within a few metres of the surface of the earth, where plant roots are present.

In practice, physical, chemical and biochemical weathering processes usually operate together and it is not always easy to differentiate particular effects.

Weathering depends on the internal structure of the minerals and the way in which the environment acts on them, that is to say, weathering is a function of internal and external factors (19). Internal factors such as energies of bond formation, and crystalline structure determine the resistance of the minerals to alteration by external factors, such as wind, water, and biological agents.

1.3.1. Physical Weathering

Physical weathering processes are more evident in rocks exposed on the surface of the earth and, particularly, in deserts and cliff areas. In these processes, the rock is broken by expanding crevices already present in them, chiefly due to freeze-thaw cycles of water in the crevices and the growth of plants. This mechanism is particularly important in areas where extreme variations in temperature are frequent.

Other important factors of physical weathering are: saline solutions, glacial displacement, and wind. Saline solutions, having access to fractures of the rocks, also brings about disintegration into blocks or grains, due to pressure set up during the growth of crystals from the solution (20), the thermal expansion of the crystals upon heating, or as hydration and dehydration takes place. Formation of gypsum and anhydrite is presented here as an example:

$$CaSO_4 \cdot 2H_2O = CaSO_4 + 2H_2O$$

Gypsum (74 cm^3) Anhydrite + Water (82 cm^3)

Glacial displacement also causes mechanical weathering. As a glacier moves across an area, it tears rock material from the surface and this detritus incorporated in the ice is transported and later deposited essentially unaltered.

Wind is an important agent of erosion and weathering in desert regions. Rock fragments transported by wind storms impinge on outcropping rocks slowly breaking them into smaller pieces. Acids generated by bacterial decomposition of plants, when present, react with minerals thus making the rock more susceptible to physical weathering. Water in these regions plays a minor role in the weathering process.

Particulate and weathered materials, from the moment of their formation, are susceptible to movement and displacement from the place of origin. The relationship between erosion, transportation and deposition of detritus as a function of current velocity and particle size is summarised in Fig. 2. It can be seen that the critical

erosion velocity is a minimum around a grain diameter of 0.3 mm, and increases for materials with particle sizes greater or less than this. Materials having particle sizes around this minimum are difficult to erode, i.e., fine sand size. Thus it is possible that the erosion of sediments of mixed grain sizes will result in the removal of relatively coarse material instead of the finer particles.

As fluids move weathered materials away from the place of origin, they are selectively sorted out in accordance with their particle sizes, shapes, and densities forming sedimentary masses composed of more homogeneous material.

1.3.2. Chemical Weathering

It has been stated at the beginning of this section that igneous, metamorphic and sedimentary rocks (formed at depth in the Earth's crust) become unstable when exposed to the atmospheric conditions present on the Earth's surface. They are attacked by water, carbon dioxide and oxygen as water penetrates through them. The reactions taking place under these circumstances follow the laws of chemical equilibria, which means that the breakdown of minerals can proceed beyond the equilibrium point only if some components are added or removed from the system or both (23).

The new minerals formed by weathering are more highly oxidized and contain more water than those present in the parent rock. However, the more basic constituents (K_2O, Na_2O, CaO) of the original rock are removed by the weathering process, giving stable products, which are depleted in bases.

Fig. 2: The effect of grain size and velocity on the erosion, transportation, and deposition of material of uniform grain size.- [After Hjulstron and Garrels (21, 22)].

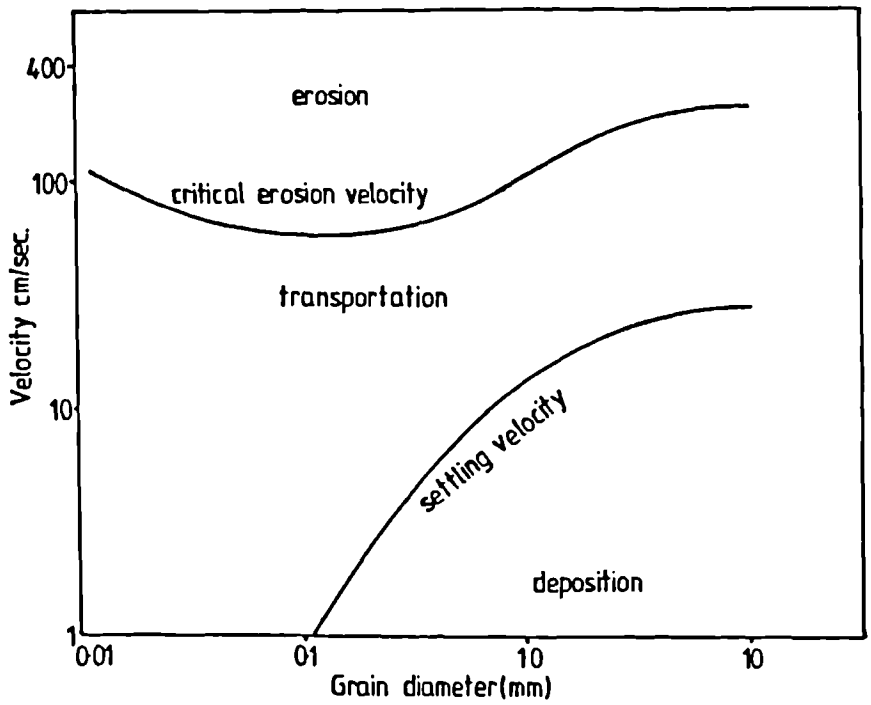

Weathering processes require water and heat. The rate at which they occur varies from a maximum in humid tropics, to a minimum at the poles. Some of the most common weathering processes are oxidation and reduction, formation of new minerals, hydration, hydrolysis and dissolution.

1.3.2.1. Oxidation and Reduction

Of particular importance in weathering processes are the oxidation of iron and sulphur. Although other elements like Mn, Cu, As, and U are also oxidized when their minerals are exposed to the atmosphere, they are not common elements in most rocks.

The reaction for fayalite given by Krauskopf (24) is taken here to illustrate the oxidation of iron.

$$Fe_2SiO_4 + 4H_2CO_3 = 2Fe^{+2} + 4HCO_3^- + H_4SiO_4$$
$$2Fe^{+2} + 4HCO_3^- + 1/2O_2 + 2H_2O = Fe_2O_3 + 4H_2CO_3$$

It seems that oxidation of iron is a two-step process. These two steps may be effected far apart when the dissolution of iron takes place in reducing conditions such as in the presence of organic matter. In the first step, ferrous ions are liberated and, in the second one, they are oxidized to ferric ions, due mainly to oxygen from the atmosphere.

Sulphur which is normally present as sulphides also undergoes oxidation, usually to sulphate. Like iron, the reaction is slow and does not take place in absence of water. Water seems to be necessary to supply acid to dissolve small amounts of sulphides before they are oxidized.

$$PbS + 2H_2CO_3 = Pb^{+2} + H_2S + 2HCO_3^-$$

$$H_2S + 2O_2 + Pb^{+2} + 2HCO_3^- = PbSO_4 + 2H_2CO_3$$

Oxidation of sulphides results in acid solutions because the dissolved metal ion undergoes hydrolysis.

$$4FeS_2 + 15O_2 + 14H_2O = 4Fe(OH)_3 + 8H_2SO_4$$

1.3.2.2. Formation of New Minerals

This is a consequence of the weathering process and it involves the precipitation of new minerals from solution and the modification of crystal structures by cation exchange and cation substitution to form other new minerals. The precipitation of calcium carbonate in soils of dry regions is an example of mineral precipitation from solutions.

$$Ca^{+2} + 3H_2CO_3 = 2CaCO_3 + 3H_2O$$

An example of substitution is the formation of vermiculite from muscovite; the original mica structure is retained, but the interlayer K^+ ions are replaced by other ions from the weathering solution.

1.3.2.3. Hydration

This results from the capacity of certain minerals to take up water into the crystal structure. In this process, a volume change takes place, setting up physical stress and causing physical disintegration (see Section 1.3.1.). An example of hydration is the formation of hydrated iron oxides

$2Fe_2O_3 + 3H_2O = 2Fe_2O_3 \cdot 3H_2O$

Hematite Limonite

1.3.2.4. Hydrolysis

This is a type of hydration reaction in which a new mineral is formed with hydroxyl ions in crystal structure.

The process is very important in initiating the decomposition of feldspars, for which the following general reactions have been proposed (18):

$$\text{Silicate} + H_2O + H_2CO_3 = \text{Cations} + OH^- + HCO_3^- + H_4SiO_4$$

$$\text{Aluminosilicate} + H_2O + H_2CO_3 = \text{Clay minerals} + \text{Cations} + OH^- + HCO_3^- + H_4SiO_4$$

The weathering of Mg-olivine illustrates the type of reaction that takes place when silicates react with water and carbon dioxide.

$$Mg_2SiO_4 + 4CO_2 + 4H_2O = 2Mg^{+2} + 4HCO_3^- + H_4SiO_4$$

It is important to note that, during the reaction, acid is consumed, which means that any unit of soil water reacting with silicate minerals becomes more alkaline as the reaction proceeds.

Silica is quite soluble at the normal soil pH and, when present in the parent material in excess over that required to form clay minerals, it is washed out in the solution.

Aluminium, on the other hand, generally remains near the site of release because it is not very soluble at the normal soil pH. Hence aluminosilicates weather to a more aluminous solid phase, a clay mineral or a hydrous oxide. Theoretical, experimental and field evidence shows that iron as well as silica and aluminium tend to remain at the place of release (25). Indeed, most of the typical oxidation colours (yellowish brown to red) present in soils or weathered rocks are due to iron oxides.

1.3.2.5. Dissolution

This is normally the first stage of the chemical weathering. The amount of rock dissolved is a function of the volume, acidity or alkalinity of the water passing its surface, the nature of the minerals present in the rock as well as the time during which water remains in contact with the weathering matrix.

Minerals vary in their response to the attack of acid water: some of them are soluble, some become gels, and some are partly soluble, leaving their framework ready for the formation of new minerals.

The dissolution processes, which result in the formation of an alumina-rich residuum with different amounts of silica, are complex as they involve the initial release of ions into solutions, and then, the reaction of these ions or minerals to give new mineral combinations. Some of the released ionic species are adsorbed on colloid surfaces, some participate in the formation of new minerals, and some of them are transported by waters.

From theoretical considerations about solubilities of rock constituents at a pH characteristic of soils, and also from experimental work, several mobility sequences have been proposed. Chesworth (25) summarised mobility sequences proposed by different authors as follows:

$Al^{+3} < Fe^{+3} < Si^{+4} < Fe^{+2} < K^{+} < Ca^{+2} = Mg^{+2} = Na^{+}$

$Si^{+4} < Al^{+3} < Fe^{+3} < Ca^{+2} < Mg^{+2} < Na^{+2} = (K^{+})$

$Al^{+3} = Fe^{+3} < Si^{+4} < K^{+} < Na^{+} < Ca^{+2} < Mg^{+2}$

$Al^{+3} = Fe^{+3} < Si^{+4} < K^{+} < Mg^{+2} < Na^{+} < Ca^{+2}$

It follows from the above sequences that, although they do not fully agree, the invariable rule is that alkaline and alkaline earth metals are more soluble than aluminium silicon and iron. As a result of this, Ca^{+2}, Mg^{+2}, Na^{+}, and K^{+} are washed away in the solution, while aluminium, silicon and iron tend to concentrate in the residual material.

The behaviour of these ionic species varies according to the environment in which the reaction takes place, pH, physical characteristics of the soil, vegetation as well as the particular mineral under consideration.

Vegetation is an important factor in the behaviour of ionic species because of the selective uptake of ions by different plants and the type of chemical substances excreted by them. Lichens, for example, excrete chelating agents that can complex ions, thus changing their mobility. Chelating agents are also important because, during their reactions, H^{+} ions are liberated, which participate in the dissolution reaction (26).

The mobility of ionic species is also affected by the permeability and topography of the soil, mountainous regions with high permeability make for higher ionic mobilities.

1.3.3. Biotic Weathering

The climate of any region conditions the type of vegetation and animal fauna that can appear there as well as the type of soil developed. Biochemical activity in weathering is difficult to assess because of the complex interdependence between soil and organisms under the influence of the climate. Indeed, it is impossible to assess the influence of a single organism on a particular type of mineral. The relationships between soil and vegetation has been dealt with by Birkeland (18). The role of plants and animals in weathering has been discussed by Carroll (27) and Ollier (28). It involves a combination of both chemical and physical effects, of which the following are the most important: splitting of rocks, due to action of burrowing animals and of plant roots; transportation of materials by animals; increase of the weathering rate, due to dissolution of respired carbon dioxide in water, which increases its acidity, and complex chemical effects, such as chelation.

According to Wilson and Jones (29), biochemical weathering (weathering in which mineral decomposition is largely controlled by the action of organic acids), prédominates in soils of cool and temperate climates. Dissolution of rock forming minerals by organic acids has been carried out experimentally by Hung and Kiang (30) and Hung and Keller (31), who have concluded that weathering of silicate minerals by complexing acids (acetic, aspartic, salicilic and tartaric acids) "may result in a different

order of mineral stability from the traditional one of Goldich which apparently applies more to inorganic reagents". Organic acids can either be produced by decomposition of organic matter, or directly by living organisms, by fungi which excrete oxalic acid (32, 33). Like chemical weathering, biochemical weathering is a complex process, due to many factors whose action often overlap and cooperate. In order to gain some understanding of these complex relations, several investigations have been undertaken to study the relationships between lichens and rocks (26, 34). Effects such as etching, secondary products, precipitation of crystalline organic salts (mainly oxalates) have been observed experimentally (35-37), and in field collected samples (38-39). It follows from the previous investigations that lichens play an important role in biotic weathering, mainly through the generation of oxalic and phenolic acids, that can react with minerals to form complexes, and that when assessing weathering processes, this should be taken into account because it may be locally relevant.

1.4. Thermodynamics of Chemical Reactions

Dealing with the energy evolved and taken up by chemical reactions and its relations to the equilibrium of the system, thermodynamics is a predictive instrument that has its greatest usefulness in the laboratory closed systems at equilibrium.

It allows the investigator to calculate equilibrium constants from thermodynamic data such as heat of reaction, heat capacities and find the change in a thermodynamic property taking place in a chemical reaction by addition and subtraction of the corresponding thermodynamic properties of

the reactants and products.

Thermodynamics is also an aid in studying geological systems. However, its applicability to this field is often limited. For many substances of geological interest, experimental data from which thermodynamic properties can be derived is scarce or lacking. Sometimes, the thermodynamic data available are for the end members of solid solution series and the effect of such solutions cannot be accounted for without further data, which is not usually available. Most geologic environments are open systems, and equilibrium is not always attained. Finally, thermodynamics gives information on what reactions are possible from the point of view of energy, but it gives no information about how fast these reactions will proceed. Despite these limitations, it is always useful to see what a particular system would look like if chemical equilibrium were attained, as it provides an approximation to the real world and indicates the direction in which changes will take place.

In this section, a brief summary of those thermodynamic concepts that are useful in the investigation of chemical reactions is given. Particular emphasis is given to reactions that occur in solutions. This summary is by no means complete and further details on these topics are found in thermodynamic and chemical equilibrium text books (40-43) as well as in geochemistry books (44, 45).

1.4.1. Internal Energy

This includes all forms of energy other than those resulting from the position of the system in space, which is assumed to remain constant (46). In other words, it is the

sum of the energies of the constituent particles of the system: molecules, atoms, ions, etc. When the system undergoes a change, for example, heat is added, or some sort of work is done upon it, the internal energy of the system changes. The actual value of the internal energy is not measurable, but changes in energy may be readily measured. The internal energy is represented by E and its units are usually calories or kilocalories. The change in energy during a chemical reaction that proceeds from an initial state E_i to a final state E_f is symbolised by ΔE and is equal to the sum of the energies of the products E_f minus the sum of the energies of the reactants E_i

$$\Delta E = E_f - E_i$$

Since the internal energy of the system varies with the amount of material present in the system, it is an extensive property of the system.

1.4.2. The First Law of Thermodynamics

The first law of thermodynamics is the energy conservation principle, and states that the change in the internal energy dE is equal to the sum of the heat transferred to the system dq, and the work done on the system dw.

$$dE = dq + dw$$

1.4.3. Enthalpy or Heat Content

Enthalpy is defined as the sum of the internal energy and the energy due to the space occupied (i.e., PV) and is

denoted by H

$$H = E + PV$$

where P is the pressure and V is the volume of the system. For most practical purposes, H = E since changes in PV are negligible with respect to variations in internal energy. This approximation however does not hold for metamorphic systems, where the pressures are high and even small variations in volume produce large variations in enthalpy.

Like E, the enthalpy has no measurable absolute value, but differences in enthalpy, ΔH, are measurable and play an important role in thermodynamics. ΔH can be measured as the heat change when a reaction takes place under constant pressure and temperature.

The enthalpy change, ΔH, of a reaction is given by the difference between the enthalpies of the products minus the enthalpy of the reactants. A negative value of ΔH means that the reaction is exothermic whereas a positive value indicates that the reaction is endothermic. The enthalpy change involved in the formation of a compound from its elements is called "heat of formation". Unless other conditions are specified, heats of formation always refer to 1 formula weight of the compound, 298K and 1 atm pressure. Heats of formation have been measured for many compounds; some of the most useful in geochemistry are given in Appendix 2 of Reference 47, and Appendix VIII of Reference 24.

The enthalpy of a system, like E, is an extensive property. Its changes are determined only by the initial and final states of the system and not by the path by which these

changes are brought about.

Changes in enthalpy are measured in heat units, calories, kilocalories or Joules.

In the absence of other data, particularly free energies, enthalpy changes can be used to predict the behaviour of chemical substances. However, this is not an infallible measure of the tendency of a reaction to take place because, although exothermic reactions tend to proceed spontaneously and endothermic reactions generally do not occur unless energy is supplied, a few endothermic reactions do take place spontaneously. Thus enthalpy changes are only a gross indicator of reactivity.

1.4.4. Heat Capacity

When heat is supplied to a given mass of a substance, the heat absorbed is proportional to the temperature rise, and the proportionality constant is termed the heat capacity of the substance. If the mass is one gram, it is called the specific heat; more important is however the molal heat capacity, which is the product of the specific heat times the formula weight.

Since the heat capacity C varies with temperature, it is better defined as

$$C = \frac{d_q}{d_T}$$

where d_q represents an infinitesimally small amount of heat

absorbed by the system when the temperature rises dT degrees. There are two commonly used heat capacities: that at constant volume

$$C_V = (\partial E/\partial T)_V$$

and that at constant pressure:

$$C_p = (\partial H/\partial T)_p$$

Heat capacities generally can be represented by means of power series involving no more than three terms as it is shown in the following equation:

$$C_p = a + bT + cT^2$$

For geochemical purposes, the first two terms give sufficient accuracy and good estimates can often be obtained by considering $C_p = a$, i.e. C_p constant. Heat capacities are normally recorded in tables by listing values of the a, b, c constants, the measurements referring to 1 atm and a specified temperature range.

The heat capacity variation during a reaction may be obtained as the sum of the heat capacities of the products minus the sum of the heat capacities of the reactants.

$$\Delta C_p = \sum C_p(\text{products}) - \sum C_p(\text{reactants}) = \Delta a + \Delta bT + \Delta cT^2$$

When the enthalpy change in a reaction is known at one temperature, heat capacities can be used to calculate the change at other temperatures.

From $C_p = (\partial H/\partial T)_p$, the heat capacity change during a reaction may be expressed as $\Delta C_p = (\partial \Delta H/\partial T)_p$ and

the integration of this equation gives:

$$\Delta H = \int_{o}^{T} \Delta C_p dT = \Delta aT + (\Delta b/2)T^2 + (\Delta c/3)T^3 + \Delta H_o$$

H_o is the constant of integration and can be calculated from the known value of ΔH at one value of temperature. The change in ΔH with temperature is small for most reactions of geochemical interest amounting to only a few kilocalories even for T ranges of 1000 K and more. The variation in enthalpy with temperature is particularly small for solid-solid reactions, but may become important for reactions involving fluids.

1.4.5. Entropy

The measure of increase in randomness of a system is called entropy (48). It is a measure of the degree of disorder. Independant of the energy changes, natural processes proceed spontaneously from states of order towards states of disorder. This natural tendency towards disorder is a second factor, besides enthalpy, that makes chemical reactions to take place.

Unlike the internal energy and enthalpy for which absolute values cannot be measured, absolute values of entropies for substances and systems can be evaluated because the third law of thermodynamics states that the entropy of a perfectly ordered crystalline solid at the absolute zero of temperature is zero.

The quantity ΔS, the entropy change, is defined as the

amount of heat absorbed by the reaction (q) divided by the absolute temperature (T), at which the heat is absorbed

$\Delta S = q/T$ for large absorption of heat and $dS = dq/T$ for an infinitesimal absorption of heat.

It follows from the above equation that the entropy units are calories per degree; this is sometimes called the conventional entropy unit: E.U.

1.4.6. The Second Law of Thermodynamics

The first law of thermodynamics says that the total energy in a natural process remains constant, but this requirement is satisfied whether the process goes towards increasing order or increasing disorder. The second law adds the requirement that the direction must be towards disorder, as it states that natural processes always lead to an overall increase in entropy.

1.4.7. The Third Law of Thermodynamics

From the definition of heat capacity and entropy change, a relation between these thermodynamic properties can be obtained as follows:

$$C_p = dq/dT \text{ or } dTC_p = dq$$

and

$$dS = dq/T$$

thus

$$dS = C_p dT/T = C d(\ln T)$$

Integration gives

$$S_2 - S_1 = \int_{T_1}^{T_2} C_p d(\ln T)$$

This equation gives the increase in entropy for a substance as the temperature changes from T_1 to T_2. Since C_p can be expressed as a function of temperature (Section 1.4.4.), this integral can be evaluated in terms of temperature. This is normally done graphically by plotting C_p against the logarithm of the temperature. By extrapolating to absolute zero, accurate values for the increase in entropy can be obtained for a substance that is heated from absolute zero to any required temperature. Comparison of experimentally determined heat capacity curves for many substances permits the generalization: "Every substance has a finite positive entropy, but at the absolute zero of temperature, the entropy may become zero, and does become so in the case of a perfect crystalline substance." (46).

The third law provides means of obtaining absolute entropies for any substance at any temperature. For example, for a pure crystalline solid that undergoes no phase change between OK and TK, the investigator needs only measure heat capacities over this temperature range, plot C_p against the logarithm of the temperature and measure the area under the curve. Values of entropies so calculated are found in tables of thermodynamic data. From these, the standard entropy change for a reaction, ΔS^{o}, can be worked out by adding entropies of products and subtracting the sum of entropies of the reactants.

1.4.8. Free Energy

When making predictions about chemical reactions, the concept of free energy is more useful than the concepts of

enthalpy and entropy. A system not at equilibrium can move towards it by releasing energy. For a system at constant temperature (T) and pressure (P), the appropriate measure of energy is the Gibbs free energy (G), which is related to the heat content of the system (H) and the entropy S by the equation

$$G = H - TS$$

where T is the absolute temperature in Kelvin. An equation for the tendency to react can now be written as

$$\Delta G = \Delta H - T\Delta S$$

indicating that the difference between the free energy of a system in a state A and the free energy of the same system in another state B at the same temperature and pressure is an indicator of the tendency of the system to pass from the state A to B. If the system under consideration is a chemical reaction, the free energy change (ΔG) is a measure of the tendency of reactants to react to give the products.

Free energies are expressed in heat units, calories and kilocalories or Joules. The sign convention is the same as for enthalpy, i.e., negative values of free energies mean energy evolved during the reaction and positive values indicate energy taken up by the reaction.

The free energy change applied to the formation of 1 mole of a compound from its elements gives rise to the concept of free energies of formation. These energies of formation are important because, as heats of formation, they can be added and subtracted to estimate the free energy

change of chemical reactions. Unless other conditions are specified, the free energy of formation for a compound refers to a reaction between its elements at 25°C and 1 atm pressure. It is also assumed that the reactants are in their most stable form under these condtions, i.e., in their standard states (T = 298.15K and p = 1 atm). Under these circumstances, free energies of formation are called standard free energies of formation, G^{o}. Values of these energies are given in standard references (47, 24).

The standard free energies of formation of the stable configuration of an element in its standard state is zero by convention. It is a universal convention. Another convention needed to calculate the free energy of ions is that the hydrogen ion at unit activity has zero free energy of formation.

Unlike enthalpies, free energy changes can be used as a criterium of equilibrium. A reaction will take place spontaneously if the value of the free energy change is negative. The reverse reaction will proceed if the free energy change is positive. If the free energy change is zero, the reaction is at equilibrium.

Closely related to free energy is the quantity called the chemical potential (μ), which is defined by the equation

$$\mu_1 = (G/ n_1)_{T,P}$$

Here the subscript i refers to a particular component in the system and n stands for the number of moles of that component in the system. The chemical potential is thus the amount, per

mole, by which G of the system changes with the addition of an infinitesimal amount of a particular component. The Gibbs free energy is an extensive property, but chemical potential is an intensive one. In a system with two or more phases coexisting at equilibrium, the chemical potential of all the components in the system must be identical in each phase. In other words, in a system at equilibrium, the chemical potential of each component is the same in all phases.

1.4.8.1. The Free Energy and the Equilibrium Constant

For a chemical reaction in which b moles of B react with d moles of D to produce y moles of Y and z moles of Z

$$bB + dD = yY + zZ$$

The equilibrium constant K is given in terms of the activities of the reactants and products as:

$$K = \frac{a_Y{}^y \cdot a_Z{}^z}{a_B{}^b \cdot a_D{}^d}$$

when all the substances present are at unit activity (i.e., 1M for substances in solution, 1 atm pressure for gases, and solids and liquids considered as pure compounds). This equilibrium constant is related to the free energy change of the reaction by the equation

$$\Delta G^o = - RT \ln K$$

The free energy change of the reaction under these conditions is termed standard free energy change. For activities other

than unity, the following equation holds:

$$\Delta G = \Delta G^{o} + RT \ln \frac{A_Y^{y} \cdot A_Z^{z}}{A_B^{b} \cdot A_D^{d}}$$

The importance of the foregoing equation lies in the fact that an equilibrium constant can be calculated from the free energies of formation of the reactants and products.

1.4.9. The Van't-Hoff Equation

The Van't-Hoff equation:

$$\frac{d\ln K}{dT} = \frac{H}{RT^2}$$

is a relation between the equilibrium constant and temperature, which permits a quantitative estimation of the variation of the equilibrium constant as the temperature varies. However, its application requires knowledge of the dependence of H on temperature. This information may be available in the form of heat capacity data (Section 1.4.4.).

In the absence of the heat capacity data, H may be assumed constant. If this is the case, integration of the Van't-Hoff equation and conversion of natural logarithm into decimal logarithm leads to the following equation:

$$\text{Log } K = \frac{-\Delta H}{2.303RT} + C$$

A plot of log K against T^{-1} is a straight line with slope $-\Delta AH/2.303R$. Thus given a set of values for the equilibrium constant for a reaction, the enthalpy change of the reaction can be computed. Also if the enthalpy change of the reaction is known, the Van't-Hoff equation can be integrated, assuming that ΔH is independant of temperature, between T_1 and T_2 to obtain the expression

$$\log K_2/K_1 = \frac{\Delta H \ (T_2 - T_1)}{2.303R \ (T_2 \ T_1)}$$

that allows the calculation of the equilibrium constant at some temperature other than that at which it was measured.

1.4.10. Activity and Fugacity

It has been pointed out previously (Section 1.4.8.) that the chemical potential is a quantity closely related to the free energy. There are two more quantities directly related to G, namely activity and fugacity, whose definitions are given in this section.

Fugacity, f, is often used in connection with gases and can be thought of as an idealized pressure. Activity (a) on the other hand, is used in connection with liquids and solids, usually in solution, and can be thought of as an idealized concentration. They are defined by the following equations:

$$\mu_i = \mu_i^{\circ} + RT \ln (a_i/a_i^{\circ})$$
$$\mu_i = \mu_i^{\circ} + RT \ln (f_i/f_i^{\circ})$$

where μ_i^o is a constant, the chemical potential of component "i" in its standard state, R is the gas constant, and T is the temperature on the Kelvin scale. The other two constants, a_i^o and f_i^o, are the activity and fugacity of the component "i" in its standard state. These are always taken, by convention, to be unity. It follows that activity and fugacity are defined by the equations

$$\mu_i = \mu_i^o + RT \ln a_i$$
$$\mu_i = \mu_i^o + RT \ln f_i$$

Several different conventions are used to define standard states (49, 50), and the choice of a particular convention is determined by convenience for solving a particular problem rather , than by any theoretical considerations. For solid solutions, solutions of two miscible liquids and for the solvent in a solution of a solid in a liquid, the standard state is commonly taken to be the pure substance at the same temperature and pressure as the solution of interest. Thus for aqueous solution, $\mu H_2O = \mu^o_{H_2O}$ and $a_{H_2O} = 1$ in pure water. For solutes in aqueous solutions, the pure solute is not a convenient standard state, and the most commonly used approach is the infinite dilution convention. According to this convention, the activity of a solute approaches its molal concentration m_i, as the concentration of dissolved species approaches zero.

$$a_i \rightarrow m_i \quad \text{as} \quad \sum m_i \rightarrow 0$$

An activity coefficient γ is defined by the equation

$\gamma = a_i/m_i$ and hence

$$\gamma \rightarrow 1 \quad \text{as} \quad \sum m_i \rightarrow 0$$

Under this convention, the standard state is a hypothetical ideal 1 m solution. An ideal solution in this context is one in which activities are equal to concentrations. For gases, the fugacity approaches the partial pressure as the total pressure on the gas approaches zero. In an ideal solution, there are no interactions between solute and solvent, or between charged species present in the solution, whereas in real solutions, such interactions are always present. As a result of this, the free energy of a real solution is different from that of an ideal solution. The relationship between free energy and activity is also different, since activities of both solute and solvent are different from their concentrations.

The activity coefficient, γ, of an uncharged species such as dissolved carbon dioxide is near unity in dilute solutions and usually rises above unity in concentrated solutions.

1.4.11. Aqueous Solutions of Electrolytes

The state of an electrolyte dissolved in water depends on the nature of the solute, the concentration of the solution as well as the presence or absence of other chemical species. Some electrolytes (e.g., NaCl, $CaCl_2$, HNO_3) are almost completely ionised, whereas others are very incompletely ionised (H_2CO_3, $HgCl_2$). Yet others are believed to form "ion pairs" at high concentration [e.g., $MgSO_4$, $Ca(NO_3)_2$]. As the concentration increases, the

formation of ion pairs (e.g., $CaNO_3^+$), or complex ions (e.g., $HgCl_4^{-2}$) increases. As the concentration decreases, the species present tend towards simple hydrated ions [$Ca(H_2O)_8^{+2}$, $Al(H_2O)_6^{+3}$].

1.4.12. Activities of Ionic Species

In solutions of electrolytes, electroneutrality imposes the condition that the number of moles of individual ions cannot be varied independently. Thus, in a system in which NaCl and H_2O are the components, the number of moles of solute and solvent can be varied independently. However, the concentration of Na^+ and Cl^- depends on the number of moles of NaCl but their concentrations are not independent variables (51). For the two components NaCl and H_2O, it is possible to measure their chemical potentials, free energies and activities by the application of thermodynamics alone. This is not possible for individual ionic species, and a number of thermodynamic developments are expressed in terms of hypothetical ionic activities knowing that only certain ionic activity products, or ratios, have physical significance.

If an electrolyte $C_{\nu_+}A_{\nu_-}$, dissociates into ν_+ cations and ν_- anions according to

$$C_{\nu_+}A_{\nu_-} = \nu_+ C + \nu_- A$$

then its activity may be written

$$a_+^{\nu_+} \cdot a_-^{\nu_-} = a_{+/-}^{\nu}$$

where $\nu = \nu_+ + \nu_-$, a_+ and a_- are the individual activities of the ionic species and $a_{+/-}$ is the so termed mean activity of the ions. Inclusion of $a_{+/-}$ in the definition of the chemical potential (and partial molal free energy) of an electrolyte component of a solution leads to the following equation:

$$\mu - \mu_o = \nu . R . T . \ln(a_{+/-})$$

which is an expression of the chemical potential of the ions in terms of their mean activities.

Like non electrolytic solutions, electrolytic solutions deviate also from ideal solutions and their deviation is greater, due to interactions of ions with each other and with the solvent, as well as ion association and changes in the dielectric constant of the solvent with the concentration of the solution.

Deviations from ideality are expressed in terms of the mean ionic activity coefficient, $\gamma_{+/-}$, which is defined as the ratio between the mean ion activity and the mean molality.

$$\gamma_{+/-} = \frac{a_{+/-}}{m_{+/-}}$$

$\gamma_{+/-}$ approaches unity when the solution approaches infinite dilution.

Although individual ion activity coefficients cannot be measured directly, the mean ionic activity coefficients

can be obtained experimentally and values for a wide range of concentrations are available (see References 41, 52, 51). From these measured mean ionic activity coefficients, it is possible to obtain values for individual activity coefficients with the aid of some assumptions.

One such assumption is that γ_+, and γ_-, the individual ionic activity coefficients for a standard electrolyte are equal over the ionic strength range of interest. Potassium chloride has been used as such a standard electrolyte for obtaining individual ion activity coefficients, assuming that $\gamma_{K^+} = \gamma_{Cl^-}$ for all possible concentrations in a pure solution. This suggestion is due to MacInnes, is often called "the MacInnes Assumption", (53) and can be expressed as follows:

$$\gamma_{+/-KCl} = [(\gamma_{K^+})(\gamma_{Cl^-})]^{1/2} = \gamma_{K^+} = \gamma_{Cl^-}$$

This relationship allows the investigator to calculate values for other ions knowing the appropriate mean ion activity coefficients. Thus, for a monovalent chloride

$$\gamma_{+/-MCl} = [(\gamma_{M^+})(\gamma_{Cl^-})]^{1/2} = [(\gamma_{M^+})(\gamma_{+/-KCl})]^{1/2}$$

and $$\gamma_{M^+} = \frac{\gamma^2_{+/-MCl}}{\gamma_{+/-KCl}}$$

for a divalent chloride

$$\gamma_{M^{+2}} = \frac{\gamma^3_{+/-MCl_2}}{\gamma_{+/-KCl}}$$

The same approximation can be applied to calculate individual activity coefficients of ions of different chlorides as an example

$$\gamma_{SO_4^{-2}} = \frac{\gamma^3_{+/-K_2SO_4}}{\gamma^2_{+/-KCl}}$$

and for a salt like $CuSO_4$, a double bridge can be used to calculate $\gamma_{Cu^{+2}}$

$$\gamma_{Cu^{+2}} = \frac{\gamma^2_{+/-CuSO_4}\gamma^2_{+/-KCl}}{\gamma^3_{+/-K_2SO_4}}$$

Calculation of individual ionic activity coefficients from the mean activity coefficients is known as the mean salt method.

1.4.13. The Debye-Hückel Theory

This is a model that allows activity coefficients for individual ions to be calculated, taking into account the effect that ionic interactions should have on the free energy. In a solution, positive ions tend to be surrounded by negative ions and negative ions by positive ions. Assuming that ions are point charges, the interactions are merely electrostatic and the ions around any particular ion follow a Boltzmann distribution. From this assumption, the following equation is derived:

$$\log \gamma_i = -AZ_i^2\sqrt{I}$$

where A is a constant depending only on pressure and temperature, Z_i is the charge of a particular ion and $I = 1/2\ m_i Z_i^2$, is the ionic strength of the solution. In the latter expression, m_i is the molality of the solution. The previous equation holds only for very dilute solutions (less than 10^{-4} mol dm^{-3}) (51). It is usually used as a method of extrapolating to infinite dilution.

At higher concentrations, the model fails and the equation should be modified to take into account the finite size of the ions, giving the equation:

$$\log \gamma_i = \frac{-AZ_i^2\sqrt{I}}{1+Ba_o\sqrt{I}}$$

where B is a constant, depending only on temperature and pressure, and a_o is the hydrated radius of the particular ion. Values of constants for use in the Debye-Hückel equation are tabulated in text books (see Reference 47). A further term has been added to the equation (54), which is justified both on theoretical and on the empirical grounds so that it improves the fit to the experimental data. An important consequence of this addition is that it predicts that activity coefficients should increase with increasing ionic strength at high concentrations, in accordance with experimental observations. According to Garrels (47), the better method for obtaining individual ion activities of ions in solutions of ionic strength higher than 0.05 is the mean salt method. Below this value, the mean salt method and the Debye-Hückel equation produce results that agree fairly well.

Although not well defined thermodynamically, individual ionic activity coefficients are important in the geochemical field, particularly to calculate solubilities of substances in various aqueous environments.

1.4.14. Thermodynamic Data

In the study of chemical reactions taking place in geological environments, two factors of predominant importance are the free energy of the reaction and the rate of the reation. Since the present investigation is not directly concerned with the rate of reaction, nothing will be said about the applicability of thermodynamic data to this field. However, the methods of estimating the thermodynamic data required to calculate the equilibrium constants needed to interpret weathering reactions will be summarised.

1.4.15. Free Energy Changes of Reactions

Several general methods are available to estimate the free energy changes accompanying reactions (41, 55). As the free energy is a thermodynamic property, it does not depend on the pathway followed by the reaction so it can be calculated by adding and subtracting the known free energies for suitable reactions, which lead to the desired product (41). From experimental studies of reactions at equilibrium, it is possible to calculate an equilibrium constant, which in turn permits calculation of the free energy of the reaction. This method is seldom applied to geological systems (55). Free energies can also be measured from electromotive force measurements (41, 55). It can be calculated from thermal data, enthalpies and entropies too (41, 55). Many free energy changes, particularly for gaseous reactions can be obtained

from spectroscopic data (41). An empirical method calculating the Gibbs free energies of reactions for compounds with composition intermediate between two components A and B, using families of compounds, has been proposed by Tardy (56).

1.4.16. Entropy

Of the greatest importance is the method of estimating entropies based upon low temperature heat capacity data, which is intimately connected to the third law of thermodynamics. A good discussion of this method is given by Kelly (55). Entropies of gaseous substances are calculated from spectroscopic data and from translational, rotational, vibrational, and electronic entropies (55), and finally, if the heat of reaction and the free energy for a reaction are known, the entropy can be calculated.

1.4.17. Free Energy of Formation of Individual Ions

Although it is not possible to measure the free energy of formation of an individual ion, for the purpose of tabulation and calculations, it is possible to separate the free energy of formation of an aqueous solute in two or more parts corresponding to the number of ions formed, and compare the free energy of ions with the free energy of a particular ion taken as a standard. Hydrogen ion has been chosen as the standard, and its free energy of formation is then taken as zero by convention. The free energies of formation of ions from their elements obtained in this way are given in tables of chemical data (57). Free energies for aqueous ions have also been estimated, using an empirical parameter that can be correlated with the Gibbs free energies of formation of hydroxides and some types of silicates (58).

1.4.18. Entropies of Aqueous Ions

Like free energies of formation of individual ions, it is not possible to measure entropies for these species. However, relative entropies can be estimated in the same way as relative free energies were obtained, by defining the entropy of the hydrogen ion as zero (59, 60). The entropies of oxy-anions and complex ions can be calculated as a function of their charge and size (61-65). These equations can be used to estimate the unknown entropy if the size of the ion is known, or to select the most reliable value from a series of discrepant experimental results.

1.4.19. Thermodynamic Properties of Minerals

As with other chemical compounds, thermodynamic properties of minerals can be obtained experimentally or empirically. In either case, they are influenced by factors such as degree of crystallinity, solid solutions, impurities, polymorphism, metastable states, and the nature of the bonds present in the mineral under consideration. Experimental determinations are difficult and, in cases such as clay minerals, experimental determination of these properties is virtually impossible because no two clays have the same composition and the data must be measured anew for every sample. However, experimental data for several minerals have been obtained. Heats and free energies of formation of gibbsite, kaolinite, halloysite, and dickite have been measured by Barany and Kelley (66). Heat and free energy of formation for muscovite was measured by Barany (67). King and Weller (68) measured low-temperature heat capacities and entropies of diaspore, kaolinite, dickite, and halloysite. A summary of experimental determinations of low-temperature

heat capacities and entropies of sodium and potassium aluminium silicates is given by Kelly (69). Heats and free energies of formation of anhydrous silicates have been summarised by Kelley (70). The free energy of formation of kaolinite and plagioclase feldspars have also been calculated from solubility measurements (71, 72).

Where calorimetric data is lacking, some sort of empirical estimation must be used. This usually involves development of a mathematical equation, which under certain assumptions, allows the researcher to estimate free energies, enthalpies, and entropies of minerals in good agreement with the available experimental data. Several methods have been used for this purpose. However, none of them are valid for all minerals. Chen (73) has proposed a method to estimate standard free energies of formation of silicate minerals at room temperature. Assuming that clay minerals are formed by a combination of silicon hydroxide with metal hydroxides, Nriagu calculated Gibbs free energies of formation for these minerals (74). Under the assumption that each silicate can be represented by oxide and hydroxide components, which possess constant Gibbs free energies of formation within the structure of the silicates, Tardy and Garrels have estimated Gibbs free energies of formation for layer silicates (75). The same authors modified this method by correlating solution energies of compounds with the solution energies of their constituent oxides to calculate Gibbs free energies of formation of hydroxides, oxides and aqueous cations (58), and monovalent and bivalent metal silicates (76). They claim that the method can be applied to many types of minerals (58).

Two important summaries of thermodynamic properties of minerals are now available: the first one, published by Robie et al. (77), and the second one, published by Helgeson et al. (78). Data for this investigation was taken from the latter publication.

1.4.20. The Standard State for Minerals

As stated by Helgeson (78), the standard state for minerals and liquids is one of unit activity of the pure solid or liquid at any pressure and temperature. It follows that the activities of components that correspond to stoichiometric minerals and pure liquids are unity at all pressures and temperatures.

1.4.21. Aqueous Solutions at High Temperatures

The physical and chemical properties of water have been widely studied at room temperature. It has been also used as a solvent to study a large number of chemical systems and, thermodynamic properties such as entropies, enthalpies, energies of reaction, activities and activity coefficients, are well known for a large number of chemical species at temperatures below 100°C.

Due to the experimental difficulties of working at high pressures and temperatures, the physical chemistry and thermodynamics of aqueous solutions at high temperatures has been studied much less thoroughly. In 1966, Cobble (79) pointed out some of the difficulties in working with water solutions at high temperatures and defined various temperature regions as follows: low temperatures between

0-60°C, moderate temperatures between 60-100°C, and high temperatures between 100-374°C. 374°C corresponds to the critical point. Temperatures above this point belong to the supercritical region. Temperatures between 364 and 384°C are regarded as belonging to the critical region. As the interest in studying aqueous solutions at high temperatures increases, either for theoretical reasons or for commercial ones (particularly hydrothermal synthesis), more and more methods are proposed to calculate thermodynamic data in order to predict thermodynamic behaviour of chemical reaction at high temperatures. As with solutions at room temperature, thermodynamic properties of solutions at high temperature can be obtained from experiments or empirical calculation. It has been noted before that it is difficult to carry out experiments at high temperatures. Variations in the physical and chemical properties of the water with temperature, changes in composition of the solutions and solubilities of minerals are amongst the factors that complicate the situation. Considerations of this type plus the search of rapid methods of producing such information led Cobble and his coworkers to propose the "Integral Heat Method" to calculate partial molal heat capacities of electrolytes at infinite dilution (80). The method involves measurements of the integral heat of reaction at infinite dilution and several temperatures of a system, which includes the electrolyte under consideration. The method has been used for sodium chloride and barium chloride (80), sodium perrhenate and perrhenic acid (81), cesium iodide (82), gadolinium chloride (83) sodium sulphate and sulphuric acid (84) from 0 to 100°C.

As part of their work on thermodynamic properties at high temperatures, Ahluwalia and Cobble used heat capacities

to analyse free energy data in order to provide better thermodynamic data at high temperatures (85). The name of the third law potential was given to the method (86), which is particularly useful in providing accurate ionic entropies. Partial molal heat capacities for hydrochloric acid have also been calculated by this method from 0 to 100°C (85). In 1964, Criss and Cobble (87), reviewing the existing thermodynamic data that could be used to calculate entropies of ions in aqueous solutions between 25 and 200°C observed that the ionic entropies of all of the cations at higher temperatures, selecting a proper standard state at each temperature, are linearly related to the entropies of the cations at other temperatures (87), and proposed equations to predict unknown entropies of ionic species up to 200°C and beyond.

This correspondence principle has been extended to the calculation and prediction of the heat capacities of electrolytes up to and above 200°C (88). Entropy values for sodium chloride solutions from 100 to 200°C, predicted by the correspondence principle, showed good agreement with experimental calorimetric determinations (89).

The temperature dependence of the thermodynamic properties for the dissociation of complexes in the range of 0-370°C has been described by Helgeson (90), in terms of functions involving the dielectric constant of water and a power series consistent with non-electrostatic interactions in the absence of a dielectric medium.

Helgeson (91) has presented a summary of thermodynamic data, which allows calculation of the solubilities of silicates, sulphides, sulphates, carbonates,

and oxides in hydrothermal solutions with high concentration of NaCl at elevated temperatures.

1.4.22. Composition, Phase and Activity Diagrams

These diagrams are used to describe the stability ranges of minerals and how these vary with environment.

1.4.22.1. Composition Diagrams

Mineral compositions can be represented by geometrical methods. These graphical devices are efficient in depicting and illustrating such information. A group of minerals can be described by reference to a number of chemical entities. The smallest number of these entities needed for such group of minerals is called the number of components needed to describe the group. Thus corundum (Al_2O_3), diaspore ($Al_2O_3.H_2O$) and Gibbsite ($Al_2O_3.3H_2O$) can be described by two components, Al_2O_3 and H_2O, and can be represented in a bar diagram, as shown in Fig. 3A. Andalusite ($Al_2Si_2O_5$), corundum (Al_2O_3), diaspore ($Al_2O_3.H_2O$), gibbsite ($Al_2O_3 . 3H_2O$), quartz (SiO_2), pyrophyllite [$Al_2Si_4O_{10}(OH)_2$] and Kaolinite ($H_4Al_2Si_2O_9$) can be described by three components: Al_2O_3, SiO_2, and H_2O, and represented in a triangular diagram (Fig. 3B). If the group of minerals needs more than three components, then the composition diagram needs more than two dimensions. Such diagrams are usually projected onto a two dimensional triangular diagram from one of the corners or edges of the multidimensional solid, which is the full representation. For example, kaolinite, pyrophyllite, muscovite, and quartz can be described by four components: Al_2O_3, SiO_2, K_2O, and H_2O, and represented in a triangular diagram by writing the

Fig. 3: Composition diagrams.

A: Bar diagram showing the composition of the minerals in the system Al_2O_3-H_2O.

B: Triangular diagram showing the composition of some of the minerals of the system Al_2O_3-SiO_2-H_2O.

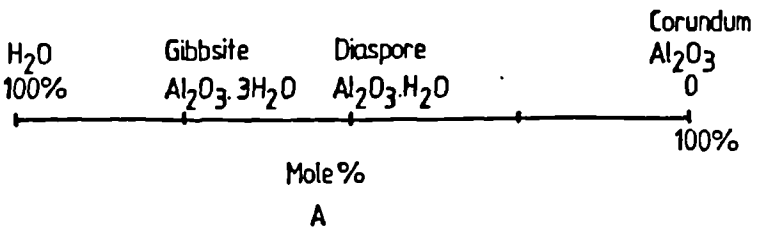

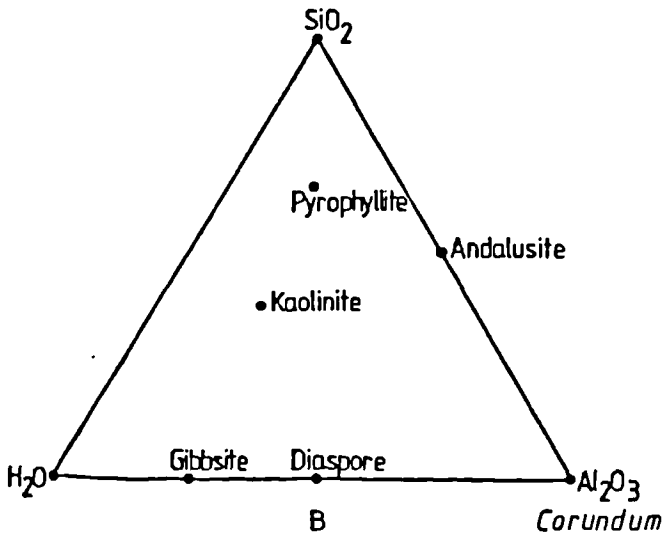

mineral formulae in terms of these oxides, eliminating water, and calculating the percentage of oxides on this water free basis (22). This is equivalent to projection from the apex of the tetrahedron (Al_2O_3, SiO_2, K_2O, and H_2O), which represents water.

1.4.22.2. Phase Diagrams

These are pressure and temperature graphs, showing the pressure and temperature regions, in which one particular equilibrium assemblage is stable. They are also known as equilibrium diagrams. A typical phase diagram is shown in Fig 4. It represents the upper stability limit for the reaction kaolinite and quartz to give pyrophyllite, line 1, and the upper limit of pyrophyllite to give kyanite, quartz and water, line 2 (see References 92 and 93).

The areas in a phase diagram each represent the range of temperatures and pressures over which one composition diagram is valid, the lines dividing off one such range from another, which requires a different composition diagram.

Phase diagrams assume that all the phases have a constant composition or that any variation in the composition is of no interest to the user. Such systems are "closed". If variations in composition are of interest, activity diagrams are needed.

1.4.22.3. Close and Open Systems

Phase diagrams represent systems in which the total chemical composition remains constant, but the composition of

Fig. 4: Phase diagram showing the stability of pyrophyllite.- [After Velde (92) and Kerrick (93)].

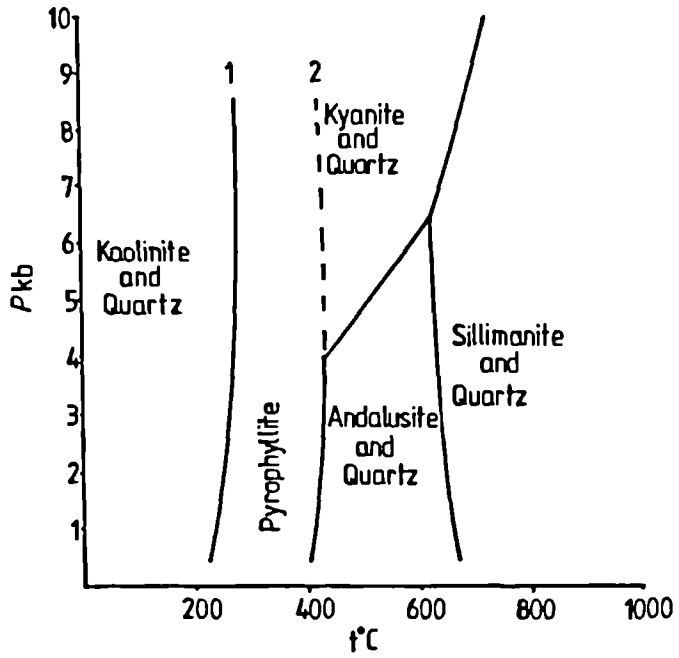

each of the constituent phases can vary, provided that some other phase within the system changes its composition to compensate for such variations. Therefore, they apply to closed systems where there is no exchange of matter with the external environment.

If the system exchanges matter with the external environment, as happens during weathering, such changes are reflected in the concentration of the mobile species [i.e., K^+, Ca^{+2}, H_4SiO_4] in the fluid phase and the system is open. Open systems can be represented by activity diagrams. Both phase and activity diagrams assume equilibrium.

1.4.22.4. Activity Diagrams

These are graphs of the activities of the mobile components (i.e., the components whose concentration vary in the variable phase), showing regions of activity corresponding to one particular composition diagram at a specified temperature and pressure. Thus the areas of an activity diagram correspond to the areas of the phase diagram in concept but show the effect of the activity of the mobile components rather than the effect of temperature and pressure. Using the available thermodynamic data, it is possible to develop qualitative diagrams that are useful to provide a graphic summary of the mineral sequences that might be expected when equilibrium is achieved. The relations between kaolinite and gibbsite have been taken from Garrels (47) as an example of an activity diagram. Assuming equilibrium between kaolinite, gibbsite, dissolved silica and water, the following reaction can be written:

Fig. 5: The solubility of gibbsite at various hydrogen ion concentrations.- [After Garrels and Christ (47)].

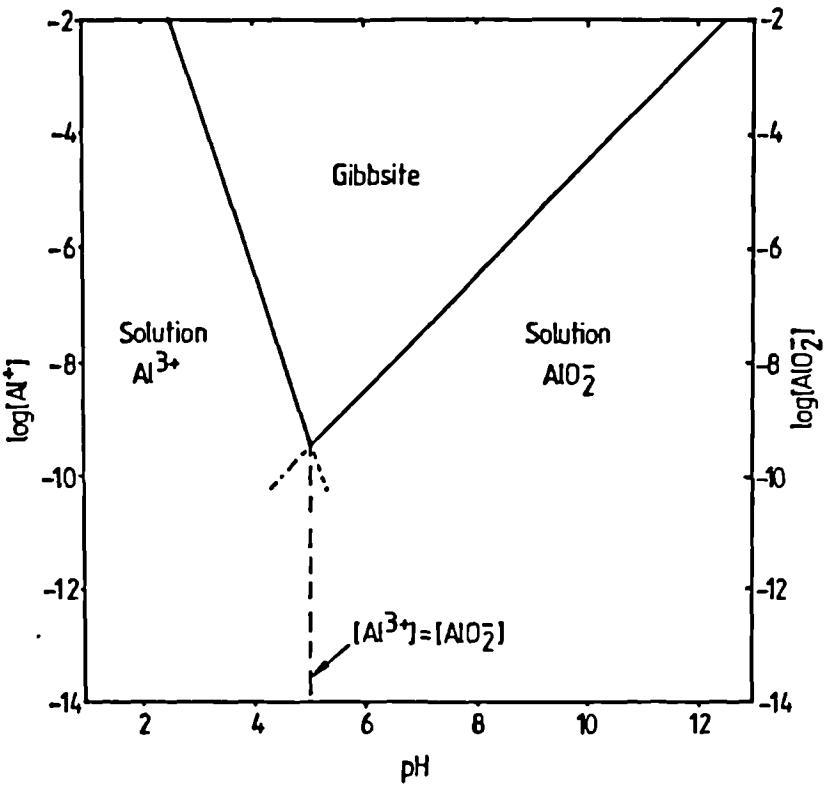

$$H_4Al_2Si_2O_9 + 5H_2O = Al_2O_3.3H_2O + 2H_4SiO_4$$

Kaolinite Gibbsite

and the equilibrium constant for this reaction is a function of the concentration of dissolved silicic acid.

$$[H_4SiO_4]^2 = K$$

The free energy of the above reaction obtained by using the data given in Reference 47 is 12.7 Kcal. From the equation relating free energies of reactions and equilibrium constants (Section 1.4.8.1.), the equilibrium constant of this reaction is:

$$K^{1/2} = [H_4SiO_4] = 10^{-4.7}$$

This means that equilibrium between gibbsite and kaolinite is attained at a fixed value of the concentration of silicic acid. Below this value, kaolinite tends to dissolve to give gibbsite and release silica in solution. Assuming also that gibbsite is in equilibrium with water, it is in equilibrium with its various dissociation products, i.e.:

$$Al_2O_3.3H_2O + 6H^+ = 2Al^{+3} + 6H_2O$$
$$Al_2O_3.3H_2O = 2H^+ + 2AlO_2^- + 2H_2O$$

Equilibrium constants for these equations can be calculated as before in the first case

$$K^{1/2} = \frac{[Al^{+3}]}{[H^+]^3}$$

and $1/2\log (K) = 5.7 = \log[Al^{+3}] + 3pH$.

In a like manner, for the second reaction

$$K^{1/2} = [H^+]\ [AlO_2^-]$$

and $1/2\log (K) = -14.6 = \log[AlO_2^-] - pH$.

Fig. 5 is a plot of the logarithmic form of the last two equilibrium constants in terms of concentration of $[Al^{+3}]$ $[AlO_2^-]$ and pH to show the stability field of gibbsite. The relations presented in Fig. 5 illustrate the behaviour of gibbsite: in acid media it dissolves to give aluminium ions, and in alkaline media it dissolves to give aluminate ions.

1.5. X-Ray Techniques

1.5.1. Generation and Characteristics of X-Rays

X-rays are generated when accelerated electrons collide with the atoms of a metal target in an X-ray tube (94). Broadly speaking, two kinds of interaction take place when an electron beam hits a target and this results in two types of X-ray spectra, namely: continuous spectra or Bremsstrahlung and discrete spectra, which are characteristic of the metal target.

When electrons hit the target anode, the impinging electrons collide with the electrons of the target material, and energy is transferred to the target electrons through this process.

Normally, electrons undergo successive collisions to transfer their energy. The excited target electrons emit photons to deexcite, producing thus a continuous or white spectrum. A plot of intensity against wavelength is a smooth curve, which begins abruptly at a short wavelength limit, rises to a maximum, and extends towards infinity. Transference of the total impinging electron energy in a single collision gives rise to the wavelength limit. Since this probability is low, the intensity at this minimum wavelength is small.

If the accelerating voltage is raised to a critical level, which is characteristic of the element of the target, the discrete spectra are produced. These spectra appear superimposed on the smooth curve in groups of peaks, which are known as K, L, M, and N series.

Characteristic radiation is emitted when the bombarding electrons have sufficient energy to remove one or more electrons from the innermost shells of the target atom. The atom then becomes unstable, due to loss of the electrons. To achieve stability, electrons from higher orbitals fill the vacancies, creating new vacancies in the higher orbitals, but of lesser degree of instability. This process continues with successive transitions between orbitals to minimise the instability. During this process, electrons undergoing transitions release energy as photons of X-ray radiation.

Electrons can be removed from the K, L, M, or N shells. If the electron removed is from the K shell, the vacancy may be filled by electrons falling from the L, M, or N shell or from outer shells. The greater probability is, however, that the vacancy be filled by electrons from the L

shell rather than from an outer one. This gives rise to a series of lines known as the K series. The line is known as $K\alpha$, if the electron comes from the L shell, $K\beta$ if it comes from the M shell, $K\gamma$ if it is an N electron and so forth. The intensity of these lines decreases from $K\alpha$ to $K\gamma$.

Similar processes, although more complex, bring about the L, M, and N series. Since the energy of the lines depends upon the energy difference between the states involved in the transition, which in turn varies from element to element, the discrete X-ray spectra are a characteristic property of each element. This is the basis of qualitative and quantitative X-ray spectrometry. For a wider view of X-rays, see References 94-96.

1.5.2. X-Ray Fluorescence

Exposure of a substance to a primary X-ray beam, produced by electron bombardment (see Section 1.5.1.) or coming from a suitable radioactive source (97) generates a secondary beam of X-rays by a fluorescent process. X-ray fluorescence deals with the production of secondary X-rays from a sample and its characterization to give qualitative and quantitative identification of the analyte. As in most X-ray methods used for analysis, X-ray fluorescence makes use of the well known relationship condensed in Bragg's Law: $n\lambda = 2d \cdot \sin(\Theta)$. where λ is the wavelength of the X-rays, d is the interplanar spacing and Θ is the incidence angle. Indeed, the technique usually relies on the use of a crystal of known d spacing to diffract different wavelengths, which in turn allow measurement of the intensity belonging to specific wavelengths.

In X-ray fluorescence analysis, each sample is exposed to a primary X-ray beam, which causes secondary fluorescent X-ray radiation from each of the elements present. The secondary radiation is then diffracted by a crystal diffraction grating and collected in a counter. The emitted X-ray spectrum is scanned by varying the angle of the crystal and the counter with reference to the incident beam. This brings about peaks at various values of Θ which in turn identifies the emitting element, because each element produces a particular wavelength.

The normal method of operation is to measure the intensities of these peaks for a series of standards of known concentration and construct a calibration graph. Concentrations of elements in samples can then be worked out from this standard graph. Qualitative X-ray fluorescence, broadly speaking, means the recognition of the elements present in a sample by the identification of the peaks present in the spectrum. Quantitative X-ray fluorescence analysis, on the other hand, is a more complex problem bacause it has to include corrections for interelement absorption, and matrix effects.

1.5.3. Diffraction of X-Rays

As with other types of electromagnetic radiation, interaction of X-rays with the electrons of the matter through which it passes leads to scattering. In an ordered environment, as in a crystal, destructive and constructive interference takes place. In certain specific directions, diffraction is the result. Two conditions must be fulfilled in order to obtain diffraction, namely: the waves emitted by all atoms present in a single plane must be in phase and the

scattering of waves by successive planes must also be in phase (98). The first condition is satisfied when the incident beam, the diffracted beam and the normal to the reflecting surface lie in the same plane, and the angle of incidence is equal to the angle of reflection. The second condition is fulfilled when the difference in the path length of two rays is equal to an integer number of wavelengths.

1.5.4. Powder Diffractometry

This is a member of the family of the so-called X-ray diffraction methods, which are based on calculations originating directly from the Bragg equation. These calculations allow identification of minerals and calculation of the structure of chemical compounds. The latter is considered as a chemical application and, by far the major geological use of the method is in the identification of minerals. This application is based upon the fact that each mineral shows a unique X-ray pattern. So, by matching exactly the X-ray pattern of an unknown and an authentic sample, chemical identity can be assumed. In addition, less successfully, as it will be shown, the method can be used for the semi-quantitative analysis of mineral mixtures. The identification of the minerals involves considerations about position of the lines in terms of the reflection angle and their relative intensities. Since the diffraction angle is determined by a particular group of planes in the single mineral, the distances between these planes, for a specific mineral, can be worked out from the Bragg equation, knowing the wavelength of the incident X-rays and the measured angle. The intensities of the lines depend on the number and kind of atomic reflection centres present in each set of planes. Tables giving d spacings and relative intensities are easily

available from mineral indexes published by international institutions (99, 100). Thus, once the d spacings are calculated, the identification of the unknown can be obtained from comparison of the experimentally obtained data with those in the tables.

1.5.4.1. Instrumentation

Three basic parts are necessary for X-ray powder diffraction analysis (98): a source of X-ray radiation "A", the diffractometer "B", and the detection and counting system "C" (see Fig. 6).

The source of X-ray radiation comprises the generator and an X-ray tube, and its function is to provide a stable source of radiation required to irradiate the sample. As is shown in Fig. 7, a filtered monochromatic beam passes through a line source "M", and a collimator system "B". It is then diffracted by the sample "S" and passes through a receiving slit "D", and a second collimator "C" into the detector. The specimen is a powder sample exposed at an angle to the incident beam. The angle is mechanically adjustable by gears. The counting and collecting slits are mounted along with the sample in such a way that any adjustment of Θ will move the collecting slit and the counter by an angle of 2Θ (101).

The detector converts the X-ray photons into voltage pulses. These pulses are then amplified and sorted out by a pulse height selector and finally counted. From here, the signal passes to either a chart recorder or a visual display. In X-ray diffraction, like in X-ray fluorescence, proportional gas counters or scintillation counters are used.

Fig. 6: Schematic representation of an X-ray diffractometer.

A: The source of X-ray radiation.

B: The diffractometer.

C: The detection and counting system.

[After Allman and Lawrence (101)]

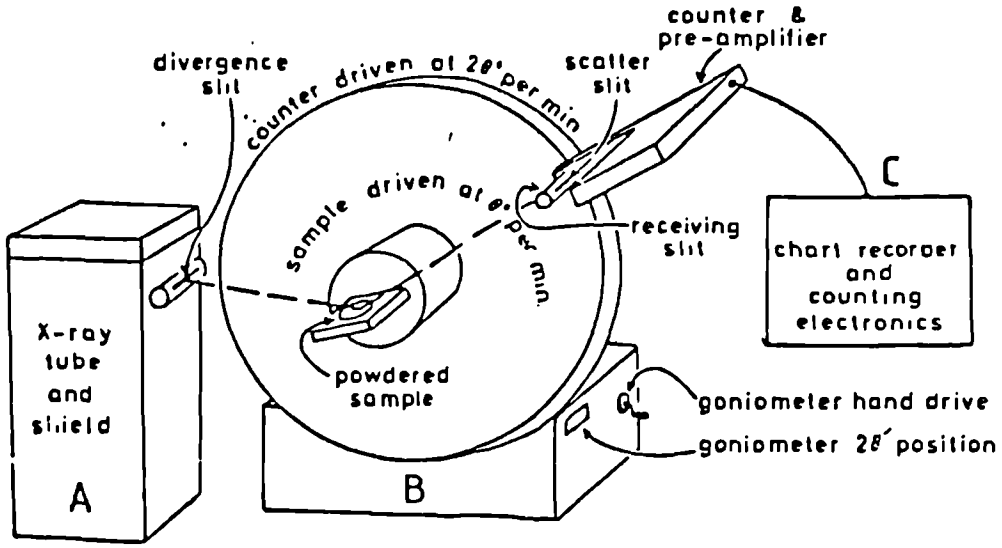

Fig. 7: Geometry of the Diffractometer.-

[After Jenkins and De Vries (98)].

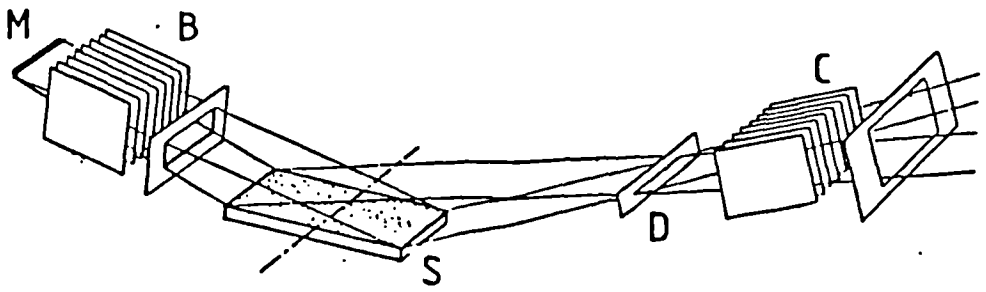

1.5.5. Factors Affecting X-Ray Fluorescence and X-Ray Diffraction Results

As in any other analytical technique, X-ray fluorescence and X-ray diffraction results are affected by the characteristics of the instrument and the analyst's skill. It is not the purpose of this section to discuss every possible error in these two techniques, but to point out the most common errors and how they affect the results. With regard to X-ray diffraction, only errors related to powder X-ray diffraction will be dealt with.

1.5.6. Errors in X-Ray Powder Diffraction Analysis

1.5.6.1. Instrumental Errors

According to Zussman (96), a small error [$\sim 0.01^{\circ}$ (2Θ)] in the position of the peaks is introduced, due to the use of a flat specimen instead of a curved sample. This error is proportional to $\cos^2(\Theta)$ and thus, it tends to zero as Θ approaches 90°.

Both absorption and fluorescence phenomena may be present in X-ray diffraction analysis and can cause pseudodoublets and high background (102).

Since the counting and recording of the photons are not simultaneous processes, the fraction of time elapsed between them introduces a constant error in 2Θ, the magnitude of which depends upon the time constant selected.

The wrong setting of the zero position in the goniometer will also introduce a constant error in the 2Θ

angle. The magnitude of both rate-meter error and zero-angle error in the calculation of d spacings is proportional to cot(Θ). Thus it tends to zero as the angle approaches 90°. The above-mentioned errors are usually small in a well designed instrument and are compensated by using suitable standards.

1.5.6.2. Specimen-Preparation Errors

Homogeneity over the range of less than 1 um, constant particle size of between 1 and 50 um, and no preferred orientation are the characteristics of an ideal sample for powder diffraction analysis. However, in practice, a sample with these characteristics is not easily prepared and some problems arise when the sample does not fulfill the above requirements.

Since the actual volume of powder used in a specimen and the penetration of the X-rays into the sample are rather small, care must be taken during the sample preparation to ensure a homogeneous and representative sample. Since only crystallites, whose reflection planes are parallel to the specimen surface give diffracted intensities, if the number of crystallites is small, there may not be a random distribution and an error in the measured intensities is the result. This error can be as much as 5-10% of the peak height (98). Sample spinning provides a larger effective surface and, thus reduces the chance of non-random orientation. Preferred orientation is an extreme case of non-random distribution and sample spinning will do little to overcome it. The best solution lies in fine grinding and careful sample preparation. Sedimentation techniques and aerosols have been used in specimen preparation in order to avoid

preferred orientation (103, 104).

Although it is not possible to separate errors affecting the identification of minerals, i.e., errors in qualitative X-ray diffraction analysis, from errors affecting the quantitative determination of the minerals, as most of them are common for both analyses, the extent to which some errors affect the two kinds of results justifies talking about errors in quantitative analysis. Quantitative results are affected by background effects that contribute to scattering and diffraction at angles other than the discrete Bragg reflections produced by the radiation employed. Some of these factors are structural defects, general radiation when unfiltered radiation is used, air scatter, secondary fluorescence radiation, absorption, and spurious lines. Spurious lines in turn are due to misalignment of the instrument, diffraction effects from the sample and radiation contaminants (103), variations in the crystal structure of the analyte minerals, due to order-disorder phenomena and solid solution (see References 105, 106 and 107, for details about order-disorder in feldspar), or overlapping peaks, whose height varies with the concentration of two or more components.

1.5.7. Errors in Quantitative X-Ray Fluorescence Analysis

Quantitative X-ray fluorescence analysis requires identification and correction of interference effects (usually matrix effects) and modification of sample through preparation processes such as dissolution, fusion and compression of pellets, and it is important to realize what problems are likely to arise during the analysis.

Errors can be caused by counting statistics, instrumental errors, i.e., wrong excitation conditions or tube type, operator errors, for instance, in preparation of the samples and standards, and influence of the matrix in the intensity we are measuring, i.e., absorption which depends upon the physical state of the sample. Absorption and surface effects are a result of non-similarity between the sample and standards.

1.5.7.1. Absorption and Enhancement Effects

These effects arise from matrix components either increasing or decreasing the measured intensity of an analyte line in a way that is different from the standards.

Absorption effects can be of two types, depending on the matrix composition. Since it is the intensity of the tube spectrum on the short wavelength side of the analyte absorption edge, which produces the analyte excitation, if other elements exist in relatively high concentrations in the sample and can absorb the tube radiation from this part of the spectrum, the effective excitation intensity experienced by the analyte is reduced. The analyte fluorescent intensity is then reduced. On the other hand, the matrix components, which have absorption edge wavelengths on the long wavelength side of the fluorescent analyte line, can absorb the analyte radiation emitted by the element of interest, and again the measured intensity of the analyte is reduced.

Enhancement of the analyte signal occurs when in the matrix one of the components present emits X-ray radiation to the short wavelength side of the analyte absorption edge because the fluorescence radiation of this matrix component

can cause excitation in addition to the analyte excitation by the X-ray tube.

Surface effects or physical interferences are due to particle size and surface variations between the sample and the standards because the scattering and absorption of primary X-rays are different, and different relative intensities are produced.

In order to minimise absorption-enhancement and physical effects, these effects must be kept the same for sample and standards.

CHAPTER II

E X P E R I M E N T A L

Major and trace element analysis was carried out using a Philips PW 1450/70 automatic X-ray fluorescence spectrometer equiped with a 60 position sample changer and a microcomputer for data processing. The major elements were analysed from fused glass discs prepared according to the method of Harvey et al. (108), which is described in Section 2.3.

2.1. Preparation of Samples for Analysis

The samples taken from localities described in Sections 4.1. and 4.2. were split into two halves: one half was kept as a reference and the other was used for analysis.

Before crushing, all weathered edges and previously exposed surfaces were removed, and the samples washed and dried. A fresh and representative part of the original rock was selected. Having done this, the samples were then handled with gloves so as to prevent any contamination, particularly of sodium, coming from sweaty hands.

2.2. Crushing the Samples

The steps followed in crushing the specimens are shown in Fig. 8. The cube shaped specimens were passed through the jaw crusher, which reduced them to a size of approximately 5mm in diameter, suitable for the tema mill, in which the samples were ground for four minutes before the homogenization and splitting process. Homogenization was

achieved by rolling the powder on a sheet of paper. The samples were split by coning and quartering (see Fig. 9).

Homogenization and splitting was required at this stage in order to obtain two portions of the same sample. A portion ground to pass a 100 mesh sieve was used for the determination of ferrous iron, water and carbon dioxide by wet analysis, as well as for making the fused bead for X-ray fluorescence determination of major elements. The second portion of the sample was further ground to pass a 250 mesh sieve. This powder was used to make the pressed pellet, with which X-ray fluorescence determination of trace elements was carried out.

To obtain a 250 mesh powder, a ball mill was used. About 10 g of 100 mesh powder was transferred to a clean agate pot along with two small agate balls and mechanically shaken for fifteen minutes.

The samples were then thoroughly homogenized again and dried in an oven at 110°C for twenty-four hours, after which they were allowed to cool in a desiccator.

2.2.1. Notes on Crushing

Every effort was made to avoid contamination of the specimens during the crushing process. Contamination may arise from several sources such as: sweaty hands, uncleaned pieces of apparatus, and residues of previous samples scattered around the bench where the crushing is being done. Therefore, it is essential to avoid touching the samples, to keep a clean working environment, and to thoroughly clean each piece of apparatus between specimens. Particular care

Fig. 8: Flow diagram for the rock crushing procedure.

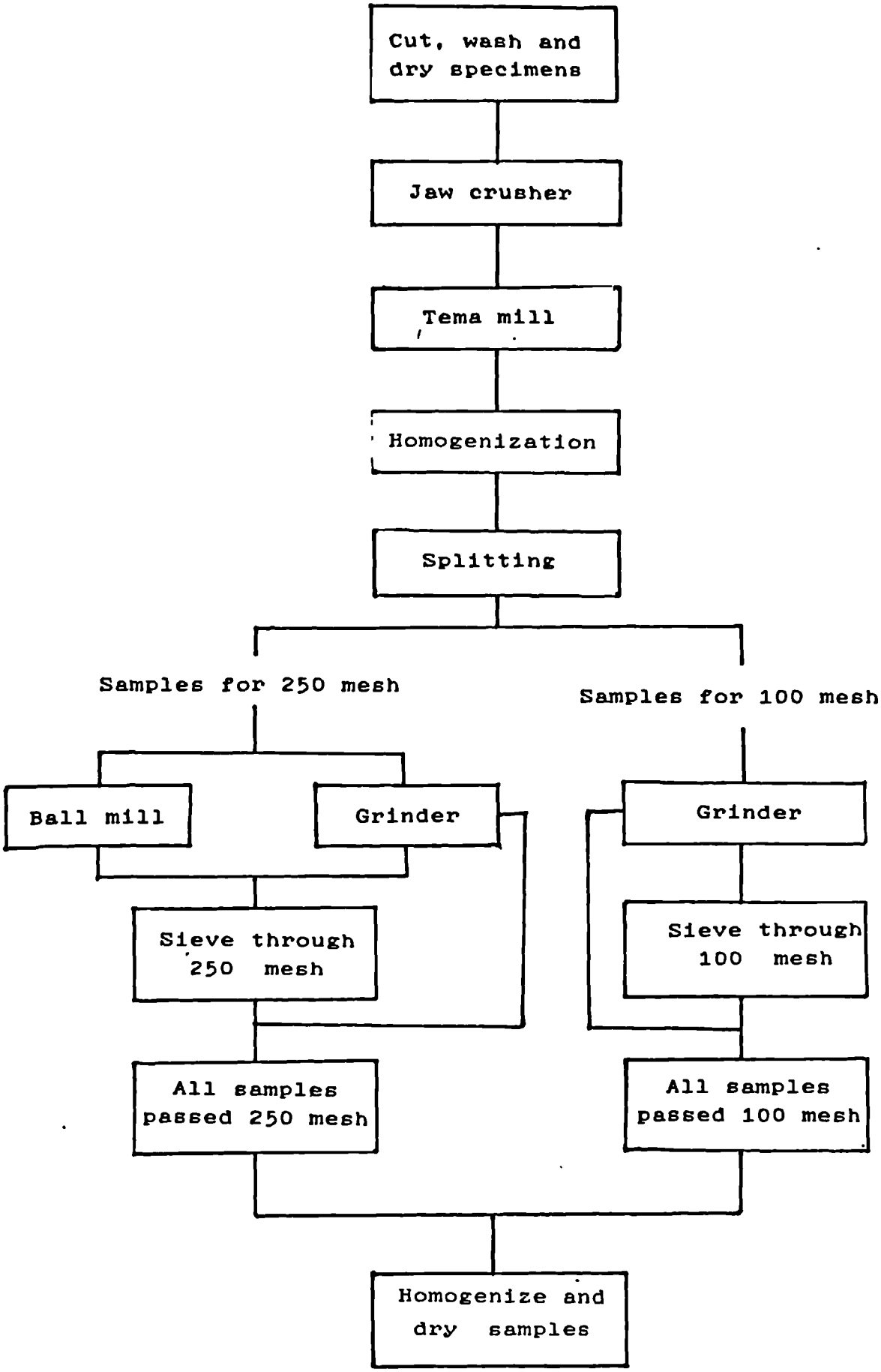

Fig 9: Steps followed to split the samples.

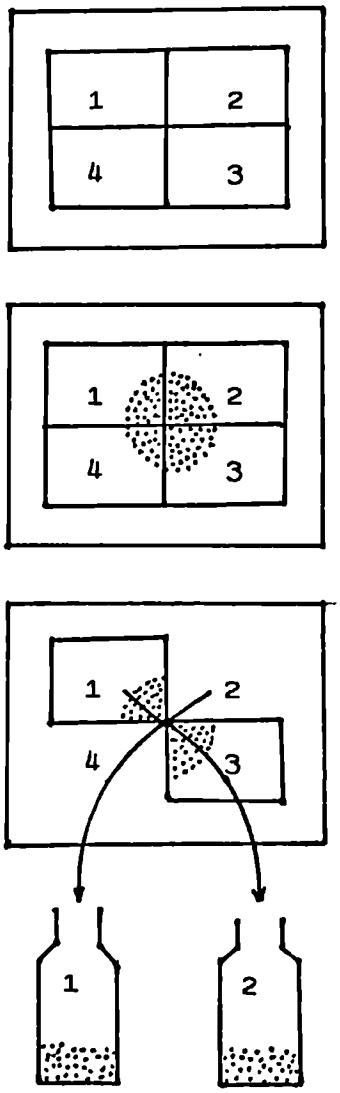

Place four overlaying sheets of paper on top of a bigger one

Distribute evenly the powder as an annular ring on the 4 pieces of paper

Take quadrants 1 and 3 and transfer the sample into a sample bottle. Do the same with quadrants 2 and 4 using another sample bottle

was taken when using the jaw crusher, which is very difficult to clean completely. Samples of similar composition were, therefore, crushed together, and when crushing different rock types, the initial portion of the second type was crushed and discarded.

In order to protect the agate rings of the tema mill, portions between 50 g and 100 g of rock chips were placed in the tema pot each time and ground for a maximum of 4 minutes. Similar precautions were taken when operating the ball mill. Only about 10 g of powder was transferred into the pot with two agate balls.

2.3. Preparation of the Fused Beads

2.3.1. Equipment Required

a) Two hot plates with adjustable temperature control to be maintained at 200 and 225 +/- 10°C.

b) A furnace capable of maintaining a temperature of 1000°C.

c) A plunger assemblage mounted on the surface of the hotter of the two plates to mould the melted flux into the final bead.

d) Six platinum gold crucibles with small bases and a capacity of about 15 cm^3 fitted with lids.

e) Blast burners, tripods, iron rings, and silica triangles. The burners should be able to maintain a temperature of 1000°C.

Other items used included an electronic balance, asbestos gloves, platinum tipped tongs, cooling blocks, a nickel shovel, nickel tongs, asbestos rings and duraluminium mounting plattens.

2.3.2. Flux

The beads were prepared using the commercially available spectro flux 105, which contains 47.03% lithium tetraborate, 36.63% lithium carbonate and 16.34% lanthanum oxide. This is the fusion mixture recommended by Norrish and Hutton (109).

2.3.3. Cleaning the Platinum Crucibles

To clean the crucibles, the process described below was followed. Some sodium carbonate was fused in them until all fused rock remaining was dissolved. After allowing some time to cool, the crucibles were gently transferred into a 10% nitric acid solution and boiled until total dissolution of carbonate and fused rock residual occurred. After cooling, the crucibles were removed with the nickel tongs, washed thoroughly with distilled water and dried in an oven at 100°C before using them. No contamination via the platinum tips was ensured by resting the tongs with tips uppermost and preventing them from coming into contact with the sodium carbonate.

Small amounts of fused rock, which normally remain after the preparation of each bead on the external walls of the crucible, were removed with the finger. This prevented the crucible being scratched, which may happen if this is done with a scalpel.

2.3.4. Procedure Used to Make the Beads

1) The fusion equipment was prepared for use: the hot plate with the plunger assembly was heated to 225 +/- 10°C and the other one was adjusted to 200 +/- 10°C. The temperatures of the furnace and the blast burners were raised to 1000°C.

2) Along with 2.000 g of flux, 0.3750 g of sample were weighed out into a crucible. The sample and crucible number were noted.

3) The crucible containing the sample and flux was placed into the furnace for 30 minutes in order to produce a homogeneous melt.

4) After that, it was removed from the furnace and placed on top of a blast burner close to the plunger assemblage and heated again until the sample was completely melted. Gentle swirling of the melt around in the crucible helped to incorporate into the melt any powder or droplets of melt on the sides of the crucible and to remove any air bubbles present.

5) The final bead was made by pouring the dull red coloured melt into the center of the mounting platten and lowering the plunger firmly against the platten for a few seconds.

6) The plunger was raised and, with the nickel shovel, the platten and the bead were quickly transferred onto the lower temperature hot plate, putting them between two asbestos blocks, in the centre of an asbestos ring. This

asbestos ring was at the same temperature as the hot plate, i.e. 200°C.

7) After thirty minutes, the asbestos blocks, keeping the bead in between, were removed from the hot plate and allowed to cool at room temperature on the bench before removing the bead for labelling and storage.

2.3.5. Notes on Making Beads

Safety precautions involved wearing gloves and safety spectacles as well as careful handling of the hot crucibles to prevent burning accidents.

There are some other facts that may lead to bead failure. Air bubbles may form in the bead mainly near the edges because either the plunger is too hot or the melt is also too hot, thus it is important to control the temperature during the process. If the plunger is raised too quickly after forming the bead, this may stick to the plunger. Failure to control the temperature during cooling of the bead may cause the bead to crack. In this investigation, when the procedure was unsuccessful, a new portion of sample was used and the process repeated.

2.4. Making the Pressed Powder Pellets

A pellet, consisting of six parts of rock to one part of binder, was prepared for trace element analysis. This pellet was prepared according to the method of Leak et al. (110), using the portion of the sample passing a 250 mesh sieve.

2.4.1. Equipment Required and Resin

a) Hydraulic press (30 ton)
b) Stainless steel plattens
c) Spexmixer
d) Polishing lap with paper and diamond paste
e) Nickel spatula
f) Polythene vials and lids
g) Glass balls
h) Phenol formaldehyde resin RO 214/1
i) Oven at 110°C

2.4.2. Procedure

1) Six grams of rock powder along with one gram of resin were weighed out and transferred to a clean polythene vial, one glass ball was added and the cap replaced.

2) To obtain a homogeneous mixture, the vial containing the sample, the resin, and the glass ball was mounted on the spexmixer and shaken for 30 minutes.

3) Then the glass ball was removed and the powder placed between two steel plattens and pressed under vacuum in a press at about 5 tons per cm^2 for one minute, after which the pressure was slowly released and the pellet removed.

4) The freshly formed pellet was put on a glass slide, ensuring that the bottom side touched the glass, which was then transferred to an oven at 110°C. After 25 minutes, the pellet was taken out of the oven and allowed to cool for subsequent analysis.

When handling the pellets, it is important to keep the fingers away from the surfaces. It is also essential not to touch the inside of the former case and the surface of the plattens with the fingers since sodium oxide is analysed from the pellet.

2.5. Ferrous Iron Determination

Ferrous iron determination was performed on rock samples which had been previously reduced to a powder, that passed a 100 mesh sieve. Ferrous analysis involved dissolution of the samples in hot sulphuric and hydrofluoric acids in a platinum crucible and subsequent titration of the solution with standard potassium dichromate solution using diphenilamine-sulphonate as indicator.

2.5.1. Reagents and Equipment Required

Analytical-reagent grade chemicals were used in the determination of ferrous iron.

a) Hydrofluoric acid
b) Sulphuric acid solution 50% V/V
c) Phosphoric acid 85% W/V
e) Boric acid

f) Potassium dichromate solution made as follows:
2.73 g of potassium dichromate dried at 130°C were dissolved in water and diluted to two litres with distilled water. Each cm^3 of this solution is equivalent to 2 mg of ferrous iron.

2.5.2. Diphenylamine-Sulphonate Indicator

A 0.2% solution of sodium diphenylamine-sulphonate was used as indicator.

Equipment involved platinum crucibles with lids, balance, a burette and beakers.

2.5.3. Cleaning the Crucibles

Before any sample was decomposed, the platinum crucibles were cleaned with about 350 ml of 50% HCl solution. The crucibles and lids were left in this solution for 15 minutes, after which they were transferred to another beaker, containing distilled water. The crucibles and lids were then heated until red on a bunsen burner flame and allowed to cool at room temperature. Crucibles were cleaned in this way after each analysis.

2.5.4. Procedure

For each sample, about 0.5 g of powder were weighed out using an electronic balance, and poured into a clean platinum crucible with a tight lid. The sample was moistened with a few drops of water to prevent any loss of sample under the acid attack, and 10 ml of 50% sulphuric acid was added. The crucible with the sample was placed on a hot plate and heated until almost boiling. At this stage, 5 ml of hydrofluoric acid were added and heating continued for 10 more minutes.

While the sample was being decomposed, the conditions

to do the titration were arranged: about 300 ml of distilled water were transferred to a 600 ml beaker and the following reagents added to it: 10 ml of 50% sulphuric acid, 10 ml of 85% phosphoric acid, 10 g of boric acid and 10 drops of indicator solution.

After decomposition of the sample, the crucible was transferred to this solution holding the lid on until the crucible was below the surface. The lid was then removed, the solution stirred and titrated until a purple end point appeared. Three replicates of each sample were analysed and the percentage of ferrous iron calculated from the following formula:

$$\% \text{ FeO} = \frac{\text{Volume of Standard Dichromate} \times 0.2}{\text{Weight of Sample}}$$

2.6. Water and Carbon Dioxide Analysis

Water and carbon dioxide were simultaneously determined in samples powdered to pass a 100 mesh sieve. Removal of water and carbon dioxide was achieved by inserting the sample into a combustion tube at 1100 to 1200°C; the gases thus produced were propelled towards the absorbers by a current of nitrogen gas. Water was absorbed on magnesium perchlorate and carbon dioxide in soda asbestos and determined gravimetrically.

2.6.1. Apparatus

The apparatus is illustrated in Fig. 10. Nitrogen gas coming from the cylinder passes through a flow regulator and

Fig. 10: Simplified apparatus used for the determination of water and carbon dioxide.

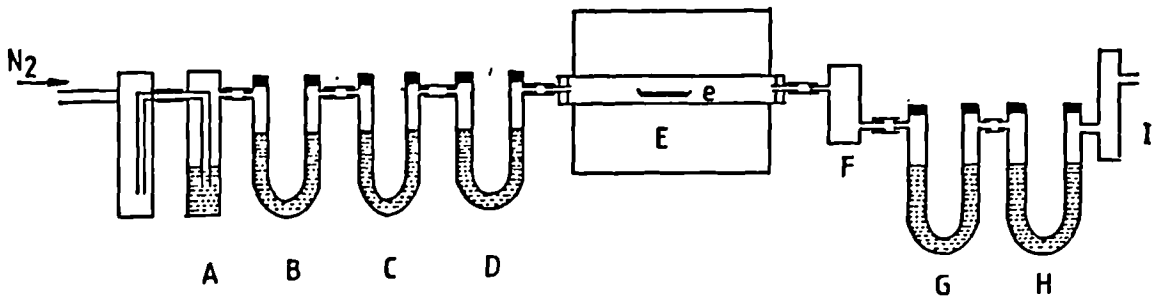

A: Sulphuric acid bubble counter.

B: U-Tube containing calcium chloride.

C: U-Tube containing soda asbestos.

D: U-Tube containing anhydrous magnesium perchlorate.

E: High-temperature furnace.

e: Sample container.

F: Water absorption tube containing anhydrous magnesium perchlorate.

G: U-Tube containing a saturated solution of chromium trioxide.

H: U-Tube containing anhydrous magnesium perchlorate.

I: Carbon dioxide absorption tube containing soda asbestos.

bubble counter (A), which contains concentrated sulphuric acid. It is then purified on passing through tubes, which contain fused calcium chloride (B), soda asbestos (C), and anhydrous magnesium perchlorate (D), respectively. The purified gas enters next into a combustion tube, which is made of mullite, and in which the sample container (e) is placed. The combustion tube is supported in a furnace (E) at 1100 to 1200°C. The nitrogen, along with water and carbon dioxide coming from the sample, enters the tube (F), which contains anhydrous magnesium perchlorate, where water is absorbed. The remaining gases pass through another tube (G) containing saturated chromium trioxide in phosphoric acid to remove any sulphur dioxide that may be present, and through a tube (H) with anhydrous magnesium perchlorate, before entering the carbon dioxide absorption tube (I). This tube is filled with soda asbestos and some anhydrous magnesium perchlorate at the end.

2.6.2. Procedure

Before any analysis was performed, the temperature in the furnace was allowed to reach 1100°C, and the nitrogen flow was regulated to about 3 litres per hour and passed through the system and absorption tubes for 20 minutes. The absorption tubes, which were cleaned and refilled with magnesium perchlorate and soda asbestos every 4 samples, were wiped carefully with a tissue and weighed to 5 decimal places using an electronic balance.

About 0.5 g of 100 mesh powder of each sample was weighed out into a previously ignited mullite boat and placed close to the entrance of the combustion tube. Nitrogen was allowed to flow for one minute, after which the weighed

absorption tube was connected, the boat with the sample was pushed to the red zone of the combustion tube and heated for 30 minutes. The absorption tubes were then removed, wiped, and reweighed to 5 decimal places.

Fifteen blanks and two standards were analysed before the sample analysis was started, in order to check the system and ensure satisfactory analyses. After this, a blank was carried out every 4 samples, except for the Fucoid Beds, for which a blank was carried out with each sample. The blanks were subtracted from the weights of water and carbon dioxide and the percentages calculated from the following formulae:

$$\%H_2O = \frac{\text{Weight of } H_2O \text{ obtained x 100}}{\text{Weight of sample taken}}$$

$$\%CO_2 = \frac{\text{Weight of Carbon Dioxide obtained x 100}}{\text{Weight of sample taken}}$$

2.7. Specific Gravity Determination

Bulk specific gravity of the rocks was determined by the principle of Archimedes (104). In order to obtain a reasonably pure homogeneous piece of rock, the external surface was cut and disposed of, thus obtaining a cube shaped specimen of about 25 g, which was used for specific gravity determination.

The samples were dried overnight in an oven at 110°C and then allowed to cool in a desiccator.

2.7.1. Procedure

Specific gravity determinations by this method involves weighing the specimen in air and calculation of its volumen by measuring the apparent loss in weight of the specimen when it is immersed in a liquid of known density.

About 25 g of each specimen were weighed out in air. Having recorded the weight of the specimens in air, the samples were left overnight immersed in water under vacuum. This was done to help draw out any air present in the pores of the specimen. The weight in water was next obtained by weighing the sample immersed in water hanging from a thread.

The specific gravity (G) was calculated as follows:

$$G = \frac{W_1}{W_1 - W_2}$$

where W_1 is the weight of the specimen in air and W_2 is the weight of the specimen in water.

2.8. Mineralogical Analysis

Mineralogical analysis was performed using a Philips PW 1050/25 automatic X-ray powder diffractometer with a PW 1120/ /00/60 generator and a Carl Zeiss-Jena Amplival Pol-U

polarising microscope. Specimens for the diffractometer were prepared according to the method suggested by Hutchinson (104) and which will be described in Section 2.8.2. Thin sections of the rocks were prepared for microscopic analysis.

2.8.1. Preparation of the Samples

Organic matter and other impurities present on the external surface of the samples were removed by cleaning the sample with a brush and then washing them thoroughly with water. The samples were then left to dry at room temperature before crushing and sieving.

A portion of about 0.4 g of each sample was subjected to X-ray diffraction analysis in order to obtain a general idea of the minerals present and to use this information in order to carry out a better mineral separation under the microscope.

The rocks were crushed in a jaw crusher, placed in a set of sieves that ranged from 22 mesh to 85 mesh and shaken for 10 minutes in order to separate the particles of different size. To remove dust present in the surface of the particles, each fraction was washed out with water and dried in an oven at 80°C for 3 hours.

The separation of the minerals was undertaken manually using a binocular microscope.

2.8.2. Specimen Preparation for the Diffractometer

A few crystals of the mineral to be analysed were placed in a clean agate mortar and ground with an agate

pestle in the presence of acetone until the gritty feeling between the pestle and the powder disappeared. This slurry was then poured evenly onto a glass slide of approximate dimensions 25x35x1 mm (104) and allowed to dry. After some time, acetone evaporated producing a thin layer of powder, which was mounted in the goniometer for analysis. Each specimen was run at two degrees 2 Θ per minute from about 4° to 56° for an average scanning time of 28 minutes.

Some difficulties faced during the specimen preparation arose from the small amount of minerals, which could be separated under the microscope; from samples which were too fine grained, it being very difficult to separate individual minerals. Sometimes, instead of a true separation of the mineral, only a concentration of it was achieved. Nonetheless, this was enough to make the mineral identification possible.

2.9. Quantitative X-Ray Diffraction

Quantitative X-ray diffraction analysis seeks to determine the modal composition of rocks from a comparison of peak heights.

In quantitative powder X-ray diffraction analyses, it is essential to have standards of precisely the same minerals as are present in the sample.

Standards were prepared using pure minerals separated from the following samples: 42, 19, 9, and 16. Separation of the minerals present in these samples under the microscope allowed isolation of potassium feldspar from sample 42, quartz and biotite from sample 19 and muscovite (illite) from

sample 9. Sample 16 was used as a source of pyrophyllite.

2.9.1. Calibration of the Instrument for Quantitative X-Ray Diffraction

a) The separated minerals were ground in a tema mill to pass a 100 mesh sieve and used as standards.

b) Standard mixtures were made of two different compositions, namely: a mixture of 50% quartz and 50% potassium feldspar and a second mixture of 64.1% of muscovite, 4.0% of pyrophyllite, 1.3% of biotite and 28.1% of quartz.

c) Specimens prepared as in Section 2.8.2. were run in the diffractometer at 2 Θ degrees per minute for an average time of 28 minutes.

d) The peak height corresponding to reflection of quartz at 2.45Å, muscovite at 10.08Å, potassium feldspar at 3.24Å, and pyrophyllite at 3.08Å were measured from duplicate analysis.

2.9.2. Selection of the Peaks

Careful observation of the diffractograms for standards and samples leads to the conclusion that the peaks noted above are relatively free from overlapping reflections and were thus selected for analysis.

2.9.3. Interpretation of the Calibration Results

Since the height of the peaks produced by a certain

component is proportional to the amount of this component present in the mixture (103), it follows that:

$$\% A = k_A H_A$$

$$\% B = k_B H_B$$

Hence

$$\frac{\% A}{\% B} = K_{A/B} \cdot \frac{H_A}{H_B}$$

If % A and % B are known and H_A and H_B measured, then $K_{A/B}$ can be calculated.

2.9.4. Calculation of the Constants Needed for Quantitative X-Ray Diffraction

Peak heights of the selected peaks for quartz, muscovite, pyrophyllite, and potassium feldspar in the two standard mixtures are given in Tables 2 and 3.

Calculation of $K_{Q/F}$, the ratio of the constants between the quartz and the potassium feldspar peaks, is presented here to illustrate the procedure followed to estimate the set of constants summarised in Table 4.

$50 = k_Q \cdot H_Q$ and $50 = k_F H_F$

$H_Q = \frac{50}{k_Q}$ and $H_F = \frac{50}{k_F}$

hence

Table 2: Determination of $K_{Q/F}$ from a mixture of 50% quartz and 50% potassium feldspar.

	Quartz	K feld.
%	50.00	50.00
2	42.80	32.10
d	2.45	3.24
H	3.02	11.78
$K_{Q/F}$		3.90

Table 3: Determination of $K_{Q/M}$, $K_{P/M}$, and $K_{P/Q}$ from a mixture of quartz (Qtz.), muscovite (Msc.) and pyrophyllite (Pyr.).

	Qtz.	Msc.	Pyr.
%	28.1	64.1	4.0
20	42.8	10.1	34.0
d	2.45	10.08	3.08
H	3.3	12.2	2.0
K	$K_{Q/M}$=1.6	$K_{P/M}$=0.4	$K_{P/Q}$=0.2

Table 4: Set of constants used in quantitative X-ray diffraction analysis of the Lewisian gneiss.

$K_{Q/F}$	$K_{Q/M}$	$K_{P/M}$	$K_{P/Q}$	$K_{F/M}$	$K_{P/F}$
3.9	1.6	0.4	0.2	0.4	0.9

Table 5: Measured height of peaks corresponding to muscovite H_M, potassium feldspar H_F, pyrophyllite H_P, and quartz H_Q for sample 17.

Sample	H_M	H_F	H_P	H_Q
17	13.11	0.00	0.90	1.92

$$K_{Q/F} = \frac{k_Q}{k_F} = \frac{50H_F}{50H_Q}$$

$$K_{Q/F} = \frac{50 \times 11.78}{50 \cdot 3.02} = 3.9$$

2.10. Quantification of the Minerals in the Samples

For each of the samples from the felsic band, a diffractogram was obtained. The height of the peaks selected for analysis was measured and compared with the standards in order to obtain an estimate of the mineral composition.

2.10.1. The Calculation

Each sample was assumed to have four components: quartz (% quartz = Q), potassium feldspar (% potassium feldspar = F), muscovite (% muscovite = M), and pyrophyllite (% pyrophyllite = P). The results give four height measurements, each being equivalent to the concentrations of one of the four minerals (H_Q, H_F, H_M, and H_P). Thus, there are four equations in four unknowns, which can be solved using the constants previously estimated and give the results shown in Table 24. The estimation of the mineral composition of sample 17 is presented here as an example to illustrate these calculations.

X-ray diffraction analysis shows that this sample contains no potassium feldspar. It contains only quartz,

pyrophyllite and muscovite. Peak heights measured on the diffractogram are for the peaks corresponding to each of the minerals present in this sample and are shown in Table 5, so

$$Q + M + P = 100 \qquad 1$$

and

$$\frac{P}{Q} = K_{P/Q} \frac{H_P}{H_Q} = 0.2 \times \frac{0.9}{1.92} = 0.09 \qquad 2$$

$$\frac{P}{M} = K_{P/M} \cdot \frac{H_P}{H_M} = 0.4 \times \frac{0.91}{13.11} = 0.03 \qquad 3$$

$$\frac{Q}{M} = K_{Q/M} \cdot \frac{H_Q}{H_M} = 1.6 \times \frac{1.92}{13.11} = 0.23 \qquad 4$$

From equation 2) $Q = \frac{P}{0.09}$ and from equation 3) $M = \frac{P}{0.03}$;

substitution in equation 1) gives a value of P = % pyrophyllite = 2.2.

From equation 2) $P = 0.09\ Q$ and from equation 4) $M = \frac{Q}{0.23}$

substitution in equation 1) gives a value of Q = % of quartz= = 18.4.

Finally, from equation 3) $P = 0.03\ M$ and from equation 4) $Q = 0.23\ M$; substitution in equation 1) gives a value of M = % of muscovite = 79.4.

CHAPTER III

PRESENT-DAY PROCESSES BEARING ON THE WEATHERING OF LEWISIAN GNEISS

Chemical weathering processes require water and heat and the rate at which they proceed is strongly influenced by these two factors. The chemical reactions through which weathering occurs follow the laws of equilibrium and can be treated as neutralization reactions in an aqueous medium in which primary minerals, constituents of the rocks, dissolve in water and bases are neutralized by carbonic acid. The products of these reactions are secondary minerals, mainly clays, that are precipitated under different environmental conditions.

Such treatment requires a knowledge of the thermodynamic controls, to determine which minerals are stable in a given environment, and hence the nature of the chemical reaction. This topic is dealt with in the first section (3.1.), where it will be shown that the nature of the reaction depends critically upon the acidity. The factors which control the acidity of natural waters are treated next (Section 3.2). The nature of the weathering products depends upon the concentration of all the dissolved species, the origin of which is discussed in Section 3.3.

The rocks preserved at Rispond represent the parent material and only rarely where preserved from present-day erosion are some of the products of the Precambrian weathering seen. It is one of the objects of this thesis to infer the composition of the water, which reacted with the parent Lewisian gneiss and produced the mineral assemblage

now found just below the Cambrian unconformity which is considered to represent a fossil soil. In order to do this, a survey of the composition of present-day natural waters is made in Section 3.4., where the minerals expected on the basis of thermodynamic equilibrium are compared with what data is available on weathering products in contact with these natural waters. Finally, in the last section (3.5.), the evolution of groundwater reacting with Lewisian gneiss is calculated by the mass balance method used by Verstraten (111) in his study of weathering in the Ardennes.

3.1. The Thermodynamic Control of Weathering

3.1.1. The Phase Rule

This is a general law dealing with phase equilibrium and can be expressed mathematically as follows: If in a system of n components, the number of degrees of freedom is f and the number of phases is p, the equation is

$$f + p = n + 2$$

Taking the case of the Lewisian gneiss as an example, the phase rule may be applied as follows: The number of components is 7 (viz. SiO_2, Al_2O_3, FeO, MgO, CaO, Na_2O, and K_2O) so n = 7; the number of degrees of freedom is 4 since temperature and pressure can vary, giving two degrees of freedom; there are also two solid solutions, whose composition can be defined only with the inclusion of two further degrees of freedom, viz., biotite, a solid solution between magnesium and iron end members, and plagioclase, a partial solid solution between calcium and sodium end members. This leads to five minerals or phases:

$$p = n - f + 2$$

$$p = 7 - 4 + 2 = 5$$

The minerals are: quartz, microcline, plagioclase, muscovite, and biotite.

Solid solutions are quite common in minerals. However, because of the simplicity of the system under consideration, which will be shown in Chapter 4 to contain mainly potassium, silicon, and aluminium, there is very little solid solution, and in this thesis, effects of solid solution will be neglected.

3.1.2. Closed and Open Systems

Since weathering profiles are open systems, a discussion of concentrations in the aqueous phase as well as the concentrations in the solid phase will be included.

It has already been pointed out that the main components of the system are K_2O, Al_2O_3, SiO_2 and H_2O, i.e. the system has four components and two degrees of freedom. Since the temperature and the pressure can vary, it follows from the phase rule that the number of phases are four.

The four phases are three minerals, either quartz, pyrophyllite, and muscovite, or quartz, muscovite, and microcline, and water, three solid phases and one fluid phase.

The above reasoning is only valid when dealing with

closed systems, i.e., those systems, in which mass does not enter or leave. However, weathering profiles are open systems, in which mass may enter or leave. This means that concentration variations of ions in the aqueous phase must be taken into consideration. In doing so, the number of components is the same (4), but the number of degrees of freedom now becomes four since, in the aqueous phase, the concentration of potassium ions and hydrogen ions are variable. Hence the number of phases in the open systems is two.

$$p = 4 - 4 + 2 = 2$$

From these two phases, one is aqueous and one is mineral. A natural water in equilibrium with a Lewisian felsic layer of an initial composition of quartz, feldspar and mica will have only one mineral present. The other minerals originally present will react together via the aqueous phase until only one mineral remains, regardless of the original composition of the rock.

Another factor that has to be taken into account when dealing with soil profiles as thermodynamic open systems is that quartz is deposited only very slowly from solutions of silicic acid that exceed the quartz solubility. Quartz does not reach equilibrium with natural waters, its solutions are often supersaturated. This is particularly important for the mobile waters of rivers, lakes and shallow groundwaters because in these waters, high concentrations of silicic acid are generated and transported.

This lack of equilibrium alters the number of components and degrees of freedom in the system, since a new

Fig. 11: Activity diagram for some minerals in the system K_2O-Al_2O_3-SiO_2-H_2O.

At 25°C and 1 atm. total pressure.

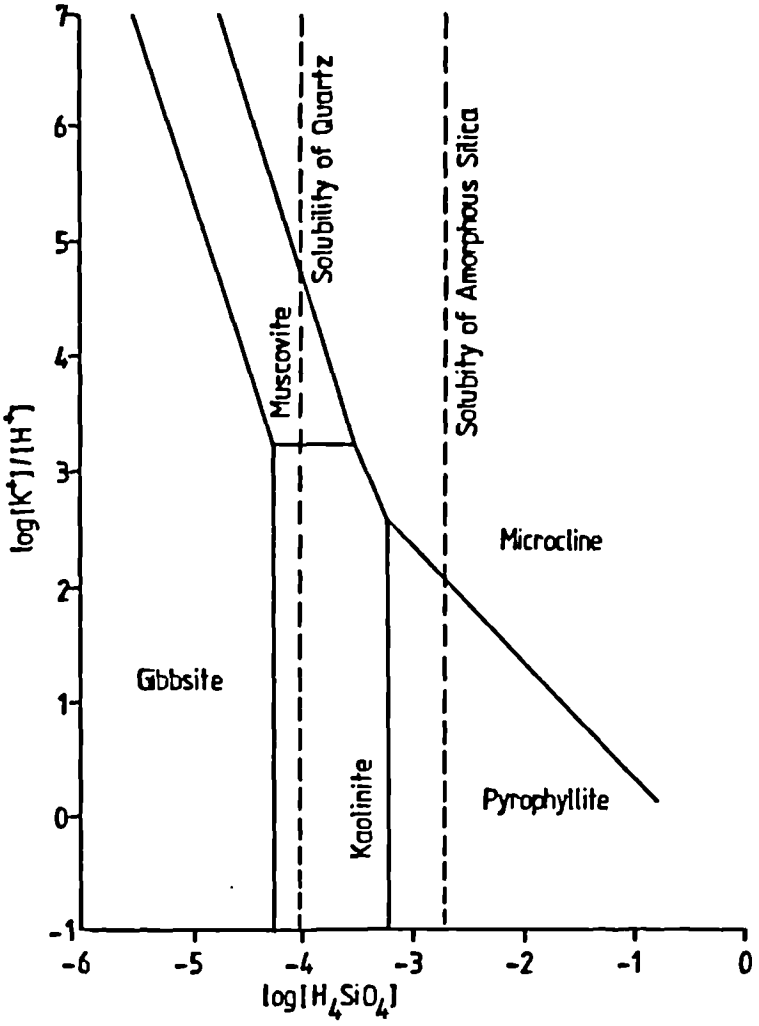

component and one more degree of freedom should be included (112, 113). It can be seen that, upon applying the phase rule with this modification, the number of phases is still two but the concentration of silicid acid has to be specified.

As thermodynamic open systems, weathering profiles are usually represented in terms of activity diagrams (22, 47). These diagrams show mineral stability fields on a graph whose axes are the activity in the aqueous phase of those species, whose concentration in the aqueous phase can vary. One such diagram, suitable for the discussion of the weathering of Lewisian gneiss (which is discussed in Chapter IV), is constructed and examined in the next section.

3.1.3. The Activity Diagram for the K_2O-Al_2O_3-SiO_2-H_2O System Open to K^+, H^+, and H_4SiO_4

An activity diagram showing stability fields for potassium feldspar, muscovite, pyrophyllite, kaolinite and gibbsite in equilibrium with natural waters, is presented in Fig. 11. The thermodynamic data used to plot this diagram are summarised in Table 6. These data have been taken from Helgeson (78, 91). Solubilities of silica and amorphous silica have been taken from Morey et al. (114, 115).

When reactions are written for the mineral compatibilities shown in Fig. 11, it is discovered that only three variables need to be considered: the concentrations of potassium ions, hydrogen ions and silicic acid. Moreover, the power to which the ratio of the concentration of potassium ions over the concentration of hydrogen ions is raised is always unity. Therefore, the mineral relations can be

Table 6: Thermodynamic data used to plot the activity diagram for the system K_2O-Al_2O_3-SiO_2-H_2O at 25°C.

Species name	Formula	ΔH Cal/Mol	S° Cal/Mol °C	ΔG° Cal
Msc.	$H_2KAl_3Si_3O_{12}$	-1427,408	69.00	-1336,301
Pyr.	$H_2Al_2Si_4O_{12}$	-1345,313	57.20	-1255,997
Mcr.	$KAlSi_3O_8$	- 949,188	52.47	- 895,374
Gbb.	$Al(OH)_3$	- 309,065	16.75	- 276,188
Kln.	$H_4Al_2Si_2O_9$	- 982,221	48.53	- 905,614
Qtz.	SiO_2	- 217,650	9.88	- 204,646
Water	H_2O	- 68,315	16.71	- 56,687
Proton	H^+	00.000	00.00	00.000
K-ion	K^+	- 60,040	24.50	- 67,349
Sil.ac.	H_4SiO_4	- 348,060	45.84	- 312,560

Abbreviations:

Msc = Muscovite

Pyr = Pyrophyllite

Mcr = Microcline

Gbb = Gibbsite

Kln = Kaolinite

Qtz = Quartz

described in a two dimensional diagram involving the ratio of the concentration of potassium ions to the concentration of hydrogen ions as one axis and the activity of silicic acid as the other (see Fig. 11).

The reactions and equilibrium constants are as follows:

1) $H_4Al_2Si_2O_9 + 5H_2O = 2Al(OH)_3 + 2H_4SiO_4$
Kaolinite Water Gibbsite Silicic Acid

$$K = [H_4SiO_4]^2 = 10^{-8.50}$$

2) $3KAlSi_3O_8 + 2H^+ + 12H_2O = H_2KAl_3Si_3O_{12} + 2K^+ + 6H_4SiO_4$
Microcline Water Muscovite Silicic Acid

$$K = \frac{[K^+]^2}{[H^+]^2} [H_4SiO_4]^6 = 10^{-14.67}$$

3) $2H_2KAl_3Si_3O_{12} + 3H_2O + 2H^+ = 2K^+ + 3H_4Al_2Si_2O_9$
Muscovite Water Kaolinite

$$K = \frac{[K^+]^2}{[H^+]^2} = 10^{6.51}$$

4) $2KAlSi_3O_8 + 2H^+ + 9H_2O = H_4Al_2Si_2O_9 + 2K^+ + 4H_4SiO_4$
Microcline Water Kaolinite Silicic Acid

$$K = \frac{[K^+]^2}{[H^+]^2} [H_4SiO_4]^6 = 10^{-7.61}$$

5) $H_2Al_2Si_4O_{12} + 5H_2O = H_4Al_2Si_2O_9 + 2H_4SiO_4$

Pyrophyllite Water Kaolinite Silicic Acid

$$K = [H_4SiO_4]^2 = 10^{-6.38}$$

6) $2KAlSi_3O_8 + 2H^+ + 4H_2O = H_2Al_2Si_4O_{12} + 2K^+ + 2H_4SiO_4$

Microcline Water Pyrophyllite Silicic Acid

$$K = \frac{[K^+]^2}{[H^+]^2} [H_4SiO_4]^2 = 10^{-1.23}$$

7) $H_2KAl_3Si_3O_{12} + H^+ + 9H_2O = 3Al(OH)_3 + K^+ + 3H_4SiO_4$

Muscovite Water Gibbsite Silicic Acid

$$K = \frac{[K^+]}{[H^+]} [H_4SiO_4]^3 = 10^{-9.49}$$

8) $2H_2KAl_3Si_3O_{12} + 2H^+ + 6H_4SiO_4 = 12H_2O + H_2Al_2Si_4O_{12} + 2K^+$

Muscovite Sil.Ac. Water Pyrophyllite

$$K = \frac{[K^+]^2}{[H^+]^2} [H_4SiO_4]^{-6} = 10^{25.64}$$

For each one of the above reactions, using the thermodynamic data presented in Table 6, the free energy of the reaction and the equilibrium constant have been calculated and are summarised in Table 7 in terms of log of (K).

Each of the fields shown in Fig. 11 represents the

Table 7: Free energies of reaction and log (K) for each one of the reactions involved in the soil profile.

Reaction No.	$\Delta G^{\circ}r$ Kcal	log(K)
1	+11.593	- 8.50
2	+20.007	-14.67
3	- 8.877	+ 6.51
4	+10.379	- 7.61
5	+ 8.698	- 6.38
6	+ 1.681	- 1.23
7	+12.951	- 9.49
8	-34.971	+25.64

range of chemical compositions of waters over which one mineral is stable once equilibrium is attained. Minerals are not stable in waters with chemical compositions that plot outside their stability fields.

It can be seen from Fig. 11 that gibbsite, a typical weathering product of tropical profiles occurs at very low concentrations of silicic acid, followed, if the potassium to hydrogen ion ratio is low, by the stability fields of kaolinite and, at still higher silica concentration, that of pyrophyllite. At high potassium to hydrogen ion ratios, increasing the silicic acid concentration results in illite and then potassium feldspar being the stable phases.

It is also clear from the same diagram that muscovite and pyrophyllite do not form a stable association. Microcline weathers directly to pyrophyllite, kaolinite or muscovite. Note that the pyrophyllite field can be reached assuming that microcline weathers first to kaolinite and then to pyrophyllite or assuming that microcline weathers first to muscovite, then to kaolinite and finally kaolinite weathers to pyrophyllite. The activity diagram is modified slightly when the mineral beidellite is taken into account. This is discussed in Section 4.11.2., in the next chapter.

It has to be emphasised that, for several reasons, the ion activity levels presented in Fig. 11 can only be considered approximate. For example, the stability field for these minerals will vary somewhat according to the crystallinity of the mineral; the lines represent the stability of minerals as determined by dissolution and other methods that determine the ion activities that such minerals will support. In nature, similar minerals may not precipitate

at the same ionic activities; some uncertainty exists in some of the mineral stability determinations and also in some of the thermodynamic values required to compute the free energy of the minerals (116). Further, as has been pointed out by Velde (92), if solid solution is ignored, thermodynamic data will be inexact; calculations of the free energy of phyllosilicates from addition of thermodynamical data of component oxides is not precise enough for detailed analysis since it does not account for configurational energy contributions to the energy of these minerals; and finally, all stable phases must be included in such diagrams and all the unstable phases must be excluded. There are several possible and important minerals, e.g., potassium montmorillonite, hydromuscovite, and illite, for which the thermodynamic data are so uncertain that they have been excluded from the activity diagram. However, it is possible that such minerals may be stable phases and should be included. All these uncertainties show that Fig. 11 should be treated as little more than a first approximation.

As a consequence of these uncertainties, the positions but not the slopes of the lines shown in Fig. 11 will be altered by any revision in the thermodynamic data for the minerals considered. Also the diagram requires the addition of fields corresponding to potassium beidellite and its solid solutions with illite. These fields will occur between the feldspar and kaolinite fields and/or the feldspar and pyrophyllite fields, depending on the unknown thermodynamic constants.

3.2. The Acidity of Natural Waters

The main reaction that occurs during the weathering of rocks can be summarised as follows:

Rock + Carbon Dioxide + Water = Secondary Mineral(s) + Bicarbonates of bases + Silicic Acid.

The weathering rate, that is, how fast this reaction occurs, depends upon several factors: the nature of the rock, the nature of the secondary minerals, the concentration of carbonic acid and the rate constant of the reaction. The nature of the rock in a particular area is assessed by field inspection. Evaluation of secondary minerals is not always easy; particularly when dealing with fine grained minerals, some insight into the secondary minerals can be gained by studying them under the microscope, by X-ray diffraction analysis, and by looking at their activity diagrams. The rate constant depends upon the particular reaction under consideration, and the mechanism by which such a reaction proceeds towards equilibrium. The rate constant also depends upon the temperature: it increases rapidly as the temperature rises. The concentration of carbonic acid affects the weathering rate since it is the major source of acidity in natural waters.

3.2.1. The Carbonate Equilibrium

The pH of most natural waters is controlled by reactions involving the ionisation of carbonic acid. Carbonic acid has two ionisation constants:

$$K_1 = \frac{[HCO_3^-][H^+]}{[H_2CO_3]} = 10^{-6.42}$$

$$K_2 = \frac{[CO_3^{-2}][H^+]}{[HCO_3^-]} = 10^{-10.43}$$

The equilibrium constant for the reaction between atmospheric CO_2 and water is

$$K_3 = \frac{[H_2CO_3]}{p\ CO_2} = 10^{-1.34}$$

where p CO_2 is expressed in atmospheres.

These three equilibria govern the concentration of carbonic acid in natural waters. The above values for the constants are at 15°C (111).

The acidity of soil water depends upon the local concentration of carbon dioxide in the soil atmosphere, which is much higher than the concentration in the general atmosphere. It must be emphasised that today these concentrations are very different. In the Precambrian, in the absence of plants, the concentration in the general atmosphere and in the soil atmosphere was probably the same. Although this concentration may well have been higher than the concentration in the present-day atmosphere (154).

The concentration of carbon dioxide in soil atmosphere is today controlled by the decomposition and respiration of plants, and is generally fairly constant. Because of this

constancy, the pH of soil waters is controlled by the amount of bases dissolved during weathering of the soil which, during dissolution, produces an equivalent concentration of bicarbonate ion.

The more weathering, the more bicarbonates; the more bicarbonates, the higher is the pH; the more carbon dioxide present in the local soil atmosphere, the lower is the pH.

$$[H^+] = K_1 K_3 \frac{[CO_2]at}{[HCO_3^-]}$$

The concentration of carbon dioxide in the general atmosphere (0.03%) is controlled by the pH of the sea water, which acts as an enormous reservoir of this gas.

The pH of the sea water is in turn governed by the balance between the total cations (mainly Na^+, K^+, Mg^{+2} and Ca^{+2}) and the anions of the strong acids (Cl^- and SO_4^{-2}). As the balance changes to increase the cations, more bicarbonate is converted to carbonate in order to produce charge balance.

In present-day oceans, the factors controlling the cation/anion balance are mainly the removal by living organisms of calcium carbonate to form shell and the respiration and metabolism of plankton, which converts organic carbon to carbon dioxide and vice versa. However, on a geological time scale, it is the balance between the supply of cations and anions by erosion and their removal in sediments, which controls this balance. Any change in the rate or nature of these processes will alter the

Fig. 12: Atmospheric carbon dioxide concentration in equilibrium with natural waters.

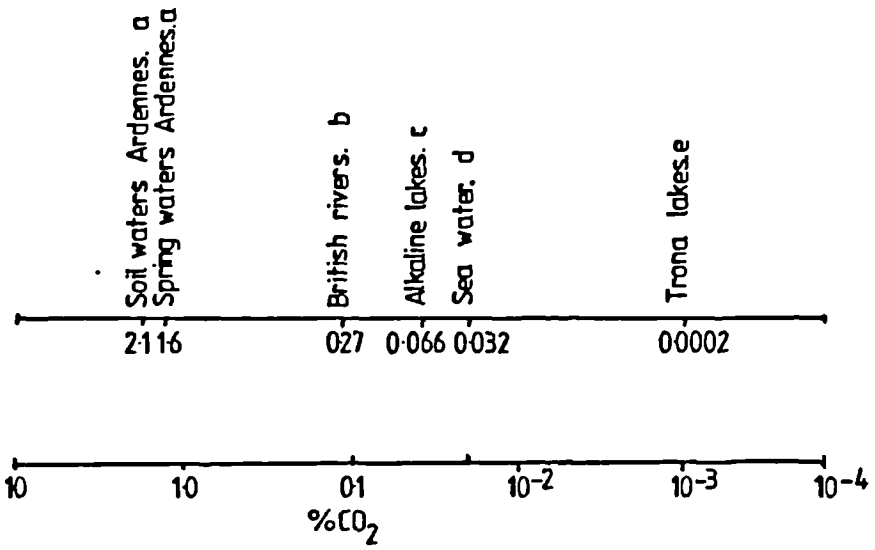

a - J.M. Verstraten (111)

b - J. Lewin (117)

c - Y.F. Kharaka et al. (118), Eugster and Hardie (119)

d - W.S. Brocker (120)

e - Eugster and Hardie (119) - Alkali Valley.

atmospheric carbon dioxide concentration (120). The processes which remove sodium, potassium and chloride from sea water are not well understood and any prediction of past atmospheric carbon dioxide concentrations is little more than speculation.

3.2.2. Carbon Dioxide Concentrations in Waters

Sea water controls the carbon dioxide concentration in the general atmosphere, but the carbon dioxide concentration in rivers, springs and lakes is governed by the difference between the carbon dioxide concentration in the soil atmosphere and the general atmosphere (see Fig. 12). Soil waters from the Haartz catchments in the Luxembourg Ardennes (111), are presented here as an example of the concentration of carbon dioxide that may be found in soil waters. The atmosphere in equilibrium with this water contains 2% of carbon dioxide. As waters leave the soil from springs and run down towards the sea as rivers, their carbon dioxide content decreases and approaches equilibrium with the general atmosphere. Note that some alkaline lakes are depleted in carbon dioxide when compared with the atmosphere. As such lakes become more and more concentrated, trona ($Na_2CO_3.NaHCO_3.2H_2O$) starts to be deposited and during this process carbon dioxide is removed from the lake in the form of sodium bicarbonate. The precipitation of calcium carbonate has the reverse effect because it is present in waters as the bicarbonate ion, which on precipitation of calcite liberates carbon dioxide.

$$Ca(HCO_3)_2 = CaCO_3 + H_2O + CO_2$$

3.3. The Origin of the Chemical Components of Natural Waters

Rainfall supplies the water that causes the chemical weathering of rocks. Rain is not pure water, but contains a wide range of dissolved substances. The chemical composition of the rain water is different from the chemical composition of ground water and varies from region to region (22). Rain is always acid and the amount of sodium chloride present from the oceans decreases towards the interior part of the continents. Rain near industrial areas commonly also contains high amounts of SO_2, CO_2, and SO_4^{-2}, mainly derived from the combustion of coal and oil (22, 121). The average chemical composition of rain water reported by Lapedes (122) and the average composition of rain water in Northern Europe as given by Carroll (123) are summarised in Table 8 along with other chemical analyses for rain water.

Drastic changes in the chemical composition of the water take place as it enters and reacts with the soil components. Since the products of these reactions vary from soil to soil, the chemical characterisation of ground waters becomes difficult. However, it is possible to give some details about pH variations in water. Generally speaking, water in contact with rocks or soil at the surface of the earth dissolves carbon dioxide, therefore becoming more acid, according to the equation:

$$H_2O + CO_2 = H^+ + HCO_3^-$$

Carbon dioxide is derived from the respiration of plant roots and the bacterial degradation of organic materials. The supply of acid soil waters is thus largely controlled by plant activity.

Table 8: Average chemical composition of rain water as reported by Lapedes (122) and average chemical composition of rain water in Northern Europe and other areas of the world.-
Concentrations are given in p.p.m.

	Na^{+}	K^{+}	Ca^{+2}	Mg^{+2}	Cl^{-}	SO_4^{-2}
Aver. chem.comp.rain	1.98	0.30	0.09	0.27	3.79	0.58
Northern Europe	2.05	0.35	1.42	0.39	3.47	2.19
Hubbard Brook 1964-77	0.11	0.06	0.14	0.04	0.42	2.74
" " 1963-74	0.12	0.07	0.17	0.05	0.51	2.87
Amazon basin	0.29	0.04	0.04	0.03	0.49	0.49
L/Valencia (Venezuela)	2.12	0.70	1.41	0.90	3.14	-
Haartz (Luxembourg)	0.67	0.25	0.74	0.07	1.93	3.94
Minnesota (USA)	0.14	0.13	0.80	0.26	0.93	3.78
Snow melt	0.02	0.015	0.02	0.02	0.20	-
Taite (N. Zealand)	5.4	0.66	0.79	0.78	9.20	-
Atlantic Coast (USA)	1.3	0.07	0.34	0.31	1.65	6.00
Mid.Atlantic (Bermuda)	3.4	1.57	0.61	0.92	6.78	3.48
Average	1.42	0.36	0.59	0.34	2.61	3.19

Table 8 (cont.)

	NO_3^-	HCO_3^-	SiO_2	NH_4^+	pH	Ref.
Aver. chem.comp.rain	-	0.12	-	-	5.7	122
Northern Europe	0.27	-	-	0.41	5.47	123
Hubbard Brook 1964-77	1.46	0.006	0.02	0.19	4.15	124
" " 1963-74	1.43	-	-	0.22	4.13	125
Amazon basin	0.13	-	0.0	-	5.03	126
L/Valencia (Venezuela)	0.21	8.18	0.18	0.40	4.28	127
Haartz (Luxembourg)	1.62	-	-	0.87	4.43	111
Minnesota (USA)	1.28	-	-	0.67	4.67	128
Snow melt	0.03	-	0.26	0.005	5.27	129
Taite (N. Zealand)	-	-	-	-	-	130
Atlantic Coast (USA)	1.56	-	-	0.34	4.22	131
Mid.Atlantic (Bermuda)	0.40	-	-	0.081	4.74	131
Average	1.19	4.10	0.12	0.43	4.63	

The concentration of hydrogen ions, expressed as pH, is of fundamental importance in weathering processes as it influences the solubility of silicon and metal oxides and may replace other cations within the structure of some minerals.

Natural waters contain the following chemical species: Na^{+}, K^{+}, Ca^{+2}, Mg^{+2}, Cl^{-}, SO_4^{-2}, NO_3^{-}, and SiO_2. The main sources of these cations and anions are rainfall, weathering and some contribution from plants, via the leaf fall. The amount each of these sources contributes to the total is difficult to assess and varies from place to place. The contribution of plants to the composition of natural waters varies from season to season and, although in some cases it may be important for the present investigation, it has been ignored because terrestrial plants were absent from the Precambrian paleosol being investigated.

Some idea of the contribution of the rainfall to the chemistry of natural waters can be gained by comparing the chemical composition of the rainfall given in Table 8 with the average river water composition and calculating the percentage of each of these species that comes from rain, as is done in Table 9. The comparison, however, cannot be made directly since evaporation has to be taken into account. Calculations given in Table 9 are made assuming evaporation of 5%. The river water composition given here is that reported by Livingston (132). It can be appreciated from Table 9 that the three largest contributions from rain waters are for sodium and chloride from marine salt, and sulphate from forest fires. The contribution for the remaining elements is very small so most of the chemical constituents of natural waters come from the weathering of rocks. There is an enormous difference in the amount of silica, which in

Table 9: Contribution of rain water to the composition of soil water.

Element	Rain water ppm	River water ppm	% from rain
Na^+	1.42	6.3	23.7
K^+	0.36	2.3	16.5
Ca^{+2}	0.59	15.0	4.1
Mg^{+2}	0.34	4.1	8.7
Cl^-	2.61	7.8	35.2
SO_4^{-2}	3.19	11.2	30.0
NO_3^-	1.19	1.0	-
HCO_3^-	4.10	58.4	7.4
SiO_2	0.12	13.1	0.1
NH_4^+	0.43	-	-
pH	4.63	7.8	-

natural waters comes mainly from the decomposition of rocks and, in some cases, from decomposition of plants that accumulate silica (133).

3.4. The Chemical Composition of Natural Waters

Precambrian waters were probably generated by processes similar to those in operation today, viz.: dissolution, reaction, and evaporation. Nevertheless, the rate and extent of these processes, and hence the composition of the waters and the nature of the minerals produced, may well differ from that occurring at the present day because the factors which control the weathering process (carbon dioxide concentration in the soil atmosphere, temperature, etc.) and the rate of evaporation (temperature, depth of soil, water table, rainfall and wind speed) will very probably have been different. Any discussion of weathering in the past, however, must start by considering the processes taking place today because these are the processes best understood. Hopefully Precambrian weathering can be understood by assuming different values for the controlling variables or by extrapolating present processes rather than by postulating completely new processes. With this end in view, a brief discussion of the chemical composition of ground and surface waters is introduced here.

3.4.1. Ground Waters

The chemistry of most of the surface and ground waters results from the interaction of rain and rocks near the surface of the earth, usually in the zone of soil formation.

A part of the solutes in surface and ground waters is

supplied by rain water but most of the substances present in these waters come from the weathering of rocks (see Section 3.3).

It is obvious that the chemical composition of these waters is influenced by the same factors that affect the weathering of rocks, that is to say climate, organisms, topography, parent material and time. These factors plus the hydrological environment in a certain region control the amount and type of species present in solutions.

It is important to emphasise that chemical attack is the most important cause of dissolution of minerals from rocks. Chemical attack in turn is governed by the amount of CO_2 present in the vicinity of the waters. Nitric and nitrous acids, produced by the decomposition of organic matter, organic acids produced by living matter, and sulphuric acid, which is produced by oxidation of sulphides also attack rocks, but the most important agent is carbonic acid.

Hydrogen ion, potassium ion and silica concentrations for ground waters from different localities, taken from Yuretich and Cerling (134), Taylor and Royer (135), Paces (136), Hopkins and Petri (137), and Verstraten (111), are given in Appendix 1 and plotted on the activity diagram shown in Fig. 13. Ground water analyses given by Yuretich are from sediments and basalts in the neighbourhood of an alkaline lake. Data taken from Paces relate to ground waters from granitic rocks and arkoses in the Bohemian massif. Chemical analyses for ground waters in Pennsylvania and several counties in South Dakota have been taken from Taylor and Royer and Hopkins and Petri respectively. Water analyses from

Fig. 13: Composition of ground waters plotted on the activity diagram for the system $K_2O-Al_2O_3-SiO_2-H_2O$ at 25°C.

Yuretich and Cerling (134)..... o
Taylor and Royer (135)..... •
Paces (136)..... *
Verstraten (111)..... x
Hopkins and Petri (137)..... +

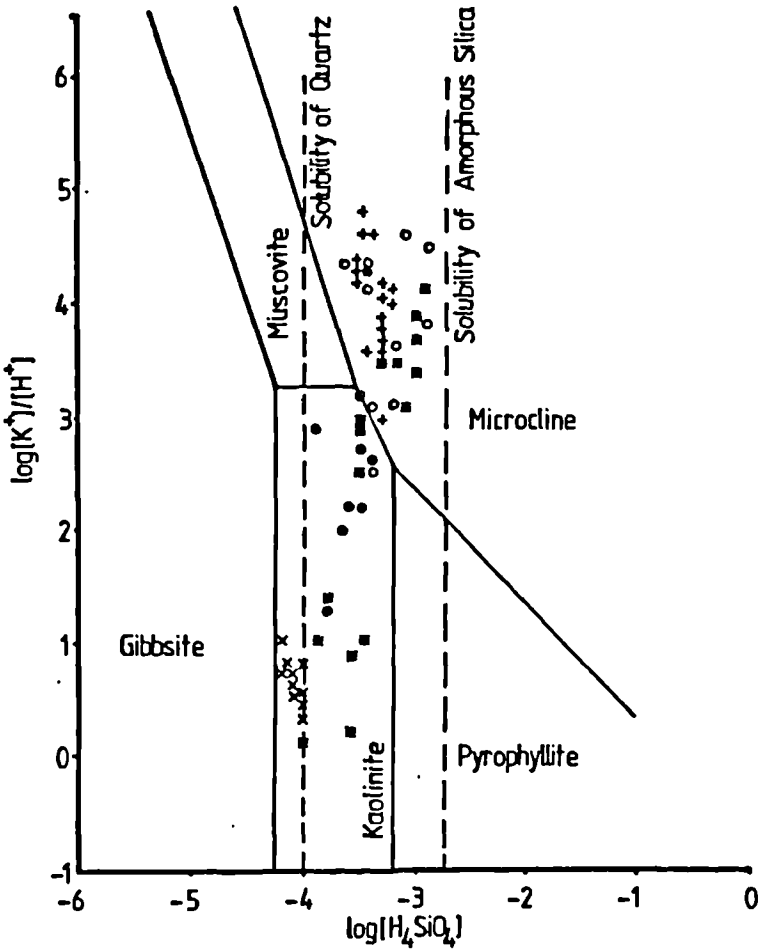

the Ardennes, presented by Verstraten, are here considered as a typical example of present-day soil water interactions in the temperate region. The position of these waters in the diagram suggests that kaolinite and microcline are the minerals that are stable in contact with these waters, the potassium feldspar being stable in the more concentrated alkaline waters, e.g., Yuretich and Cerling (134), Hopkins and Petri (137).

3.4.2. Geothermal Waters

Waters that penetrate deep into the earth may be heated from below by contact with hot rocks or by the ascent of hot emanations, including superheated steam, which raises the temperature of the water which then emerges at the surface of the earth as geysers or as hot springs.

According to Arnorsson et al. (138), the chemical composition of geochemical systems is dynamic and governed by the rate of leaching of the various chemical components from the chemical constituents of the primary rock and the kinetics of the formation and alteration of minerals (138). The composition of the waters, however, is also affected by external variables acting on the system such as temperature and pressure.

Hydrogen ion, silica and potassium concentrations for geothermal waters from Iceland are summarised in Appendix 2 and plotted on the activity diagram shown in Fig. 14. Data have been taken from Arnorsson et al., Tables 1 and 2 (138). Chemical compositions for waters with temperatures outside the range 18-24°C have not been included.

Fig. 14: Composition of geothermal waters plotted on the activity diagram for the system K_2O-Al_2O_3-SiO_2-H_2O at 25°C.

Arnorsson et al. (138)..... o

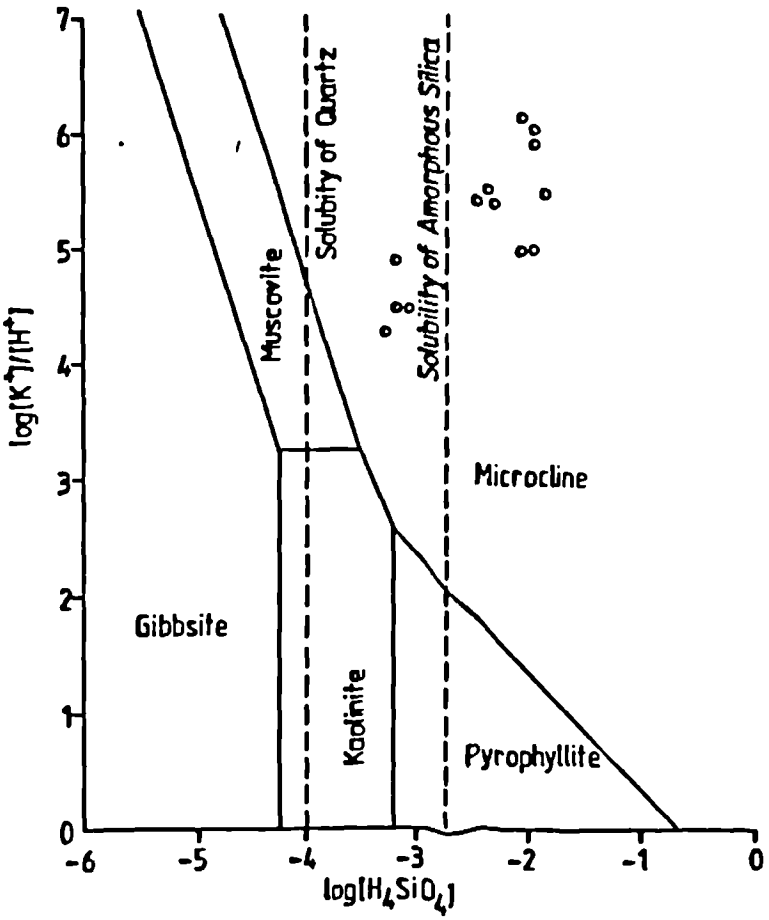

It is clear from Fig. 14 that potassium feldspar is the stable mineral in equilibrium with geothermal waters, and in fact, is one of the minerals with which these waters equilibrate (138).

3.4.3. River and Stream Waters

River and stream water chemistry is more complex than ground water chemistry because it consists of a variable mixture of waters that have reached the channel by different routes. Because ground waters remain in contact with rocks for longer periods of time than stream waters, they generally have a higher concentration of dissolved solids when compared with waters that reach the stream by some surface route or after a short residence in the soil. During dry seasons, the stream flow is dominated by ground water drainage, therefore, the concentration of solutes in the water tends to be high. During wet seasons, this concentration tends to be low because the stream flow is dominated by rain water or subsurface flow so, for most streams, there exists an inverse correlation between discharge and the concentration of total dissolved solids as is illustrated in Fig. 15.

As may be expected, stream water chemistry varies with the geology of the drainage basin, but rivers are a mixture of a variety of waters with different chemical compositions coming from different lithologies. There is also a gross correlation between total dissolved solids and the climate and hydrology. Streams in arid regions tend to have a higher concentration than streams in humid regions. The content of dissolved solids in streams is sometimes increased by concentrated waters coming from mines or oil fields and by the addition of industrial and municipal wastes or drainage

Fig. 15: Variation of totally dissolved solids concentration with stream discharge for the Athi River, Kenya.- [After Dunne and Leopold (139)].

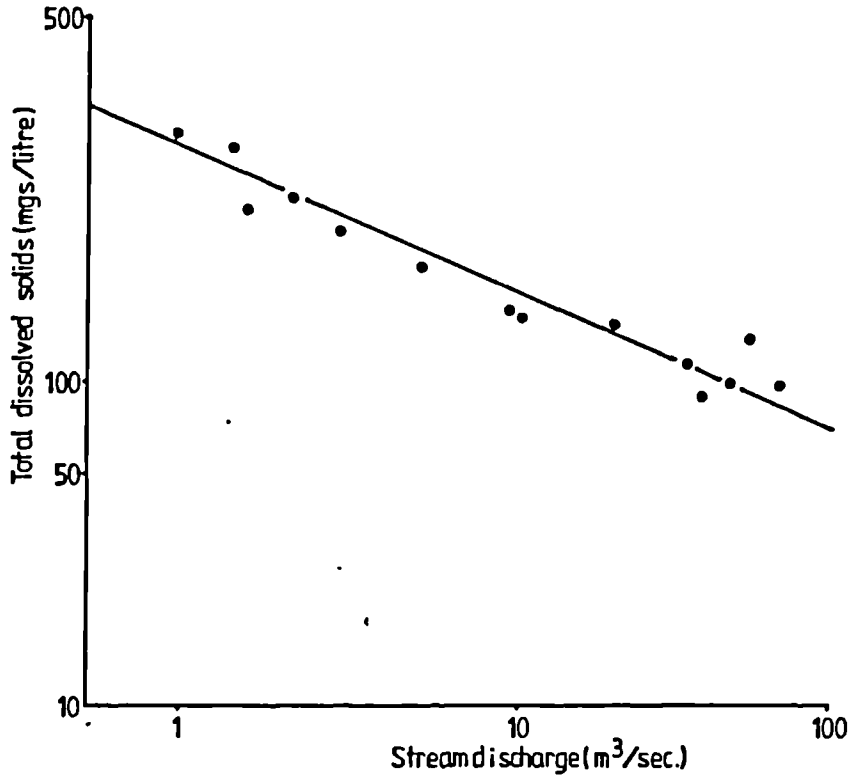

from irrigated lands, although clearly these processes are modern and could not have operated in the geological past.

Hydrogen ion, potassium and silica concentrations for several rivers and streams are summarised in Appendix 3 and plotted on the stability field diagram in Fig. 16. Data for rivers and streams have been taken from Yuretich and Cerling (134), Dunne and Leopold (139), Stallard and Edmond (140), Johnson et al. (125), Keller (141), Love (142-144), Miller (145), Oltman (146), and Verstraten (111). The composition of rivers and stream waters plot in the fields of kaolinite and microcline, indicating that these minerals are stable in these waters.

3.4.4. Lakes

The chemical composition of lakes, like other surface waters, is controlled by three major mechanisms: atmospheric precipitation, rock type and the evaporation-crystallization process (147). Other second-order factors, which may be of local importance are climate, vegetation and human influence (147). However, Feth (148) has criticized this approach as being based upon extrapolation of incomplete data across large regions.

The chemical composition of lakes with drainage may differ greatly from closed ones because, in undrained lakes, only crystallization removes the dissolved load from the lake. Although in most lakes the chemical constituents of their waters do not accumulate beyond the potable range, in some cases, the lake becomes saline. Saline lakes occur because the rate of evaporation is faster than the rate of

Fig. 16: Composition of rivers and stream waters plotted on the activity diagram for the system K_2O-Al_2O_3-SiO_2-H_2O at 25°C.

Stallard and Edmond (140)..... +
Keller (141)..... o
Love (142-144)..... Δ
Miller (145)..... ×
Verstraten (111)..... ●
Dunne and Leopold (139)..... □

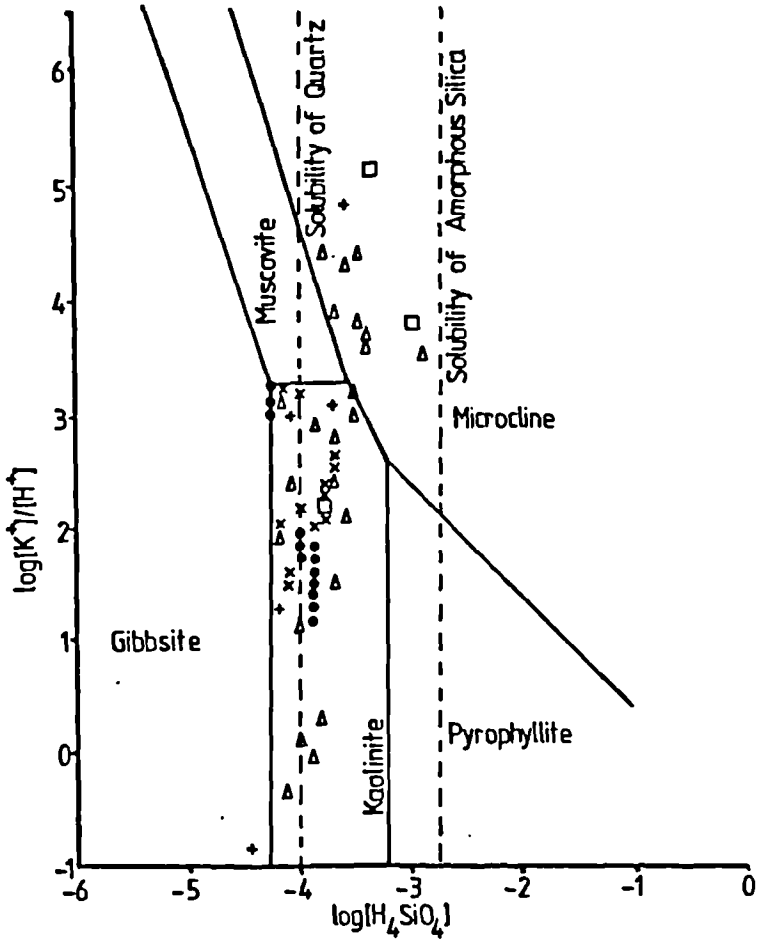

inflow or because the inflow is saline or both.

The net effect of evaporation is to remove pure water from solution so that the concentration of all dissolved species tends to increase. It also involves loss of carbon dioxide as the water approaches equilibrium with the atmosphere. Initially, calcium carbonate starts to precipitate and will continue to do so until virtually all the calcium is removed from the solution. At this stage, removal of magnesium starts by precipitation of dolomite or the silicate sepiolite until essentially all magnesium is consumed (149).

$$Mg^{+2} + 3H_4SiO_4 + 2HCO_3^- = MgSi_3O_6(OH)_2 + 6H_2O + 2CO_2$$

or

$$Mg^{+2} + 2HCO_3^- + CaCO_3 = CaMg(CO_3)_2 + CO_2 + H_2O$$

In either case, there is an increase in alkalinity and the final result of this concentration process is a strongly alkaline solution.

Hydrogen ion, potassium and silica concentrations for some alkaline and fresh-water lakes have been summarised in Appendix 4 and plotted on the stability fields diagram shown in Fig. 17. Chemical analyses of waters from these lakes have been taken from Kharaka et al. (118), Olafsson (150), Yuretich and Cerling (134), Gac et al. (151), Mitten et al. (152), Phillips (153), Eugster and Hardie (119), and Talling and Talling (155).

It can be seen from Fig. 17 that fresh-water lakes

Fig. 17: Composition of waters from fresh and alkaline lakes plotted on the activity Diagram for the system K_2O-Al_2O_3-SiO_2O-H_2O at 25°C.
Data taken from References 118, 119, 134, 150, 151, 152, 153, 155.

Fresh lakes ..... ●
Alakine lakes ... o

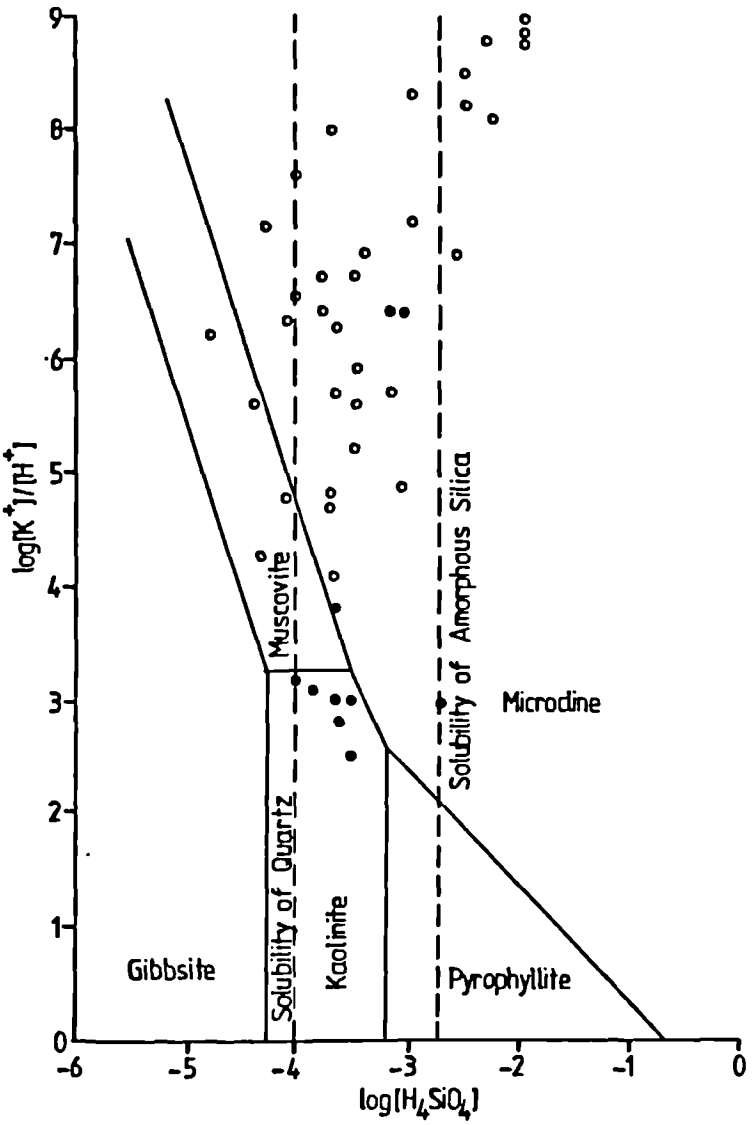

plot in the field of kaolinite and microcline, indicating that these minerals are stable in these waters. Alkaline lakes plot in the field of microcline and muscovite, which means that these minerals are stable in alkaline lakes.

3.4.5. Oceanic Waters

Determination of sodium, potassium, magnesium, calcium, and strontium, carried out on samples of water from the major oceans over many years has led to the conclusion that the concentration of these elements in sea water is constant (156). The ratio of potassium to chlorinity for the major oceans, as given by Riley and Tongudai (156) is shown in Table 1o, to emphasise the previous statement.

The concentration of potassium in normal sea waters is 380 ppm (122, 157, 158). For the purpose of this work, this value of 380 ppm has been accepted and used.

Most variations in the composition of sea water arise from the removal of elements by organisms living in surface sea water and the later release of these elements due to the destruction of biologically produced particles in deeper waters.

Marine plants living in the surface of the seas give off oxygen and extract carbon dioxide and other nutrients from the sea to produce organic matter. Plants are consumed by animals, some of which also extract calcium, and silica to make carbonate or silica shells or tests. During the downward rain of particles produced by plants and animals in surface waters, destruction of organic matter by bacteria and animals release carbon dioxide back into the water column at depth

Table 10: K/Cl ratio for the main oceans and seas of the world.-
[After Riley and Tongudai (156)].

Ocean/Sea	K/Cl
Atlantic	0.0206
Pacific	0.0206
Indian	0.0206
N. Seas	0.0205
S. Seas	0.0206
Mediterranean	0.0206

and consumes dissolved oxygen. Some of these particles dissolve and release dissolved silica after the death of their parent organism and some of them eventually reach the bottom of the sea and accumulate as siliceous sediments. Carbonate particles, on the other hand, are stable in surface waters and accumulate readily in shallow areas of the sea floor, but in deeper waters, where the temperature is low and the pressure is high, they dissolve rapidly in the presence of abundant carbon dioxide from the decomposition of organic matter.

Silicon concentration in oceans is affected by geochemical and biological activity and there is a wide variation in the distribution of this element. However, the general tendency is for an increased silica concentration towards the bottom of the ocean (159). Mainly derived from alteration of silicates from the earth's crust (160-162) its surface concentration is governed by the growth of diatoms and radiolarians, which consume nearly all the soluble surface silica to form their tests. Its concentration varies in the range of 0.02 to 3 ppm for surface waters and around 8-10 ppm for the deep waters of the Pacific Ocean (159).

It has been pointed out before (see Section 3.2.1.) that the acidity of sea water is governed by the ratio of the concentrations of the bicarbonate and carbonate ions

$$[H^+] = K_2 \frac{[HCO_3^-]}{[CO_3^{-2}]}$$

At the present day, this ratio is governed mainly by biological activity in surface waters and the decomposition

Fig. 18: Composition of marine water plotted on the activity diagram for the system $K_2O-Al_2O_3-SiO_2-H_2O$ at 25°C.
Data taken from References 122, 157, 159, 165, 166, 167, 168, 171 and 172.

Oceanic waters ..... o

Interstitial waters ... ●

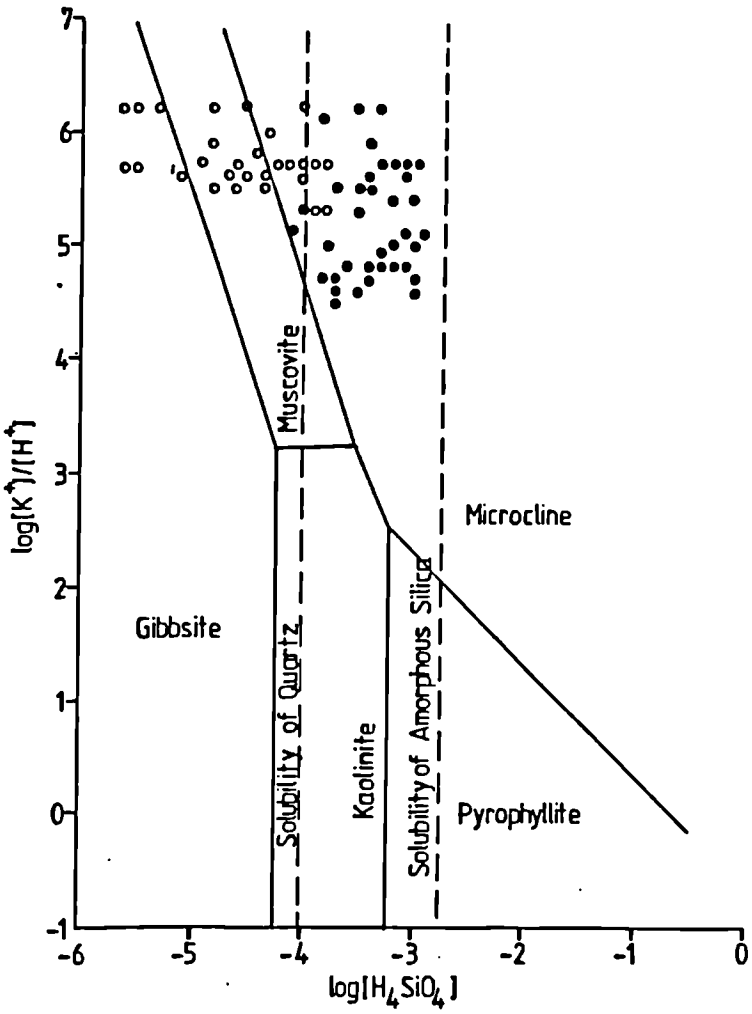

of these surface animals and plants at depth. The result of these processes is the removal of carbon from the surface and its reintroduction at depth. To maintain the same anion-cation balance, the surface water has more of the doubly charged carbonate ion and, hence, it is more alkaline whereas the deep water has more of the singly charged bicarbonate and is more acidic (120). It is also influenced by changes in temperature and gaseous exchange with the atmosphere. Usually, values of pH increase as the temperature rises because the solubility of carbon dioxide falls and the balance of carbonic acid between sea water and the atmosphere reaches equilibrium.

At great depths, sea water is subjected to high pressures under which conditions, the dissociation constants of carbonic acid alter and the result is a further decrease of pH. Values for the pH of surface waters have been reported between 8.0 and 8.3 (163). At great depths in the ocean, pH is lower; values as low as 7.36 (157) and 7.63 (164) have been reported.

Hydrogen ion, potassium and silica concentration for surface and deep oceanic waters are summarised in Appendix 5, and plotted on the stability fields diagram shown in Fig. 18. Data on the chemical analysis of these waters have been taken from: Mackin and Aller (165), Lapedes (122), Fairbridge (157), Fairbridge and Boyle et al. (157, 159), Berner and Shink et al. (166, 167), and Fyfe et al. (168).

Note that oceanic waters plot in the stability fields of gibbsite, muscovite and microcline. Surface oceanic waters, waters with pH 8.0 or over (Appendix 5) plot towards the lower concentrations of silicic acid because these waters

are depleted in silica by the action of diatoms and radiolarians (120, 163).

3.4.6. Interstitial Waters from Marine Sediments

The chemical composition of interstitial solutions of sediments reflects the nature of the original fluids buried with the sediments, and the reactions between the fluid and the solids of the sediments, thus providing a means of studying the early stages of diagenesis of sediments (169, 170).

The interpretation of compositional changes and the identification of reactions is complicated, due to the fact that many reactions may take place at the same time and the composition of these waters records only the net reaction. However, the following diagenetic processes have been identified:

a. dolomitization,
b. recrystallization of calcium carbonate
c. devitrification of silicates,
d. uptake of cations, mainly Mg^{+2} and K^{+}, but also Na^{+}, Ca^{+2}, Li^{+}, by authigenic silicate formation, and
e. replacement of iron in clays by magnesium as a result of sulphate reduction and ion exchange reactions (162).

Hydrogen ion, potassium and silica concentrations for some interstitial waters from marine sediments, taken from Sayles and Manheim (171), and Manheim and Schug (172) are presented in Appendix 6 and plotted on the stability fields diagram illustrated by Fig. 18. It can be appreciated from this figure that they plot in the field of microcline,

revealing that, in such waters, the concentrations of potassium ions, hydrogen ions and silicic acid are those that correspond to equilibrium activities with potassium feldspar.

3.4.7. Minerals Known to Be in Equilibrium with Natural Waters

The identification of the minerals formed during weathering or authigenically formed at normal temperatures is very difficult. The minerals are very fine grained, form complex mixtures, and are difficult to separate. Most soils consist of mixtures of clay minerals, and the residuals of the parent rock, often moved a considerable distance from their original location. Nonetheless, the general picture agrees with the thermodynamic conclusions drawn in the earlier parts of this section.

The formation of clay minerals from feldspars is probably the most important single weathering process of humid environments. Kaolinite is the end product of weathering in an acid environment (24) with good drainage in temperate climates. In alkaline solutions, montmorillonite is the end product. In potassium-rich environments such as alkaline lakes, illite is the stable clay mineral (24).

Illite is the most common clay mineral found in marine sediments suggesting that montmorillonite is slowly converted into illite in the presence of the abundant potassium of sea water (24). Kaolinite and glauconite are also common dominant minerals of some shallow marine sediments.

In tropical climates, weathering goes beyond the

formation of clay minerals because the soil is so leached of bases that the composition of the ground water enters the gibbsite field. The end products of such weathering are ferric and aluminium oxides, giving rise to the so-called lateritic soils (24).

3.5. The Changing Composition of a Water during the Weathering of Potassium Feldspar

During the process, carbon dioxide from the soil atmosphere dissolves in water and attacks potassium feldspar. This process can be represented by one of the following equations:

$$\underset{\text{Microcline}}{KAlSi_3O_8} + CO_2 + 8H_2O = \underset{\text{Gibbsite}}{Al(OH)_3} + HCO_3^- + K^+ + 3H_4SiO_4$$

$$2\underset{\text{Microcline}}{KAlSi_3O_8} + 2CO_2 + 11H_2O = \underset{\text{Kaolinite}}{H_4Al_2Si_2O_9} + 2K^+ + 2HCO_3^- + 4H_4SiO_4$$

$$2\underset{\text{Microcline}}{KAlSi_3O_8} + 2CO_2 + 6H_2O = \underset{\text{Pyrophyllite}}{H_2Al_2Si_4O_{12}} + 2K^+ + 2HCO_3^- + 2H_4SiO_4$$

The carbon dioxide consumed by these reactions is replaced almost immediately from the local soil atmosphere. The production of carbon dioxide by the respiration and decomposition of plants is balanced by its diffusion into the general atmosphere, thus maintaining a constant concentration in the soil atmosphere; hence, the concentration of carbonic acid in the soil water also remains constant. This will be true throughout the weathering process. The dissolution of

Fig. 19: The changing composition of acid and neutral water during the weathering of potassium feldspar.

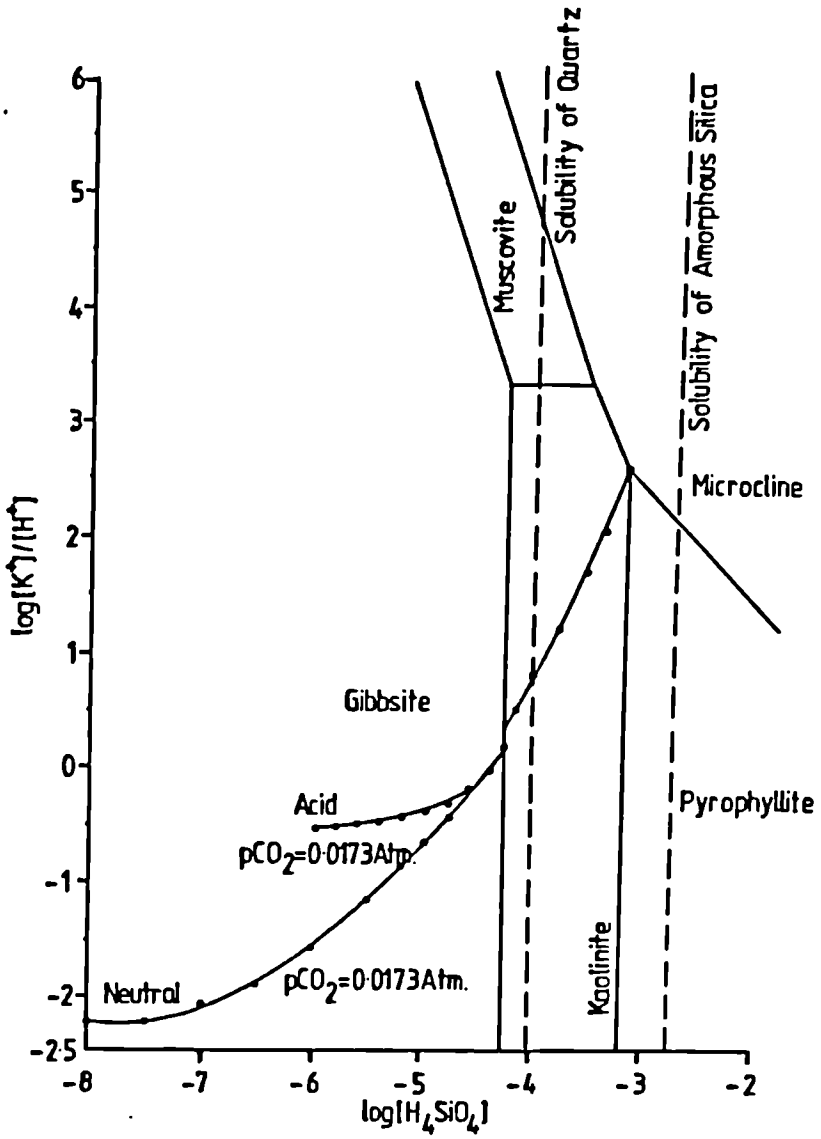

bases (as cations) is balanced by the convertion of carbon dioxide into the bicarbonate ion (an anion) and as the weathering proceeds, the concentration of bicarbonates increases continuously, the carbon being supplied by carbon dioxide from the soil atmosphere. While the carbonic acid concentration remains constant and the bicarbonate concentration increases, the pH increases steadily as weathering continues. Thus, during the weathering process, the concentration of bases, bicarbonate ions and silicic acid increases as the rock dissolves, but the hydrogen ion concentration decreases as the increasing bicarbonate concentration suppresses the ionisation of carbonic acid.

Which one of the three above-mentioned reactions actually occurs depends upon the composition of the soil water. The mineral product is determined by the field in the activity diagram, in which the composition of the water lies. Thus, very acid rain water, with low potassium and silicic acid concentrations, lies in the gibbsite field, and the first reaction takes place. As the weathering proceeds, the increasing silicic acid concentration causes the water to enter the kaolinite field when the second reaction occurs and after more weathering, the pyrophyllite field when the last reaction takes place.

This evolution of ground water is shown in Fig. 19, a diagram which assumes complete equilibrium, all the gibbsite produced in the gibbsite field being converted into kaolinite before the kaolinite field is entered. However, the changes in the concentrations of potassium and hydrogen ions in the ground water due to the conversion of kaolinite to pyrophyllite by the reaction

$$H_4Al_2Si_2O_9 + 2KAlSi_3O_8 + 2H^+ = 2K^+ + 2H_2Al_2Si_4O_{12} + H_2O$$

are such that only a small proportion of the kaolinite previously generated has been converted to pyrophyllite when the composition of the aqueous phase reaches the triple point where microcline is stable and further reaction ceases.

This discussion assumes that the ground water stays in contact with the feldspar long enough to reach equilibrium. In normal weathering, this will not happen and the water would be removed whilst it is still in the kaolinite field. This is because the amount of gibbsite produced is very small and pyrophyllite is produced only in the last stages of the process.

The mathematical equations used for these calculation are very simple if it is assumed that only one mineral is being weathered. This is not very likely in real weathering but it is a reasonable approximation for a Lewisian gneiss composed mainly of quartz and microcline because the quartz would be attacked very slowly. To calculate the path shown in Fig. 19, it was assumed that weathering had proceeded to a point represented by a certain silicic acid concentration (S). This was enough to determine which field was being considered and hence determine the stable mineral. The potassium concentration was then calculated:

$$[K] = k_o + (S - S_o)/n$$

where k_o equals the concentration of potassium in rain water, and S_o equals the concentration of silica also in rain water. The constant n represents the number of moles of silicic acid generated in the weathering reaction for each

mol of potassium produced, i.e., for gibbsite: n = 3, for kaolin: n = 2, and for pyrophyllite: n = 1 (see the chemical equations given at the beginning of this section).

The rain water initially contained free acid as well as potassium and silicic acid. The amount of anions required to balance the potassium and hydrogen cations in the rain water was given the symbol "a". It is now possible to calculate the pH from the two equations:

$$[HCO_3^-] + a = [H^+] + [K^+]$$

$$[H^+] = \frac{[CO_2] \times 10^{-7.76}}{[HCO_3^-]}$$

let $b = a - [K^+] = a - K_o - (S - S_o)/n = [H^+] - [HCO_3^-]$

and $c = [CO_2] \cdot 10^{-7.76}$

then $b = [H^+] - [HCO_3^-] = [H^+] - \frac{c}{[H^+]}$

hence $$[H^+]^2 - b[H^+] - c = o$$

$$[H^+] = \frac{b + \sqrt{b^2 + 4c}}{2}$$

The numbers required for the two axes of the activity diagram (viz., $[K^+]/[H^+]$ and $H_4SiO_4 = S$) can now be obtained.

The results of these calculations, Appendixes 7-10, and Figures 19 and 20, show that potassium feldspar will usually weather to kaolinite and will produce pyrophyllite only when the concentration of carbon dioxide in the soil atmosphere is very high (lower curve Fig. 20). Waters produced in this way will never pass through the muscovite field because the concentration of carbon dioxide in the ground water would be so low (10^{-5}% CO_2), that weathering would be very slow.

Illite (a clay mineral with a composition and structure close to muscovite) is a very common product of weathering from potassium feldspar and several of the natural waters discussed in Section 3.4. were in equilibrium with this mineral. However, these waters have been produced by evaporation, e.g. sea water, and alkaline lakes. It is also possible to produce illite from the weathering of basalts and other mafic rocks, which contain minerals, e.g. olivine, that produce a large amount of bicarbonate and a small concentration of silicic acid:

$$Mg_2SiO_4 + 4CO_2 + 4H_2O = 2Mg(HCO_3)_2 + H_4SiO_4$$

This will move the lines on the activity diagram nearer the muscovite field. However, Lewisian gneiss does not contain such minerals and can only produce muscovite by evaporation of the ground waters.

It has been emphasised throughout this chapter that the rate of weathering is increased as the concentration of carbonic acid dissolved in water increases. It has also been pointed out that the amount of carbon dioxide present in the soil atmosphere is higher than the amount of carbon dioxide present in the general atmosphere and that this is due to

Fig. 20: The changing composition of a water during the weathering of potassium feldspar at two different carbon dioxide concentrations.

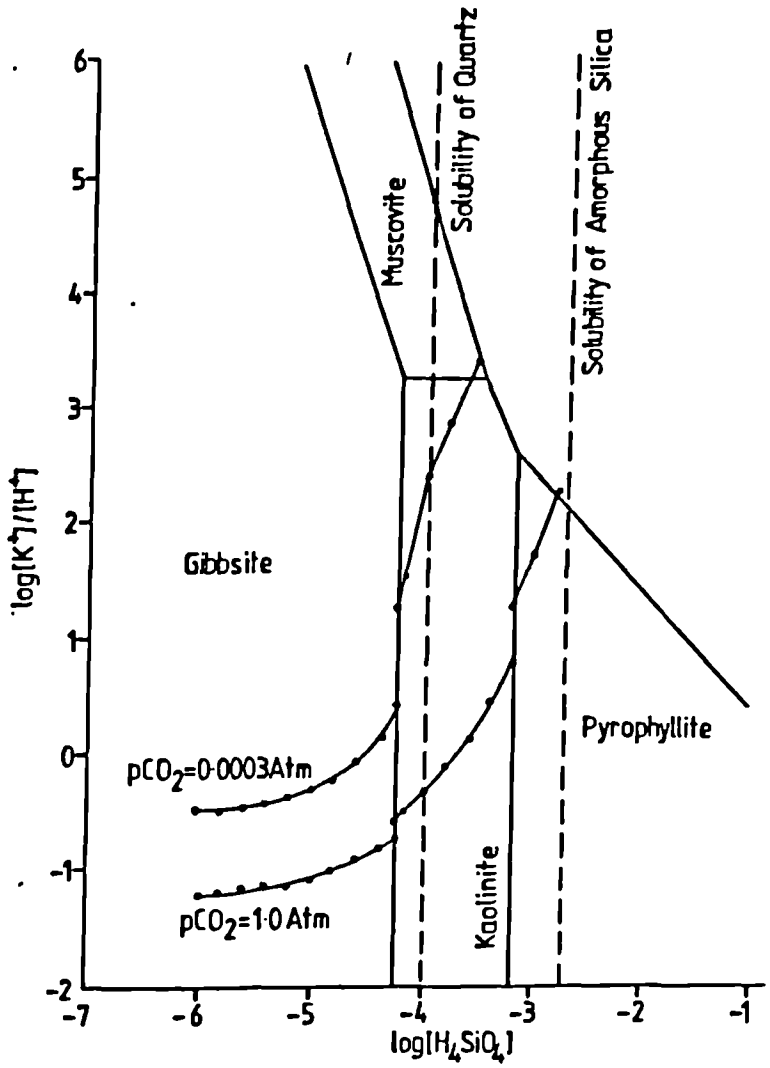

biological activity. Since in the Precambrian land plants had not yet evolved, the concentration of carbonic acid dissolved in waters must have been lower. Hence the rate at which weathering occurred must have been lower too. This assumes that marine plants had evolved sufficiently to remove the carbon dioxide present in the primitive atmosphere, which is assumed to have occurred by the end of the Precambrian (173). Weathering probably proceeded under alkaline conditions.

CHAPTER IV

RESULTS AND DISCUSSION

4.0. Introduction

In simple terms, weathering has been considered as the disintegration or decay of rocks in situ. Ollier (28) has defined it in more complex terms as "The breakdown and alteration of materials near the earth's surface to products that are more in equilibrium with newly imposed physicochemical conditions".

Weathering processes are complex, and few generalizations can be made about the rate of weathering due to the numerous factors that influence them. However, climate, and physical and chemical composition of the bedrock are of great significance. Weathering processes are accelerated by the reaction between acid water and the mineral constituents of the rocks. Acid waters result mainly from the dissolution of carbon dioxide, which in turn is produced chiefly by the respiration of plants, degradation of organic matter and bacterial action.

In the Precambrian Lewisian, terrestrial plants had not evolved [they did not appear until the Devonian (174)]. In the absence of plants, the amount of carbon dioxide present in the soil atmosphere was relatively low. Therefore, the rate at which weathering occurred was probably lower than it is today. The different sections of this chapter will show that the weathering profile, which developed in the Lewisian rock beneath the Cambrian unconformity, is similar to weathering profiles being developed in present day weathering

Fig. 21: Map of Northwest Scotland showing the Cambrian, Lewisian and Torridonian rocks and the five localities sampled.

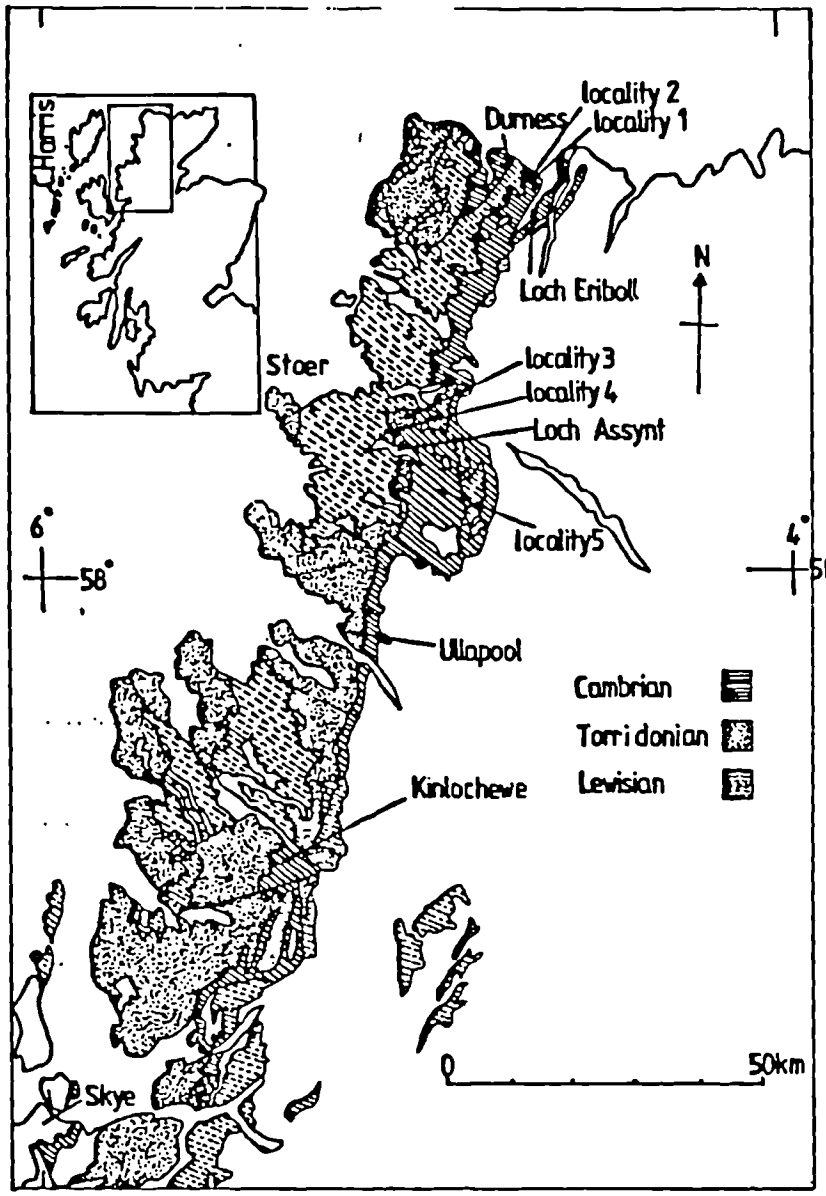

and it will be concluded that weathering processes in the Precambrian were similar to modern weathering processes in arid regions.

Thermodynamic interpretation of chemical and mineralogical analyses of fresh and weathered gneisses leads to the conclusion that potassium feldspar was first weathered to kaolinite, or smectite (potassium beidellite), which was later converted to illite by evaporated ground waters. These minerals were subsequently converted, at the higher temperatures produced by subsequent burial, to the minerals observed in the samples, viz., illite to muscovite (sericite) and kaolinite (or potassium beidellite) to pyrophyllite and quartz.

4.1. Collection of the Samples

Samples for this investigation were collected from several localities (see Fig. 21). In the neighbourhood of Durness, two localities were selected:

a. Locality One, (NC 438 661), close to a telegraph hut, southwest of Rispond, and

b. Locality Two, (NC 441 658), on the beach close to Rispond.

In the neighbourhood of Loch Assynt, two further localities were also selected:

c. Locality Three, (NC 240 292), close to Loch Na Gainmhich, and

d. Locality Four, (NC 222 256), east of Loch Na Dunaiche.

Finally, samples of Fucoid Beds were taken from

e. Locality Five, (NC 250 157), in the neighbourhood of Loch Awe.

Sample number, classification and distance from the unconformity for the samples (where measurable) are given in Table 11.

4.2. Nature of the Samples

Samples from locality one are granitic gneiss and muscovite, whereas samples from locality two are mainly granitic gneiss and pegmatites (see Table 11). The sample from locality three is a Lower Cambrian green shale. The Torridonian samples from locality four are sandstones, and the Fucoid Beds from locality five are argillites and dolomites.

Although five localities were sampled, the most important samples for this project are from localities one and two, where the rocks immediately beneath the unconformity could be sampled (see Fig. 21). A view of locality two on the beach close to Rispond is shown in Fig. 22. In this locality, the Cambrian overlies the Lewisian with a remarkable planar unconformity, which can be seen at the entrance to the cave shown in Fig. 23.

Field inspection of this locality will confirm that the Lewisian gneiss consists of at least two kinds of material:

Fig. 22: View of locality two looking west where the Cambrian overlies the Lewisian.

Fig. 23: Entrance to the cave showing the unconformity between the Cambrian and the Lewisian.

felsic bands and mafic bands. Both felsic and mafic bands have been sampled although sampling of the mafic band was not very successful, as will be shown later.

Major and trace element analyses performed on the samples from these five localities by X-ray fluorescence spectrometry are summarised in Tables 12, 13, 14 and 15. Ferrous oxide, carbon dioxide, water, and specific gravity (SG) are also included in these tables (see Section 4.3.). Accuracy, precision, and detection limits for major and trace elements are given in Appendixes. 11 and 12, respectively.

4.3. Results of the Chemical Analyses

Table 11: Sample number, classification and other characteristics for each of the forty-three samples included in this investigation.

Sample No.	Classification	Locality*	D.f.U.	Other Comments
1	Dolomite	5	-	
2	Argillite	5	-	
3	Dolomitic Arg.	5	-	
4	" "	5	-	Not analysed
5	Green Shale	3	-	
6	Granitic Gneiss	1	ind.	
7	" "	1	ind.	
8	" "	1	ind.	
9	Massive Msc.	1	ind.	
10	Granitic Gneiss	1	ind.	
11	Intermediate Gn.	2	2.0	
12	" "	2	2.5	
13	" "	2	3.0	
14	" "	2	4.0	
15	" "	2	5.0	
16	Granitic Gneiss	2	1.0	
17	" "	2	2.0	
18	" "	2	3.5	
19	" "	2	5.0	
20	Granitic Pegm.	2	1.5	
21	Amphibolite	2	3.0	
22	"	2	5.0	
23	Granitic Gneiss	2	4.0	
24	" "	2	3.0	
25	" "	2	2.0	
26	" "	2	1.0	
27	" "	2	0.0	
28	Sandstone	4	0.0	Torridonian
29	"	4	0.7	Cambrian
30	"	4	1.6	Unconformity
31	"	4	4.1	
32	"	4	5.8	Torridonian
33	"	4	8.5	Sandstones
34	"	4	5.8	
35	"	4	0.0	
36	Intermediate Gn.	2	14.0	
37	" "	2	14.0	
38	Granitic Pegm.	2	14.0	
39	Amphibolite	2	14.0	
40	Granitic Gneiss	2	11.0	

Table 11 (cont.)

Sample No.	Classification	Locality*	D.f.U.	Other Comments
41	" "	2	7.0	
42	" "	2	7.0	
43	Gneiss + Pegm.	2	50.0m	

* Locality 1 Map Reference NC 438 661
" 2 " " NC 441 658
" 3 " " NC 240 292
" 4 " " NC 222 256
" 5 " " NC 250 157

Abbreviations:

D.f.U. = Distance from Unconformity
Arg. = Argillite
Msc. = Muscovite
Gn = Gneiss
Pegm. = Pegmatite
ind. = indeterminate

Table 12: Major and trace element analysis plus H_2O, FeO, CO_2, and specific gravity for Fucoid Bed samples.- Localities 3 and 5. *, ^.

	1	2	3	5
SiO_2	10.31	59.60	51.39	53.34
TiO_2	0.08	0.68	0.51	0.98
Al_2O_3	2.40	17.91	11.26	29.17
Fe_2O_3	3.35	1.62	0.63	1.72
FeO	3.44	2.15	1.61	0.15
MnO	0.23	0.04	0.09	0.01
MgO	15.12	1.95	5.09	0.68
CaO	24.82	0.26	7.42	0.05
Na_2O	0.13	0.03	0.09	0.07
K_2O	1.22	11.99	8.92	9.16
P_2O_5	0.46	0.15	0.15	0.05
H_2O	0.64	1.95	0.89	4.38
CO_2	36.84	0.67	11.44	0.15
Total Fe	7.18	4.01	2.42	1.88
T O T A L	99.04	99.00	99.49	99.91
Zr	90	212	355	317
Y	26	25	20	15
Sr	2650	82	92	121
U	0	2	2	2
Rb	24	176	84	160
Th	3	17	4	11
Pb	1	9	5	5
Ga	8	19	11	47
Zn	b.d.l.	26	5	7
Cu	10	4	1	b.d.l.
Ni	2	25	9	27
Co	2	12	1	2
Cr	14	77	46	440
Ce	53	102	66	86
Ba	54	687	621	671
La	12	52	30	49
S.G.	2.94	2.70	2.70	2.82

b.d.l. = below detection limits. S.G. = Specific Gravity.

* = Major constituents given as a percentage of weight of the sample dried at 110°C.

^ = Trace elements are given in p.p.m.

Table 13: Major and trace element analysis plus H_2O, FeO, CO_2 and specific gravity for the felsic band samples.- Localities 1 and 2. *, ^.

	6	7	8	9	10	16
SiO_2	71.73	75.84	61.55	47.32	54.93	57.57
TiO_2	0.14	0.06	0.91	0.04	1.05	0.44
Al_2O_3	15.85	12.93	25.17	34.39	23.55	30.73
Fe_2O_3	1.64	0.57	1.08	1.23	4.05	0.73
FeO	0.31	0.05	0.04	0.08	0.71	0.01
MnO	0.01	0.01	0.00	0.02	0.02	0.01
MgO	0.84	0.49	0.37	0.50	1.86	0.32
CaO	0.02	0.10	0.02	0.04	0.02	0.02
Na_2O	0.17	0.76	0.12	0.17	0.04	0.13
K_2O	8.64	9.20	7.66	10.97	9.60	4.55
P_2O_5	0.01	0.01	0.02	0.01	0.02	0.02
H_2O	1.45	0.36	2.99	4.22	3.74	4.77
CO_2	0.21	0.06	0.18	0.15	0.18	0.13
Total Fe	1.98	0.62	1.12	1.32	4.84	0.75
TOTAL	101.02	100.44	100.11	99.14	99.77	99.43
Zr	38	29	196	20	192	150
Y	2	1	3	2	6	5
Sr	154	272	45	24	11	11
U	1	1	1	3	2	3
Rb	144	138	81	168	180	57
Th	b.d.l.	b.d.l.	0	3	0	b.d.l.
Pb	21	33	1	39	b.d.l.	b.d.l.
Ga	21	15	28	47	44	27
Zn	8	2	b.d.l.	26	6	b.d.l.
Cu	2	4	b.d.l.	2	0	b.d.l.
Ni	7	b.d.l.	24	b.d.l.	72	9
Co	b.d.l.	b.d.l.	b.d.l.	b.d.l.	6	4
Cr	b.d.l.	0	167	b.d.l.	862	17
Ce	3	5	34	2	95	8
Ba	755	1082	85	323	298	36
La	b.d.l.	5	23	3	43	3
S.G.	2.69	2.61	2.78	2.86	2.85	2.83

Table 13 (cont.)

	17	18	19	20	23	24
SiO_2	60.13	61.08	66.03	70.66	66.75	64.41
TiO_2	0.92	0.31	0.21	0.04	0.23	0.25
Al_2O_3	25.89	21.45	16.52	20.75	17.07	17.11
Fe_2O_3	1.34	3.23	1.23	0.44	1.37	1.33
FeO	0.01	0.50	0.46	0.01	0.56	0.58
MnO	0.01	0.02	0.02	0.00	0.02	0.02
MgO	0.45	1.45	1.02	0.27	1.39	1.37
CaO	0.02	0.03	0.13	0.06	0.03	0.11
Na_2O	0.27	0.02	0.37	0.04	0.12	0.17
K_2O	7.60	7.74	12.41	3.81	11.32	12.33
P_2O_5	0.03	0.02	0.05	0.20	0.02	0.07
H_2O	3.50	3.43	1.08	2.80	1.42	1.23
CO_2	0.07	0.08	0.03	0.09	0.04	0.16
Total Fe	1.35	3.78	1.74	0.45	1.99	1.97
TOTAL	100.24	99.36	99.56	99.17	100.34	99.14
Zr	174	122	97	29	106	117
Y	14	18	4	15	7	8
Sr	36	28	81	1136	67	91
U	3	1	2	1	1	1
Rb	98	207	169	49	158	164
Th	4	1	b.d.l.	b.d.l.	b.d.l.	b.d.l.
Pb	1	1	3	14	4	4
Ga	28	24	12	26	16	17
Zn	b.d.l.	36	24	1	20	17
Cu	b.d.l.	2	b.d.l.	2	5	3
Ni	21	17	8	b.d.l.	10	11
Co	5	9	3	b.d.l.	5	1
Cr	47	10	1	b.d.l.	2	7
Ce	52	24	11	141	24	12
Ba	47	384	486	31	586	734
La	40	22	2	81	8	5
S.G.	2.80	2.79	2.63	2.75	2.68	2.65

Table 13 (cont.)

	25	26	27	40	41	42
SiO_2	66.15	64.21	55.56	71.02	64.49	69.11
TiO_2	0.34	0.57	0.76	0.21	0.37	0.07
Al_2O_3	22.72	24.84	30.08	13.96	17.42	15.76
Fe_2O_3	0.32	0.36	0.27	0.84	1.46	0.61
FeO	0.01	0.01	0.01	0.72	0.65	0.14
MnO	0.01	0.01	0.01	0.02	0.02	0.01
MgO	0.32	0.35	0.34	0.95	1.54	0.59
CaO	0.02	0.06	0.03	0.11	0.20	0.06
Na_2O	0.11	0.31	0.00	0.24	0.23	1.12
K_2O	6.86	4.89	8.70	11.15	11.31	12.25
P_2O_5	0.05	0.19	0.02	0.06	0.12	0.04
H_2O	2.87	3.49	3.91	0.65	1.95	0.82
CO_2	0.13	0.12	0.05	0.25	0.05	0.08
Total Fe	0.33	0.37	0.29	1.64	2.18	0.76
TOTAL	99.91	99.41	99.74	100.18	99.81	100.66
Zr	145	299	163	133	99	40
Y	11	42	3	10	3	9
Sr	161	1177	23	139	88	87
U	3	0	3	4	1	2
Rb	83	76	90	163	115	104
Th	7	19	5	12	b.d.l.	32
Pb	4	4	3	28	5	9
Ga	27	23	35	11	19	17
Zn	b.d.l.	b.d.l.	b.d.l.	15	16	b.d.l.
Cu	b.d.l.	7	2	4	b.d.l.	1
Ni	0	1	0	4	12	b.d.l
Co	b.d.l.	b.d.l.	1	1	3	b.d.l
Cr	11	17	40	9	12	2
Ce	72	142	37	46	13	76
Ba	42	37	44	1117	425	298
La	79	33	19	27	5	38
S.G.	2.77	2.78	2.82	2.63	2.68	2.61

b.d.l. = below detection limits. S.G. = Specific Gravity.

* = Major constituents given as a percentage of weight of the sample dried at 110°C.

^ = Trace elements are given in p.p.m.

Table 14: Major and trace element analysis plus H_2O, FeO, CO_2 and specific gravity for the Torridonian sandstones.- Locality 4. *, ^.

	28	29	30	31	32	33
SiO_2	86.44	83.00	84.54	84.19	82.69	83.25
TiO_2	1.38	0.19	0.20	0.01	0.26	0.16
Al_2O_3	6.24	8.87	7.61	8.03	8.17	8.01
Fe_2O_3	0.90	0.60	0.90	1.03	1.84	1.55
FeO	0.05	0.06	0.07	0.07	0.07	0. 7
MnO	0.01	0.01	0.02	0.01	0.04	0.04
MgO	0.42	0.52	0.48	0.44	0.49	0.49
CaO	0.03	0.03	0.03	0.03	0.07	0.02
Na_2O	0.01	0.07	0.04	0.03	0.03	0.02
K_2O	3.45	6.17	5.59	5.79	5.62	5.69
P_2O_5	0.03	0.02	0.02	0.04	0.05	0.04
H_2O	0.78	0.73	0.76	1.12	0.78	0.70
CO_2	0.09	0.06	0.11	0.11	0.11	0.17
Total Fe	0.95	0.67	0.98	1.10	1.92	1.61
TOTAL	99.83	100.33	100.37	100.90	100.22	100.21
Zr	959	79	87	58	103	76
Y	23	8	7	8	13	9
Sr	60	89	90	94	92	94
U	4	2	2	1	1	1
Rb	47	90	84	95	88	84
Th	10	b.d.l.	1	1	1	1
Pb	7	6	5	5	8	8
Ga	5	10	6	7	9	7
Zn	5	2	b.d.l.	4	9	1
Cu	49	11	31	b.d.l.	b.d.l.	b.d.l.
Ni	6	2	3	4	6	3
Co	6	2	b.d.l.	b.d.l.	1	0
Cr	43	17	12	8	21	34
Ce	78	22	34	46	36	56
Ba	453	766	975	757	705	705
La	36	12	16	24	17	28
S.G.	2.65	2.64	2.63	2.64	2.61	2.63

Table 14 (cont.)

	34	35
SiO_2	79.47	92.98
TiO_2	0.38	0.37
Al_2O_3	9.77	3.90
Fe_2O_3	2.75	0.52
FeO	0.11	0.05
MnO	0.00	0.02
MgO	0.60	0.35
CaO	0.03	0.03
Na_2O	0.36	0.05
K_2O	6.79	1.98
P_2O_5	0.02	0.02
H_2O	1.01	0.47
CO_2	0.10	0.16
Total Fe	2.87	0.58
TOTAL	101.39	100.90
Zr	142	237
Y	9	7
Sr	84	43
U	3	2
Rb	102	25
Th	4	b.d.l.
Pb	11	1
Ga	10	3
Zn	2	3
Cu	4	8
Ni	6	0
Co	b.d.l.	b.d.l.
Cr	27	72
Ce	26	29
Ba	792	319
La	17	17
S.G.	2.67	2.61

b.d.l. = below detection limit. S.G. = Specific Gravity.

* = Major constituents given as a percentage of weight of the sample dried at 110°C.

^ = Trace elements are given in p.p.m.

Table 15: Major and trace element analysis plus H_2O, FeO, CO_2 and specific gravity for samples from the basic band. Localities 1 and 2. *, ^.

	11	12	13	14	15	21
SiO_2	48.56	46.45	39.83	50.45	43.37	48.21
TiO_2	1.72	1.77	1.63	1.41	1.71	0.67
Al_2O_3	29.95	30.66	26.64	23.92	27.79	14.13
Fe_2O_3	2.76	2.84	3.89	3.63	3.84	3.29
FeO	0.37	0.49	8.76	4.62	4.34	7.37
MnO	0.01	0.00	0.02	0.02	0.02	0.21
MgO	1.26	1.18	4.07	2.73	2.68	9.91
CaO	0.05	0.02	0.06	0.07	0.05	8.18
Na_2O	0.33	0.22	0.16	0.28	0.00	1.27
K_2O	9.46	10.90	7.70	7.39	9.59	2.28
P_2O_5	0.04	0.02	0.04	0.04	0.03	0.05
H_2O	4.07	4.41	6.31	4.82	5.41	2.70
CO_2	0.18	0.14	0.12	0.24	0.27	0.09
Total Fe	3.17	3.38	13.62	8.77	8.67	11.48
TOTAL	98.76	99.10	99.23	99.62	99.10	98.36
Zr	98	100	110	81	97	48
Y	25	27	26	13	13	19
Sr	16	9	11	23	6	68
U	2	4	4	1	5	2
Rb	115	139	103	105	141	76
Th	b.d.l.	0	0	1	0	2
Pb	0	2	1	3	b.d.l.	1
Ga	37	29	24	35	25	13
Zn	1	b.d.l.	25	14	23	65
Cu	7	33	75	38	2	134
Ni	390	183	634	203	130	135
Co	37	17	230	102	72	53
Cr	463	410	361	369	303	243
Ce	9	17	10	0	12	6
Ba	138	179	136	121	179	205
La	14	5	6	6	3	b.d.l.
S.G.	2.83	2.89	2.90	2.91	2.91	3.00

Table 15 (cont.)

	22	36	37	38	39	43
SiO_2	47.76	57.04	70.93	67.62	43.14	71.16
TiO_2	0.66	0.55	0.26	0.21	1.15	0.24
Al_2O_3	13.96	18.13	15.57	17.58	16.01	14.69
Fe_2O_3	3.21	1.65	0.70	1.46	10.90	0.52
FeO	7.39	4.06	0.92	0.79	3.65	1.00
MnO	0.22	0.09	0.02	0.03	0.22	0.03
MgO	10.31	4.35	1.01	0.96	8.42	0.10
CaO	9.13	3.55	1.86	2.37	8.67	1.64
Na_2O	1.89	4.77	5.85	5.58	1.61	3.07
K_2O	1.24	2.39	1.37	2.19	2.95	5.57
P_2O_5	0.05	0.16	0.01	0.08	0.06	0.07
H_2O	2.41	1.51	0.28	0.75	2.24	0.57
CO_2	0.04	0.06	0.11	0.10	0.12	0.01
Total Fe	11.43	6.17	1.73	2.34	14.96	1.62
TOTAL	98.27	98.31	98.89	99.72	99.14	98.67
Zr	48	117	94	102	83	153
Y	18	12	3	3	26	5
Sr	156	304	227	441	210	549
U	1	1	b.d.l.	1	1	2
Rb	27	65	29	38	72	118
Th	b.d.l.	0	b.d.l.	0	b.d.l.	8
Pb	7	10	9	12	14	12
Ga	13	21	16	19	20	15
Zn	86	81	20	19	170	21
Cu	105	10	b.d.l.	4	8	5
Ni	133	79	1	2	93	8
Co	62	19	0	b.d.l.	52	b.d.l.
Cr	235	111	23	22	132	4
Ce	0	24	11	9	12	75
Ba	105	295	224	142	325	1726
La	b.d.l.	10	10	3	b.d.l.	45
S.G.	3.00	2.76	2.67	2.67	3.12	2.66

b.d.l. = below detection limit. S.G. = Specific Gravity.

* = Major constituents are given as percentage by weight of the sample dried at 110°C.

^ = Trace elements are given in p.p.m.

4.4. The Kronberg Weathering Diagram

Kronberg and Nesbit (175) have proposed a diagram for the quantification of present-day weathering in terms of two molar ratios: the ratio $(CaO + Na_2O + K_2O)/(Al_2O_3 + CaO + Na_2O + K_2O) = y$, as a measure of the degree of breakdown of feldspars, and the ratio $(SiO_2 + CaO + Na_2O + K_2O)/(Al_2O_3 + SiO_2 + Na_2O + K_2O + CaO) = x$, as a measure of the enrichment during weathering of silicon and aluminium oxide in phases such as quartz, kaolinite and gibbsite.

The diagram is illustrated in Fig. 24. The point y=1, x=1 represents the pure bases, pure K_2O in the case of this investigation. The point y=0, x=1.0 represents pure silicon oxide. The point y=0, x=0 represents pure aluminium oxide.

Currently, values of y and x for fresh rocks are around 0.5 and 0.9. These rocks contain a large amount of bases, which are steadily removed by weathering as soluble bicarbonates. The analysis of waters therefore reveals a large proportion of bases in the residue after evaporation (175), whereas the rocks that are left behind are depleted in bases and move down towards the point y=0, x=0, with more aluminium and more silica and less bases. As the weathering proceeds, more and more bases are washed away, until eventually all the bases are removed and silica starts to be removed. If the weathering process goes on undisturbed for long periods of time under good drainage conditions, silicon oxide is also totally removed and the resulting weathering product is pure aluminium oxide and iron oxide, characteristic of the lateritic soils commonly found in tropical environments. Such rocks will be represented on the diagram close to the point x=0, y=0.

Fig. 24: Kronberg weathering diagram for Lewisian gneiss from the felsic band.- The lines represent the limits of present-day weathered gneiss.

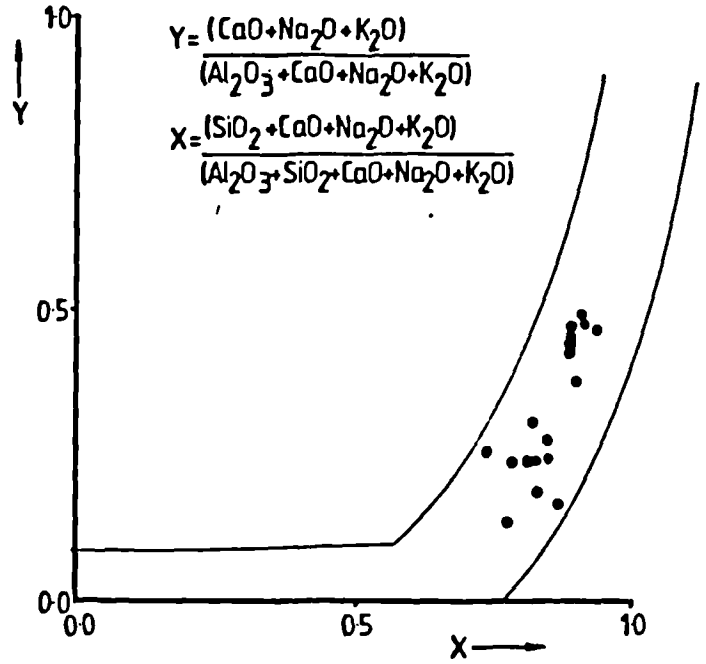

Fig. 25: Kronberg weathering diagram for Torridonian sandstones.

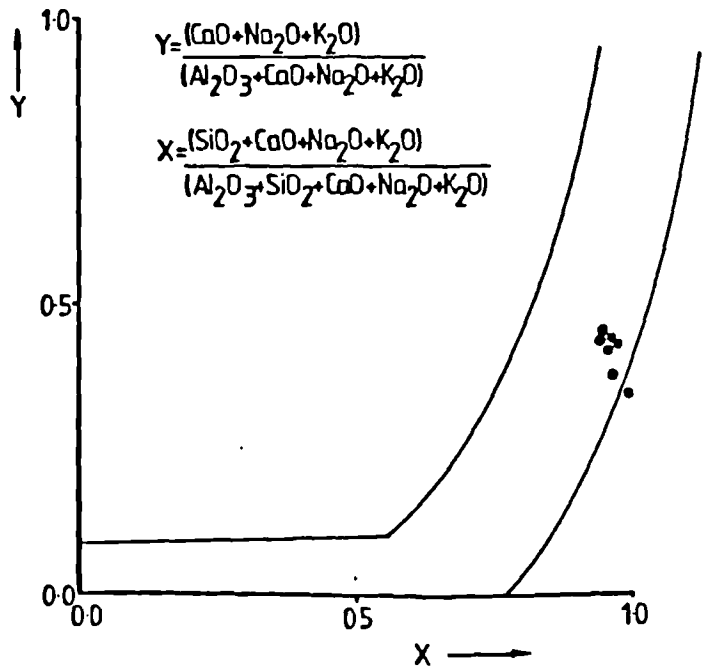

Table 16: Values x and y ratios for Lewisian gneiss from the felsic band.

Sample No.	x	y	Sample No.	x	y
6	0.89	0.38	20	0.86	0.17
7	0.92	0.47	23	0.88	0.42
8	0.82	0.25	24	0.88	0.45
9	0.73	0.26	25	0.84	0.25
10	0.81	0.31	26	0.82	0.19
16	0.77	0.14	27	0.78	0.24
17	0.81	0.25	40	0.91	0.48
18	0.84	0.28	41	0.88	0.43
19	0.88	0.46	42	0.90	0.49

The molar ratios calculated from the chemical analysis of our samples of Lewisian gneiss are shown in Table 16 and plotted in Fig. 24. It can be seen in the figure that there is a group of rocks with y values around 0.45. These are the unweathered gneiss, which contain a large proportion of potassium feldspar. Moving down the diagram, there is a group of samples with y values around 0.25. Their composition is mainly mica and quartz. Further down the diagram, there is another group of samples with the lowest y values, around 0.15. They are composed mainly of mica and pyrophyllite. At this stage, potassium feldspar has been fully removed from the samples, which are very close to the unconformity.

This fits very well with the present-day weathering path and shows that the section of the rock sampled is actually a weathering profile.

Similarly, y and x values for the Torridonian sandstones are shown in Table 17 and plotted in Fig. 25. Note that in contrast to x and y values for the Lewisian gneiss, x and y values for these rocks do not follow the chemical weathering path. The unweathered rocks do lie within the band of compositions of present-day chemically weathered rocks, but as we go down the sequence towards the most weathered sample, they move away from the chemical weathering path. As the weathering goes on, bases are washed away and aluminium goes into very fine-grained clay minerals. These Torridonian sandstones are river deposits and, as the sandstones are transported, the fine aluminous clay particles are removed, leaving deposits of nearly pure quartz. Therefore, the Torridonian sandstones follow the mechanical weathering path.

A plot of y (bases over bases plus alumina) against

Fig. 26: Chemical change versus depth of weathering.

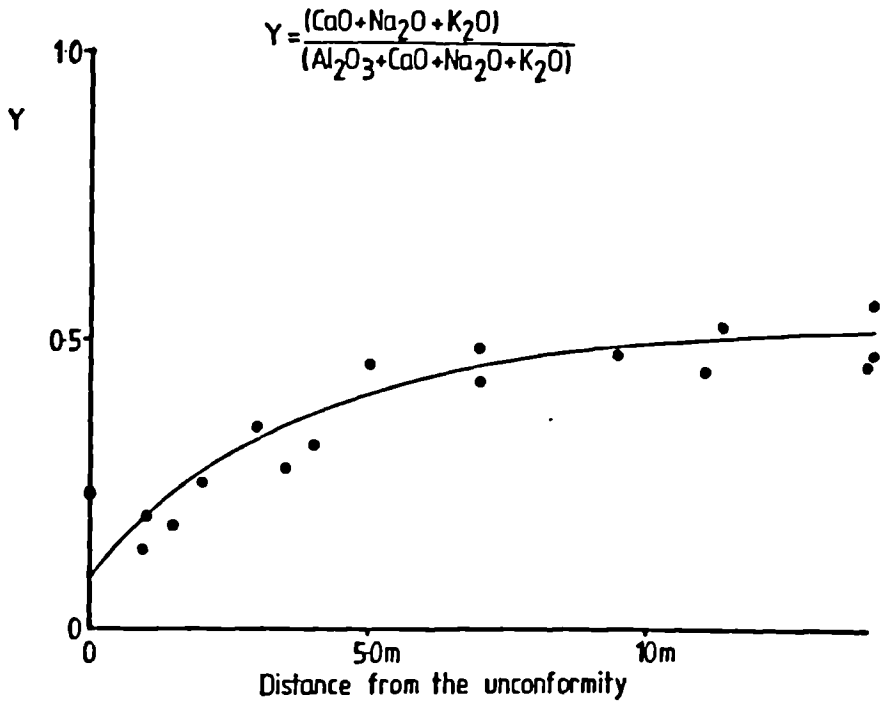

Table 17: Values x and y ratios for the Torridonian sandstones.

Sample No.	x	y	Sample No.	x	y
28	0.96	0.38	32	0.95	0.43
29	0.94	0.44	33	0.95	0.44
30	0.95	0.44	34	0.94	0.45
31	0.95	0.44	35	0.98	0.37

Table 18: Values of y ratios and distance from the unconformity for the Lewisian gneiss from the felsic band.

Sample No.	y	D.f.U.	Sample No.	y	D.f.U.
6	0.38	-	20	0.17	1.5
7	0.47	-	23	0.42	4.0
8	0.25	-	24	0.45	3.0
9	0.26	-	25	0.25	2.0
10	0.31	-	26	0.19	1.0
16	0.14	1.0	27	0.24	0.0
17	0.25	2.0	40	0.48	11.0
18	0.28	3.5	41	0.43	7.0
19	0.46	5.0	42	0.49	7.0

D.f.U. = Distance from Unconformity.

depth of the sample (distance from the unconformity) is shown in Fig. 26. It can be seen that samples closer to the unconformity (the weathering surface) are more weathered than samples away from the unconformity. Distances from the unconformity and values of y are summarised in Table No. 18.

The position of the profile just below the unconformity; the nature of the chemical changes observed; a loss of potassium and silica (the greatest loss being from the shallowest samples); and the similarity of the weathering diagram to that of modern weathering; all of these indicate that the samples represent a fossil soil, although not necessarily an unchanged one.

4.5. The Chemical Composition of Weathered Gneiss

The chemical composition of weathered gneiss taken at 5.0m, 3.5m, 2.0m and 1.0m beneath the Cambrian unconformity in the longest and most distinct feldspathic zone is given in Table 19 and illustrated in Fig. 27. The sample collected at 1.0m from the unconformity belongs to the most weathered material, whereas the sample taken at 5.0m is nearest to the parent material. It can be seen that the amount of aluminium present in the rocks increases from the sample at 5.0m (the parent material) to the sample at 1.0m (the weathered rock). Unlike the aluminium oxide, the potassium oxide decreases from the parent material to the weathered material. A decrease in silicon oxide is also observed. This is exactly what happens in present-day weathering and is reproduced in the weathering of these Precambrian gneiss.

The important point to note, however, is the small size of the shaded area in the figure (Fig. 27). This represents

Fig. 27: Chemical composition of weathered gneiss taken at various distances from the Cambrian unconformity.

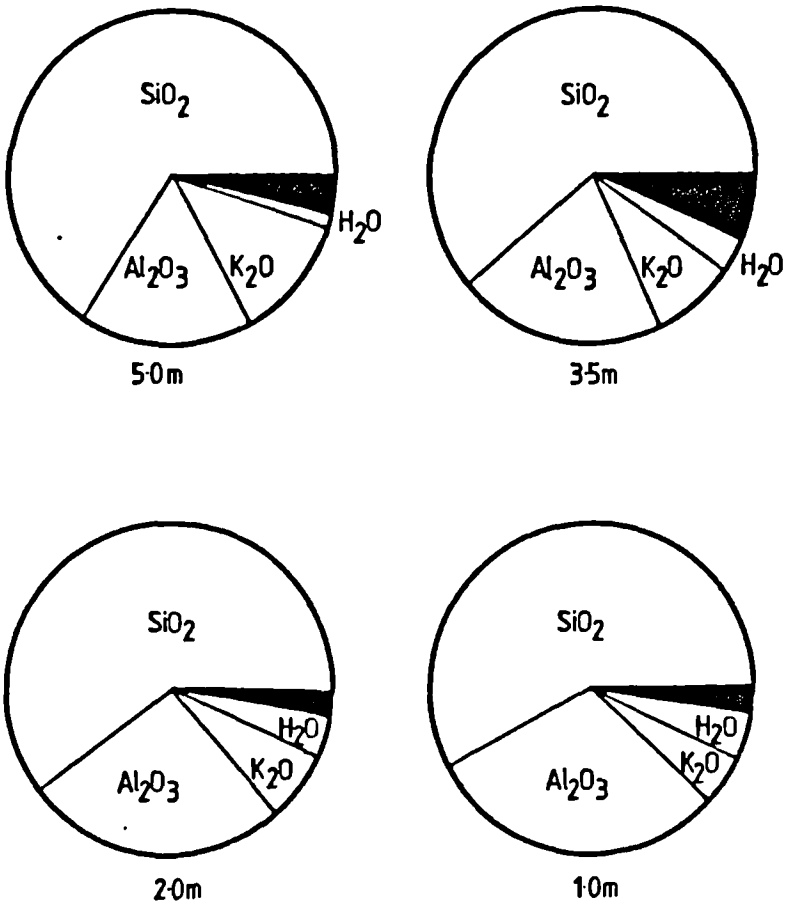

Table 19: Chemical composition of four samples taken at various distances beneath the Cambrian unconformity.

Oxides	5.0m	3.5m	2.0m	1.0m
SiO_2	66.03	61.08	60.13	57.57
TiO_2	0.21	0.31	0.92	0.44
Al_2O_3	16.52	21.45	25.89	30.73
Fe_2O_3	1.23	3.23	1.34	0.73
FeO	0.46	0.50	0.01	0.01
MnO	0.02	0.02	0.01	0.01
MgO	1.02	1.45	0.45	0.32
CaO	0.13	0.03	0.02	0.02
Na_2O	0.37	0.02	0.27	0.13
K_2O	12.41	7.74	7.60	4.55
P_2O_5	0.05	0.02	0.03	0.02
H_2O	1.08	3.43	3.50	4.77
CO_2	0.03	0.08	0.07	0.13
T O T A L	99.56	99.36	100.24	99.43

Fig. 28: Chemical composition of rocks and minerals from the weathering profile.

+ Rocks

o Minerals

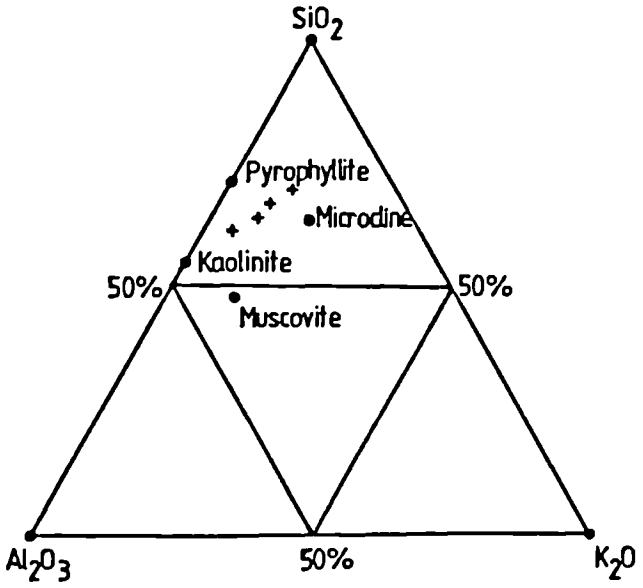

the remaining components of the rock except water. It can be seen that the rocks are mainly made of silicon oxide, aluminium oxide, potassium oxide and water. Such a four component system can be represented in three dimensions, and projected onto a triangular diagram (22), similar to the one shown in Fig. 28. The chemical composition of the minerals kaolinite ($H_4Al_2Si_2O_9$), pyrophyllite ($H_2Al_2Si_4O_{12}$), microcline ($KAlSi_3O_8$), muscovite ($H_2KAl_3Si_3O_{12}$), and quartz (SiO_2), which occur in this system, are also shown in this diagram. This simple diagram results from the simplicity of the chemical composition of the parent gneiss (i.e., absence of sodium, calcium, and magnesium) and enables a more comprehensible discussion of the thermodynamics of the weathering reactions to be made.

4.6. The Mineral Composition of the Weathered Gneiss

A mineralogical analysis of the samples (16, 17, 18 and 19) described in the previous section from the most suitable feldspathic zone was performed by X-ray diffraction and polarized light microscopy. Two estimates of the proportions of the minerals present in the samples were made: the first by semi-quantitative X-ray diffraction and the second by a normative calculation from the chemical analysis. The results of the mineralogical analysis are summarised in Table 20 and the estimated proportions of the minerals in Table 21. It follows from the qualitative and semi-quantitative mineralogical results that the parent material, the furthest sample from the unconformity, is mainly made of quartz, microcline, and a small amount of muscovite. There is very little change in the mineral composition of the samples between 2.0m and 3.5m below the unconformity, and which are

Table 20: Qualitative mineralogical analysis of gneiss taken at various distances from the Cambrian unconformity
++ = mineral is abundant in the sample. + = mineral present in the sample in relatively large amounts. (+) = scarcely distinguishable under the microscope
- = not seen under microscope.

D.f.U.	Quartz	Pyroph.	Muscov.	Microcl.
5.0m	++	-	(+)	++
3.5m	++	-	++	-
2.0m	++	-	++	-
1.0m	+	++	++	-

Table 21: Semi-quantitative mineralogical analysis of gneiss taken at various distances from the Cambrian unconformity

Sample No.	D.f.U.	Quartz		Pyroph.		Muscov.		Mcr.	
		1	2	1	2	1	2	1	2
19	5.0	32.0	16.0	0.0	0.0	42.0	9.0	26.0	64.0
18	3.5	19.0	31.0	6.0	0.0	76.0	51.0	0.0	7.0
17	2.0	19.0	27.0	2.0	4.0	79.0	63.0	0.0	0.0
16	1.0	7.0	2.0	31.0	56.0	62.0	37.0	0.0	0.0

1) Results from X-ray diffraction analysis.

2) Estimated from the chemical analysis.

D.f.U. = Distance from unconformity.

mainly made of quartz and muscovite. Potassium feldspar disappears in the sample closest to the unconformity and a large amount of pyrophyllite is present instead.

Some of the microphotographs taken from thin sections of the samples are shown in Figs. 29, 30 and 31. The presence of potassium feldspar, quartz and a small amount of mica can be seen in Fig. 29, which represents the fresh gneiss or parent material. The next figure (Fig. 30) shows the presence of fresh and altered potassium feldspar, which is being converted into muscovite (sericite) by the weathering process.

Pyrophyllite can be seen in Fig. 31; note that it appears in contact with muscovite and quartz as if it were produced by a reaction between muscovite and quartz. It will be seen later in this chapter that this is not in agreement with the thermodynamic predictions.

The presence of pyrophyllite was unexpected. However, the chemical analysis of sample 16, with an excess of aluminium over muscovite and the absence of kaolinite, and the X-ray diffraction pattern supported by the microscopic identification, are conclusive. Further evidence is given in Table 22, which shows an electron microprobe analysis of the mineral in thin section.

A graphic representation of the weathering profile has been drawn (Fig. 32), which summarises the above comments. It can be concluded from the Kronberg diagram that these rocks actually represent a weathering profile. Nevertheless, there is a difficulty: there should not be any pyrophyllite since this is metastable at the assumed weathering temperature

Fig. 29: Photomicrograph of a fresh gneiss showing potassium feldspar (K), quartz (Q), and small amounts of muscovite (M) and biotite (B).- Sample 19.

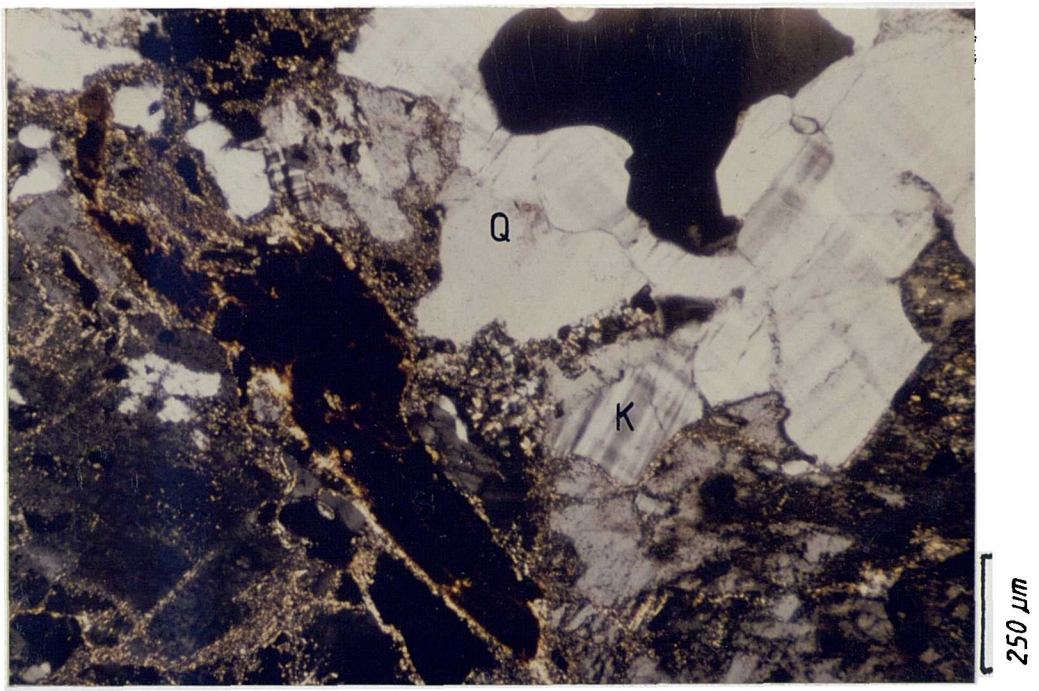

Fig. 30: Photomicrograph of an altered gneiss showing fresh (K) and partially altered potassium feldspar (K^1).- Sample 19.

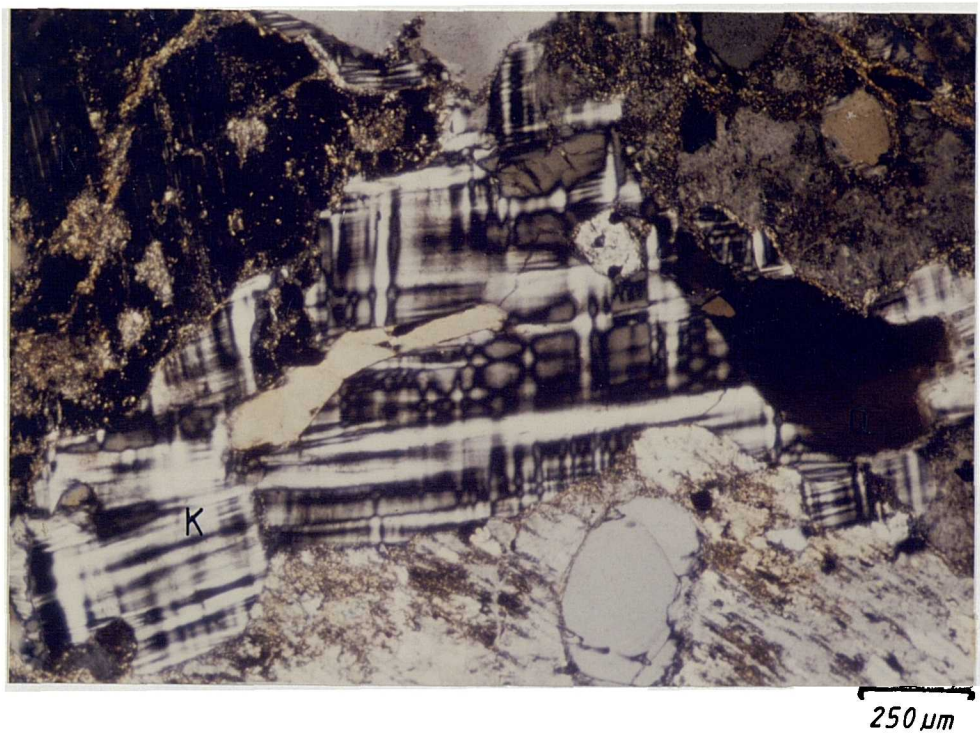

Fig. 31: Photomicrograph of an altered gneiss showing pyrophyllite (P), quartz (Q) and muscovite (M).- Sample 20.

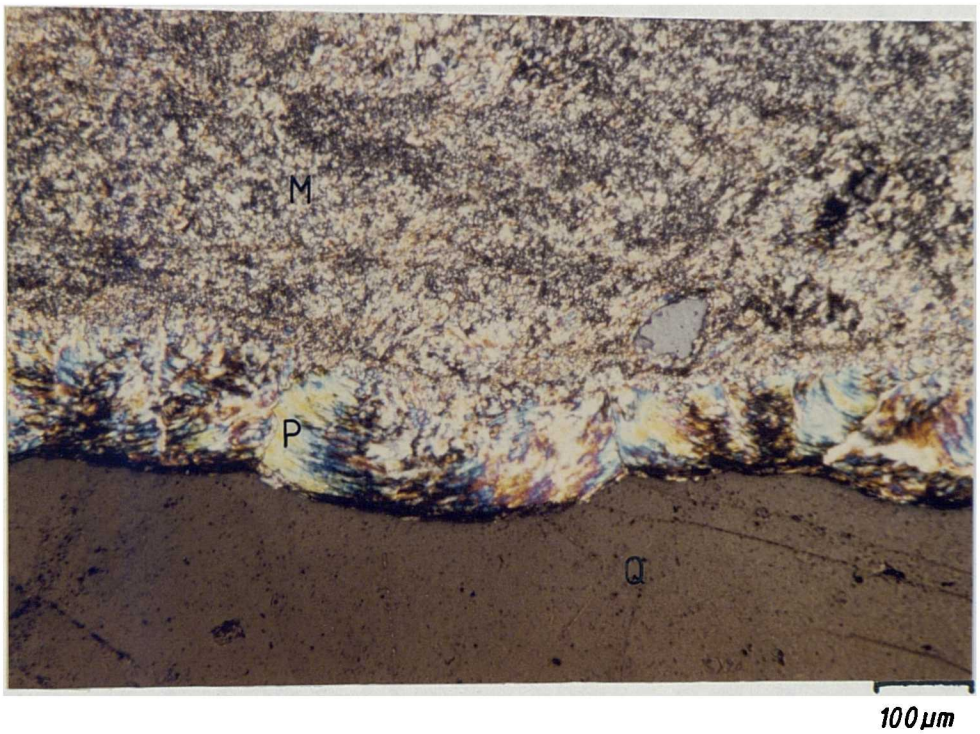

Table 22: Microprobe analysis of pyrophyllite.- Sample 26.

% Oxides	Experimental	Theoretical
K_2O	0.0375	-
Na_2O	0.1111	-
CaO	0.0143	-
MgO	0.0077	-
MnO	0.0085	-
Al_2O_3	27.9882	28.2918
Fe_2O_3	0.0942	-
SiO_2	65.1631	66.7081
H_2O	-	5.0000
T O T A L	93.4264	99.9999

(25°C) and there is geological evidence (Section 4.8.) that these rocks have not been heated much above 200°C, which is too low to affect conversion of kaolinite and quartz to pyrophyllite.

When the composition of all of the weathered gneiss samples from the felsic band are included in the triangular diagram (Fig. 33), although a general trend towards the pyrophyllite field can be discerned, the situation becomes very confused. This is due to the very variable amount of quartz in the parent gneiss (see Table 13).

The situation is also theoretically ambiguous because a line showing stable associations of minerals can either be drawn from quartz to muscovite or from pyrophyllite to microcline, as illustrated in Figures 34A and 34B. Note that, in the system represented in Fig. 34A, pyrophyllite and microcline do not form a stable association, while in the system represented in Fig. 60B they do.

In the reaction

$$KAlSi_3O_8 + H_4Al_4Si_8O_{24} = 2H_2KAl_3Si_3O_{12} + 8SiO_2$$

Microcline Pyrophyllite Muscovite Quartz

microcline reacts with pyrophyllite to give muscovite and quartz or vice versa. The composition diagram changes from Fig. 34A, on the right of the reaction, to Fig. 34B, on the left of the reaction.

The free energies of formation for the minerals involved in the above reaction are summarised in Table 6. ΔG°_r,

Fig. 32: Weathering profile from the Cambrian unconformity.

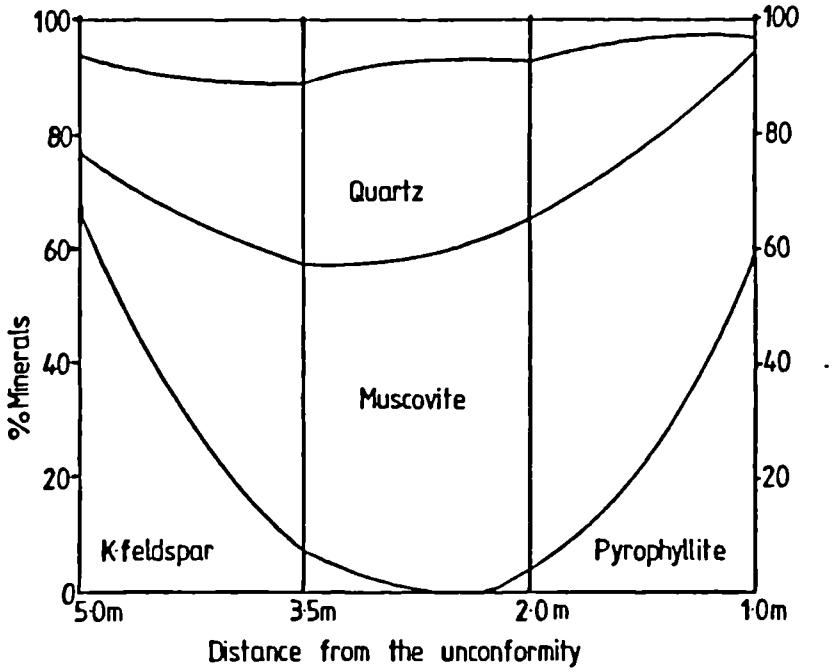

the free energy of the reaction worked out from these values(*) gives a value of -1,262,785 calories, indicating that muscovite and quartz should exist together. In other words, the thermodynamic calculation suggests that the composition diagram of Fig. 34A represents the natural equilibrium at all conceivable temperatures and pressures.

4.7. Comparison of the Mineral Composition of Weathered Feldspathic Gneiss with the Thermodynamic Composition Diagram

The mineralogical analysis of all the samples of the fresh and the weathered gneiss taken from the felsic band is given in Table 23 and illustrated in Fig. 35. All samples contain muscovite and quartz. There is a group of samples, marked as x in Fig. 35, that contain potassium feldspar. There is a group of samples, marked as ⊙ in the same figure that contain pyrophyllite, but none of the samples contain both pyrophyllite and potassium feldspar. As has been pointed out when discussing the thin section, the parent material (Fig. 29) consists mainly of potassium feldspar, and quartz, with minor muscovite and biotite. The muscovite present in the original material is well crystallized but uncommon. The muscovite seen in the weathered samples (Figs.

(*) $\Delta G^{\circ}_{r} = G^{\circ}_{f}$ products $- G^{\circ}_{f}$ reactants

$\Delta G^{\circ}_{r} = (2\ G^{\circ}_{f}$ muscovite $+ 8\ G^{\circ}_{f}$ Quartz) $-$

$- (2\ G^{\circ}_{f}$ microcline $+\ G^{\circ}_{f}$ pyrophyllite

$\Delta G^{\circ}_{r} = [2(-1,336,301) + 8(-204,616] - [2(-895,374) +$

$(-1,255,997)]$

$\Delta G^{\circ}_{r} = -1,262,785$ calories

Fig. 33: The composition of fresh and altered gneiss taken from the felsic band.

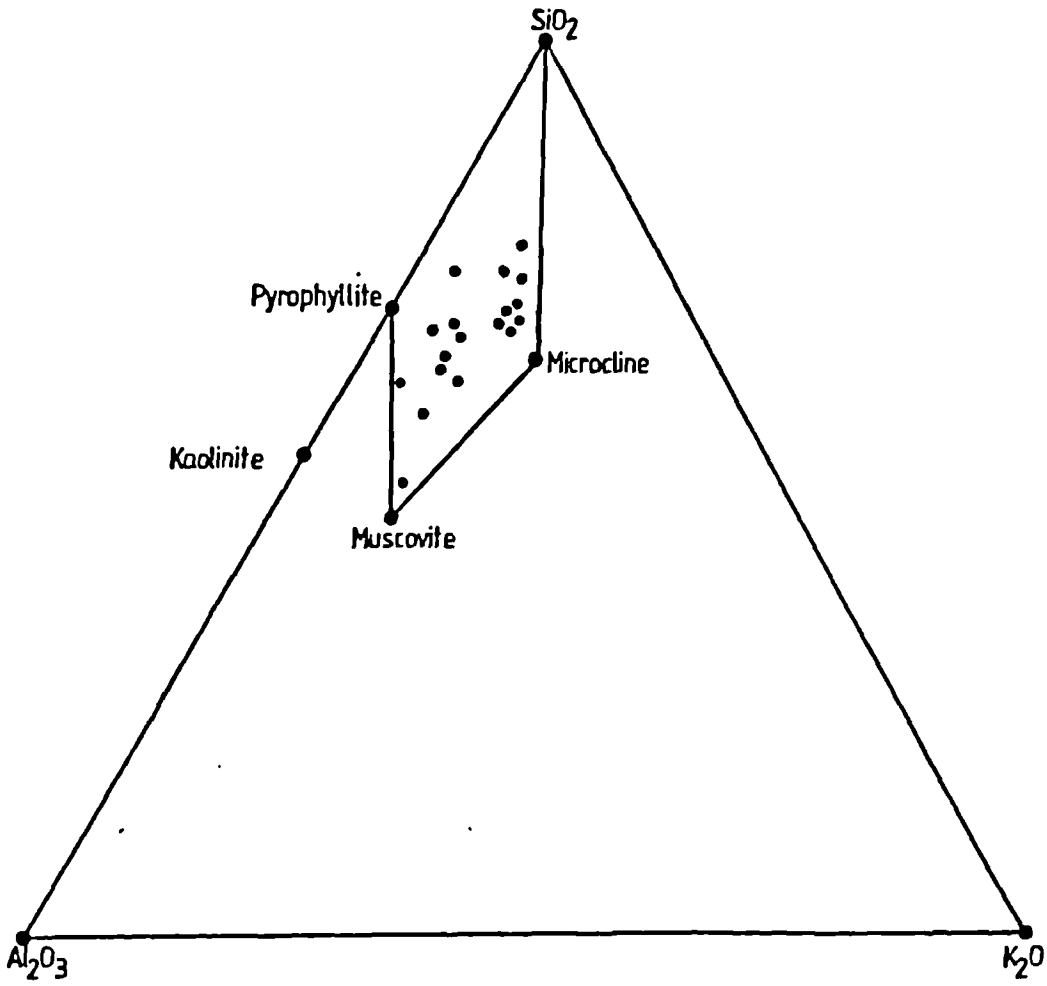

Fig. 34: Two different stable associations of the minerals quartz, pyrophyllite, microcline, and muscovite.

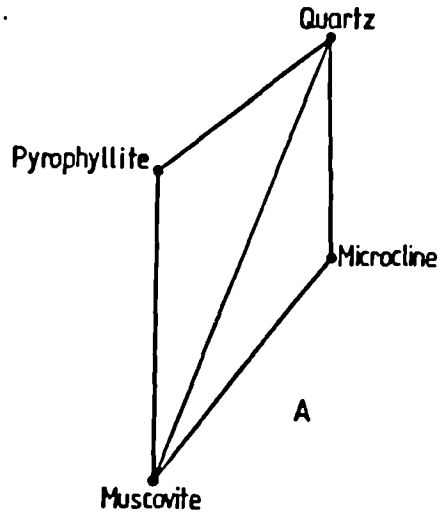

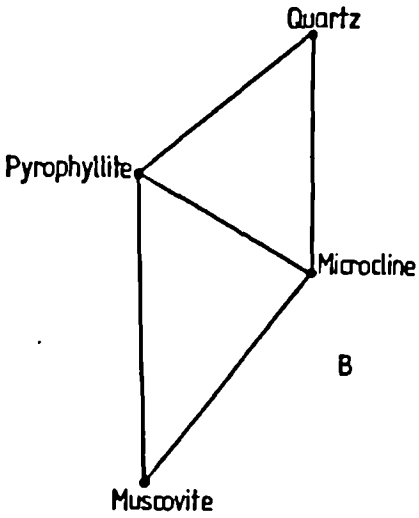

Table 23: Mineralogical analysis of the Lewisian gneiss from the felsic band.-

++ = the mineral is abundant in the sample. + = mineral present in the sample in relatively large amounts. (+)= the mineral is scarcely distinguished under the microscope. - = mineral not seen under the microscope.

Sample No.	D.f.U.*	K-feld.	Msc.	Qtz.	Pyroph.
6	ind.**	++	++	++	-
7	"	++	-	++	-
8	"	-	++	++	-
9	"	-	++	++	-
10	"	-	++	++	-
16	1.0	-	++	+	++
17	2.0	-	++	++	-
18	3.5	-	++	++	-
19	5.0	++	(+)	++	-
20	1.5	-	++	++	++
23	4.0	++	++	++	-
24	3.0	++	++	+	-
25	2.0	-	++	++	-
26	1.0	-	++	++	++
27	0.0	-	++	++	+
40	11.0	++	++	++	-
41	7.0	++	++	++	-
42	7.0	++	+	++	-

* = Distance from unconformity.

** = indeterminate.

30 and 31) is sericite. Fresh and sericitised feldspar, which is being converted into muscovite, can be seen in the same section (Fig. 30).

From these results, it is clear that, as the samples progress from barely altered gneiss (Samples 6, 7, 19, 23, 24, 40, 41, 42) to partly altered gneiss (Samples 8, 9, 10, 17, 18, 25), the potassium feldspar is converted into muscovite and disappears. Further weathering gives samples with pyrophyllite (16, 20, 26, 27), all of which were taken close to the unconformity. These results agree with the thermodynamic predictions given in the previous section viz potassium feldspar and pyrophyllite are incompatible and before pyrophyllite can appear as a weathering product, all the microcline must be converted into muscovite.

However, the diagram shown in Fig. 34B corresponds to a closed system at a temperature of about 350°C. At some temperature below this (see next section), pyrophyllite becomes unstable with respect to quartz and kaolinite in the closed system. It is still possible for pyrophyllite to be formed as a weathering product, however, because the silica activity of natural waters often exceeds that of quartz (see Chapter III, Section 3.1.2.).

4.8. The Stability of Pyrophyllite

The lower limit of the stability field of pyrophyllite is given by its formation from kaolinite and quartz, whereas the upper limit is marked by its breakdown to andalusite plus quartz (or kyanite plus quartz); in both cases, high pressures have been used in the experiments to measure these limits (176). Work on the lower limit of pyrophyllite before

Fig. 35: Comparison of the mineralogical composition of weathered gneiss with the thermodynamic composition diagram.

x = Samples containing potassium feldspar

⊙ = Samples containing pyrophyllite

● = samples containing neither potassium feldspar nor pyrophyllite.

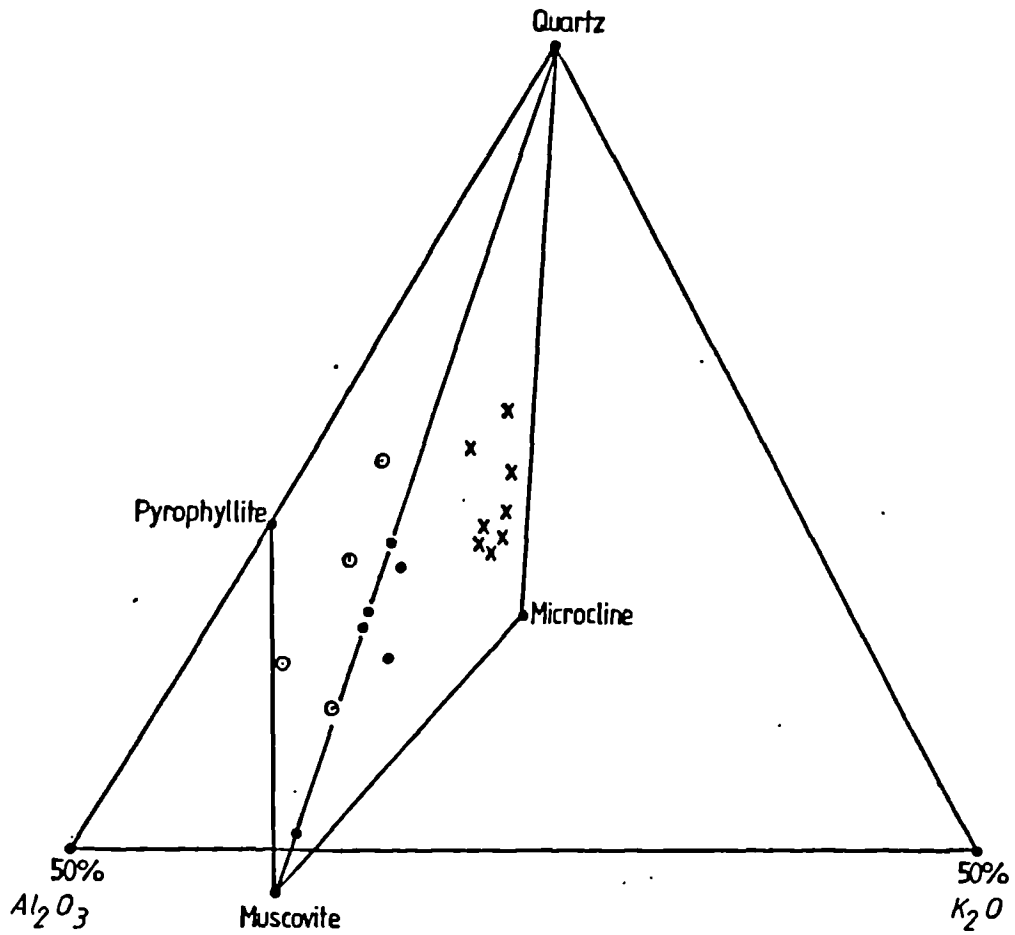

1970 has been summarised by Thompson (177). Values of temperatures ranged between 420°C (178) and 310°C (179) at 2kb and he concluded that the lower limit should be 345 +/- 10°C at this pressure (177). Later investigators have proposed values somewhat lower [see Day (176) and Velde (92)] suggesting that insuficient time was allowed by previous researchers, whose experiments had not reached equilibrium.

According to Velde (92), the lower limit of pyrophyllite is known with precision (250°C), and for the purpose of this discussion, this value is accepted.

The upper limit of stability of pyrophyllite is not so well known. Work on this limit before 1968 has been summarised by Kerrick (93). Values for the temperature at 2kb ranged from 580°C (180) to 400°C [obtained by Hemley (181) and cited by Kerrick]. From his own experimental work, Kerrick proposed 410 +/- 15°C at 1.8kb and 430 +/- 15°C at 3.9kb. There is a large variation in the data, but the lowest values have been reported by Hemley (181), Kerrick (93) and Day (176), who has reported a value around 375°C at 2kb. According to Winkler (182), the lower values given by Hemley and Kerrick appear to represent the upper stability field of pyrophillite. The value reported by Day is lower, but it is an estimated one. See also Haas and Holdaway (183), who reported a value of 384°C.

The Cambrian and Torridonian rocks of the northern Highlands of Scotland were deposited upon a stable platform (6). Illite crystallinity and colour index measurements of microfossils imply that it is extremely unlikely that the higher of the temperatures suggested (cf 350°C) has ever been reached by the samples being examined. However, the more

recent lower temperature suggested by Velde (92) is a possibility. A temperature of 250°C has also been suggested by Johnson (184). It is known that the more northern rocks (such as the samples being discussed) have been heated to a higher temperature than those in the south (185), and it would be of great interest to examine soils from below the Cambrian unconformity from a southern region of the Highlands.

4.9. The Origin of Pyrophyllite

The stability field of pyrophyllite discussed in the previous section, the conditions in which it has been synthesized (186-188), studies of its solid solutions and its formation in nature (189-190) have all been reported. These reports leave little doubt that pyrophyllite is a mineral stable only at elevated temperatures and pressures.

Three possible modes of origin have been suggested for pyrophyllite:

a. The hydrothermal alteration of kaolinite by high temperature and silica-rich, geothermal waters;
b. the metamorphism of rocks containing kaolinite and quartz after deep burial; and
c. the direct precipitation of pyrophyllite during weathering from acid waters containing high concentrations of silica, in excess of the solubility of quartz.

The geothermal origin of pyrophyllite in areas with hot springs was documented by: Ellis (191), Iwao (192), and Zen (193) in New Zealand, Iceland, Japan, USA. and USSR. The

absence of an extensive vein system or a typical hydrothermal zonation from the area around Rispond, where the samples were taken, argues against this origin for the pyrophyllite below the Cambrian unconformity.

The direct precipitation of pyrophyllite in soils is possible (see Chapter III, Fig. 11). This mechanism involves waters with a very high silica content. Suitable waters are produced by the decomposition of plant remains in nutrient poor tropical soils and are characteristic of the presence of vegetation. The absence of vegetation in the Precambrian argues against this mechanism; nor could suitable waters be produced by the evaporation of silicic acid solutions from the dissolution of silicate rocks because such solutions always contain bicarbonates, which would produce upon evaporation an alkaline water in equilibrium with illite (see Chapter III, Section 3.4.7.).

The origin of pyrophyllite from quartz and kaolinite is the common origin in metamorphic rocks (194). The only difficulty with this origin for the pyrophyllite below the Cambrian unconformity is the temperature required, which is usually assumed to be 300-350°C. Nonetheless, this is the mechanism preferred by this study (see Section 4.8.). It should be pointed out that kaolinite is not necessary as a source of aluminium; any mineral with aluminium in excess of that in mica is suitable (e.g., gibbsite or potassium beidellite).

4.10 Semi-Quantitative Mineralogical Analysis

A comparison of two estimates of the mineral composition for the samples is presented in this section. A preliminary

estimate of the mineral composition was made by X-ray diffraction on the basis of single peak calibration curves. The heights of only four peaks were measured to estimate the proportion of each of four minerals, viz., quartz (d-2.45Å), microcline (d-3.24Å), muscovite (d-10.08Å), and pyrophyllite (d-3.05Å). As most of the X-ray diffraction spectrum was discarded, the results are not very satisfactory (see Sections 2.9. and 4.10.1.).

Another estimate was made from the chemical analysis under the assumption that the rock is either made of muscovite, quartz and pyrophillite or muscovite, quartz and potassium feldspar (that is on the basis of Fig. 34A).

The results of both estimates are summarised in Table 24 and illustrated in Fig. 36. However, note that in the table only the more abundant minerals are recorded; other minerals, that may be present in the samples in small amounts were not detected by X-ray diffraction and their estimated amount from the chemical analysis can be seen in Appendix 13. The calculations were carried out using a computer programme, which is given in Appendix 14. Although the two estimates of the mineral composition are not in good agreement, generally speaking, they agree with the previous observations. There is a group of samples with a large amount of potassium feldspar, another group of samples with pyrophyllite in them, and a third group of samples containing neither pyrophyllite nor potassium feldspar.

The length of the lines joining the two estimates of mineral composition in Fig. 36 represents the difference between them, and is largely due to the error in the semi-quantitative X-ray diffraction analysis. These lines

Fig. 36: Comparison of two estimates of the mineral composition of weathered Lewisian gneiss taken from the felsic band.

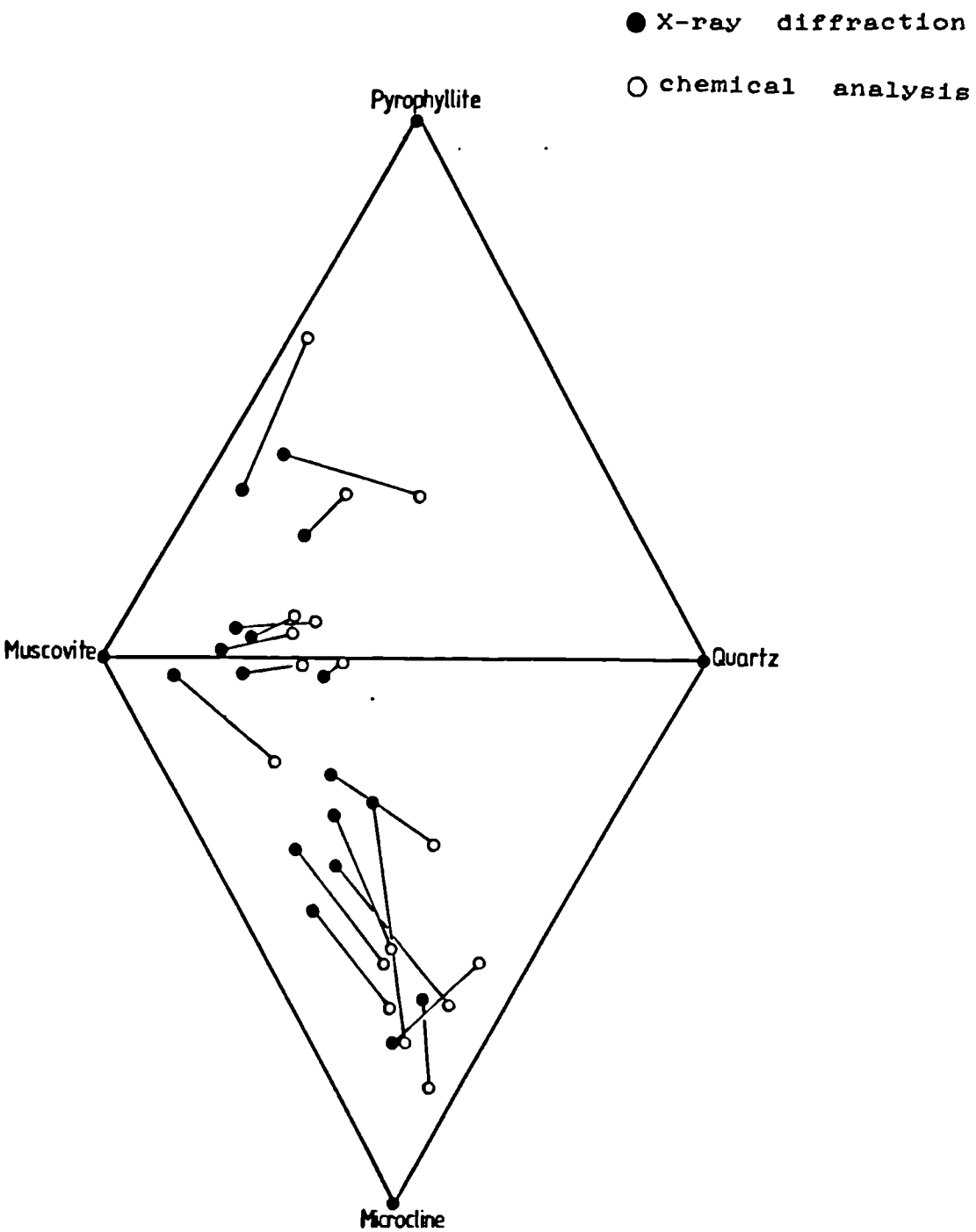

Table 24: Comparison of two estimates of the mineral composition of the Lewisian gneiss from the felsic band.- 1: from the X-ray diffraction analysis. 2: from the chemical analysis.

Sample No.	D.f.U. m	Mcr. 1	Mcr. 2	Msc. 1	Msc. 2	Qtz. 1	Qtz. 2	Pyroph. 1	Pyroph. 2
6	ind.	22	33	50	27	27	38	0	0
7	ind.	71	56	15	8	14	36	0	0
8	ind.	3	1	72	65	22	31	3	1
9	ind.	12	5	29	89	48	4	10	0
10	ind.	3	17	83	57	11	18	3	0
16	1.0	0	1	62	38	7	2	31	56
17	2.0	0	2	79	65	19	27	2	4
18	3.5	0	7	76	57	19	31	6	0
19	5.0	26	68	42	13	32	16	0	0
20	1.5	0	1	52	32	11	36	37	30
23	4.0	28	52	46	24	24	23	2	0
24	3.0	45	62	40	19	12	16	2	0
25	2.0	2	1	62	58	34	38	2	2
26	1.0	2	3	54	42	21	23	23	30
27	0.0	2	0	72	74	22	18	4	7
40	11.0	38	62	42	10	20	27	0	0
41	7.0	33	54	48	23	15	20	4	0
42	7.0	63	79	14	4	23	16	0	0

D.f.U. = Distance from Unconformity.

ind. = indeterminate

represent an average error of about 15%.

From the above-mentioned figure, it can also be seen that estimates for the group of samples containing little pyrophyllite present a better agreement when compared to the other two groups, the reason for this being that they are almost a two-component system (muscovite and quartz), which is easier to analyse than a multicomponent system.

4.10.1. Sources of Error in Quantitative X-Ray Diffraction

In view of the large discrepancies between the X-ray diffraction results and the chemical calculations observed above, an attempt was made to improve the results by measuring all the peaks in the X-ray diffraction spectra. However, many difficulties were encountered and, due to lack of time, the attempt was abandoned. A few of these difficulties are discussed in this section so that the complexity of the problem can be appreciated.

Quantitative X-ray diffraction analysis is influenced by several factors (see Sections 1.7., 1.7.1., 1.7.2.). Some of them are:

1. Order-disorder phenomena and solid solution.
2. Non-uniform sample thickness or coarse sample grinding.
3. Overlapping peaks.
4. Absorption and fluorescence.

1. The crystal structures of the minerals involved in this investigation are very complex and vary with the composition of the solid solutions, which alter the crystal structure and, consequently affect the intensity

and position of the peaks. The distribution of aluminium atoms in the silicate structure is such that every fourth silicon atom is exchanged for an aluminium atom and the charge balance is maintained by potassium ions. Any variation in this distribution affects the diffractogram pattern and is known as order-disorder phenomena. Therefore, to get good results, it is necessary to have the right minerals with the correct amount of solid solution and order-disorder as standards. This can only be achieved by separating the minerals from the samples and using these pure separates as standards. Separation of the minerals from the samples under the microscope is a difficult and time-consuming process, particularly because the rocks are very fine grained. As a result of this, there is not enough sample to construct a calibration graph with many points.

2. It is not always easy to get a uniform thickness of the surface to be irradiated; variations in thickness affect the relative height of the peaks because certain planes may be enhanced. A similar enhancement of certain reflections occurs when the sample has been ground too coarsely and platy or fibrous minerals become oriented whilst preparing the sample for the X-ray diffraction analysis.

3. X-ray diffraction patterns contain many peaks and, when dealing with samples containing many minerals, some of these peaks are certain to overlap. When they do, the peak height (or area) of each one affects the peak height (or area) of the other. Corrections are possible but depend on the separation of the peaks, and individual calibration is needed for each such pair.

4. Interaction of X-rays with the minerals produces absorption and fluorescence, which also affects the X-ray diffraction analysis.

Unfortunately, although each of these errors could be coped with separately, there was simply insufficient time to optimise a technique and obtain satisfactory quantitative X-ray diffraction analyses. The only alternative to this method of quantitative mineralogical analysis - the use of the polarised microscope - was precluded because of the fine grain size of the sericite in the samples near the unconformity. Even the samples far from the unconformity gave underestimates for muscovite because of the neglect of sericite within feldspar grains.

4.11. Genesis of the Rocks Immediately Below the Cambrian Unconformity

The previous sections have shown that the rocks being discussed:

a. progress from a potassium feldspar-quartz gneiss to pyrophyllite-muscovite rock by first converting the potassium feldspar into muscovite and then some of the muscovite to pyrophyllite (Sections 4.6. and 4.7.),

b. have been heated to a temperature of around 250°C to produce the pyrophyllite from some precursor (Sections 4.6., 4.7. and 4.8.).

It is quite possible for the muscovite also to have been produced by action of heat on a mixture of kaolinite and potassium feldspar such as would be produced by the acid

weathering of Lewisian gneiss. The reaction would be

$$H_4Al_2Si_2O_9 + KAlSi_3O_8 = H_2KAl_3Si_3O_{12} + H_2O + 2SiO_2$$
Kaolinite Microcline Muscovite Quartz

However, this is not considered likely because muscovite is a common detrital mineral, both in the Torridonian and, in the form of illite, in the Cambrian in this region. This detrital muscovite appears to be present in too large a quantity to have originated from the small amount present in the fresh Lewisian gneiss (this is particularly true of the Cambrian Fucoid Beds, which contain large amounts of detrital illite). Therefore, the muscovite is believed to have originated from the alkaline weathering of the microcline, which is abundantly present in the Lewisian and which would produce illite on alkaline weathering (see Chapter III, Section 3.4.7.).

This argument is supported by the very common reports of illite in Precambrian paleosols [Gay and Grandstaff (195); Button (196), and Button and Tyler (197, 198)] suggesting that such alkaline weathering was common in this period even though it is rare today.

There are three possibilities:

a. both pyrophyllite and muscovite were formed in the soil,
b. neither muscovite nor pyrophyllite was formed in the soil, or
c. muscovite was formed in the soil (as illite) but pyrophillite was not.

The first possibility a. can be eliminated because

illite requires alkaline conditions while pyrophyllite needs acid ones (see Chapter III, Sections 3.1.3. and 4.9). However, the effect of a variable aluminium activity, similar to the variable silicon activity considered in Chapter III, Section 3.1.2., has not been discussed. This will be done in the next section (4.11.1.), where it will be shown not to alter the situation.

The remaining two possibilities represent differing weathering environments. Abundant rainfall and unrestricted drainage would produce low concentration of potassium and moderately acid (pH 6) soil waters. Corresponding to case b., kaolinite would be the dominant product of weathering. The original gneiss would be weathered to a varying extent with depth because of the varying access to percolating waters, which would produce soils with varying kaolinite/microcline ratios that on burial and metamorphism could produce muscovite or pyrophyllite depending on the ratio of kaolinite to potassium feldspar. The difficulty with this explanation is that it does not explain the abundance of detrital illite. Also to get muscovite in the metamorphosed rock by this mechanism, it is essential to have the correct ratio of kaolinite to potassium feldspar, which is a very unlikely coincidence. In the actual rock, however, there is a wide zone with very little pyrophyllite or potassium feldspar in strong disagreement with this mechanism (see Figs.32 and 35).

The possibility c. corresponds to an arid environment with restricted drainage. Weathering at the surface during periods of rainfall would produce a surface soil composed of kaolinite but evaporation during dry periods would produce an alkaline solution at depth, which is conducive to the weathering of potasium feldspar to illite. The assumption of

kaolinite as a precursor is supported by the reported presence of this mineral as a precursor in archaean rocks (199). This is a favoured hypothesis because the major effect of the absence of plants in the Precambrian will certainly be the destabilising of soils. The effect will be similar to the famous "dust bowl" of Kansas and Dakota in the USA in the 1930's, when removal of the stabilising grasslands by ploughing produced removal of the soil by wind and rain (200). This would certainly have been the general state of affairs in the Precambrian. Soils would not accumulate except in areas of restricted drainage. These would be lakes in temperate regions, and in the tropics they would be areas occasionally flooded but usually the water would be strongly evaporated to a concentrated alkaline solution. These two alternative environments are illustrated in Fig. 37.

There remains only one further possibility: the weathering of potassium feldspar to a smectite clay. Potassium smectites are not well-known minerals, but this is probably due to the difficulty of purifying and analysing clays rather than to the absence of potassium smectites in nature. The well-known clay minerals are just those minerals which occur pure in nature. The mixed clays, usually produced by weathering, cannot be separated and would be expected to contain some potassium smectite. This last possibility is discussed in Section 4.11.2., and will be shown to be a likely candidate also involving evaporation in an arid environment.

4.11.1. Non-Equilibrium with Respect to Aluminium

Just as it is possible to have non-equilibrium with quartz, enabling high silica activities which stabilize

Fig. 37: Precambrian Weathering Environments

U N C O N F O R M I T Y

Much Kaolinite Little Feldspar and Quartz		Pyrophyllite Muscovite Quartz		Kaolinite Illite Quartz	¦
One mole of Kaolinite to every mole of Feldspar together with Quartz	HEAT ---->	Muscovite Quartz	HEAT <----	Illite Quartz	D E P
Much Feldspar Little Kaolinite With Quartz		Quartz Feldspar Muscovite		Illite Feldspar Quartz	T H
Gneiss		Gneiss		Gneiss	¦

Acid Weathering | Present-Day Rock | Alkaline Weathering

pyrophyllite, so it is also possible, indeed very likely, that in natural waters non-equilibrium with gibbsite may occur, allowing high aluminium concentrations. The question naturally arises as to the effect of this on stability of pyrophyllite. Could such high alumina activities allow the precipitation of pyrophyllite in more alkaline solutions at the expense of kaolinite?

This question is answered by Fig. 38, where the activities of alumina and silica are plotted on the same diagram. The lines plotted on this diagram represent the solubility products of the various minerals:

Gibbsite:

$Al(OH)_3 + H_2O = Al(OH)_4^- + H^+$

$pA = 15.8 - pH$

Kaolinite:

$H_4Al_2Si_2O_9 + 7H_2O = 2Al(OH)_4^- + 2H^+ + 2H_4SiO_4$

$pA = 20.0 - pH - pS$

Pyrophyllite:

$H_2Al_2Si_4O_{12} + 12H_2O = 2Al(OH)_4^- + 2H^+ + 4H_4SiO_4$

$pA = 23.2 - pH - 2pS$

where

$pA = -\log_{10}[Al(OH)_4^-]$

$pS = -\log_{10}[H_4SiO_4]$

$pH = -\log_{10}[H^+]$

The dotted lines correspond to the various solubility limits for solutions supersaturated with respect to gibbsite [$K_{so} = 10^{-15.8}$ (201)], aged aluminium hydroxide, [K_{so} =

Fig. 38: Effect of non-equilibrium with respect to aluminium on the stability of pyrophyllite.

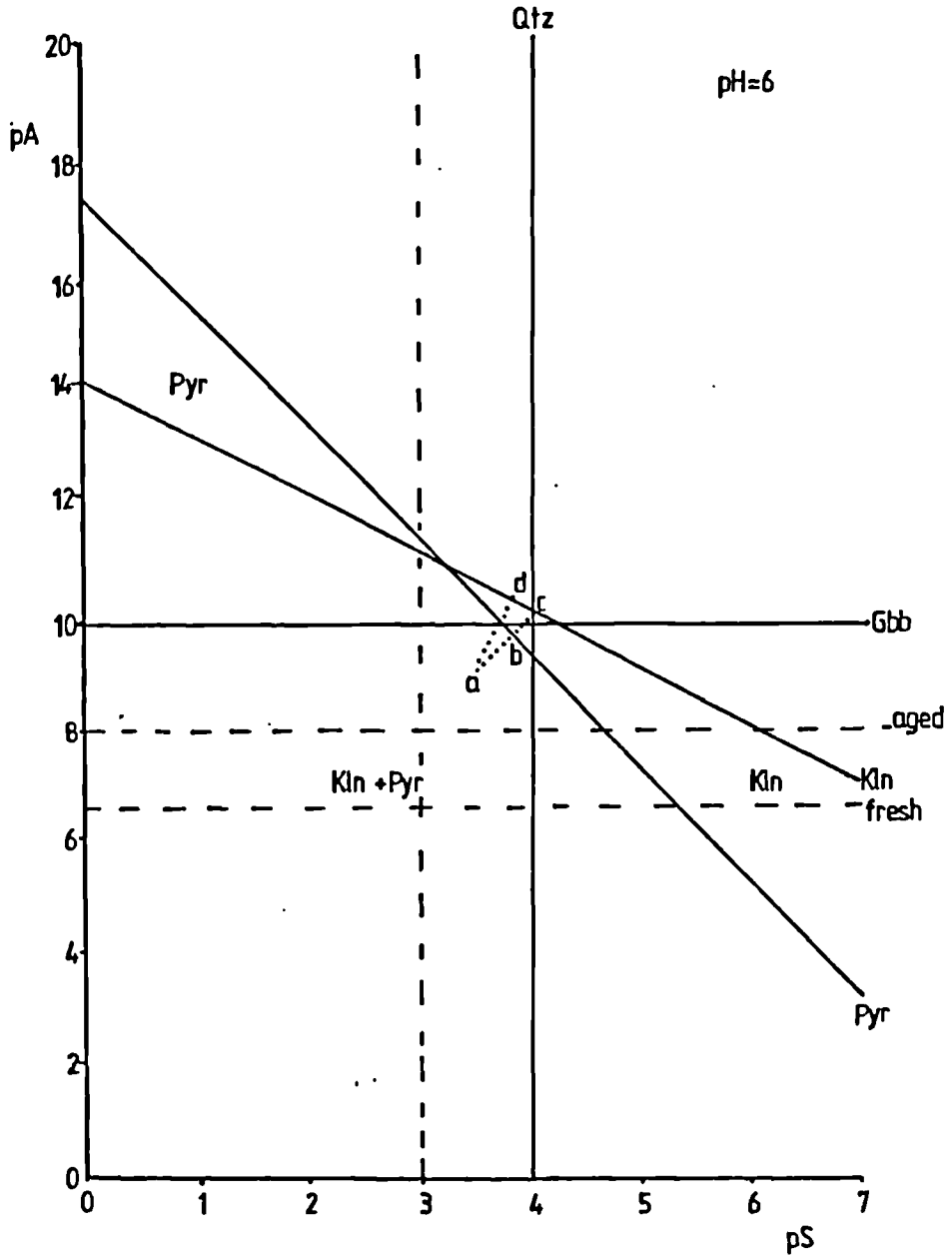

= $10^{-13.9}$ (202)] and freshly precipitated aluminium hydroxide [K_{so} = $10^{-12.6}$ (202)]. Aluminium activities higher than the latter cannot be sustained even for a short period, whilst activities lower than those for aged aluminium hydroxide can be sustained for several months.

Solutions whose composition lies in the field marked "Kln" are supersaturated with respect to kaolinite; those in the field marked "Pyr" are supersaturated with respect to pyrophyllite; those in the field marked "Kln + Pyr" are supersaturated with respect to both. Thus a solution with a composition represented by the point "a" ([Al]=10^{-9} molar); ([Si]=$3x10^{-4}$ molar) which, according to the activity diagram previously used, would be in equilibrium with kaolinite, can in fact deposit pyrophyllite.

However, this is an unstable situation. Such a solution will change its composition as it deposits the minerals. If kaolinite is deposited, its composition moves along the line "a-d" until the kaolinite solubility product is reached when further changes cease. However, if pyrophyllite is deposited, the line "a-c" is followed, with the silica concentration falling faster because the precipitated pyrophyllite contains more silica. When the point "b" is reached, further precipitation of pyrophyllite is impossible, but the precipitation of kaolinite can still occur; and if equilibrium is to be reached, then theoretically the previously precipitated pyrophyllite would be redissolved so that the more insoluble kaolinite could be precipitated. Hence it is concluded that supersaturation with respect to kaolinite as well as gibbsite is needed if pyrophyllite is to be precipitated in waters of such low silica activity.

There is no evidence in nature that pyrophyllite has less tendency to supersaturate than kaolinite. Kaolinite is an often reported constituent of soils, whereas pyrophyllite has never been observed to be in equilibrium with soil waters. Hence there is no reason whatever to suppose that the pyrophyllite observed at the Cambrian unconformity was originally precipitated as a product of the weathering of potassium feldspar. The conclusion drawn in Section 4.9., that this pyrophyllite is a product of low-grade metamorphism due to burial, is thus confirmed.

4.11.2. The Significance of Smectites

The only smectite which needs to be considered is potassium beidellite. The absence of magnesium from the parent gneiss rules out trioctahedral smectites and the similar absence of sodium and calcium rules out the common form of beidellite. All the activity diagrams presented before have ignored potassium beidellite because reliable thermodynamic data are absent. In the absence of such data, the rather sketchy activity diagram of Velde (92) will be used. This diagram (Fig. 39) is purely qualitative: the axes have no scales, the slope of the beidellite-kaolinite line is too shallow (*), and pyrophyllite has been omitted. Nevertheless, it gives a reasonable qualitative picture of the effect this mineral will have on the weathering products of potassium feldspar.

(*) The slope of the line is governed by the stoichiometry of the reaction:

$2H^+ + 3\text{Beidellite} + 23H_2O = 7\text{Kaolinite} + 8H_4SiO_4 + 2K^+$

and is -2/8, whereas Velde uses a slope of zero.

Fig. 39: Activity diagram for the weathering of potassium feldspar including potassium beidellite.- [After B. Velde (92).]

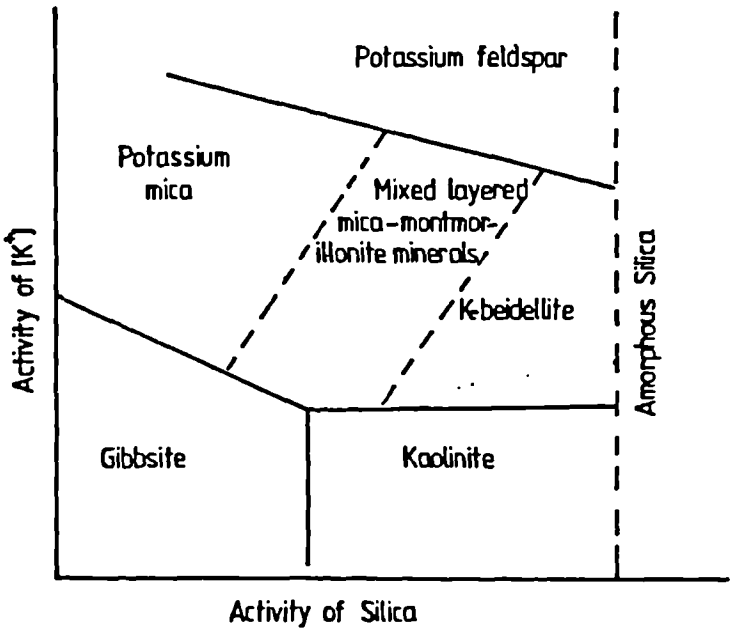

Velde (92) has shown that potassium beidellite forms a mixed-layer clay mineral with illite. The stability field of this mixed-layer mineral in the new diagram (Fig. 39) separates the stability field of kaolinite from that of potassium feldspar. This agrees much better with the paleosol profile found at Rispond than the diagram given in Chapter III. The presence of this stability field, due to the mixed-layer mineral, allows a steady progression from a weathering product, mostly illite, to one with a high proportion of beidellite, which on heating would give rocks having the observed mineralogy.

Weathering by fresh rainfall at the surface would automatically enter the mixed-layer field if weathering proceeded for enough time and evaporation of the solution resulting at any stage would give a solution in the deeper parts of the profile in the illite field. In the deepest part of the profile, the soil will consist of illite and potassium feldspar. Closer to the surface, it will be a mixture of the mixed-layer mineral having a large proportion of illite, with some residual feldspar. At the surface, the soil will consist of a mixed-layer mineral having a large proportion of beidellite. During burial and low grade metamorphism, the beidellite would produce pyrophyllite and muscovite near the surface, and the illite at depth would produce muscovite, which is exactly the pattern revealed in Section 4.6. (see Fig. 40). All of these products would also contain quartz, which is very incompletely removed during weathering. The production of pyrophyllite then corresponds to the reaction

$$3H_4K_{2/3}Al_{4.2/3}Si_{7\ 1/3}O_{24} = H_4K_2Al_6Si_6O_{24} + 2H_4Al_4Si_8O_{24}$$

Beidellite Muscovite Pyrophyllite

Fig. 40: Genesis of Paleosol near Rispond

Mixed layer Illite/Beidellite and Quartz		Pyrophyllite Muscovite and Quartz	Sample 16 (1m)
Illite, some mixed-layer Illite/Beidellite Some Potassium Feldspar, and Quartz	HEAT ---->	Muscovite and Quartz	Sample 17 (2m)
Potassium Feldspar, Illite Quartz		Potassium Feld-Quartz and and Muscovite	Sample 18(3.5m)
Gneiss		Gneiss	Sample 19 (5m)
Original Profile	Burial and very low grade Metamorphism	Present Minerals	

4.12. Precambrian Weathering

Although chemical weathering in Precambrian environments has been widely observed, few Precambrian paleosoils have been studied chemically in detail. Kalliokaski (203) studied the chemistry and mineralogy of Precambrian paleosols in Northern Michigan and concluded that "The rate of weathering is an unknown. In the probable absence of soil organisms, they may have been considerably below present-day rates under comparable climatic and geographic conditions.". Studies of Archaean chemical weathering by Shau and Henderson (204) led them to conclude that weathering profiles are more a response to local environmental conditions within the rock than a result of the composition of the atmosphere. Some more detailed studies of Precambrian weathering have been carried out by Gay and Grandstaff (195), Button (196), and Button and Tyler (197, 198). In an attempt to understand the environment under which Precambrian weathering took place, Gay and Grandstaff (195) studied the chemistry and mineralogy in two Canadian localities. In one locality, the minerals of the parent rock, actinolite, sphene and epidote, were fully destroyed and replaced by clay minerals, which were themselves recrystallized and altered to form fine grained sericite. Gay and Grandstaff also noted an increase of K_2O in the weathering products. In the second locality, microcline and plagioclase were altered first to clay minerals and then to sericite. Retention of potassium in the paleosol was observed, which in the opinion of the authors, probably resulted from both the formation of illite during weathering and later diagenesis, which replaced the clay minerals with sericite. Retention of quartz in this paleosol was explained in terms of diagenetic formation of quartz as cement. Both

weathering profiles present similarities to present-day weathering environments, i.e., gley soils formed under anoxic or reducing ground water conditions, and spodosols formed in moderate weathering conditions. Precambrian soil profiles reported by Button (196) and by Button and Tyler in South Africa (197, 198) show sericite and quartz as the main weathering products. Characteristic of the paleosols is the high K_2O, Al_2O_3 and TiO_2 contents relative to the parent material. Concentration of Al_2O_3 and TiO_2 was assigned to residual origin, whereas the large increase in K_2O was believed to be due to residual enrichment and addition during diagenesis by potassium bearing ground waters.

Despite the similarities to the present day reported by Gay and Grandstaff (195) and revealed by this work, the environmental conditions in which Precambrian weathering took place as well as other factors associated with them, such as concentration of potassium in the weathering products, are not well understood. It has been said [Perel'man (173)] that the late Precambrian soils were alkaline and poorly developed.

The work reported in this thesis was initiated in collaboration with Professor Russell, one of whose interests lies in the genesis of the Aberfeldy Celsian barite and base metal deposit, which he believes to have been formed by precipitation from alkaline solutions having a high concentration of aluminium (1). Basing his thesis on the laboratory work of Tamm (205), and Garrells and Howard (206) he assumes that the feldspar is hydrolysed to hydrogen feldspar producing a very alkaline solution, which could dissolve large amounts of aluminium (15).

That this process is the initial step in the weathering of potassium feldspar is not doubted. However, the dissolution of the hydrogen feldspar produced is the slowest step and will control the rate of the weathering reaction, and hence the overall chemical reaction (which will be of the form written in Chapter III, Section 3.5.). Finally Tamm's alkaline pH of 10.7 represents equilibrium with a carbon dioxide free water, which seems an unlikely contingency in the Precambrian because it is generally assumed that the spread of plant life has lowered, not increased the atmospheric carbon dioxide levels. Hence it seems more likely that the alkaline solutions were produced by evaporation of more acid solutions than by direct dissolution of the feldspar.

Undoubtedly, aluminium will be more soluble in these alkaline solutions (a solution saturated with both kaolinite and amorphous silica at pH 10 would contain 3 $\mu g\ dm^{-3}$, whereas at pH 11, it would contain 30 $\mu g\ dm^{-3}$). Nonetheless, the solubility is very low and the source of aluminium must have been a solid aluminosilicate (kaolinite, illite, beidellite etc.) mobilised by the increased solubility in alkaline solution (or alternatively by higher temperatures than that assumed, i.e. 25°C).

The concentration of potassium in Precambrian paleosols requires the development of illite as a weathering product, which in turn needs high potassium concentrations and alkaline conditions. The absence of land vegetation would by itself have increased the amount of potassium in the environment because in land plants the ratio of potassium to sodium is about ten to one, whereas in rocks it is about one to one. Thus at the present day, a large amount of potassium

is locked away in the land vegetation (roughly 0.3% of the biomass). In the Precambrian, this potassium would have been present in the natural waters. However, this potassium by itself does not appear sufficient to explain the widespread development of illite. As explained in Section 4.11., the absence of land plants has a second more important consequence: the mechanical destabilisation of the soils. Most modern soils are held in position by plant roots. In the absence of this binding, fine clay particles would have been either blown or washed away. Hence a more probable explanation for the concentration of potassium in Precambrian soils is that both the soils and the potassium were concentrated in the same place, viz., enclosed basins with poor drainage where the clay particles would settle out and the potassium be concentrated by evaporation. The concentration of potassium by evaporation also explains the alkaline conditions because the bases in the waters would be present as bicarbonates and, upon evaporation, loss of carbonic acid as carbon dioxide would produce the alkaline solution needed to ensure the stability of illite. If a mixed-layer illite-beidellite mineral were also precipitated, a wider range of conditions would be possible involving less alkaline conditions and a smaller concentration of potassium. However, acid conditions are ruled out as this would produce kaolinite rather than illite.

4.13. The Basic Band

An attempt was also made to sample rocks from the more basic band in the Lewisian gneiss in order to investigate the removal of iron and magnesium during the weathering process. Major and trace element analyses for these samples are presented in Table 15. The mineralogical analysis is

Table 25: Mineralogical analysis of the Lewisian gneiss from the basic band.-

++ = mineral is abundant in the sample.

+ = mineral present in relatively large amounts.

- = mineral not seen under the microscope.

Sample No.	D.f.U.	K-Feld	Hornblend	Chlorite	Muscovite	Qtz
11	2.0	-	-	-	++	++
12	2.5	-	-	-	++	+
13	3.0	-	-	++	++	+
14	4.0	-	-	++	++	+
15	5.0	-	-	++	++	-
21	3.0	-	++	++	++	+
22	5.0	-	++	++	++	+
36	14.0	++	++	++	++	+
37	14.0	++	-	++	++	++
38	14.0	++	-	++	++	++
39	14.0	-	++	++	+	-
43	50.0m	++	-	-	++	++

D.f.U. = Distance from Unconformity.

summarised in Table 25, along with the distances beneath the unconformity for each sample. Examination of these tables shows that there is no regular variation in either the chemical or the mineral species, suggesting that the sampling process was not very successful. Collection of samples from basic bands is particularly difficult because these bands are very discontinuous, and it was not possible to follow one band of uniform composition for more than a metre or two. Also the composition of these bands is very variable being seldom constant for more than a metre in the localities studied. Finally the rocks were very fine grained and it was not possible to identify all the components present.

4.14. Conclusions

It is concluded that the rocks below the Cambrian unconformity at Rispond represent a fossil soil profile. These rocks contain pyrophyllite formed by low-grade metamorphism at temperatures around 250°C. Three possible modes of origin have been considered and that involving the weathering of potassium feldspar to kaolinite alone in an acid environment rejected. The two mechanisms involving the weathering of the feldspar to illite in an arid alkaline environment with restricted drainage are considered to be more likely. The illite produced in these mechanisms was further weathered to produce, in the one case kaolinite, and in the other one potassium beidellite as a mixed-layer mineral with illite. These two mechanisms can be mixed in any proportion, the exact amount of potassium beidellite present depending upon the relative thermodynamic stabilities of kaolinite and beidellite. As the latter is unknown, further accuracy cannot at present be achieved.

CHAPTER V

DETERMINATION OF AMMONIA IN ROCKS

5.1. General

Proteins break down naturally to produce ammonia decomposition, which is accelerated by temperature. This ammonia may then contribute to the formation of an ammonium feldspar (buddingtonite) because of the similarity in ionic radius and charge between the ammonium ion and the potassium ion. Thus the ammonium ion may be present in chemical sediments or muds, if available at the time of formation of the rock.

The presence of abundant potassium feldspar in the Fucoid Beds and the existence of trace fossil planolites in such rocks as well as the temperature to which they have been heated (about 200°C), which is high enough to decompose any organic matter that may have ben present at the time of their formation, provide conditions suitable for the substitution of ammonium for potassium ions to take place. Therefore, it was decided to investigate the possible existence of an ammonium feldspar in 22 samples from the Cambro-Ordovician succesion in Northwest Scotland. This investigation involved the design of a suitable method of releasing and collecting the ammonia expelled from the matrix and its subsequent determination by the Indophenol-Blue method as described in this chapter.

5.2. Nitrogen in Rocks

Appreciable quantities of nitrogen are present in rocks, the amount of which varies from place to place and seems to be independent of the type of rock (207). It has been reported (207-210) that a considerable amount of this nitrogen exists as ammonium ions held within the structure of the silicate minerals. Similarities in ionic radius, about 1.43 Å for NH_4^+ (207), and charge, suggest that this ion might substitute alkali metals, particularly K^+ (radius 1.33 Å), in minerals. Other forms of nitrogen may also be found in rocks. Atomic nitrogen may be dissolved as solid solutions within various mineral phases of the rocks, and molecular nitrogen may be present in small crystalline cavities (210).

It is improbable that nitrogen exists as nitrides in rocks (211). However, Baur (212) has explained the presence of large amounts of nitrogen in chondrites as partly due to the presence of the mineral sionite (Si_2N_2O), a mineral that has been discovered (213) in this type of rock. At about the time of its discovery, the mineral was synthesised (214) and its crystalline structure established (215). Regardless of the method of extraction used for the chemical analysis, the larger part of nitrogen detected is in the form of ammonia, which by no means implies that this is the form present in the rock sample. The possibility that mixtures of hydrogen and nitrogen could react in presence of KOH to form potassamide at the time of their release for chemical analysis has been pointed out (216). Chemical analysis for ammonia in aqueous extracts from fluorite and other minerals have revealed the presence of high concentrations of combined nitrogen (217, 218). This is obviously related to the well

known fact that ammonium chloride is a typical product of fumarole and volcanic activity (217, 218). It was under hydrothermal conditions that Eugster and Munoz found that NH_4^+ may enter micas (219). Incorporation of this ion into mineral structures has been confirmed by Sterne et al. (220) and Erd et al. (221), who have described natural ammonium illites and the new mineral Buddingtonite. This mineral will be dealt with later in this section. The ammoniacal nitrogen content of silicates is very variable: from 41.4 µg/g in orthoclase (222) up to 7.95% in buddingtonite (221). Excluding this mineral, the higher values are reported for micas (211, 222, 223). Small amounts of nitrogen present as NO_3^- have also been reported. Wlotzka (211) analysed nitrate-nitrogen in rocks and reported between 5-20 µg/g in surface sediments, some in saline clays and limestones but none in average clays and sandstones (211).

5.3. The Determination of Total Nitrogen

Although some nitrogen may be extracted from silicate rocks by leaching with water, this is unlikely to give any real indication of the total amount of nitrogen present in the specimen. Reported methods for this determination include ignition in vacuum and the chemical decomposition of the sample by either alkalis or acids. Gibson and Moore (210, 224) developed a high-temperature-fusion technique using helium as carrier gas for the determination of nitrogen in rocks and meteorites. Samples were fused in a graphite crucible at 2400°C, and the combustion products injected to a gas chromatograph after the removal of carbon dioxide and water in order to quantify the nitrogen.

Wlotzka (211) decomposed the rocks with sodium hydroxide in a closed system and dissolved the melt in water. Oxidised forms of nitrogen present were reduced by Devarda's alloy to Ammonia, which was distilled and collected in standard acid and determined by the Nessler method.

Stevenson (222) determined total nitrogen in silicates and rocks by fusing the samples in a completely sealed tube at a temperature of 420°C for a minimum period of 90 minutes. A Kjeldahl distillation apparatus was employed to recover the ammonia, which was determined by the Nessler method. A modification of the method used by Dhariwal (225) for determination of fixed nitrogen in soils has been used by Stevenson to determine fixed ammonia in rocks (208). In this method, the rock is first treated with potassium hydroxide and the residue dissolved with a mixture of hydrochloric and hydrofluoric acids. The ammonium released by hydrofluoric acid is distilled with alkali into standard acid and estimated by means of Nessler's reagent.

It is clear from the above literature that determination of nitrogen in rocks involves two different steps, namely, release of the analyte from the sample and its quantification. Both processes bear inherent difficulties and limitations. Total release of nitrogen from the sample depends upon the way in which the analyte is held in the matrix and the method employed for its release. Total determination of the analyte depends mainly upon the sensitivity of the method of analysis. The reported results rely on the skill of the investigator to perform the analysis since contamination may occur in either step.

5.4. Buddingtonite, an Ammonium Feldspar

This was the first ammonium aluminosilicate found in nature and occurs in Quaternary andesite and older rocks hydrothermally altered by ammonia-bearing hot-spring waters below the water table at the Sulphur Bank quicksilver mine, Lake County, California (221). The mineral is also widely distributed in the rocks of the Meade Peak Member of the Phosphoria formation in Southeastern Idaho (226), and in the Condor Oilshale Deposit, Queensland, Australia (227).

The chemical composition of buddingtonite is presented in Table 26 and its formula is (221):

$$(NH_4)_2O \cdot Al_2O_3 \cdot 6SiO_2 \cdot H_2O$$

Buddingtonite is present in ammonium-rich environments and its origin has been attributed to reaction between ammonium-rich hot spring waters with plagioclase (277), and also to diagenetic processes (266, 227) in presence of ammonia formed by the decomposition of organic material under anoxic conditions.

5.5. Substitution of NH_4^+ for K^+

In 1958 Dharival and Stevenson observed that many soils have the ability to fix considerable amount of ammonium, which was attributed to a replacement by ammonium for interlayer cations such as Ca^{++}, Mg^{++}, Na^+, and H^+.

From subsequent observations and taking into account the similarity of the ionic radius of NH_4^+ and K^+, 1.43Å and 1.33Å respectively, plus their unit charge, several

Table 26: Chemical analysis of Buddingtonite.- After Erd et al. (221).

OXIDE	%
SiO_2	63.80
Al_2O_3	19.16
Fe_2O_3	1.85
MgO	0.21
CaO	0.04
BaO	0.26
Na_2O	0.06
K_2O	0.62
$(NH_4)_2O$	7.95
H_2O	3.28
H_2O^-	0.88
TiO_2	0.99
S	1.59
TOTAL	100.69

workers, amongst them Stevenson (209), suggestted that ammonium might be a substitute for K^+ in minerals. Although as early as 1900 substitution of ammonium for alkali metals had already been suggested in silicate minerals (228, 229), the hypothesis gained support and was proved only in the nineteen-sixties, when:

a. ammonium micas were synthesised (219),

b. evidence of the presence of NH_4^+ in sericites (230) and muscovites (231-233) was obtained (from infrared and chemical analysis), and

c. buddingtonite was found in nature (221).

Later investigations have revealed the presence of naturally occurring ammonium illites (220, 234), which have been subjected to infrared studies to show the presence of NH_4^+.

5.6. Relevance of the Project

In speculations on the origin of life, it is sometimes suggested that the early atmosphere contained both molecular nitrogen and nitrogen in a combined form (216, 154). According to Rayleigh (216) this type of hypothesis is not necessary as ammoniacal nitrogen, or perhaps organic nitrogen, is present in igneous rocks, and would be available in the course of denudation. This in turn would explain why the earth did not lose its nitrogen when its temperature was higher.

The presence of Si_2N_2O in a meteorite is interesting

since it implies the existence of nitrogen in the environment in which the meteorite crystallized (213). However, there exists the possibility that this nitrogen has been added during the terrestrial life of the meteorite (224). The presence of nitrogen in rocks is also interesting inasmuch as it provides information about the conditions of the formation of the rocks.

Buddingtonite has not only provided information about its geological environment of formation, but also, since it has been found associated with oilshales (227) and it decomposes at about the same temperature as oil is released from the shale, it may become a commercial source of ammonia, as a secondary product of the exploitation of these shales. It follows from the above discussion that there is an ample justification for research on nitrogen compounds in geological environments as indicators of rock-forming conditions, economic interest and clues about the probably unknown conditions in which the origin of life took place.

5.7. Aim of the Project

It has been stated (see Section 5.3.) that determination of ammonia in rocks requires two steps that involve release of the ammonia in a first place and its quantification in a second. Moreover, since usually the amount of ammonia in rocks is small, a highly sensitive method of analysis is required. The total nitrogen content of rocks, ranging from granite to dunite is about 20 +/- 10 ppm (207).

The purpose of this investigation was twofold:

1. To search for an ammonium feldspar in some Cambro-Ordovician rocks in Northwest Scotland.

2. To develop an alternative method of releasing the ammonia present in feldspathic rocks and determining it by the indophenol blue method, which was selected on the grounds of its reported high sensitivity.

5.8. The Indophenol Blue Method

As early as 1859, Berthelot had already described the blue colour produced by the reaction of ammonia with phenol in the presence of hypochlorite (235), which is the basis of the indophenol blue method. As the intensity of the colour is proportional to the concentration of ammonia present in the solution by measuring, the optical density of the colour at 630 nm, the unknown concentration of ammonia can be worked out from a previously standardised calibration curve.

Since then, this reaction has been widely studied and modified in several ways. Although Thymol (236-242), M-Cresol (243), Guaiacol (244), O-phenylphenol (245) have been employed instead of phenol, in some cases, Chloromina-T has been added in place of Hypochlorite (246-247). No catalysts have been used in some experiments (248-252). Several catalysts have been proposed and used in others: Manganese (II) has been used by Russell (253), (who also noted that copper ions tend to inhibit the development of the colour), and others (254-256); Nitroprusside (257-263), and Acetone (264-265) have also been used. Combinations of these catalysts have been utilized too, for example, a mixture of nitroprusside and acetone was used in the determination of ammonia in plasma by Fenton (266). Investigating the

catalytic action of both sodium nitroprusside and acetone, Horn et al. (267) came to the conclusion that the reaction is catalysed by sodium ferrous nitritopentacyanide, a complex formed by reaction of nitroprusside and NaOH, and not by the nitroprusside itself as had previously been thought. These results were later confirmed by other investigators (268). From a similar investigation, Harwood (269) concluded that sodium nitroprusside is a better catalyst than acetone and reported an increase in sensitivity. Using chloromina-T instead of hypochlorite, Namiki et al. developed a technique for the determination of nitrogen in metals, which involves extraction with isobutyl alcohol (270). Other modifications and studies of the reaction include the use of hypobromite instead of hypochlorite (271), kinetic investigations (272-273), and automation of the method (274-276).

The use of a particular catalyst, the temperature, the pH of the solution, the order of addition of reagents, timing and the relative concentrations of sodium hydroxide and phenol are factors, which affect the sensitivity and reproducibility of the indophenol method.

Earlier investigators observed the high sensitivity of the method (248-250, 253, 254, 277) but often experienced difficulties in obtaining reproducibility. Bolletter et al. (252) have illustrated the fundamental chemistry of the method as follows:

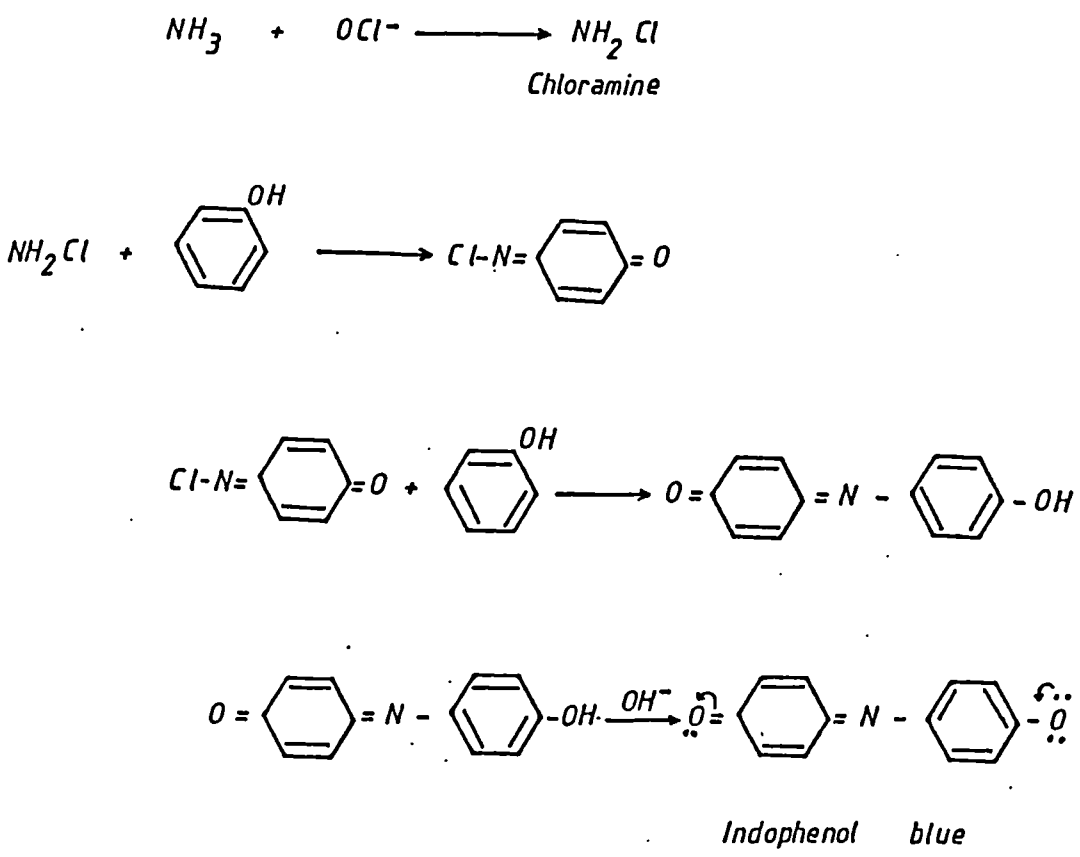

The method has been used for the determination of NH_3 in sea water (246, 255, 278), soil extracts (274), natural waters (251, 271), metallurgical analyses (236, 270), biological fluids (250, 260, 266-268, 279), urea (257, 258), petroleum stocks (277) and boiler feed water (265). Apart from its application to ammonia analysis in soil extracts, nothing is known about its application for ammonia determination in rocks.

It is known that copper (II) ions cause low results, but this interference has been overcome by adding EDTA (265). Other interferences due to hydroxylamine, certain aminoacids and urea in the development of the colour can be eliminated by distillation to isolate the ammonia (255) or by solvent extraction (247, 270). In order to quantify the amount of NH_3 present in the Fucoid Bed rocks, the method described by Tetlow and Wilson (265) was used for the estimation of the

ammonia. This method will be briefly summarised later on.

5.9. EXPERIMENTAL

5.9.1. Sample Preparation

Samples for this investigation were provided by the Department of Applied Geology. The samples were first cut into two halves. The analysis was performed on one half, which was crushed in a jaw crusher and then powdered in a Tema mill to pass a 200 mesh sieve. The powder was then stored in polythene bottles.

5.9.2. Release and Collection of Ammonia

In order to release the ammonia from the rocks, the powdered sample was fused in a nitrogen-free nickel crucible with sodium hydroxide. An argon stream flowing at 0.5 l/m propelled the gases towards a 10^{-3} M standard HCl solution, in which the ammonia is dissolved for subsequent analysis by the indophenol blue method.

5.9.3. Apparatus

To fuse and collect the ammonia, the apparatus shown in Fig. 41 was designed. It consists of three main parts:

a. a nickel tube "A", in which the fusion takes place,

b. a glass tube "B", in which the hydrochloric acid solution dissolves the ammonia, and

c. a glass head "C" that, fitted on top of the tubes "A" and "B", allows the gases released from the fusion to pass to the HCl solution propelled by an argon flow coming through tube "D".

5.9.4. Procedure

1) Twenty-five ml of ammonia-free water were place in the receiving tube "B" (see Fig. 41).

Five grams of analytical reagent grade sodium hydroxide were weighed out and transferred to the nickel tube "A".

3. The glass head "C" was fitted on top of tubes "A" and "B" and the apparatus set up on iron supports suitable for heating with a bunsen burner.

4. The argon flow was adjusted at about 0.5 l/min and the sodium hydroxide fused by heating the tube with the burner. This step took about eight minutes.

5. The system was allowed to cool for eight minutes, the glass head removed and the nickel tube brought to room temperature under tap water.

6. One ml of ammonia-free water was added on top of the solidified sodium hydroxide, the glass head replaced, the argon flow adjusted, and the sodium hydroxide fused again. This step lasted about twelve minutes.

7. The system was allowed to cool as in Point 5 and the nickel tube cooled under tap water.

Fig. 41: Schematic diagram of the apparatus used to free and collect the ammonia.

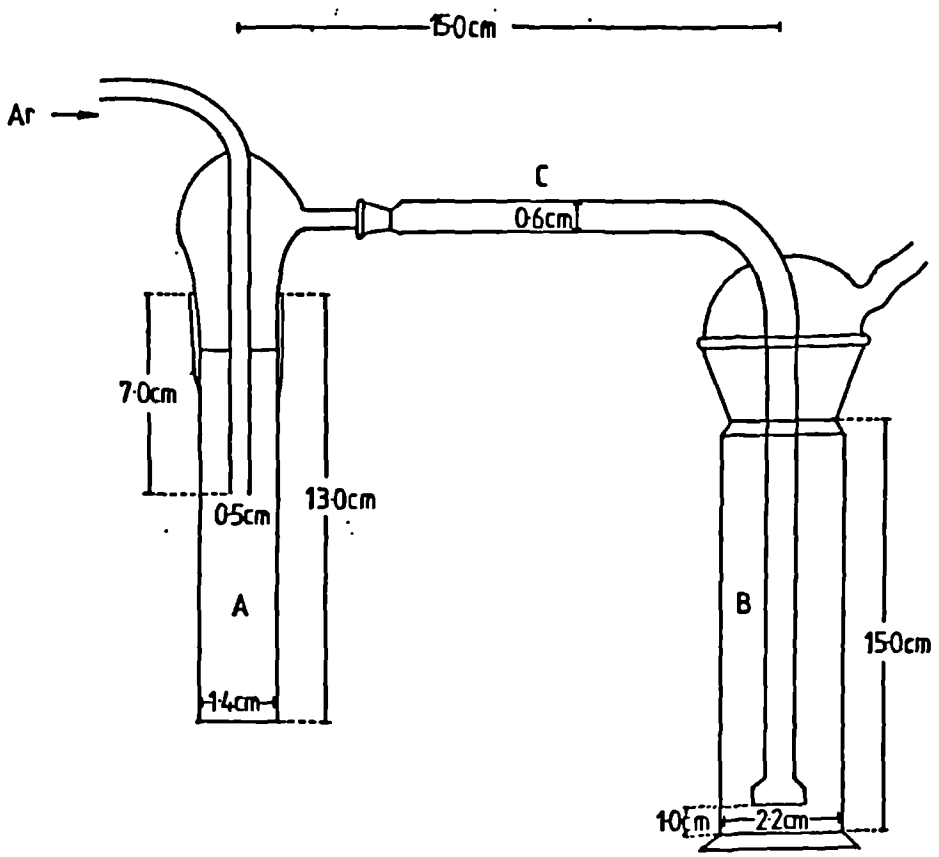

8. Adding no water at this time, the glass head was replaced, the apparatus set up, the gas flow adjusted and the sodium hydroxide fused once more. This step took about eight minutes.

9. The system was allowed to cool as in "5" and "7", and the nickel tube cooled under tap water before doing the blank.

5.9.5. Blank Determination

1. Having discarded the water that was in tube "B" during the previous fusions, 25 ml of 10^{-3} M HCl were transferred into this tube.

2. On top of the solid sodium hydroxide in the nickel tube, 0.2 ml of nitrogen-free water were added, the glass head replaced, the apparatus set up, the argon flow adjusted, and the sodium hydroxide fused after gentle evaporation of the water. This step took about ten minutes.

3. The system was allowed to cool, the glass head removed, the porous plug at the end of the glass head was carefully washed and this water added to the HCl solution before making up to 50ml.

4. This HCl solution was split into two 25 ml calibrated flasks and kept for later analysis.

5. The receiving tube "B" was thoroughly washed with ammonia-free water and another 25 ml of 10^{-3} M HCl transferred into it before the addition of the sample on top of the sodium hydroxide for fusion.

5.9.6. Addition of the Sample

The steps following the addition of the sample are described below and illustrated in Fig. 43.

1. Between 0.1 and 1.0g of the sample to be analysed were weighed out and transferred into the nickel tube with the help of the cups designed for this purpose (see Fig. 42).

2. The cup containing the sample was securely fitted onto its glass support, making use of the ground glass joint (Fig. 43.2).

3. The cold nickel tube containing the solid sodium hydroxide was inverted (Fig. 43.1) and the cup with the sample lowered into the tube by handling it carefully from its support (Fig. 43.3) until it reached the sodium hydroxide.

4. Next the nickel tube was quickly set upright, holding the cup tightly against the sodium hydroxide (Fig. 43.4), thus leaving the sample on top of the center of the sodium hydroxide as is shown in Fig. 43.5.

5. The cup was carefully taken out, 0.2 ml of water added, the glass head replaced and the argon flow adjusted as before and the fusion performed.

6. As in the blank determination, the porous plug at the end of the glass head was washed and this water added to the HCl solution, the solution diluted and split into two 25ml flasks and kept for analysis. The fusion of the sample took about fifteen minutes.

Fig. 42: The cup used for the addition of the sample.

1 - Glass cup with ground joint.

2 - Glass support for the cup with ground joint.

3 - Cup fitted on the glass support ready to introduce the sample.

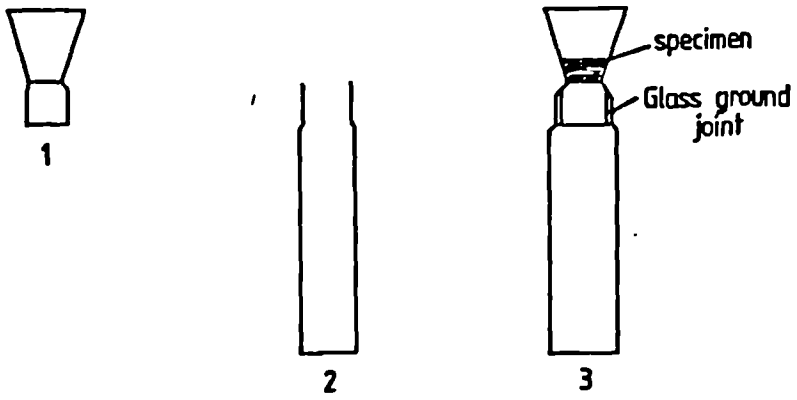

Fig. 43: Steps followed in the addition of the sample.

1 - Nickel tube with solid NaOH inverted.

2 - Cup with sample in its support.

3 - Cup and sample placed in the nickel tube.

4 - Sample being deposited on top of the NaOH.

5 - Sample ready to be fused.

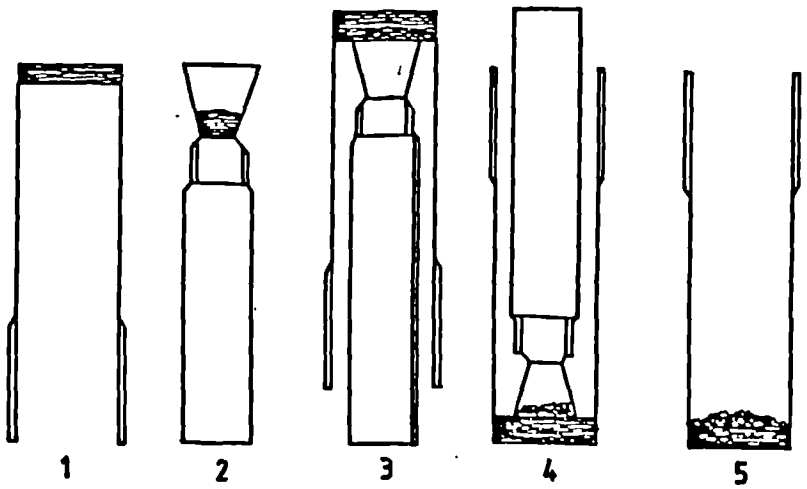

5.9.7. Cleaning the Nickel Tube

Before fusion of any sample was performed, the nickel tube was thoroughly cleaned. 5.0g of sodium hydroxide were fused and removed every day in the morning before any blank or sample was fused for analysis.

After the fusion of each sample, the tube was cleaned by refusing the melt with a further 10.0g of sodium carbonate. The residue was dissolved in abundant water under the tap. Alternatively, the tube can be cleaned simply by washing it under the water tap but this is a time-consuming process.

5.9.8. Method of Analysis and Reagents

To estimate the ammonia in the solutions coming from the fusion of the samples, the Indophenol blue method, as suggested by Tetlow and Wilson (265) was followed without any modification.

Analytical-reagent grade chemicals were used. Water for this investigation was collected daily after passing distilled water through a column of amberlite IR-120 cation exchange resin. This was done to ensure a very low ammonia content in it.

5.9.8.1. EDTA Solution

The EDTA solution was made up by dissolving 60g of the reagent in about 900 ml of water without heating and diluting it with water to 1 litre. The solution was stored in a glass bottle and was used for the analysis of all the samples.

5.9.8.2. Sodium hydroxide 5N

200 gr of sodium hydroxide were dissolved in water at room temperature, transferred to a 1l calibrated flask and diluted to the mark with water. The solution was then stored in a polythene bottle and its normality measured by titrating it with standardised hydrochloric acid.

5.9.8.3. Sodium Phenate Solution

100 ml of this solution were made up daily by dissolving 12.5g of phenol in 27 ml of 5N NaOH and making up to the mark in a 100 ml calibrated flask. The solution was prepared immediately before it was required for use.

5.9.8.4. Acetone

Analytical-reagent grade acetone was used.

5.9.8.5. Sodium Hypochlorite Solution

One per cent w/V available chlorine. This solution was prepared from a solution containing about 12% available chlorine. The concentration of available chlorine was determined by the iodometric method given by Vogel (280). 500 ml of this solution were made up each time and changed every four weeks. The solution was stored in a dark bottle and kept out of the direct sunlight.

5.9.8.6. Standard Ammonium Chloride Solution "A"

A 1000 ppm ammonia solution was made up by

dissolving 3.141g of ammonium chloride, dried at 100°C, in water and diluting it to the mark in a 1l calibrated flask. The solution was stored in a glass bottle.

5.9.8.7. Standard Ammonium Chloride Solution "B"

500 ml of 100 ppm of ammonia solution were prepared by transferring 50 ml of solution "A" with a pipette into a 500 ml calibrated flask and diluting it to the mark with water. The solution was stored in a glass bottle.

5.9.8.8. Standard Ammonium Chloride Solution "C"

50 ml of solution "B" were added with a pipette to a 100 ml calibrated flask and diluted to the mark with water to obtain a 10 ppm solution of ammonia. This solution was used to make the standards for the calibration curve.

5.9.9. Estimation of Ammonia

To each of the 25 ml portions of the solution containing the NH_3 released from the fusion, the reagents stated by Tetlow and Wilson (265) were added following their instructions as follows:

a. First, 1.0 ml of EDTA solution was added. The flask was stoppered and the contents mixed by gently swirling.

b. Second, 0.3 ml of acetone were added, the flask stoppered and the content mixed by swirling.

c. Third, 10.0 ml of phenate solution were added, followed after mixing by 5 ml of sodium hypochlorite and the

solution mixed once more by swirling. The solution was immediately diluted to 50 ml with water, the flask stoppered and the contents mixed by inversion. The flasks were then placed in a water bath at 25°C for sixty minutes, after which they were removed and the absorbance of the solution measured at 630 nm in a Shimazdu spectrophotometer, using 10-mm plastic cuvettes, with water in the reference cuvette. After use, the flasks were washed with abundant water every day, filled with water and set aside until they were required again next day. The cuvettes were also thoroughly washed with abundant water and kept in water in a beaker for subsequent use.

5.9.10. Preparation of the Calibration Curve

Suitable amounts of ammonia solution "C" were added to 50 ml calibrated flasks in order to construct a calibration curve in the range of 0 to 120 µg of ammonia and subjected to the analytical procedure described in Section 5.9.9. The calibration curve is shown in Fig. 44.

5.9.11. Advantages and Limitations of the Method

The method here described for the determination of ammonia in rocks can be carried out cheaply in any laboratory, provided that there is a nickel tube, argon and a patient operator. It has also the advantage of needing little sample.

Limitations for a wide application of the method arise mainly from the release of the ammonia from the rocks and these can be described as follows:

Fig. 44: The calibration curve for the determination of ammonia in rocks.

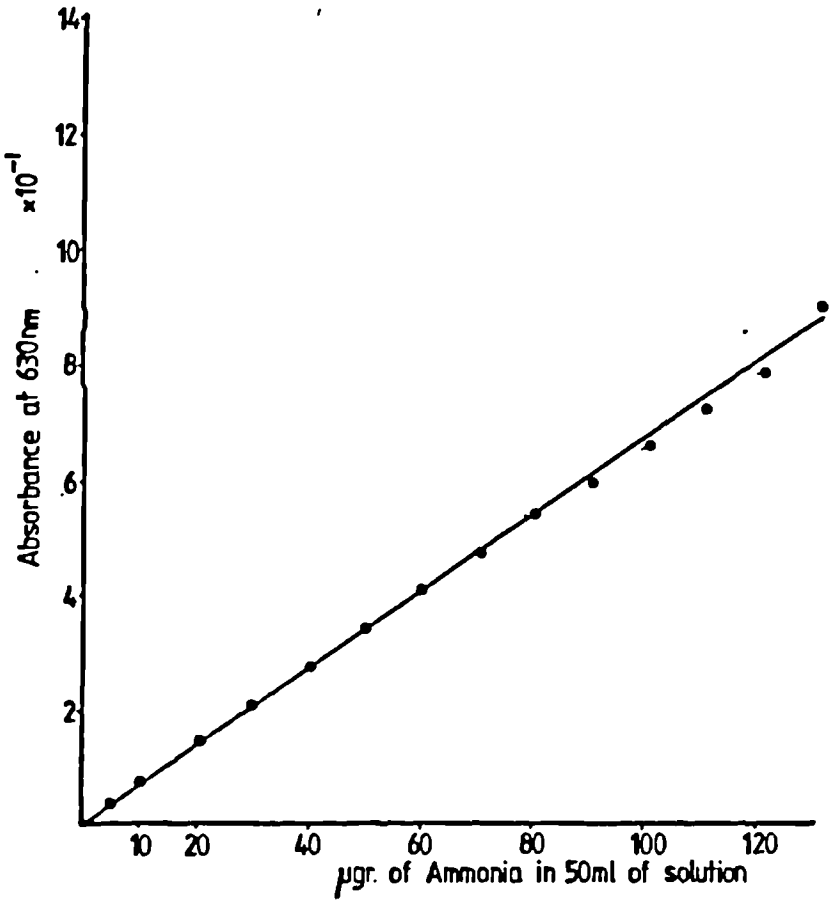

Table 27: Time spent in each of the operations involved in the process of expelling the ammonia from the rocks for analysis.

OPERATION	TIME (minutes)
First fusion of NaOH	8
Cooling	8
Second fusion of NaOH	12
Cooling	8
Third fusion of NaOH	8
Cooling	8
Blank	10
Cooling	8
Sample	15
Cleaning	35
T O T A L	120

5.9.11.1. Required Time

It follows from the section under "Procedure" that a total of two hours are required to prepare a replicate of sample for analysis (see Table 27). This in turn means that, preparing four replicates of each sample, only one sample can be analysed in a day, if no mistakes are made. This is a handicap particularly when a large number of samples must be analysed.

5.9.11.2. Ejection of the Sample

Ejection of the sample can cause the loss of some solid before total decomposition can occur. This can happen for any one of three following causes:

1. If the argon flow is released too fast, some powder is blown out and sticks to the walls of the tube.

2. When the rate of heating is too fast, the effervescence of the sodium hydroxide is violent and some sample comes out as dust, which again sticks to the walls of the tube.

3. Finally, as a consequence of a fast heating rate, water may condense in the upper part of the nickel tube and, quite often, it condenses in the glass head, which warms up more slowly than the metal. A drop of this water falling on top of the hot fused mixture, causes sputtering of the mixture, which will remain on the walls of the tube. The result is always low values for the ammonia content.

5.9.11.3. Leaking of Ammonia

Leaking may occur at the junction of the glass head and the metal, due to differences in expansion coefficients of the nickel and the glass. This would cause low results. However, such difficulty has been overcome by putting a thin "teflon" tape between the glass and the metal surfaces. Two springs pull the glass head tightly to the metal, preventing any gas from escaping.

5.9.11.4. Heating of the Receiving Solution

Due to the high temperature at which the decomposition of the sample is achieved, both argon and gases coming out of the fusion pass, while still hot, to the hydrochloric acid solution thus raising its temperature. This may cause loss of ammonia through evaporation. In order to avoid this, the flask containing the hydrochloric acid solution was immersed in a beaker of cold water.

5.9.11.5. The Amount of Sample

The amount of sample added in each fusion must be kept below 1g. This is the upper limit. Samples over one gram may not be fully decomposed. 0.5g of sample is considered an ideal amount. Theoretically, there is no lower limit for the amount of sample as long as it can be accurately weighed out and the recoveries of the method were measured with 5 mg of ammonium phosphomolybdate.

5.9.11.6. Use of Plastic Cells

Although these were used in the present

investigation their use is not recommended because, no matter how carefully they are handled and washed, they soon become dark and do not match. A change of cell when the analysis is in progress affects the reproducibility of the results. This difficulty was overcome by keeping the cells in water overnight.

5.9.11.7. Addition of the Water

Once the sample has been deposited in the nickel tube, care has to be taken during the addition of the 0.2 ml of water. This should be done slowly and against the walls of the tube since dropping the water on top of the sample will cause ejection of powder and consequent low results. This is particularly so if the amount of sample is very small and the ammonia content is high.

5.9.11.8. Other Comments

Due to the conditions in which the fusion of the sample is carried out, high temperature and fused sodium hydroxide, special safety precautions have to be taken:

1. Always handle the crucible with a strong pair of tweezers and wear gloves.

2. The tube should always be handled only when the sodium hydroxide is fused.

3. When cooling the tube under the tap water, do it slowly and check that no water gets into the tube since this will give rise to a high blank.

Table 28: Recoveries of Ammonia.

Test No.	$\mu g\ NH_3$	
1	137.00	Average of 4 blanks = 0.62 μg
2	134.25	
3	135.92	Total NH_3 recovered =
4	138.23	= 134.84 μg - 0.62 μg =
5	126.68	= 134.22 μg in 5 $x10^{-3}g$
6	135.82	
7	141.17	= 2.68% of NH_3 in the salt
8	131.66	
9	137.39	The theoretical value is 2.72%
10	125.31	
11	136.50	hence % recovery is 98.5%
12	128.90	
13	137.50	However the purity of the salt
14	138.30	
15	138.00	is not known.
$\bar{X}$	134.84	
σ_{n-1}	4.63	
R.S.D.	3.4%	

5.10. *Results and Discussion*

5.10.1. Recoveries

Before any samples were analysed, the recovery of ammonia during the fusion step was tested by using 5 mg of ammonium phosphomolybdate, following exactly the procedure described in Section 5.9.4. However, in order to weigh accurately and add such small amount of sample properly, very small glass cups with appropriate supports were designed. The results obtained are given in Table 28 and are very satisfactory.

5.10.2. Analysis of Samples

Twenty-two samples of shales and dolostones from the Fucoid Beds and a sample of buddingtonite were analysed by the previously described method. With few exceptions, four replicates of each sample were performed and the results are given in Table 29. Also included in this table are the nature of the rock and the relative standard deviation for the four replicates. The results are illustrated in Fig. 45. It can be seen from the table and Fig. 5 that a large amount of NH_3 is present in feldspar-rich shales and that quartzites contain the smallest amount of ammonia. These results agree with previous investigations (207, 222, 223). Barker (207) stated that feldspars contain higher amounts of ammonia than that of its coexisting quartz and reported that the amount of nitrogen in alkali feldspars range from 3 ppm to 125 ppm. Although the highest values have been reported in buddingtonite (221), and micas (211, 222, 223), relatively high values in shales are not uncommon (222), usually associated with high organic carbon content, indicating that

Fig. 45: The distribution of ammonia in different types of rocks.

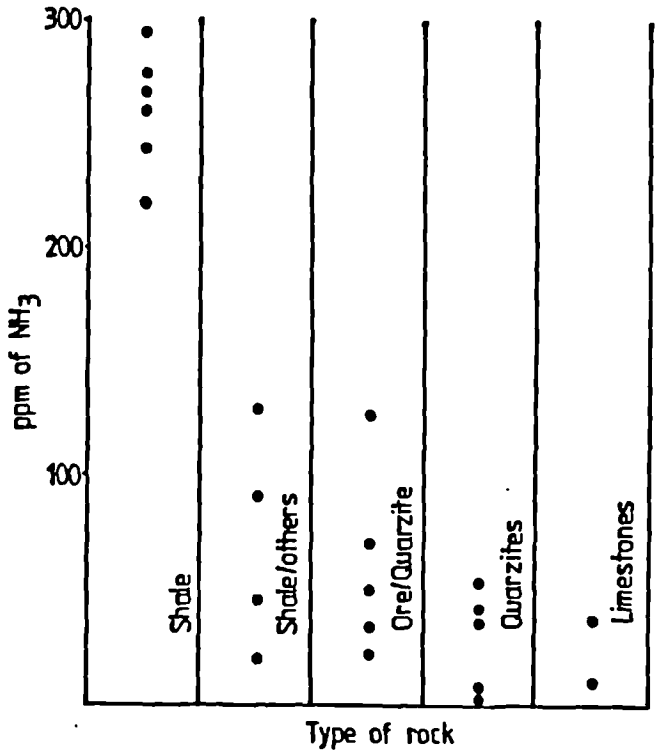

Table 29: Results obtained for twenty-two samples from the Cambro-Ordovician formation in Northwest Scotland, and a buddingtonite specimen.

Sample	Kind of Rock	ppm.NH_3	Replicate	R.S.D.%
1	Ore-Quartzite	128.0	4	2.7
2	Quartzite	55.0	4	2.6
3	Shale	263.0	4	0.4
4	Quartzite	7.3	4	6.3
5	Quartzite	43.6	4	4.1
6	Quartzite	5.6	4	5.0
7	Ore-Quartzite	22.0	4	2.3
8	Carbonate	37.5	4	10.5
9	Ore-Quartzite-Shale	35.6	4	2.8
10	Ore-Quartzite	52.2	4	6.1
11	Ore-Quartzite	73.0	4	2.2
12	Quartzite	36.6	4	2.1
13	Carbonate/Ore	11.6	4	4.2
14	Quartzite/Shale	20.3	4	1.5
15	Carbonate/Shale	93.0	4	1.7
16	Shale	221.4	4	0.6
17	Shale	245.0	4	2.2
18	Shale	276.8	4	1.2
19	Shale/Carbonate	132.3	5	2.7
20	Shale	270.0	4	2.0
21	Shale	295.5	4	2.4
22	Feldspar	46.7	5	5.6
23	Buddingtonite	3.24%	6	2.0

this type of rock was formed in the presence of organic matter (281).

Six replicates of the mineral buddingtonite were carried out using 0.1g of sample and the percentage of ammonia was found to be 3.24%. This value, compared with that reported for the pure mineral, 7.95% (221), is low. However, the purity of the sample is not known. In order to check this result, the amount of NH_3 present in the buddingtonite sample was determined by the method used by Erd et al. (221), i.e., expelling the ammonia from the mineral with a strong solution of sodium hydroxide and collecting it in an excess of acid for subsequent titration of the excess of acid with a standardised solution of sodium hydroxide. Due to the small amount of sample available, only two replicates were made by this method and the percentage of ammonia was found to be 3.19%, which, compared with 3.24% obtained from the fusion of the sample, shows good agreement.

5.10.3. The Blanks

A total of twenty-seven blanks were determined during the application of the method to the analysis of rocks. The values for such blanks are given in Table 30. A histogram of the blanks is shown in Fig. 46. The maximum amount of ammonia in the blank (2 µg) corresponds to 4 ppm on the 0.5g sample recommended.

5.10.4. Detection Limit

The detection limit as defined by Roos (282, 283) is:

$$D.L. = 1.645 \sqrt{2}s$$

Fig. 46: A histogram for the blanks obtained in the analysis of rocks for ammonia.

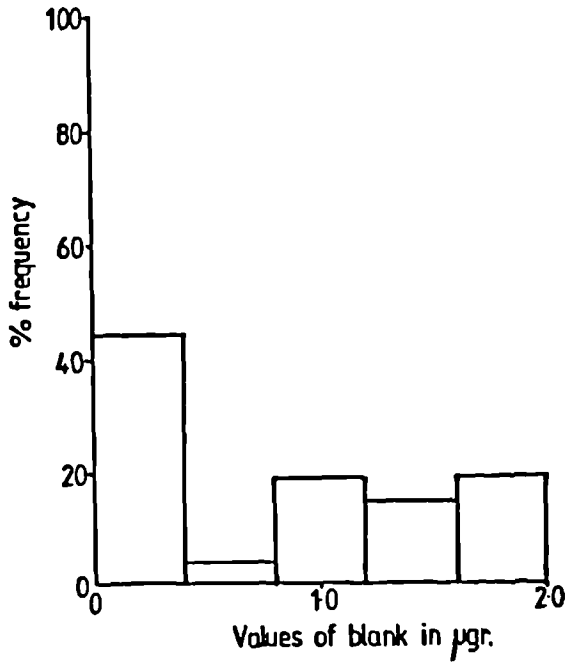

Table 30: Value of the blanks for ammonia in rocks.

Blank No.	µg NH_3	
1	0.3	$\bar{x}$ = 0.71 µg.
2	1.5	
3	0.1	The standard deviation
4	0.0	
5	0.1	of the blank was
6	1.2	
7	1.9	0.71 µg.
8	0.0	
9	0.1	
10	0.9	
11	0.0	
12	1.9	
13	1.6	
14	1.1	
15	0.0	
16	0.2	
17	1.7	
18	0.0	
19	0.0	
20	0.0	
21	1.5	
22	1.8	
23	0.1	
24	0.8	
25	0.5	
26	1.1	
27	0.8	

where S stands for the standard deviation of the blanks.

$$D.L. = 1.645\ \sqrt{2} \times 0.71 = 1.7\ \mu g$$

This is equal to 1.7 ppm on 1g sample.

5.10.5. Conclusions

1. It follows from the results that the amount of ammonia present in the rocks is very low. If all the ammonia is present as buddingtonite, it represents about 0.3% of the mineral in the shales and even less in other rock types.

2. The highest ammonia content is present in shales and probably comes from the remains of organic material present at the time when the rocks were formed.

3. The ammonia content in the sample of buddingtonite is low, but the purity of the sample is unknown.

4. The method has a precision of +/- 2.0% for large amounts of ammonia and +/- 5.0% for samples around 30 ppm.

A P P E N D I X E S

Appendix 1: pH, potassium (ion) and silica concentrations for ground waters from different localities.- Concentrations of K^+ and silica in umol l^{-1}.

pH	K^+	SiO_2	$\log\frac{[K^+]}{[H^+]}$	$-\log[H_4SiO_4]$	Ref.
4.4	63.9	259.6	0.2	3.6	136
4.85	102.3	258.0	0.9	3.6	"
5.25	51.2	126.5	1.0	3.9	"
4.4	51.2	91.5	0.1	4.0	"
5.0	115.1	299.6	1.0	3.5	"
5.0	89.5	296.2	0.9	3.5	"
5.96	25.6	166.4	1.4	3.8	"
6.51	127.9	346.1	2.6	3.5	"
6.50	89.5	312.9	2.5	3.5	"
6.9	593.8	1015.1	3.7	3.0	"
7.0	734.1	965.2	3.9	3.0	"
7.0	286.5	535.9	3.5	3.3	"
6.60	271.1	451.0	3.0	3.3	"
6.90	409.2	574.1	3.5	3.2	"
6.75	217.4	722.3	3.1	3.1	"
6.6	3007.8	1184.8	4.1	2.9	"
7.1	43.5	321.2	2.7	3.5	134
7.0	122.8	414.4	3.1	3.3	"
7.6	163.7	577.5	3.8	3.2	"
8.6	58.8	246.3	4.4	3.6	"
7.9	299.2	441.0	4.4	3.4	"
6.8	243.0	306.2	3.2	3.5	"
6.3	176.5	402.7	2.5	3.4	"
6.9	156.0	665.7	3.1	3.2	"
7.1	145.8	713.9	3.3	3.1	"

Appendix 1 (cont.)

pH	K^+	SiO_2	$\log\frac{[K^+]}{[H^+]}$	$-\log[H_4SiO_4]$	Ref.
7.6	209.7	1233.2	3.9	2.9	134
7.6	145.8	1218.2	3.8	2.9	"
8.2	746.8	382.8	5.1	3.4	"
7.6	30.7	366.1	3.1	3.4	135
7.4	20.5	299.6	2.7	3.5	"
7.2	51.2	118.2	2.9	3.9	"
7.2	25.6	366.1	2.6	3.4	"
6.8	25.6	233.0	2.2	3.6	"
7.3	97.2	432.7	3.3	3.3	"
6.4	35.8	249.6	2.0	3.6	"
5.7	38.4	166.4	1.3	3.8	"
6.9	17.9	332.8	2.1	3.5	"
7.1	25.6	299.6	2.5	3.5	"
4.8	32.00	110.00	0.31	3.96	111
5.0	35.00	98.00	0.54	4.00	"
5.0	33.00	105.00	0.52	3.98	"
5.18	37.00	98.00	0.75	4.00	"
5.30	36.00	103.00	0.90	3.99	"
5.05	26.00	110.00	0.46	3.96	"
4.77	31.00	94.00	0.26	4.00	"
4.91	29.00	93.00	0.37	4.03	"
4.90	46.00	74.00	0.56	4.13	"
5.19	39.00	83.00	0.78	4.10	"
4.91	36.00	82.00	0.47	4.10	"
5.41	37.00	71.00	0.98	4.15	"
5.20	30.00	71.00	0.68	4.15	"

Appendix 1 (cont.)

pH	K^+	SiO_2	$\log\frac{[K^+]}{[H^+]}$	$-\log[H_4SiO_4]$	Ref.
5.35	23.00	73.00	0.71	4.14	111
5.22	34.00	100.00	0.75	4.00	"
5.02	30.00	99.00	0.50	4.00	"
7.7	306.92	549.18	4.19	3.26	137
8.0	767.30	366.12	4.88	3.44	"
8.0	409.23	432.68	4.61	3.36	"
7.9	199.50	565.82	4.20	3.25	"
7.6	485.96	299.55	4.29	3.52	"
7.5	332.50	432.68	4.02	3.36	"
7.5	204.61	399.40	3.81	3.40	"
7.5	306.92	532.53	3.99	3.27	"
7.9	117.65	515.89	3.97	3.29	"
7.7	217.40	465.97	4.04	3.33	"
7.6	332.50	582.46	4.12	3.23	"
7.6	332.50	465.97	4.12	3.33	"
7.7	332.50	449.33	4.22	3.35	"
7.5	460.38	465.97	4.16	3.33	"
7.6	690.57	316.19	4.44	3.50	"
7.9	232.75	399.40	4.27	3.40	"
7.5	741.73	515.89	4.37	3.29	"
7.3	168.81	183.06	3.53	3.74	"
8.0	166.25	432.68	4.22	3.36	"
7.5	153.46	382.76	3.69	3.42	"
7.5	186.71	465.97	3.77	3.33	"
7.3	186.71	432.68	3.57	3.36	"
7.4	40.92	499.25	3.01	3.30	"

Appendix 1 (cont.)

pH	K^+	SiO_2	$\log\frac{[K^+]}{[H^+]}$	$-\log[H_4SiO_4]$	Ref.
7.0	281.34	482.61	3.45	3.32	137
7.6	306.92	532.53	4.09	3.27	"
7.7	741.73	499.25	4.57	3.30	"
7.6	86.96	482.61	3.54	3.32	"
7.2	383.65	465.97	3.78	3.33	"
7.6	204.61	499.25	3.91	3.30	"
7.5	485.96	465.97	4.19	3.33	"
7.2	383.65	499.25	3.78	3.30	"
8.1	158.58	366.12	4.30	3.44	"
8.1	219.96	449.33	4.44	3.35	"
7.7	332.50	316.19	4.22	3.50	"

Appendix 2: pH , potassium ion and silica concentrations for some geothermal waters in Iceland.-
Concentrations in umol l^{-1}.

pH	K^+	SiO_2	$\log\frac{[K^+]}{[H^+]}$	$-\log[H_4SiO_4]$	Ref.
9.31	42.50	624.10	4.94	3.20	138
9.91	2.30	497.60	4.30	3.30	"
9.92	4.10	835.41	4.53	3.10	"
9.69	5.63	607.42	4.44	3.22	"
7.53	31,843.10	8,896.70	6.03	2.05	"
6.38	43,992.00	10,500.92	5.02	2.00	"
9.30	138.11	2,992.20	5.44	2.52	"
9.28	158.83	4,207.02	5.50	2.40	"
8.82	342.73	4,676.32	5.40	2.33	"
9.02	741.73	9.577.30	5.90	2.02	"
8.52	920.80	12,760.90	5.50	1.90	"
9.33	652.21	7,368.95	6.14	2.13	"
8.20	613.84	7.427.20	5.00	2.13	"

Appendix 3: pH, potassium ion and silica concentrations for several rivers of the world.-
Concentrations in um l^{-1}.

pH	K^+	SiO_2	$\log\frac{[K^+]}{[H^+]}$	$-\log[H_4SiO_4]$	Ref.
7.1	58.8	332.8	2.9	3.5	134
4.64	3.81	40.44	-0.78	4.40	140
7.50	36.60	196.04	3.10	3.71	"
8.5	178.01	244.00	4.80	3.61	"
4.90	5.90	73.72	-0.33	4.13	125
8.1	15.3	51.60	3.3	4.3	141
8.1	17.9	53.25	3.3	4.3	"
8.0	17.9	49.93	3.2	4.3	"
8.1	12.8	48.30	3.2	4.3	"
8.0	20.5	53.30	3.3	4.3	"
7.4	53.7	66.6	3.1	4.2	142
6.6	20.5	59.9	1.9	4.2	"
6.9	125.3	296.2	3.0	3.5	"
6.9	63.9	154.8	2.7	3.8	"
4.7	24.3	91.5	0.1	4.0	"
4.5	69.1	149.8	0.3	3.8	"
7.1	63.9	154.8	2.9	3.8	"
4.4	35.8	119.8	-0.1	3.9	"
4.1	33.2	118.2	-0.4	3.9	"
5.7	28.1	93.2	1.1	4.0	"
6.7	46.0	199.7	2.4	3.7	"
6.9	33.2	81.5	2.4	4.1	143
7.8	127.9	191.4	3.9	3.7	"
8.3	173.9	299.6	4.5	3.5	"

Appendix 3 (cont.)

pH	K^+	SiO_2	$\log\frac{[K^+]}{[H^+]}$	$-\log[H_4SiO_4]$	Ref.
8.3	112.5	166.4	4.4	3.8	143
8.4	87.0	224.7	4.3	3.6	144
8.4	99.7	332.8	4.4	3.5	"
8.0	48.6	416.0	3.7	3.4	"
7.6	35.8	291.2	3.2	3.5	"
7.7	71.6	366.1	3.6	3.4	"
6.7	6.39	208.0	1.5	3.7	"
7.1	10.2	233.0	2.1	3.6	"
7.5	230.2	916.1	3.8	3.0	139
8.3	562.7	416.4	5.1	3.4	"
6.8	25.6	166.6	2.2	3.8	"
6.35	11.00	113.00	1.40	1.40	111
6.69	16.00	105.00	1.90	4.00	"
6.51	15.00	116.00	1.70	3.90	"
6.51	13.00	129.00	1.60	3.90	"
6.30	10.00	118.00	1.30	3.90	"
6.50	15.00	109.00	1.70	4.00	"
6.30	11.00	124.00	1.30	3.90	"
6.41	15.00	123.00	1.60	3.90	"
6.39	9.00	124.00	1.30	3.90	"
6.35	14.00	128.00	1.50	3.90	"
6.4	25.00	100.00	1.80	4.00	"
6.5	18.00	128.00	1.70	3.90	"
6.2	14.00	123.00	1.30	3.90	"
6.15	12.00	114.00	1.20	3.90	"
6.50	16.00	133.00	1.70	3.90	"

Appendix 3 (cont.)

pH	K^+	SiO_2	$\log\frac{[K^+]}{[H^+]}$	$-\log[H_4SiO_4]$	Ref.
6.46	15.00	135.00	1.60	3.90	111
7.0	17.90	154.77	2.25	3.81	145
7.0	23.02	166.42	2.36	3.78	"
7.1	17.90	166.42	2.35	3.78	"
7.2	20.46	183.06	2.51	3.74	"
7.0	10.23	58.25	2.01	4.23	"
7.0	10.23	114.83	2.01	3.94	"
7.2	12.79	166.42	2.31	3.78	"
7.2	15.35	161.42	2.39	3.79	"
7.1	15.35	166.42	2.29	3.78	"
7.0	12.79	166.42	2.11	3.78	"
7.33	17.90	183.06	2.58	3.74	"
6.7	10.23	79.88	1.71	4.10	"
6.4	7.67	63.24	1.28	4.20	"
6.7	7.67	73.22	1.58	4.14	"
8.0	10.23	79.88	3.01	4.10	"
8.1	12.79	104.84	3.21	3.98	"
7.1	12.79	88.20	2.21	4.05	"
7.8	15.35	64.90	2.99	4.19	"
8.0	15.35	59.91	3.19	4.22	"
8.0	17.90	68.23	3.25	4.17	"
7.1	10.23	149.78	2.1	3.8	146
6.5	15.35	149.78	1.6	3.8	"
7.1	10.23	149.78	2.1	3.8	"
6.5	15.35	149.78	1.6	3.8	"

Appendix 4: pH, potassium ion, and silica concentration for some fresh and alkaline lakes.-

Concentration in um l^{-1}.

pH	K^+	SiO_2	$\log\frac{[K^+]}{[H^+]}$	$-\log[H_4SiO_4]$	Ref.
9.70	8133.41	108.20	7.61	4.00	118
9.70	29547.60	3449.00	8.20	2.50	"
9.00	2122.90	74.90	6.30	4.13	"
7.1	220.0	1830.6	3.4	2.7	150
9.2	514.1	329.5	5.9	3.5	134
9.9	81290.60	5580.00	8.81	2.30	151
9.7	58800.96	2990.51	8.50	2.52	"
9.3	7430.05	1060.10	7.20	3.00	"
9.7	191500.84	9151.30	9.00	2.05	"
9.7	176039.70	9520.72	8.95	2.02	"
8.1	5678.04	183.10	5.85	3.74	152
8.6	33889.20	54.92	7.13	4.30	"
7.6	21407.74	316.20	5.93	3.50	"
7.9	58315.42	166.42	6.70	3.80	"
7.8	8286.90	199.70	5.72	3.70	"
7.6	43.48	299.60	3.23	3.52	153
7.4	40.92	266.30	3.01	3.60	"
8.1	94.63	216.34	4.10	3.70	"
8.8	133.00	765.52	4.92	3.12	"
6.9	35.81	316.20	2.50	3.50	"
10.1	226354.29	9019.80	9.45	2.04	119
9.8	99493.58	10733.9	8.80	1.97	"
9.2	281.34	599.10	5.65	3.22	"

Appendix 4 (cont.)

pH	K^+	SiO_2	$\log\frac{[K^+]}{[H^+]}$	$-\log[H_4SiO_4]$	Ref.
9.7	41690.11	915.29	8.32	3.04	119
7.8	82868.69	316.19	6.72	3.50	"
9.5	2608.83	2363.12	6.92	2.63	"
9.6	29924.8	232.98	8.08	3.63	"
7.0	56.2	281.24	2.7	3.5	155
8.0	97.1	69.9	4.7	4.1	"
7.1	94.6	144.78	3.0	3.8	"
9.3	161.1	43.27	5.5	4.3	"
8.0	168.8	44.93	4.2	4.3	"
7.0	166.2	111.5	3.2	3.9	"
7.2	406.6	183.06	3.8	3.7	"
8.1	391.3	183.06	4.6	3.7	"
9.6	107.4	302.88	5.6	3.5	"
8.89	2020.5	33.28	6.2	4.4	"
9.1	2301.9	108.17	6.4	3.9	"
9.1	2174.0	149.78	6.4	3.8	"

Appendix 5: pH, potassium ion and silica concentrations for surface and deep oceanic waters.-
Concentrations in umol l^{-1}.

pH	K^+	SiO_2	$\log\frac{[K^+]}{[H^+]}$	$-\log[H_4SiO_4]$	Ref.
7.7	9719.2	75.0	5.7	4.1	165
8.2	9719.2	99.9	6.2	4.0	122
7.8	9719.2	0.3	5.7	6.5	157
8.2	9719.2	49.9	6.2	4.3	"
7.6	9719.2	49.9	5.6	4.3	168
8.21	9719.2	2.3	6.2	5.6	157-159
7.76	9719.2	2.6	5.7	5.6	"
7.55	9719.2	25.0	5.5	4.6	"
7.71	9719.2	94.8	5.7	4.0	"
7.70	9719.2	158.0	5.7	3.8	"
7.36	9719.2	156.4	5.3	3.8	"
8.21	9719.2	32.2	6.2	4.5	"
7.70	9719.2	74.8	5.7	4.1	"
7.59	9719.2	100.8	5.6	4.0	"
7.71	9719.2	131.0	5.7	3.9	"
8.21	9719.2	3.3	6.2	5.5	"
8.21	9719.2	2.7	6.2	5.6	"
7.76	9719.2	3.2	5.7	5.5	"
7.60	9719.2	7.2	5.6	5.1	"
7.57	9719.2	16.0	5.5	4.8	"
7.71	9719.2	68.5	5.7	4.2	"
7.70	9719.2	159.7	5.7	3.8	"
7.36	9719.2	143.1	5.3	3.8	"

Appendix 5 (cont.)

pH	K^+	SiO_2	$\log\frac{[K^+]}{[H^+]}$	$-\log[H_4SiO_4]$	Ref.
8.21	9719.2	2.7	6.2	5.5	157-159
7.71	9719.2	13.1	5.7	4.9	"
7.70	9719.2	68.9	5.7	4.2	"
7.36	9719.2	120.5	5.3	3.9	"
8.21	9719.2	5.0	6.2	5.3	"
8.21	9719.2	16.6	6.2	4.7	"
7.76	9719.2	25.0	5.7	4.6	"
7.60	9719.2	31.0	5.6	4.5	"
7.71	9719.2	66.6	5.7	4.2	"
7.36	9719.2	148.1	5.3	3.8	"
8.21	9719.2	5.2	6.2	5.3	"
7.60	9719.2	23.3	5.6	4.6	"
7.57	9719.2	51.5	5.5	4.3	"
7.7	9719.2	145.0	5.7	3.8	"
7.7	9719.2	70.5	5.7	4.1	166-167
7.9	9719.2	16.0	5.9	4.8	"
7.8	9719.2	38.9	5.8	4.4	"
7.8	9719.2	36.6	5.8	4.4	"

Appendix 6: pH, potassium ion and silica concentration for interstitial water from marine sediments. Concentrations in umol l^{-1}.

pH	K^+	SiO_2	$\log\frac{[K^+]}{[H^+]}$	$-\log[H_4SiO_4]$	Ref.
7.69	1099.80	221.33	4.73	3.70	172
7.78	946.34	437.70	4.76	3.40	"
7.60	1176.50	141.45	4.70	3.85	"
7.76	920.76	401.10	4.72	3.40	"
8.27	2506.52	988.52	5.70	3.01	"
7.04	5601.31	795.47	4.80	3.10	"
6.89	4834.00	286.24	4.60	3.54	"
7.4	4322.47	165.60	5.00	3.80	"
7.0	6752.26	386.10	4.80	3.41	"
7.95	2736.71	657.35	5.40	3.20	"
7.78	1892.68	69.40	5.10	4.16	"
7.83	5089.77	204.70	5.54	3.70	"
7.4	1053.20	575.80	5.42	3.24	"
7.33	4706.12	602.43	5.00	3.22	"
7.75	1713.64	178.10	5.00	3.75	"
7.01	3580.75	178.10	4.60	3.75	"
7.10	4834.01	535.86	4.80	3.30	"
7.05	4629.39	813.78	4.72	3.09	"
8.62	3145.94	169.75	6.12	3.80	"
7.6	11499.31	459.31	5.70	3.34	171
7.5	10199.70	199.70	5.51	3.70	"
8.1	11599.00	459.31	6.20	3.34	"
7.6	11199.70	710.60	5.65	3.15	"

Appendix 6 (cont.)

pH	K^+	SiO_2	$\log\frac{[K^+]}{[H^+]}$	$-\log[H_4SiO_4]$	Ref.
7.7	10100.00	820.44	5.70	3.10	171
7.8	8599.9	610.75	5.7	3.2	"
7.5	11199.7	429.36	5.5	3.4	"
7.2	7399.3	920.29	5.0	3.0	"
7.4	8900.7	109.84	5.3	4.0	"
7.0	5498.8	890.33	4.7	3.0	"
7.0	4700.9	1000.17	4.6	3.0	"
7.6	10599.0	399.40	5.6	3.4	"
7.2	8800.9	1199.87	5.1	2.9	"
7.5	10998.0	319.52	5.5	3.5	"
7.4	10199.7	920.29	5.4	3.0	"
7.3	7000.3	1209.85	5.1	2.9	"
7.9	11199.7	389.42	5.9	3.4	"
8.1	11900.8	319.52	6.2	3.5	"
7.4	8701.2	319.52	5.3	3.5	"
7.0	8099.9	459.31	4.9	3.3	"
7.1	9299.7	710.60	5.1	3.1	"
7.5	11000.2	199.70	5.5	3.7	"
7.2	7399.3	750.54	5.1	3.1	"
7.0	6900.6	610.75	4.8	3.2	"
7.0	5900.5	239.64	4.8	3.6	"

Appendix 7: The composition of water produced by weathering potassium feldspar.

Rain water: pH = 6.56, pK = 5.0, $[H_4SiO_4] = 10^{-6}$, $pCO_2 = 0.0173$ atm.

$[H_4SiO_4]$	$[H_3SiO_3^-]$	$[HCO_3^-]$	$[CO_3^{-2}]$	$[K^+]$	$[H^+]$
10.00×10^{-9}	1.72×10^{-13}	1.72×10^{-5}	3.66×10^{-11}	9.97×10^{-8}	1.75×10^{-5}
3.16×10^{-8}	5.44×10^{-13}	1.72×10^{-5}	3.66×10^{-11}	1.07×10^{-7}	1.75×10^{-5}
10.00×10^{-8}	1.72×10^{-12}	1.72×10^{-5}	3.67×10^{-11}	1.29×10^{-7}	1.74×10^{-5}
3.16×10^{-7}	5.46×10^{-12}	1.72×10^{-5}	3.7×10^{-11}	2.02×10^{-7}	1.71×10^{-5}
10.00×10^{-7}	1.73×10^{-11}	1.73×10^{-5}	3.73×10^{-11}	4.29×10^{-7}	1.73×10^{-5}
3.16×10^{-6}	5.60×10^{-11}	1.77×10^{-5}	3.89×10^{-11}	1.15×10^{-6}	1.69×10^{-5}
6.31×10^{-6}	1.15×10^{-10}	1.83×10^{-5}	4.13×10^{-11}	2.20×10^{-6}	1.64×10^{-5}
10.00×10^{-6}	1.90×10^{-10}	1.90×10^{-5}	4.44×10^{-11}	3.43×10^{-6}	1.59×10^{-5}
1.58×10^{-5}	3.17×10^{-10}	2.00×10^{-5}	4.96×10^{-11}	5.38×10^{-6}	1.50×10^{-5}
2.51×10^{-5}	5.48×10^{-10}	2.18×10^{-5}	5.91×10^{-11}	8.47×10^{-6}	1.37×10^{-5}
3.98×10^{-5}	9.95×10^{-10}	2.45×10^{-5}	7.75×10^{-11}	1.34×10^{-5}	1.20×10^{-5}
5.62×10^{-5}	1.62×10^{-9}	2.89×10^{-5}	1.03×10^{-10}	1.88×10^{-5}	1.04×10^{-5}
5.62×10^{-5}	2.03×10^{-9}	3.61×10^{-5}	1.62×10^{-10}	2.82×10^{-5}	8.30×10^{-6}
6.31×10^{-5}	2.46×10^{-9}	3.90×10^{-5}	1.88×10^{-10}	3.16×10^{-5}	7.70×10^{-6}
1.00×10^{-4}	5.52×10^{-9}	5.52×10^{-5}	3.77×10^{-10}	5.00×10^{-5}	4.44×10^{-6}
1.58×10^{-4}	1.31×10^{-8}	8.26×10^{-5}	8.46×10^{-10}	7.93×10^{-5}	3.63×10^{-6}
2.51×10^{-4}	3.21×10^{-8}	1.28×10^{-4}	2.02×10^{-9}	1.23×10^{-4}	2.36×10^{-6}
3.98×10^{-4}	7.97×10^{-8}	2.00×10^{-4}	4.97×10^{-9}	1.99×10^{-4}	1.50×10^{-6}
6.31×10^{-4}	2.00×10^{-7}	3.16×10^{-4}	1.24×10^{-9}	3.16×10^{-4}	9.50×10^{-7}
6.31×10^{-4}	3.98×10^{-7}	6.30×10^{-4}	4.93×10^{-8}	6.31×10^{-4}	4.76×10^{-7}

Appendix 8: The composition of water produced by weathering potassium feldspar.

Rain water: pH = 4.56, pK = 5.0, $[H_4SiO_4] = 10^{-6}$, $pCO_2 = 0.0173$ atm.

$[H_4SiO_4]$	$[H_3SiO_3^-]$	$[HCO_3^-]$	$[CO_3^{-2}]$	$[K^+]$	$[H^+]$
1.10×10^{-6}	9.2×10^{-12}	8.38×10^{-6}	8.72×10^{-12}	1.00×10^{-5}	3.58×10^{-5}
1.58×10^{-6}	1.33×10^{-11}	8.41×10^{-6}	8.78×10^{-12}	1.02×10^{-5}	3.57×10^{-5}
2.51×10^{-6}	2.13×10^{-11}	8.47×10^{-6}	8.9×10^{-12}	1.05×10^{-5}	3.54×10^{-5}
3.98×10^{-6}	3.41×10^{-11}	8.57×10^{-6}	9.10×10^{-12}	1.10×10^{-5}	3.50×10^{-5}
6.31×10^{-6}	5.50×10^{-11}	8.72×10^{-6}	9.44×10^{-12}	1.17×10^{-5}	3.44×10^{-5}
10.00×10^{-6}	8.98×10^{-11}	8.98×10^{-6}	9.99×10^{-12}	1.29×10^{-5}	1.34×10^{-5}
1.58×10^{-5}	1.49×10^{-10}	9.41×10^{-6}	1.10×10^{-11}	1.50×10^{-5}	3.19×10^{-5}
2.51×10^{-5}	2.55×10^{-10}	1.02×10^{-5}	1.28×10^{-11}	1.80×10^{-5}	2.95×10^{-5}
3.98×10^{-5}	4.6×10^{-10}	1.15×10^{-5}	1.65×10^{-11}	2.30×10^{-5}	2.60×10^{-5}
5.62×10^{-5}	7.53×10^{-10}	1.34×10^{-5}	2.22×10^{-11}	2.84×10^{-5}	2.24×10^{-5}
5.62×10^{-5}	9.84×10^{-10}	1.75×10^{-5}	3.80×10^{-11}	3.78×10^{-5}	1.71×10^{-5}
6.31×10^{-5}	1.22×10^{-9}	1.93×10^{-5}	4.62×10^{-11}	4.12×10^{-5}	1.55×10^{-5}
1.00×10^{-4}	3.17×10^{-9}	3.17×10^{-5}	1.25×10^{-10}	5.97×10^{-5}	9.46×10^{-6}
1.58×10^{-4}	8.10×10^{-9}	5.68×10^{-5}	3.99×10^{-10}	8.89×10^{-5}	5.29×10^{-6}
2.51×10^{-4}	2.53×10^{-8}	1.00×10^{-4}	1.26×10^{-9}	1.35×10^{-4}	2.98×10^{-6}
3.98×10^{-4}	6.89×10^{-8}	1.73×10^{-4}	3.71×10^{-9}	2.09×10^{-4}	1.73×10^{-6}
6.31×10^{-4}	1.82×10^{-7}	2.89×10^{-4}	1.03×10^{-8}	3.25×10^{-4}	1.04×10^{-6}
6.31×10^{-4}	3.80×10^{-7}	6.03×10^{-4}	4.51×10^{-8}	6.41×10^{-4}	5.00×10^{-7}

Appendix 9: The composition of water produced by weathering potassium feldspar.

Rain water: pH = 4.56, pK = 5.0, $[H_4SiO_4] = 10^{-6}$, $pCO_2 = 0.0003$ Atm.

$[H_4SiO_4]$	$[H_3SiO_3^-]$	$[HCO_3^-]$	$[CO_3^{-2}]$	$[K^+]$	$[H^+]$
10.00×10^{-7}	1.09×10^{-11}	1.89×10^{-7}	2.55×10^{-13}	9.97×10^{-6}	2.76×10^{-5}
1.58×10^{-6}	1.73×10^{-11}	1.90×10^{-7}	2.60×10^{-13}	1.02×10^{-5}	2.74×10^{-5}
2.51×10^{-6}	2.79×10^{-11}	1.92×10^{-7}	2.64×10^{-13}	1.05×10^{-5}	2.71×10^{-5}
3.98×10^{-6}	4.50×10^{-11}	1.96×10^{-7}	2.74×10^{-13}	1.10×10^{-5}	2.66×10^{-5}
6.31×10^{-6}	7.32×10^{-11}	2.02×10^{-7}	2.90×10^{-13}	1.17×10^{-5}	2.59×10^{-5}
10.00×10^{-6}	1.22×10^{-10}	2.12×10^{-7}	3.20×10^{-13}	1.30×10^{-5}	2.46×10^{-5}
1.58×10^{-5}	2.09×10^{-10}	2.30×10^{-7}	3.76×10^{-13}	1.49×10^{-5}	2.27×10^{-5}
2.51×10^{-5}	2.83×10^{-10}	2.66×10^{-7}	5.03×10^{-13}	1.8×10^{-5}	1.97×10^{-5}
3.98×10^{-5}	8.04×10^{-10}	3.52×10^{-7}	8.81×10^{-13}	2.30×10^{-5}	1.48×10^{-5}
5.62×10^{-5}	1.76×10^{-9}	4.55×10^{-7}	2.12×10^{-12}	2.84×10^{-5}	9.57×10^{-6}
5.62×10^{-5}	7.96×10^{-9}	2.46×10^{-6}	4.32×10^{-11}	3.78×10^{-5}	2.12×10^{-6}
6.31×10^{-5}	1.76×10^{-8}	4.84×10^{-6}	1.67×10^{-10}	4.12×10^{-5}	1.08×10^{-7}
1.00×10^{-4}	1.28×10^{-7}	2.23×10^{-5}	3.55×10^{-9}	5.96×10^{-5}	2.34×10^{-7}
1.6×10^{-4}	4.65×10^{-7}	5.11×10^{-5}	1.86×10^{-8}	8.89×10^{-5}	1.02×10^{-7}
2.51×10^{-4}	1.39×10^{-6}	9.63×10^{-5}	6.61×10^{-8}	1.35×10^{-4}	5.42×10^{-8}
3.98×10^{-4}	3.82×10^{-6}	1.70×10^{-4}	1.99×10^{-7}	2.09×10^{-4}	3.13×10^{-8}
6.31×10^{-4}	1.00×10^{-5}	2.76×10^{-4}	5.43×10^{-7}	3.25×10^{-4}	1.89×10^{-8}
6.31×10^{-4}	2.09×10^{-5}	5.76×10^{-4}	2.34×10^{-6}	6.46×10^{-4}	9.06×10^{-9}

Appendix 10: The composition of water produced by weathering potassium feldspar.

Rain water: pH = 4.56, pK = 5.0, $[H_4SiO_4] = 10^{-6}$, pCO_2 = 1 atm.

$[H_4SiO_4]$	$[H_3SiO_3^-]$	$[HCO_3^-]$	$[CO_3^{-2}]$	$[K^+]$	$[H^+]$
10.00×10^{-7}	2.05×10^{-12}	1.19×10^{-4}	3.02×10^{-11}	9.97×10^{-6}	1.46×10^{-4}
1.58×10^{-6}	3.25×10^{-12}	1.19×10^{-4}	3.03×10^{-11}	1.02×10^{-5}	1.46×10^{-4}
2.51×10^{-6}	5.16×10^{-12}	1.19×10^{-4}	3.04×10^{-11}	1.05×10^{-5}	1.50×10^{-4}
3.98×10^{-6}	8.20×10^{-12}	1.19×10^{-4}	3.05×10^{-11}	1.09×10^{-5}	1.46×10^{-4}
6.31×10^{-6}	1.30×10^{-11}	1.20×10^{-4}	3.06×10^{-11}	1.17×10^{-5}	1.45×10^{-4}
10.00×10^{-6}	2.07×10^{-11}	1.20×10^{-4}	3.09×10^{-11}	1.30×10^{-5}	1.45×10^{-4}
1.58×10^{-5}	3.31×10^{-11}	1.21×10^{-4}	3.14×10^{-11}	1.49×10^{-5}	1.44×10^{-4}
2.51×10^{-5}	5.30×10^{-11}	1.23×10^{-4}	3.21×10^{-11}	1.80×10^{-5}	1.42×10^{-4}
3.98×10^{-5}	8.57×10^{-11}	1.25×10^{-4}	3.33×10^{-11}	2.30×10^{-5}	1.39×10^{-4}
5.62×10^{-5}	1.24×10^{-10}	1.27×10^{-4}	3.47×10^{-11}	2.84×10^{-5}	1.36×10^{-4}
5.62×10^{-5}	1.28×10^{-10}	1.32×10^{-4}	3.73×10^{-11}	3.77×10^{-5}	1.32×10^{-4}
6.31×10^{-5}	1.46×10^{-10}	1.34×10^{-4}	3.83×10^{-11}	4.12×10^{-5}	1.30×10^{-4}
1.00×10^{-4}	2.47×10^{-10}	1.43×10^{-4}	4.40×10^{-11}	5.96×10^{-5}	1.21×10^{-4}
1.58×10^{-4}	4.38×10^{-10}	1.60×10^{-4}	5.48×10^{-11}	8.89×10^{-5}	1.09×10^{-4}
2.51×10^{-4}	8.21×10^{-10}	1.90×10^{-4}	1.70×10^{-11}	1.35×10^{-4}	1.18×10^{-5}
3.98×10^{-4}	1.67×10^{-9}	2.43×10^{-4}	1.26×10^{-10}	2.09×10^{-4}	1.16×10^{-5}
6.31×10^{-4}	3.69×10^{-9}	3.39×10^{-4}	2.46×10^{-10}	3.25×10^{-4}	5.13×10^{-5}
6.31×10^{-4}	6.86×10^{-9}	6.31×10^{-4}	8.51×10^{-10}	6.41×10^{-4}	2.76×10^{-5}
1.00×10^{-3}	1.71×10^{-8}	9.89×10^{-4}	2.10×10^{-9}	1.00×10^{-3}	1.76×10^{-5}
1.58×10^{-3}	4.23×10^{-8}	1.57×10^{-3}	5.26×10^{-9}	1.59×10^{-3}	1.11×10^{-5}
2.51×10^{-3}	1.08×10^{-7}	2.50×10^{-3}	1.33×10^{-8}	2.52×10^{-3}	6.99×10^{-6}
3.98×10^{-3}	2.72×10^{-7}	3.96×10^{-3}	3.35×10^{-8}	3.99×10^{-3}	4.40×10^{-6}

Appendix 11.- Summary Statistics: Major Elements.

Element	SiO_2	TiO_2	Al_2O_3	Fe_2O_3	MnO
Count rate error %	0.6	0.8	1.0	1.0	3.0
Std. error of estimate wt.%	0.54	0.03	0.52	0.15	0.01
Calibration lower	8.00	0.00	0.00	0.00	0.00
range upper	80.00	3.20	23.00	14.80	0.20
Detection limit wt.%	0.086	0.018	0.087	0.045	0.012
Accuracy +/- wt.% (average deviations of 11 standards)	0.46	0.11	0.36	0.10	0.008
precision c%: G-SL	0.76	1.55	0.75	1.45	11.1

Element	MgO	CaO	Na_2O	K_2O	P_2O_5
Count rate error %	1.5	0.6	0.7	0.6	1.6
Std. error of estimate wt.%	0.30	0.09	0.20	0.07	0.01
Calibration lower	0.00	0.00	0.00	0.00	0.00
range upper	50.00	32.50	5.40	5.00	0.60
Detection limit wt.%	0.165	0.006	0.155	0.002	0.018
Accuracy +/- wt.% (average deviations of 11 standards)	0.13	0.17	0.26	0.09	0.02
precision c%: G-SL	6.47	1.34	4.35	1.03	4.35

Appendix 12.- Summary Statistics: Trace Elements.

El.	C.R.E.%	S.E.of e.ppm.	U.L. ppm.	D.L. ppm.	Precis. c% G-TH
Zr	0.7	10	300	2.7	1.7
Y	0.9	4	150	1.4	2.4
Sr	0.9	14	800	1.5	0.9
U	4.0	1	100	9.4	55.9
Rb	0.9	9	600	1.7	4.3
Th	3.0	4	400	11.5	20.6
Pb	6.0	9	100	11.6	12.1
Ga	3.0	3	100	2.4	4.1
Zn	2.0	12	1400	1.8	1.6
Cu	1.5	8	400	4.4	10.9
Ni	1.5	12	2500	4.8	14.6
Co	0.5	3	250	3.2	4.9
Cr	1.2	22	3200	1.9	5.9
Ce	2.2	8	500	3.2	2.0
Ba	0.9	10	2500	12.3	2.7
La	2.5	6	250	3.9	6.1

El. = Element

C.R.E.% = Counting rate error %

S.E.of e.ppm. = Std. error of estimate ppm.

U.L.ppm. = Upper limit ppm.

D.L.ppm. = Detection limit ppm.

Precis. = Precision

Appendix 13: Normative mineral calculations for the Lewisian gneiss from the felsic band.

Mineral	6	7	8	9	10
Quartz	37.71	35.99	30.86	4.27	17.90
(Microcline)	(31.90)	(49.03)	(0.00)	(3.03)	(16.77)
(Albite)	(1.43)	(6.42)	(1.01)	(1.43)	(0.33)
(Anorthite)	(0.09)	(0.49)	(0.09)	(0.19)	(0.09)
Feldspar	33.44	55.95	1.11	4.67	17.20
(Phlogopite)	(2.89)	(1.69)	(0.00)	(1.72)	(6.41)
(Annite)	(0.43)	(0.00)	(0.00)	(0.10)	(0.00)
(Ferric-easton.)	(0.00)	(0.00)	(1.58)	(0.00)	(0.00)
(Ferric-sidero.)	(0.00)	(0.00)	(0.00)	(0.00)	(0.00)
Biotite	3.33	1.69	1.58	1.82	6.41
Muscovite	24.16	6.02	63.53	86.62	51.03
Goethite	1.82	0.63	1.03	1.36	4.50
Pyrophyllite	0.00	0.00	1.04	0.00	0.00
(Clinochlore)	(0.00)	(0.00)	(0.00)	(0.00)	(0.00)
(Brunsvigite)	(0.00)	(0.00)	(0.00)	(0.00)	(0.00)
(Thuringite)	(0.00)	(0.00)	(0.00)	(0.00)	(0.00)
Chlorite	0.00	0.00	0.00	0.00	0.00
Serpentine	0.00	0.00	0.00	0.00	0.00
Talc	0.00	0.00	0.00	0.00	0.00
Ilmenite	0.26	0.10	0.08	0.07	1.49
Rutile	0.00	0.00	0.86	0.00	0.26
Luecite	0.00	0.00	0.00	0.00	0.00
Kaolinite	0.00	0.00	0.00	0.00	0.00
T O T A L	100.75	100.40	100.13	98.85	98.84
SiO_2	+ 0.00	+ 0.00	+ 0.00	+ 0.00	+ 0.00
TiO_2	+ 0.00	+ 0.00	+ 0.00	+ 0.00	+ 0.00
Al_2O_3	+ 0.00	+ 0.00	+ 0.00	+ 0.00	+ 0.00
Fe_2O_3	+ 0.00	+ 0.00	+ 0.00	+ 0.00	+ 0.00
FeO	+ 0.00	+ 0.00	+ 0.00	+ 0.00	+ 0.00
MnO	+ 0.01	+ 0.01	+ 0.00	+ 0.02	+ 0.02
MgO	+ 0.00	+ 0.00	+ 0.00	+ 0.00	+ 0.00
CaO	+ 0.00	+ 0.00	+ 0.00	+ 0.00	+ 0.00
Na_2O	+ 0.00	+ 0.00	+ 0.00	+ 0.00	+ 0.00
K_2O	+ 0.00	+ 0.00	+ 0.00	+ 0.00	+ 0.00
P_2O_5	+ 0.01	+ 0.01	+ 0.02	+ 0.01	+ 0.02
H_2O	+ 0.03	- 0.04	- 0.09	+ 0.08	+ 0.69
CO_2	+ 0.21	+ 0.06	+ 0.18	+ 0.15	+ 0.18
Total Fe	+ 0.00	+ 0.00	+ 0.00	+ 0.00	+ 0.00

Easton. = eastonite
Sidero. = Siderophyllite

Appendix 13 (cont.)

Mineral	16	17	18	19	20
Quartz	1.91	27.12	31.38	16.23	36.03
(Microcline)	(0.00)	(0.00)	(6.52)	(64.38)	(0.00)
(Albite)	(1.09)	(2.28)	(0.16)	(3.13)	(0.33)
(Anorthite)	(0.09)	(0.09)	(0.14)	(0.64)	(0.29)
Feldspar	1.19	2.38	6.84	8.15	0.63
(Phlogopite)	(0.00)	(0.00)	(5.00)	(3.51)	(0.00)
(Annite)	(0.00)	(0.00)	(0.52)	(0.64)	(0.00)
(Ferric-easton.)	(1.37)	(1.93)	(0.00)	(0.00)	(1.15)
(Ferric-sidero.)	(0.00)	(0.00)	(0.00)	(0.00)	(0.00)
Biotite	1.37	1.93	5.52	4.16	1.15
Muscovite	37.40	62.76	50.75	8.77	31.31
Goethite	0.67	1.29	3.59	1.36	0.37
Pyrophyllite	56.21	3.57	0.00	0.00	29.58
(Clinochlore)	(0.00)	(0.00)	(0.00)	(0.00)	(0.00)
(Brunsvigite)	(0.00)	(0.00)	(0.00)	(0.00)	(0.00)
(Thuringite)	(0.00)	(0.00)	(0.00)	(0.00)	(0.00)
Chlorite	0.00	0.00	0.00	0.00	0.00
Serpentine	0.00	0.00	0.00	0.00	0.00
Talc	0.00	0.00	0.00	0.00	0.00
Ilmenite	0.02	0.02	0.58	0.39	0.02
Rutile	0.42	0.90	0.00	0.00	0.02
Luecite	0.00	0.00	0.00	0.00	0.00
Kaolinite	0.00	0.00	0.00	0.00	0.00
T O T A L	99.23	100.00	98.69	99.08	99.15
SiO_2	+ 0.00	+ 0.00	+ 0.00	+ 0.00	+ 0.00
TiO_2	+ 0.00	+ 0.00	+ 0.00	+ 0.00	+ 0.00
Al_2O_3	+ 0.00	+ 0.00	+ 0.00	+ 0.00	+ 0.00
Fe_2O_3	+ 0.00	+ 0.00	+ 0.00	+ 0.00	+ 0.00
FeO	+ 0.00	+ 0.00	+ 0.00	+ 0.00	+ 0.00
MnO	+ 0.01	+ 0.01	+ 0.02	+ 0.02	+ 0.00
MgO	+ 0.00	+ 0.00	+ 0.00	+ 0.00	+ 0.00
CaO	+ 0.00	+ 0.00	+ 0.00	+ 0.00	+ 0.00
Na_2O	+ 0.00	+ 0.00	+ 0.00	+ 0.00	+ 0.00
K_2O	+ 0.00	+ 0.00	+ 0.00	+ 0.00	+ 0.00
P_2O_5	+ 0.02	+ 0.03	+ 0.02	+ 0.05	+ 0.20
H_2O	+ 0.15	+ 0.28	+ 0.53	+ 0.37	- 0.17
CO_2	+ 0.13	+ 0.07	+ 0.08	+ 0.03	+ 0.09
Total Fe	+ 0.00	+ 0.00	+ 0.00	+ 0.00	+ 0.00

Easton. = eastonite
Sidero. = siderophyllite

Appendix 13 (cont.)

Mineral	23	24	25	26
Quartz	22.83	16.16	38.25	23.44
(Microcline)	(50.59)	(60.10)	(0.00)	(0.00)
(Albite)	(1.01)	(1.43)	(0.93)	(2.62)
(Anorthite)	(0.14)	(0.54)	(0.09)	(0.29)
Feldspar	51.75	62.08	1.02	2.92
(Phlogopite)	(4.79)	(4.72)	(0.00)	(0.00)
(Annite)	(0.83)	(0.84)	(0.00)	(0.00)
(Ferric-eastonite)	(0.00)	(0.00)	(1.37)	(1.50)
(Ferric-siderophyllite)	(0.00)	(0.00)	(0.00)	(0.00)
Biotite	5.63	5.57	1.37	1.50
Muscovite	17.85	12.84	56.93	40.18
Goethite	1.52	1.48	0.21	0.24
Pyrophyllite	0.00	0.00	1.51	30.25
(Clinochlore)	(0.00)	(0.00)	(0.00)	(0.00)
(Brunsvigite)	(0.00)	(0.00)	(0.00)	(0.00)
(Thuringite)	(0.00)	(0.00)	(0.00)	(0.00)
Chlorite	0.00	0.00	0.00	0.00
Serpentine	0.00	0.00	0.00	0.00
Talc	0.00	0.00	0.00	0.00
Ilmenite	0.43	0.47	0.02	0.02
Rutile	0.00	0.00	0.32	0.55
Luecite	0.00	0.00	0.00	0.00
Kaolinite	0.00	0.00	0.00	0.00
T O T A L	100.03	98.62	99.68	99.13
SiO_2	+ 0.00	+ 0.00	+ 0.00	+ 0.00
TiO_2	+ 0.00	+ 0.00	+ 0.00	+ 0.00
Al_2O_3	+ 0.00	+ 0.00	+ 0.00	+ 0.00
Fe_2O_3	+ 0.00	+ 0.00	+ 0.00	+ 0.00
FeO	+ 0.00	+ 0.00	+ 0.00	+ 0.00
MnO	+ 0.02	+ 0.02	+ 0.01	+ 0.01
MgO	+ 0.00	+ 0.00	+ 0.00	+ 0.00
CaO	+ 0.00	+ 0.00	+ 0.00	+ 0.00
Na_2O	+ 0.00	+ 0.00	+ 0.00	+ 0.00
K_2O	+ 0.00	+ 0.00	+ 0.00	+ 0.00
P_2O_5	+ 0.02	+ 0.07	+ 0.05	+ 0.19
H_2O	+ 0.22	+ 0.26	+ 0.15	+ 0.08
CO_2	+ 0.04	+ 0.16	+ 0.13	+ 0.12
Total Fe	+ 0.00	+ 0.00	+ 0.00	+ 0.00

Appendix 13 (cont.).

Mineral	27	40	41	42
Quartz	17.56	26.97	19.58	15.61
(Microcline)	(0.00)	(59.21)	(50.60)	(69.39)
(Albite)	(0.00)	(2.03)	(1.94)	(9.47)
(Anorthite)	(0.14)	(0.54)	(0.99)	(0.29)
Feldspar	0.14	61.79	53.54	79.17
(Phlogopite)	(0.00)	(3.27)	(5.31)	(2.03)
(Annite)	(0.00)	(1.26)	(0.75)	(0.18)
(Ferric-eastonite)	(1.45)	(0.00)	(0.00)	(0.00)
(Ferric-siderophyllite)	(0.00)	(0.00)	(0.00)	(0.00)
Biotite	1.45	4.53	6.06	2.21
Muscovite	72.42	5.07	17.34	2.15
Goethite	0.15	0.93	1.62	0.67
Pyrophyllite	7.04	0.00	0.00	0.00
(Clinochlore)	(0.00)	(0.00)	(0.00)	(0.00)
(Brunsvigite)	(0.00)	(0.00)	(0.00)	(0.00)
(Thuringite)	(0.00)	(0.00)	(0.00)	(0.00)
Chlorite	0.00	0.00	0.00	0.00
Serpentine	0.00	0.00	0.00	0.00
Talc	0.00	0.00	0.00	0.00
Ilmenite	0.02	0.39	0.70	0.13
Rutile	0.74	0.00	0.00	0.00
Luecite	0.00	0.00	0.00	0.00
Kaolinite	0.00	0.00	0.00	0.00
T O T A L	99.55	99.71	98.87	99.97
SiO_2	+ 0.00	+ 0.00	+ 0.00	+ 0.00
TiO_2	+ 0.00	+ 0.00	+ 0.00	+ 0.00
Al_2O_3	+ 0.00	+ 0.00	+ 0.00	+ 0.00
Fe_2O_3	+ 0.00	+ 0.00	+ 0.00	+ 0.00
FeO	+ 0.00	+ 0.00	+ 0.00	+ 0.00
MnO	+ 0.01	+ 0.02	+ 0.02	+ 0.01
MgO	+ 0.00	+ 0.00	+ 0.00	+ 0.00
CaO	+ 0.00	+ 0.00	+ 0.00	+ 0.00
Na_2O	+ 0.00	+ 0.00	+ 0.00	+ 0.00
K_2O	+ 0.00	+ 0.00	+ 0.00	+ 0.00
P_2O_5	+ 0.02	+ 0.06	+ 0.12	+ 0.04
H_2O	+ 0.21	+ 0.14	+ 0.74	+ 0.55
CO_2	+ 0.05	+ 0.25	+ 0.05	+ 0.08
Total Fe	+ 0.00	+ 0.00	+ 0.00	+ 0.00

Appendix 14: Computer program designed to perform the normative mineral calculations for the Lewisian gneiss from the felsic band.

```
1 rem "norm/2-anal-sil"
10 dim na$(100),ra(20),nm$(30),ma(30,30),m(30),k(30)
11 rem na$ is the name of the analyte
13 rem ra is the rock analysis
15 rem nm$ is the mineral name
17 rem ma is the mineral analysis
20 poke 59468,14
30 open4,4,7:print#4:close4
31 rem printer to buisness mode
40 c$=chr$(29):b1$="(":b2$=")":ss$=chr$(160)
41 rem c$=skip,ss$=shifted space-for formated printing
100 data "SiO2","TiO2","Al2O3","Fe2O3","FeO","MnO","MgO","CaO","Na2O","K2O"
110 data "P2O5","H2O","CO2","tot-Fe","Zr","Y","Sr","U","Rb","Th","Pb","Ga","Zn"
120 data "Cu","Ni","Co","Cr","Ce","Ba","La","SG"
130 fori=1to31:read na$(i):next
140 data"Quartz","(Microcline)","(Albite)","(Anorthite)","Feldspar"
150 data"(Phlogopite)","(Annite)","(Ferric-eastonite)"
154 data "(Ferric-siderophyllite)","Biotite"
160 data"Muscovite","Goethite","Pyrophyllite"
170 data "(Clinochlore)","(Brunsvigite)","(Thuringite)","Chlorite"
172 data"Serpentine","Talc","Ilmenite","Rutile"
180 data"Luecite","Kaolinite"
190 fori=1to23:read nm$(i):next
200 data 100,0,0,0,0,0,0,0,0,0,0,0,0
210 data 64.77,0,18.30,0,0,0,0,0,0,16.92,0,0
220 data 68.74,0,19.44,0,0,0,0,0,11.82,0,0,0
230 data 43.20,0,36.64,0,0,0,0,20.16,0,0,0,0
240 data 0,0,0,0,0,0,0,0,0,0,0,0
```

Appendix 14 (cont.)

```
250 data 43.21,0,12.21,0,0,0,28.98,0,0,11.29,0,4.31
260 data 35.21,0,9.95,0,42.12,0,0,0,0,9.20,0,3.52
270 data 0,0,40.09,47.10,0,0,0,0,0,9.26,0,3.54
280 data 29.38,0,14.95,7.81,0,0,19.71,0,0,0,0,3.53
290 data 0,0,0,0,0,0,0,0,0,0,0,0
300 data 45.27,0,38.38,0,0,0,0,0,0,11.83,0,4.52
310 data 0,0,0,89.86,0,0,0,0,0,0,0,10.14
320 data 66.71,0,28.29,0,0,0,0,0,0,0,0,5.00
330 data 32.43,0,18.34,0,0,0,36.27,0,0,0,0,12.96
340 data 25.26,0,14.29,0,50.35,0,0,0,0,0,0,10.1
350 data 14.25,0,24.18,10.94,34.08,0,0,0,0,0,0,8.55
360 data 0,0,0,0,0,0,0,0,0,0,0,0
370 data 43.36,0,0,0,0,0,43.64,0,0,0,0,13.00
380 data 63.36,0,0,0,0,0,31.89,0,0,0,0,4.75
390 data 0,52.65,0,0,47.35,0,0,0,0,0,0,0
400 data 0,100,0,0,0,0,0,0,0,0,0,0
410 data 37.99,0,32.23,0,0,0,0,0,0,29.78,0,0
420 for m=1to22:for c=1to12:read ma(m,c):next:next
430 data 0,1,1,1,0,1,1,1,1,0,0,0,0,1,1,1,0,0,0,0,0,0
440 fori=1to22:read k(i):next
500 gosub1000:rem input
510 gosub1500:rem "Albite,Anorthite"
520 gosub2000:rem"Leucite,Serpentine,   Phlogopite"
530 gosub3000:rem"Ilmenite,Rutile,Annite"
540 gosub4000:rem"K-feldspar,Muscovite ,Clinochlor"
550 gosub5000:rem"Brunsvigite,Thuringite,Goethite,Fe-Biotite"
560 gosub6000:rem"Pyrophyllite"
570 gosub7000:rem"Talc,Quartz,Feldspar,Biotite,Chlorite"
580 gosub8000:rem output
900 end
1000 input"sample number";ns
1100 dopen#1,"index-anal-sil",d1
1110 dopen#2,"file-anal-sil",d1
1120 rs%=4*ns-3
1130 record#1,(rs%)
1140 input#1,a$:ns%=val(a$)
1150 record#2,(ns%)
1160 fori=1to13
1170 input#2,a$:ra(i)=val(a$)
1180 next
1190 n$=""
1200 for i=1to3
1210 input#1,a$
1220 n$=n$+a$
1230 next
1290 dclose
```

Appendix 14 (cont.)

```
1400 return
1500 x=ra(9)/ma(3,9)
1510 m=3:gosub9000
1520 m(3)=100*x
1550 x=ra(8)/ma(4,8)
1560 m=4:gosub9000
1570 m(4)=100*x
1900 return
2000 a=ra(7)/ma(6,7):b=ra(10)/ma(6,10)
2010 x=a*(b>=a)+b*(a>b):x=-x
2020 m(6)=100*x
2030 m=6:gosub9000:rem"Phlogopite"
2040 x=ra(10)/ma(22,10)
2050 m(22)=100*x
2060 m=22:gosub9000:rem"Luecite"
2070 x=ra(7)/ma(18,7)
2080 m(18)=100*x
2090 m=18:gosub9000:rem"Serpentine"
2900 return
3000 a=ra(2)/ma(20,2):b=ra(5)/ma(20,5)
3010 x=a*(b>=a)+b*(a>b):x=-x
3020 m(20)=x*100
3030 m=20:gosub9000:rem"Ilmenite"
3040 x=ra(2)/ma(21,2)
3050 m(21)=x*100
3060 m=21:gosub9000:rem"Rutile"
3070 x=ra(5)/ma(7,5)
3080 m(7)=x*100:rem"Annite"
3090 m(22)=m(22)-x*100*218.25/511.91
3100 ra(5)=ra(5)-x*ma(7,5)
3110 ra(1)=ra(1)-x*100*60.09/511.91
3120 ra(12)=ra(12)-x*100*18.02/511.91
3900 return
4000 a=ra(1)/ma(2,1)*6/4
4010 b=m(22)*ma(22,10)/ma(2,10)/100
4020 x=a*(b>=a)+b*(a>=b):x=-x
4030 m(2)=100*x:rem"K-feldspar"
4040 ra(1)=ra(1)-x*ma(2,1)*4/6
4050 m(22)=m(22)-m(2)*ma(2,10)/ma(22,10)
4100 a=ra(3)*3/2/ma(11,3)
4110 b=m(2)*ma(2,10)/ma(11,10)/100
4120 x=a*(b>=a)+b*(a>b):x=-x
4130 m(11)=100*x:rem"Muscovite"
4140 ra(3)=ra(3)-x*ma(11,3)*2/3
4150 ra(12)=ra(12)-x*ma(11,12)
4160 m(2)=m(2)-100*x*ma(11,10)/ma(2,10)
4200 a=ra(3)/ma(14,3)
4210 b=m(18)*ma(18,7)/ma(14,7)
4220 x=a*(b>=a)+b*(a>b):x=-x
```

Appendix 14 (cont.)

```
4230 m(14)=100*x:rem"Clinochlor"
4240 ra(1)=x*100*120.18/3335.22+ra(1)
4250 ra(3)=ra(3)-x*100*611.64/3335.22
4260 ra(12)=ra(12)-x*100*72.06/3335.22
4270 m(18)=m(18)-x*100*2771.7/3335.22
4900 return
5000 goto5050
5050 a=ra(4)/479.1:b=ra(3)/305.84:c=m(6)/4173.15
5060 x=a:ifa>bthenx=b
5070 ifx>cthenx=c
5080 m(8)=x*5190.24:rem"Ferric-Eastonite"
5090 m(6)=m(6)-4173.15*x
5100 ra(3)=ra(3)-305.84*x
5110 ra(4)=ra(4)-479.1*x
5114 ra(1)=ra(1)+240.36*x
5120 a=ra(4)/479.1:b=ra(3)/305.84:c=m(7)/5119.1
5130 x=a:ifa>bthenx=b
5140 ifx>cthenx=c
5150 m(9)=6136.14*x:rem"Ferric-Siderophyllite"
5160 ra(3)=ra(3)-305.84*x
5170 ra(4)=ra(4)-479.1*x
5180 m(7)=m(7)-5119.1*x
5190 ra(1)=ra(1)+240.36*x
5200 a=ra(4)/3194:b=ra(3)/2446.56
5210 c=m(15)/11416.32
5220 x=a*(b>=a)+b*(a>b):x=-x
5230 x=x*(c>x)+c*(x>c):x=-x
5240 m(17)=16864.4*x:rem"thuringite"
5250 ra(1)=ra(1)+480.72*x
5260 ra(3)=ra(3)-2446.56*x
5270 ra(4)=ra(4)-3194*x
5280 ra(12)=ra(12)-288.24*x
5290 m(15)=m(15)-11416.32*x
5300 x=ra(4)/ma(12,4)
5310 m(12)=100*x:rem"geothite"
5320 m=12:gosub9000
5400 a=ra(1)/ma(2,1)*6/4
5410 b=m(22)*ma(22,10)/ma(2,10)/100
5420 x=a*(b>a=a)+b*(a>b):x=-x
5430 m(2)=m(2)+100*x:rem "Microcline" ex qtz from ferric-btt
5440 m(22)=m(22)-100*x*ma(2,10)/ma(22,10)
5900 return
6000 a=m(6)/8346.3:b=ra(3)/3262.08
6010 c=ra(1)/2163.24
6020 x=a*(b>=a)+b*(a>b):x=-x
```

Appendix 14 (cont.)

```
6030 x=x*(c>=x)+c*(x>c):x=-x
6040 m(14)=m(14)+x*6670.44:rem"Clinochloore"
6050 m(11)=m(11)+x*7965.9:rem"Muscovite"
6060 ra(1)=ra(1)-x*2163.24
6070 ra(3)=ra(3)-x*3262.08
6080 ra(12)=ra(12)-x*864.72
6100 a=m(8)/4068.36:b=m(7)/8190.48
6110 c=ra(1)/2884.32:d=ra(3)/3669.84
6120 a=a*(b>=a)+b*(a>b):a=-a
6130 c=c*(d>=c)+d*(c>d):c=-c
6140 x=a*(c>=a)+c*(a>c):x=-x
6150 m(16)=m(16)+10118.64*x:rem"Thuringite"
6160 m(11)=m(11)+9559.08*x:rem"Muscovite"
6170 ra(1)=ra(1)-2884.32*x
6180 ra(3)=ra(3)-3669.84*x
6190 ra(12)=ra(12)-864.72*x
6200 m(8)=m(8)-4068.36*x
6210 m(7)=m(7)-8190.48*x
6300 a=m(7)/10238.1:b=ra(3)/3262.08
6310 c=ra(1)/2163.24
6320 x=a*(b>=a)+b*(a>b):x=-x
6330 x=x*(c>=x)+c*(x>c):x=-x
6340 m(15)=m(15)+8562.24*x:rem"Brunsvigite"
6350 m(11)=m(11)+7965.9*x:rem"Muscovite"
6360 ra(1)=ra(1)-2163.24*x
6370 ra(3)=ra(3)-3262.08*x
6380 ra(12)=ra(12)-864.72*x
6390 m(7)=m(7)-10238.1*x
6500 a=ra(3)/ma(13,3)
6510 b=ra(1)/ma(13,1)
6520 x=a*(b>=a)+b*(a>b):x=-x
6530 m(13)=100*x:rem "Pyrophyllite"
6540 m=13:gosub9000
6600 a=ra(3)/101.94:b=m(13)/360.32
6610 x=a*(b>=a)+b*(a>b):x=-x
6620 m(23)=516.30*x:rem "Kaolinite"
6630 ra(3)=ra(3)-x*101.94
6640 m(13)=m(13)-x*360.32
6650 ra(12)=ra(12)-54.05*x:rem "H2O"
6900 return
7000 a=ra(1)/240.36:b=m(18)/554.33
7010 x=a*(b>=a)+b*(a>b):x=-x
7020 m(18)=m(18)-x*554.33
7030 m(19)=m(19)+758.67*x
7040 ra(1)=ra(1)-240.36*x
7050 ra(12)=ra(12)+36.03*x
```

Appendix 14 (cont.)

```
7060 m(1)=ra(1):ra(1)=0
7070 m(10)=m(6)+m(7)+m(8)+m(9):rem "Biotite"
7080 m(17)=m(14)+m(15)+m(16):rem "Chlorite"
7100 m(5)=m(2)+m(3)+m(4):rem "Feldspar"
7900 return
8000 open2,4,2
8010 print#2,"aaaaaaaaaaaaaaaaaaaaaaaaa      azzz.99a"
8020 close2
8021 rem formats printer
8030 open4,4
8040 print#4,"number of sample";ns
8050 print#4,"--------------------"
8060 print#4,"name of sample ";n$
8070 print#4:print#4
8080 print#4,"mineral                                  %"
8090 print#4:close4
8100 open4,4,1:tt=0
8110 fori=1to23
8114 if k(i)=0 then p1$=ss$+c$:p2$=p1$
8116 if k(i)=1 then p1$=b1$+c$:p2$=b2$+c$
8118 if k(i)=0 then tt=tt+m(i)
8120 print#4,nm$(i)c$p1$m(i)p2$
8130 next
8132 p1$=ss$+c$:p2$=ss$+c$
8134 print#4,"Total"c$p1$,tt,p2$
8140 close4
8150 open2,4,2
8160 print#2,"aaaaaaaaaaaaaaaaaaaaa     szz.99"
8170 close2
8180 open4,4,1
8300 print#4:print#4
8310 print#4,"residual analysis"
8320 print#4,"------------------":print#4
8330 print#4,"component                    %"
8340 print#4
8350 fori=1to14
8360 print#4,na$(i)c$ra(i)
8370 next
8380 print#4:print#4
8390 close4:open4,4,0
8400 print#4,"-----------------------------------------"
8410 print#4:print#4
8500 close4
8900 return
9000 for c=1to12
9010 ra(c)=ra(c)-x*ma(m,c)
9020 next
9090 return
9091 rem subtract components of mineral 'm' from rock analysis
```

REFERENCES

R E F E R E N C E S

1. M.J. Russel, A.J. Hall, R.C.R. Willan, I. Allison, R. Anderton, G. Bowes; On the Origin of the Aberfeldy Celsian + Baryte + Base Metal Deposits, Scotland. In: Prospecting in Areas of Glaciated Terrain, Inst. Min. Metal. 159 (1984).

2. J.P.B Lovell; The British Isles through Geological Time, George Allen and Unwin, London (1977).

3. J.A.G. Thomas; British Stratigraphy, George Allen and Unwin, London (1974).

4. A.H. Truesdell and B.F. Jones; J. Res. U.S. Geol. Survey, 2, 233 (1974).

5. J.W. Cowie; The Cambrian of Spitzbergen and Scotland. In: Cambrian of the British Isles, Norden and Spitzbergen, by C.H. Holland, 123, John Wiley and Sons, London (1974).

6. G.Y. Craig; Geology of Scotland, Scottish Academic Press, Edinburgh (1983).

7. N.G. Berridge; Natural Environment Research Council, Institute of Geological Sciences. Rep. No. 69/5, London (1969).

8. R. Anderton, P.H. Bridges, M.R. Leeder and B.W. Sellwood; A Dynamic Stratigraphy of the British Isles, George Allen and Unwin, London (1979).

9. R. Anderton, D.R. Bowes; Proc. Royal Soc. Edinburgh, 83B, 31 (1983).

10. T.R. Owen; The Geological Evolution of the British Iles, Pergamon Press, Oxford (1976).

11. R.C. Selley; J. Sed. Petrol., 35, 366 (1965).

12. A.D. Stewart; Torridonian Rocks of Western Scotland. In: Precambrian: A Correlation of Precambrian Rocks in the British Isles, Geol. Soc. Spec. Rep. No. 6 (1973).

13. S.H.U. Bowie, M.J. Gallagher, D. Ostle, J. Dawson; Trans. Inst. Min. Met., 75, B125 (1966).

14. K. Swett; Interpretation of Depositional and Diagenetic History of Cambrian Ordovician Succession of N.W. Scotland. In: North Atlantic Geology and Continental Drift. Am. Ass. Pet. Geologists. Mem. 12 (1969).

15. M.J. Rusell, I. Allison; Scott. J. Geol., 21, 113 (1985).

16. P.J. Brand; Soct. J. Geol., 1, 285 (1965).

17. K. Swett; J. Sed. Petrol., 35, 928 (1965).

18. P. W. Birkeland; Pedology, Weathering and Geomorphological Research, Oxford Univ. Press, London (1974).

19. T.R. Patton; The Formation of Soil Material, George Allen and Unwin, London (1978).

20. R.W. Cooke, I.J. Smalley; Nature, 220, 1227 (1968).

21. F. Hjulström; Transportation of Detritus by Moving Water. In: Recent Marine Sediments: A Symposium, Am. Ass. Petrol. Geol., Tulsa, Oklahoma (1939).

22. R.M. Garrels, F.T. Mackenzie; Evolution of Sedimentary Rocks, W.W. Norton and Company, New York (1971).

23. F.C. Loughnan; Chemical Weathering of Silicate Minerals, Am. Elsevier Publishing Cia., New York (1969).

24. K.B. Krauskopf; Introduction to Geochemistry, McGraw-Hill Inc., Tokio (1979).

25. W. Chesworth; Am. J. Science, 24, 69 (1973).

26. T.A. Jackson, W.D. Keller; Am. J. Science, 269, 446 (1970).

27. D. Carrol; Rock Weathering, Plenum Press, New York (1970).

28. C.D. Ollier; Weathering, Ed. by K.M. Clayton, Oliver and Boyd, Edinburgh (1969).

29. M.J. Wilson, D. Jones; Lichen Weathering of Minerals: Implications for Pedogenesis. In: Residual Deposits. By R.C.L. Wilson, Geol. Soc. Special Publication No. 11, Butler and Tanner, London (1983).

30. W.H. Huang and W.C. Kiang; Am. Min., 57, 1849 (1972).

31. W.H. Huang and W.D. Keller; Am. Min., 55, 2076 (1970).

32. D. Jones, M.J. Wilson, J.M. Tait; Lichenologist, 12, 277 (1980).

33. M.J. Wilson, D.J. Jones, W.J. McHardy; Lichenologist, 13, 167 (1981).

34. A. Schatz; Agr. and Food Chem., 11, 112 (1963).

35. M.J. Wilson, W.J. McHardy; J. of Microscopy, 120, 291 (1980).

36. D. Jones, M.J. Wilson, W.J. McHardy; J. of Microscopy, 124, 95 (1981).

37. K. Cromack et al.; Soil. Biol. Biochem., 11, 463 (1979).

38. W.C. Graustein, K. Cromack, Ph. Sollins; Sci., 198, 1252 (1977).

39. M.J. Wilson, D. Jones, J.D. Russell; Min. Mag., 43, 837 (1980).

40. K. Debnigh; The Principles of Chem. Equil., Cambridge Univ. Press, Cambridge (1981).

41. I.M. Klotz, R.M. Rosenberg; Chemical Thermodynamics, W.A. Benjamin, Inc. Menlo Park, California (1972).

42. G.N. Lewis, M. Randall; Thermodynamics and the Free Energy of Chemical Substances, McGraw-Hill Inc., London (1923).

43. F.D. Rossini; Chemical Thermodynamics, Wiley, New York, (1950).

44. R.A. Berner; Principles of Chem. Sedimentology, McGraw-Hill Book Company, New York (1971).

45. A.H. Brownlow; Geochemistry, Prentice Hall, Inc., Englewood Cliffs, N.J. (1979).

46. S. Glastone; Textbook of Physical Chemistry, MacMillan and C., London (1968).

47. R.M. Garrels, Ch.L. Christ; Solutions, Minerals and Equilibria, Harper and Row, New York (1965).

48. G.E. MacWood, F.H. Verhoek; J. Chem. Education, 38, 334 (1961).

49. L.H. Adams; Chemical Review, 19, 1 (1936).

50. R. Powell; Equilibrium Thermodynamics in Petrology and Introduction, Harper and Row, London (1978).

51. H.S. Harned, B.B. Owen; The Physical Chemistry of Electrolytic Solutions, Reinhold Publishing Corporation, New York (1958).

52. R.A. Robinson, R.H. Stokes; Electrolyte Solutions, Butterworth, London (1959).

53. D.A. MacInnes; J. Am. Chem. Society, 41, 1086 (1919).

54. C.W. Davies; Ion Association, Butterworth, Washington (1962)

55. K.K. Kelley and E.G. King; Bull. Bur. Mines No. 592, U.S. Government Printing Ofice, Washington (1961).

56. Y. Tardy; Am. J. Science, 279, 217 (1979).

57. J.G. Stark, H.G. Wallace; Chemistry Data Book, John Murray, London (1984).

58. Y. Tardy, R.M. Garrels; Geoch. et Cosm. Chem. Acta, 40, 1051 (1976).

59. W.M. Latimer, R.M. Buffington; J. Am. Chem. Society, 48, 2297 (1926).

60. R.E. Powell, W.L. Latimer; J. Chem. Phys., 19, 1139 (1951).

61. R.E. Connick, R.E. Powell; J. Chem. Phys., 21, 2206 (1953).

62. J.W. Cobble; J. Chem. Phys., 21, 1443 (1953).

63. J.W. Cobble; J. Chem. Phys., 21, 1446 (1953).

64. J.W. Cobble; J. Chem. Phys., 21, 1451 (1953).

65. A.M. Couture, K.J. Laidler; Can. J. Chem., 35, 202 (1957).

66. R. Barany, K. K. Kelley; Bureau of Mines. Rep. of Inv. No. 5825, U.S. Dep. of Interior (1961).

67. R. Barany; Bureau of Mines. Rep. of Inv. No. 6356, U.S. Dep. of Interior (1963).

68. E.G. King, W.W. Weller; Bureau of Mines. Rep. of Inv. No. 5810, U.S. Dep. of Interior (1961).

69. K.K. Kelley et al.; Bureau of Mines. Rep. of Inv. No. 4955, U.S. Dep. of Interior (1953).

70. K.K. Kelley; Bureau of Mines. Rep. of Inv. No. 5901, U.S. Dep. of Interior (1961).

71. J.A. Kittrick; Am. Min., 51, 1457 (1966).

72. W.H. Huang, W.C. Kiang; Am. Min., 58, (1973).

73. Ch. Chen; Am. J. of Sci., 275, 801 (1975).

74. J.O. Nriagu; Am. Min., 60, 834 (1975).

75. Y. Tardy, R.M. Garrels; Geoch. et Cosm. Chem. Acta, 38, 1101 (1974).

76. Y. Tardy, R.M. Garrels, Geoch. et Cosm. Chem. Acta, 41, 87 (1977).

77. R.A. Robie, B.S. Hemingway, J.R. Fisher; Geol. Surv. Bull. 1452, U.S. Gov. Print. Office, Washington (1978).

78. H.C. Helgeson, J.M. Delany, H.W. Nesbitt, D.K. Bird; Am. J. Science, 278A, 1107 (1978).

79. J.W. Cobble; Sci., 152, 1479 (1966).

80. C.M. Criss, J.W. Cobble; J. Am. Chem. Soc., 83, 3223 (1961).

81. J.C. Ahluwalia, J.W. Cobble; J. Am. Chem. Soc., 86, 5377 (1964).

82. R.E. Mitchell, J.W. Cobble; J. Am. Chem. Soc., 86, 5401 (1964).

83. E.C. Jekel, C.M. Criss, J.W. Cobble; J. Am. Chem. Soc., 86, 5404 (1964).

84. W.L. Gardner, E.C. Jekel, J.W. Cobble; J. Phys. Chem., 73, 2017 (1968).

85. J.C. Ahluwalia, J.W. Cobble, J. Am. Chem. Soc., 86, 5381 (1964).

86. J.W. Cobble; Thermodynamics. In: Annual Review of Physical Chemistry by H. Eyring, Palo Alto, California, 15 (1966).

87. C.M. Criss, J.W. Cobble, J. Am. Chem. Soc., 86, 5385 (1964).

88. C.M. Criss, J.W. Cobble; J. Am. Chem. Soc., 86, 5390 (1964).

89. W.L. Gardner, R.E. Mitchell, J.W. Cobble; J. Phys. Chem., 73, 2025 (1969).

90. H.C. Helgeson; J. Phys. Chem., 71, 3121 (1967).

91. H.C. Helgeson; Am. J. Sci., 267, 729 (1969).

92. B. Velde; Clays and Clay Minerals in Natural and Synthetic Systems, Elsevier Scientific Publishing Co, Amsterdam (1977).

93. D. Kerrick; Am. J. Science, 266, 204 (1968).

94. E.W. Nuffield; X-Ray Diffraction Methods, John Wiley and Sons, New York (1966).

95. R. Jenkins, J.L. De Vries; Practical X-Ray Spectrometry The MacMillan Press, London (1970).

96. J. Zussman; Physical Methods in Determinative Mineralogy, Academic Press, London (1977).

97. D.A. Skoog, D.M. West; Principles of Instrumental Analysis, Holt-Saunders International, Tokio (1980).

98. R. Jenkins, J.L. De Vries; An Introduction to X-Ray Powder Diffractometry, N.V. Philips (1970).

99. J.C.P.D.S. Mineral Powder Diffraction File. Search Manual (1980).

100. J.C.P.D.S. Mineral Powder Diffraction File. Data Book (1980).

101. M. Allman, D.F. Lawrence; Geological Laboratory Techniques, Blandon Press, London (1972).

102. L.K. Frevel; Ind. and. Eng. Chem., 16, 210 (1944).

103. H.P. Klug, L.E. Alexander; X-Ray Diffraction Procedures, John Wiley and Sons, New York (1954).

104. Ch. S. Hutchinson; Laboratory Handbook of Petrographic Techniques, John Wiley and Sons, New York (1974).

105. R.A. Yund and J. Tullis; Subsolidus Phase Relations in the Alkali Feldspars with Emphasis on Coherent Phases. In: Feldspar Mineralogy, Vol. 2, Min. Soc. Am., Chapter 6 (1983).

106. H.D. Megaw; The Architecture of Feldspars. In: The Feldspars, Proceedings of NATO Advanced Study Institute. By W.S. McKenzie, J. Zussman, Manchester (1974).

107. M.E. Cherry, L.T. Trembath; Am. Min. 64, 66 (1970).

108. P.K. Harvey, D.M. Taylor, R.D. Hendry, F. Bancroft; X-Ray Spectrometry, 2, 33 (1973).

109. K. Norrish, J.T. Hutton; Geoch. et Cosm. Chem. Acta, 33, 431 (1969).

110. B.E. Leake et al.; Chemical Geology, 5, 7 (1969-1970).

111. J.M. Verstraten; Water-Rock Interaction, Geo. Books, Norwich (1980).

112. J.B. Thompson, Am. J. Science, 253, 65 (1955).

113. D.S. Korzhinski; Eighteenth Intern. Geol. Congress Proc., Sec. A, 50 (1950).

114. G.W. Morey, R.O. Fournier, J.J. Rowe; J. Geoph. Research, 69, 1995 (1964).

115. G.W. Morey, R.O. Fournier, J.J. Rowe; Geoch. et Cosm. Chem. Acta, 26, 1029 (1962).

116. J.A. Kittrick; Clays and Clay Minerals, 17, 157 (1969).

117. J. Lewin; British Rivers, G. Allen and Unwin, London (1981).

118. Y.F. Kharaka et al.; Geoch. et Cosm. Chem. Acta, 48, 823 (1984).

119. H.P. Eugster, L.A. Hardie, Saline Lakes. In: Lakes: Chemistry, Geology and Physics. By Abraham Lerman. Chapter 8, Springer-Verlag, New York (1978).

120. W.S. Brocker; Chemical Oceanography, Harcourt Brace Jovanovich, Inc., New York (1974).

121. T. Pearce; New Scientist, Vol. 95, 419 (1982).

122. D.N. Lapedes; McGraw-Hill Encyclopaedia of the Geological Sciences, London (1978).

123. D. Carroll, Geol. Survey, Water-Supp. Paper, 1535-G., Washington (1962).

124. G.E. Likens, F.H. Bormann, J.S. Eaton; Variations in Precipitation and Stream Water Chemistry of the Hubbard Brook Experimental Forest during 1964-1977. In: Effects of Acid Precipitation on Terrestrial Ecosystems. By T.C. Hutchinson and H. Hava, Plenum Pres, London (1980).

125. N.M. Johnson et al.; Geoch. et Cosm. Chem. Acta, 45, 1421 (1981).

126. R.F. Stallard, J.M. Edmond; J. Geoph. Research, 86, 9844 (1981).

127. W.M. Lewis; Wat. Res. Res., 17, 169 (1981).

128. E. Gorham, W.E. Dean, J.E. Sanger; Limnol. Ocean., 28, 287 (1983).

129. H.M. Seip; Acid Snow - Snowpack Chemistry and Snowmelt. In: Effects of Acid Precipitation on Terrestrial Ecosystems. By T.C. Hutchinson, Plenum Press, London (1980).

130. G.G.C. Claridge; Studies in Element Balances in a Small Catchment at Taite, New Zealand. In: Results of

Research on Representative and Experimental Basins. UNESCO, Vol. 2 (1970).

131. T.M. Church, J.N. Galloway; J. Geoph. Research, 87, 11013 (1982).

132. D.A. Livingstone; Geol. Survey Prof. Paper 440-G, Hington (1963).

133. J.A. McKeague, M.G. Cline; Silica in Soils. In: Advances in Agronomy, Vol. 15, Academic Press, 339 (1963).

134. R.F. Yuretich, T.E. Cerling; Geoch. et Cosm. Chem. Acta, 47, 1099 (1983).

135. L.E. Taylor, D.W. Royer; Pennsylvania Geol. Survey, Water Res. Rep. 52 (1981).

136. T. Paces; Geoch. et Cosm. Chem. Acta, 36, 217 (1972).

137. W.B. Hopkins, L.R. Petri; South Dak. Geol. Surv. Water Res. Rep. No. 1, Vermillion (1962).

138. S. Arnorsson, E. Gunnlaugsson, H. Svavarsson; Geoch. et Cosm. Chem. Acta, 47, 547 (1983).

139. T. Dunne, L.B. Leopold; Water in Environmental Planning, Ch. 20, W.H. Freeman and Co., San Francisco (1978).

140. R.F. Stallard, J.M. Edmond; J. Geoph. Research, 88, 9671 (1983).

141. H.M. Keller; Factors Affecting Water Quality of Small Mountain Catchments. In: Results of Research on Representative and Experimental Basins, Vol. 2, UNESCO (1970).

142. S.K. Love; Geol. Survey Water-Suppl. Paper 1947, Washington (1967).

143. S.K. Love; Geol. Survey Water-Suppl. Paper 1950, Washington (1966).

144. S.K. Love; Geol. Survey Water-Suppl. Paper 1951, Washington (1967).

145. J.P. Miller; Geol. Survey Water-Suppl. Paper 1535-F, Washington (1961).

146. R.E. Oltman; Geol. Survey Circular 552, Washington (1968).

147. R.J. Gibbs; Science, Vol. 170, 1088 (1970).

148. J.H. Feth; Science, 172, 870 (1971).

149. R.M. Garrels, F.T. McKenzie; Origin and Chemical Composition of some Springs and Lakes. In: Equilibrium Concepts in Natural Water Systems. Am. Chem. Society (1967).

150. J. Olafsson; Limn. and Ocean., 25, 779 (1980).

151. J.Y. Gac et al.; Chemical Model for Origin and Distribution of Elements in Salts and Brines during

Evaporation of Waters. Application to some Saline Lakes of Tibesti, Chad. In: Origin and Distribution of the Elements, Physics and Chemistry of the Earth, Vol. 11, L.H. Ahrens, Pergamon Press, London (1979).

152. H.T. Mitten, C.H. Scott, Ph.G. Rosene; Geol. Survey Water-Suppl. Paper 1859-B, Washington (1968).

153. K.N. Phillips; Geol. Survey Water-Suppl. Paper 1859-E, Washington (1968).

154. H. Clemmey, N. Badham; Geology, 10, 141 (1982).

155. J.F. Talling, I.B. Talling; Int. Revueges. Hydrobiol. 50, 421 (1965).

156. J.P. Riley, M. Tongudai; Chem. Geol., 2, 263 (1967).

157. R.W. Fairbridge; The Encyclopaedia of Oceanography, Van Nostrand Reinhold Co., New York (1966).

158. F.T. MacKenzie, R.M. Garrels; J. of Sed. Petrology, 36, 1075 (1966).

159. E.A. Boyle, F.R. Sclater, J.M. Edmond; Earth and Plan. Science Letters, 37, 38 (1977).

160. F.A.J. Armstrong; Silicon. In: Chemical Oceanography, Vol. 1, Ch. 10, by J.P. Riley, G. Skirrow, Academic Press, London (1965).

161. F.T. MacKenzie et al.; Sci., 155, 1404 (1967).

162. F.T. MacKenzie, R.M. Garrels; Sci., 150, 57 (1965).

163. H.W. Harvey; The Chemistry and Fertility of Sea Waters, Cambridge Univ. Press, Cambridge (1966).

164. G.W. Moore, C.E. Robertson, H.D. Nygren; Geol. Survey Prof. Paper 450-B (1962).

165. J.E. Mackin, R.C. Aller; Geoch. et Cosm. Chem. Acta, 48, 281 (1984).

166. R.A. Berner; Geoch. et Cosm. Chem. Acta, 29, 947 (1965).

167. D.R. Schink, N.L. Guinasso, K.A. Fanning; J. Geoph. Res. 80, 3013 (1975).

168. W.S. Fyfe, N.J. Price, A.B. Thompson; Fluids in the Earth's Crust, Elsevier, Amsterdam (1968).

169. F.T. Manheim; Interstitial Waters of Marine Sediments. In: Chemical Oceanography. V. 6, Ch. 32, By Riley-Chester, Academic Press, London (1976).

170. F.T. Manheim, F.L. Sayles; Composition and Origin of Interstitial Waters of Marine Sediments, based on deep sea drill cores. In: The Sea, Vol. 5, Ch. 16. By E.D. Goldberg, Wiley and Sons, New York (1974).

171. F.T. Syles, F.T. Manheim; Geoch. et Cosm. Chem. Acta, 39, 103 (1975).

172. F.T. Manheim, D.M. Schug; Interstitial Waters of Black Sea Coves. In: Initial Reports of the Deep Sea Drilling

Project, V. XLII, Part 2, Ch. 23, US. G.P.O. Washington (1978).

173. A.I. Perel'man; Int. Geol. Rev., 4, 253 (1962).

174. A.C. Seward; Plant Life through the Ages. A Geological and Botanical Retrospect, Ch. IX, Cambridge at the Univ. Press, London (1931).

175. B.I. Kronberg, H.W. Nesbit, J. of Soil Sci., 32, 453 (1981).

176. H.W. Day; Am. J. Sci., 276, 1254 (1976).

177. A.B. Thompson; Am. J. Sci., 268, 454 (1970).

178. R.M. Carr, W.S. Fyfe; Geoch. et Cosm. Chem. Acta, 21, 99 (1960).

179. B. Velde, J. Kornprobst; Contr. Min. and Petrol., 21, 63 (1969).

180. R. Roy, E.F. Osborn; Am. Mineralogist, 39, 853 (1954).

181. J.J. Hemley; Am. Geophys. Union Trans., 48, 224 (1966) [Abs.].

182. H.Q.F. Winkler; Petrogenesis of Metamorphic Rocks, Springer-Verlag, Berlin (1974).

183. H. Haas, M.J. Holdaway; Am. J. Science, 273, 449 (1973).

184. M.R.W. Johnson, S.P. Kelley, G.J.H. Oliver, D.A. Winter; J. Geol. Soc. London, 142, 863 (1985).

185. C.Downie; Trans. Roy. Soc. Edinburgh (Earth Sci.), 71, 69 (1982).

186. D. Eberl; Am. Min., 64, 1091 (1979).

187. Ph. E. Rosenberg, G. Cliff; Am. Min., 65, 1217 (1980).

188. Ph. E. Rosenberg; Am. Min., 59, 254 (1974).

189. M.L. Sykes, J.B. Moody; Am. Min., 63, 96 (1978).

190. B.L. Reed, J.J. Hemley; U.S. Geol. Survey Prof. Paper 550-C, C162 (1966).

191. A.J. Ellis; The Chemistry of Some Explored Geothermal Systems. In: Geochemistry of Hydrothermal Ore Deposits. Ch. 11, by H.L. Barnes, Holt, Reinhart and Winston, New York (1967).

192. S. Iwao; Clay and Silica Deposits of Volcanic Affinity in Japan. In: Volcanism and Ore Genesis, p. 267, by T. Tatsumi, Univ. Tokio Press, Tokio (1970).

193. E-An Zen; Am. Min., 46, 52 (1961).

194. M. Frey, Sedimentology, 15, 261 (1970).

195. A.L. Gay, D.E. Grandstaff; Precambrian Research, 12, 349 (1980).

196. A. Button; Economic Geology Research Unit, University of the Witwatersrand, Johannesburg. Information Circular No. 133 (1979).

197. A. Button, N. Tyler; Economic Geology Research Unit, University of the Witwatersrand, Johannesburg. Information Circular 135 (1979).

198. A. Button, N. Tyler; Economic Geology, 75th Aniversary, Volume 686 (1981).

199. R.L. Stanton; Economic Geology, 78, 422 (1983).

200. A. Holmes, D.L. Holmes; Principles of Physical Geology, Nelson BAS, over Wallop, Hampshire (1979).

201. R.E. Slade; Z. Electrochem., 17, 261 (1911).

202. R. Fricke, "Kolloid Z.", 49, 229 (1929).

203. J. Kalliokoski; Geological Society of Am. Bull., 86, 371 (1975).

204. M. Schau, J.B. Henderson; Precambrian Research, 20, 189 (1983).

205. O. Tamm; Chemie der Erde, 4, 420 (1930).

206. R.M. Garrels, P. Howard; Clays and Clay Min. Mongr., 2, 68, (1959).

207. D.S. Barker; Am. Min., 49, 851 (1964).

208. F.J. Stevenson; Sci., 130, 221 (1959).

209 F.J. Stevenson, Geoch. et Cosm. Acta, 26, 797 (1962).

210. E.K. Gibson, C.B. Moore; Anal. Chem., 42, 461 (1970).

211. F. Wlotzka; Geoch. et Cosm. Acta, 24, 106 (1961).

212. W.H. Baur; Nature, 22, 461 (1972).

213. C.A. Andersen, K. Keit, B. Mason; Sci., 146, 256 (1964).

214. C. Brosset, I. Idrestedt; Nature, 201, 1211 (1964).

215. I. Idrestedt, C. Brosset; Acta Chem. Scand., 18, 1879 (1964).

216. L. Rayleigh; Proc. Royal. Soc., CLXXA, 451 (1939).

217. V.F. Volynets, T.M. Sushchevskaya; Trans. from "Geokhimiya No. 1", 58-63 (1972).

218. V.A. Klyakhin, N.F. Levitskiy; Geoch. Int., 6, 193 (1969).

219. H.P. Eugster, J. Munoz; Sci., 151, 683 (1966).

220. E.J. Sterne, R.C. Reynolds, H. Zantop; Clays and Clay Min., 30, 161 (1982).

221. R.C. Erd, D.E. White, J.J. Fahey, D.E. Lee; Am. Min., 49, 831 (1964).

222. F.J. Stevenson; Anal. Chem., 32, 1704 (1960).

223. A.P. Vinogradov, K.P. Floresnkii, V.F. Volynets; Geoch. Int., 10, 905 (1963).

224. C.B. Moore, E.K. Gibson; Sci., 163, 174 (1969).

225. A.P.S. Dhariwal, F.J. Stevenson; Soil Sci., 86, 343 (1958).

226. R.A. Gulbrandsen; J. Res. U.S. Geol. Surv., 2, 693 (1974).

227. F.C. Loughnan, F.I. Roberts; Min. Mag., 47, 327 (1983).

228. F.W. Clarke, G. Steiger; Am. J. Sci., 9, 117 (1900).

229. F.W. Clarke, G. Steiger; Am. J. Sci., 9, 345 (1900).

230. T. Yamamoto, M. Nakahira; Am. Min., 51, 1775 (1966).

231. W. Vedder; Geoch. et Cosm. Acta, 29, 221 (1965).

232. S. Higashi; Mineralogical Journal, 9, 16 (1978).

233. A.V. Karyakin, V.F. Volynets, G.A. Kriventsova; Geoch. Int., 10, 326 (1973).

234. E.J. Sterne; Econ. Geology, 79, 1406 (1984).

235. M. Berthelot; Rep. de Chimie. App., 1, 284 (1859).

236. H. Goto, Y. Kakita, I. Atsuya; Sci. Rep. Res. Inst., Tohoku Univ., Ser A., 19, 50 (1967).

237. F. Hiroshi, S. Yoshitaka, H. Shizo; Bunseki Kagaku, 20, 131 (1971) (Ch. A).

238. F. Hiroshi, S. Yoshitaka; Bunseki Kagaku, 20, 1038 (1971) (Ch. A).

239. H. Hiroshi, Y. Hideyo; Bunseki Kagaku, 19, 1564 (1970) (Ch. A).

240. H. Hiroshi, Y. Hideyo; Bunseki Kagaku, 19, 1081 (1970) (Ch. A).

241. H. Hiroshi, Y. Hideyo; Bunseki Kagaku, 19, 1136 (1968) (Ch. A).

242. M. Katsuhiko, S. Kunio, N. Masakichi; Bunseki Kagaku, 19, 1255 (1970).

243. Y. Ryoji, M. Takao, U. Michiko; Yakugaku Zasshi, 89, 1534 (1969) (Ch. A).

244. Y. Ryoji, M. Takao; Yakugaku Zasshi, 89, 804 (1969) (Ch. A).

245. Y. Ryoji, M. Takao; Yakugaku Zasshi, 88, 1383 (1968) (Ch. A).

246. B.S. Newell; J. Mar. Biol. Ass. U.K., 46, 271 (1967).

247. P.J. Rommers, J. Visser., Analyst., 94, 653 (1969).

248. P. Thomas; Bull. de la Soc. de Chim. de Fr., 11, 796 (1912).

249. H. Borsook; J. of Biol. Chem., 110, 481 (1935).

250. D.D. Van Slyke, A. Hiller; J. of Biol. Chem., 102, 499 (1933).

251. R.T. Emmet; Anal. Chem., 41, 1648 (1969).

252. W.T. Bolleter, C.J. Bushman, P.W. Tidwell; Anal. Chem. 33, 592 (1961).

253. J.A. Russell; J. of Biol. Chem., 156, 457 (1944).

254. P.G. Scheurer, F. Smith; Anal. Chem., 27, 1617 (1955).

255. J.P. Riley; Anal. Chem. Acta, 9, 575 (1953).

256. J.R. Rossum, P.A. Villarruz; J. Am. Water Works Ass., 55, 657 (1963).

257. A.L. Chaney, E.P. Marbach; Clin. Chem., 8 130 (1962).

258. J.K. Fawcett, J.E. Scott; J. Clin. Path., 13, 156 (1960).

259. B. Lubochinsky, J.P. Zalta; Bull. Ste. Chim. Biol., 36, 1364 (1954).

260. L.T. Mann; Anal. Chem., 35, 2179 (1963).

261. R.L. Searcy, N.M. Simms, J.A. Foreman, L.M. Bergquist; Clin. Chim. Acta, 12, 170 (1965).

262. M.W. Weatherburn; Anal. Chem., 39, 971 (1967).

263. J.L. Ternberg, F.B. Hershey; J. Lab. and Clin. Med., 56, 766 (1960).

264. A.B. Crowther, R.S. Large; The Analyst, 81, 64 (1956).

265. J.A. Tetlow, A.L. Wilson; Analyst., 89, 453 (1964).

266. J.C.B. Fenton; Clin. Chim. Acta, 7, 163 (1962).

267. D.B. Horn, C.R. Squire; Clin. Chim. Acta, 17, 99 (1967).

268. T.E. Weichselbaum, J.C. Hagerty; Anal. Chem., 41, 848 (1969).

269. J.E. Harwood, D.J. Huyser; Water. Res., 4, 501 (1970).

270. M. Namiki, Y. Kakita, H. Goto; Talanta, 77, 813 (1964).

271. V.G. Datsko, V.T. Kaplin; Gidrokhim. Materialy., 29, 230 (1959).

272. C. Patton, S.R. Crouch; Anal. Chem., 49, 464 (1977).

273. B. Singh; The Indophenol Blue Reaction: a Kinetic Investigation, M.Sc. Thesis, Dept. P. and App. Chem., Univ. of Strathclyde (1977).

274. A.R. Selmer-Olsen; Analyst, 96, 565 (1971).

275. B. Chapman, G.H. Cooke, R. Whitehead; Water Poll. Cont., 66, 185 (1967).

276. J.E. Harwood, D.H. Huyser; Water Res., 4, 695 (1970).

277. E.D. Noble; Anal. Chem., 27, 1413 (1955).

278. B. Newell, G.D. Point; Nature, 201, 36 (1964).

279. R.H. Brown, G.D. Duda, S. Korkes, P. Handler; Arch. Bioch. and Bioph., 66, 301 (1957).

280. A.I. Vogel; Textbook of Quantitative Inorganic Analysis, Longman, London (1981).

281. E. Hutchinson; Am. Scientist, 32, 178 (1944).

282. J.K. Bundy, G.C. Goode; Anal. Chim. Acta, 37, 394 (1967).

283. J.B. Roos; Analyst, 87, 832 (1962).